



UNIVERSITAT DE
BARCELONA

Ecomorphological discrimination of vertebrate sister species with recent phylogenetic divergence using novel non-destructive morphometric methods

Discriminación ecomorfológica de especies hermanas de vertebrados con divergencia filogenética reciente utilizando nuevos métodos morfométricos no-destructivos

Javier Hilario Santos Santos

ADVERTIMENT. La consulta d'aquesta tesi queda condicionada a l'acceptació de les següents condicions d'ús: La difusió d'aquesta tesi per mitjà del servei TDX (www.tdx.cat) i a través del Dipòsit Digital de la UB (diposit.ub.edu) ha estat autoritzada pels titulars dels drets de propietat intel·lectual únicament per a usos privats emmarcats en activitats d'investigació i docència. No s'autoritza la seva reproducció amb finalitats de lucre ni la seva difusió i posada a disposició des d'un lloc aliè al servei TDX ni al Dipòsit Digital de la UB. No s'autoritza la presentació del seu contingut en una finestra o marc aliè a TDX o al Dipòsit Digital de la UB (framing). Aquesta reserva de drets afecta tant al resum de presentació de la tesi com als seus continguts. En la utilització o cita de parts de la tesi és obligat indicar el nom de la persona autora.

ADVERTENCIA. La consulta de esta tesis queda condicionada a la aceptación de las siguientes condiciones de uso: La difusión de esta tesis por medio del servicio TDR (www.tdx.cat) y a través del Repositorio Digital de la UB (diposit.ub.edu) ha sido autorizada por los titulares de los derechos de propiedad intelectual únicamente para usos privados enmarcados en actividades de investigación y docencia. No se autoriza su reproducción con finalidades de lucro ni su difusión y puesta a disposición desde un sitio ajeno al servicio TDR o al Repositorio Digital de la UB. No se autoriza la presentación de su contenido en una ventana o marco ajeno a TDR o al Repositorio Digital de la UB (framing). Esta reserva de derechos afecta tanto al resumen de presentación de la tesis como a sus contenidos. En la utilización o cita de partes de la tesis es obligado indicar el nombre de la persona autora.

WARNING. On having consulted this thesis you're accepting the following use conditions: Spreading this thesis by the TDX (www.tdx.cat) service and by the UB Digital Repository (diposit.ub.edu) has been authorized by the titular of the intellectual property rights only for private uses placed in investigation and teaching activities. Reproduction with lucrative aims is not authorized nor its spreading and availability from a site foreign to the TDX service or to the UB Digital Repository. Introducing its content in a window or frame foreign to the TDX service or to the UB Digital Repository is not authorized (framing). Those rights affect to the presentation summary of the thesis as well as to its contents. In the using or citation of parts of the thesis it's obliged to indicate the name of the author.



UNIVERSITAT DE BARCELONA

Departament de Biologia Evolutiva, Ecologia i Ciències Ambientals,
Programa de Doctorat en BIODIVERSITAT

Museo Nacional de Ciencias Naturales,
Consejo Superior de Investigaciones Científicas

“Ecomorphological discrimination of vertebrate sister species with recent phylogenetic divergence using novel non-destructive morphometric methods”

“Discriminación ecomorfológica de especies hermanas de vertebrados con divergencia filogenética reciente utilizando nuevos métodos morfométricos no-destructivos”

Memòria presentada per **Javier H. Santos-Santos** per optar al grau de Doctor per la Universitat de Barcelona.

Javier H. Santos-Santos

Els directors de tesi:

Tutor:

Dr. David Vieites Rodríguez

Museo Nacional de Ciencias Naturales,
Consejo Superior de Investigaciones Científicas

Dr. Javier María Ferrer Parareda

Departament de Biologia Evolutiva, Ecologia
i Ciències Ambientals,
Universitat de Barcelona

Cover: Isaac Pozo

Design: Javier H. Santos-Santos

Illustrations: Javier H. Santos-Santos

ACKNOWLEDGEMENTS

First of all I want to thank my parents, Eugene and Isabel, because without their support I would have never been able to study that which fulfills my curiosity or had the opportunity to perform this thesis. Their care, and insistence in bringing out my best, has made this work possible.

I am enormously grateful to my director David Vieites, for having taking me up in his line of work, for including me in several enriching auxiliary research projects, for endowing me with extensive fieldwork experience and having granted me the possibility of travelling to exotic Mayotte and Madagascar, for his recurrent vital optimistic turnarounds of my unenthusiastic temperament in the face of complications in the development of the thesis, and for the transmission of his bureaucratic wisdom in the application and management of research projects.

I want to appreciate the potential travelling expenses and time saved by my tutor Xavier Ferrer, who uninterestedly was always attentive to facilitate my paperwork at the University of Barcelona throughout the five years I performed my thesis. But more than for these vain matters, I appreciate his permanent good humor, his initiative to create networking, and his generous provisioning of resources to perform my investigations whilst my stays at the UB.

I would also like to give a special thanks to Dominique Adriaens, whose direction, especially in my earliest years, paved the way for my interest in morphological and functional evolution. His mentorship and persistence has provided me with the precision and consistency distinctive of anatomical description that has become the gist of my work. I would like to show appreciation to all of those with whom I crossed paths under his supervision at the Evolutionary Morphology of Vertebrates Lab (UGent) with special mention to Barbara De Kegel and her technical support.

I am thankful to Cristina Paradela from the Service of Non-destructive Techniques (MNCN-CSIC) and to Manuel Dierick from the Center for X-ray Tomography (UGCT), for our long hours together developing the CT protocols and CT reconstructions indispensable for the elaboration of this project; there are indeed technical caveats when scanning mandatorily submerged samples...

I am also grateful to Emily Standen for introducing me to the fascinating and complex world of biomechanics. Her extensive practical training in various aspects of this field has made me respect the multifaceted preparation and elaboration necessary to execute biomechanical experiments. I also want to show my appreciation to everyone with whom I interacted at the Comparative and Evolutionary Biomechanics Lab (UOttawa), for their help and company during our intense working hours together. I cannot leave out either while my Canadian stay Brett Culbert and Vance Trudeau and his lab members Michal Galus, Maria Vu, and Brad Weiler for their company and assistance in wood frog anatomizing and hunting, respectively.

Although not yet represented in my work, I want to mention the people I met at Aalborg University during my courses on musculoskeletal modeling techniques Miguel Nobre Castro, Michael Skipper Andersen, and Jon Rasmussen. Their training with AnyBody Technology© raised inspiring conversations on the prospective future paths and potential applications of my research.

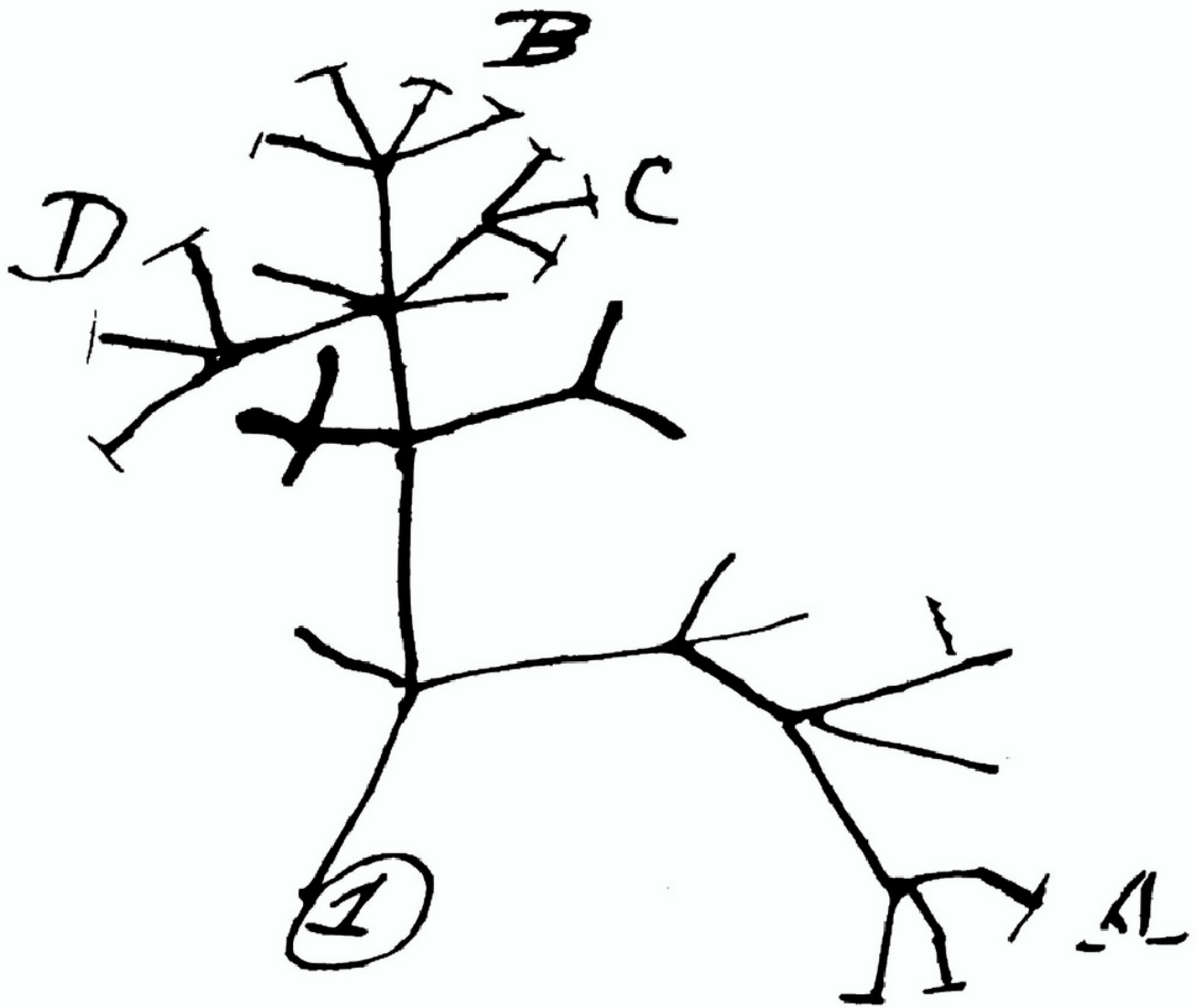
And lastly, I would like to thank the National Museum of Natural History (MNCN-CSIC), for hosting me during all these years, allowing me to use their installations, for its inspiring collections and exhibitions on biodiversity and evolution, its humanizing educational activities in which I have had the opportunity to take part, its stimulating journal clubs, and to my colleagues also in pursuit of their doctorate with whom I have shared the anxieties and joys of the development of the thesis, publications, and project accomplishments. In special, of the numerous PI's I have had the luck to interact with during my years at this institution, I also want to express my gratitude to Markus Bastir who has always been predisposed to assist me in the development of my projects and statistical analyses.

To these, and to everyone else who I have not mentioned expressly (*i.e.* personal friends, workshop colleagues, etc.) I thank you for your support and encouragement towards the completion of my thesis during the hard times and the good. I am sure that our relationship will continue to flourish albeit the conclusion of the current project.

INDEX

Prelude	<i>i</i>
General Introduction	1
Thesis Structure	8
References	11
Objectives	13
Director's Report	17
Section I: Lake Victoria Cichlids	21
Chapter 1. Divergent ontogenies of trophic morphology in two closely related haplochromine cichlids	23
Chapter 2. Ontogenetic shape development in a non-natural Lake Victoria haplochromine hybrid	55
Section II: Malagasy Mantellids	85
Chapter 3. Hidden in plain sight: two new species of the genus <i>Blommersia</i> from the oceanic island of Mayotte	87
Chapter 4. Descriptive skeletal anatomy of <i>Blommersia alexi</i> sp. nov.	109
Chapter 5. Morphological variation in <i>Blommersia</i> pelvic shape coincides with muscular architecture and parallels genus phylogenetic evolution	185
Section III: Wood Frog Locomotor Biomechanics	215
Chapter 6. Kinematic performance and muscle activation patterns during post-freeze locomotion in wood frogs (<i>Rana sylvatica</i>)	217
Integrative Discussion	249
Conclusions	269

PRELUDE



HISTORICAL CONTEXT OF EVOLUTIONARY BIOLOGY

The main concern in evolutionary biology since its origins has been the identification and comprehension of the processes that promote the divergence and creation of novel species and biodiversity generation. Throughout its modern history the field of Biology advanced on this enterprise initially with the application of Natural Selection theory (Darwin, 1859) combined with Mendelian Genetics (Mendel, 1865) [*i.e.* differential survival and reproduction of inheritable randomly generated alleles through competition], and progressively with the development of the Modern Evolutionary Synthesis [*i.e.* “Neo-Darwinism”: Dobzhansky, 1937; Huxley, 1942; Mayr, 1942], which incorporates the addition of biogeographical (Wallace, 1871), population genetics/dynamics (Haldane, 1924; Wright, 1942), quantitative genetics (Fisher, 1930), paleontological (Simpson, 1944), and [plant] hybridization and polyploidy (Stebbins, 1966) processes. What was unbecoming in this line of reasoning, however, is thinking that random mutation has all the directions of possible mutation-space available to diversify in, when there are physiological biases (Alberch et al., 1979) that limit the possibilities of the variation generation upon which natural selection will act upon *a posteriori*; and there are also constructional constraints (Gould & Lewontin, 1979) and embryological contingency (Alberch, 1982; Smith et al., 1985) that link with these physiological/developmental processes. In the late 20th century as the Modern Synthesis was succumbing before these evidences, other conceptual frameworks followed: the theory of island biogeography concerning migration and extinction rates (MacArthur & Wilson, 1967), sociobiology in relation to social behavior (Wilson, 1975), evolutionary developmental biology (aka evo-devo) integrating embryology with genetics and evolution (Gould, 1977; Jacob, 1977), and the Extended Evolutionary Synthesis (Pigliucci, 2007) and Post-modern Evolutionary Synthesis (Koonin, 2009) movements, which call for the incorporation of gene duplication (Ohno, 1970), sex evolution (Smith, 1978), extended phenotype (Dawkins, 1978), phenotypic plasticity (Via & Lande, 1985), niche construction (Odling-Smee, 1988), multilevel selection (aka group selection; Wilson & Sober, 1994), evolvability (Wagner & Altenberg, 1996), transgenerational epigenetic inheritance (Jablonka & Raz, 2009), and reticulate evolution [induced by horizontal gene transfer (Keeling & Palmer, 2008), hybridization (Stebbins, 1959; Mallet, 2007), infectious heredity (Brinton, 1967), symbiosis (Margulis & Fester, 1991), and symbiogenesis (Mereschkowsky, 1910)] processes into the Evolutionary Synthesis’ toolkit.

The main perception arising out of this historical process is that Natural Selection is not enough to describe all of the processes shaping the evolution of living organisms. However, these new developments in evolutionary biology should not be viewed as a belittlement of Darwin's work; but on the contrary, as the fruitful development of his initial passion to describe the natural processes governing the biological world at an integrative, organismal scale. The main motivation behind the discrepancy with an explanation based solely on Natural Selection comes over the source of variation on which Natural Selection can operate. The main motivators of the Modern Synthesis emphasized adaptation to occur solely at the genetic level, however even Darwin took for granted the Lamarckian idea of inheritance of acquired characteristics resulting from use or disuse (Darwin, 1859). In the current tome I examine the evolutionary process primarily from a morphological point of view, vindicating my approach by the fact that modification of the phenotype can precede change in the genotype, phenotypic variation occurs in various individuals of a population simultaneously, adaptation can be caused by either Natural Selection or environmental induction (*e.g.* ecomorphological phenotypic plasticity), non-genetic inheritance or cultural transmission, phenotypic variation is predominantly positive [as opposed to neutral], and that rapid evolution can occur from Natural Selection acting synchronously with other evolutionary processes, (Pigliucci & Finkelman, 2014).

REFERENCES

Alberch P (1982) Developmental constraints in evolutionary processes. In *Evolution and Development*, pp. 313-332. Springer.

Alberch P, Gould SJ, Oster GF, Wake DB (1979) Size and shape in ontogeny and phylogeny. *Paleobiology*, **5**, 296-317.

Brinton Jr CC (1967) Contributions of pili to the specificity of the bacterial surface, and a unitary hypothesis of conjugal infectious heredity. In *The Specificity of Cell Surfaces*, pp. 37-70. Englewood Cliffs, NJ: Prentice-Hall, Inc.

Darwin C (1859) *On the Origin of Species*, Routledge.

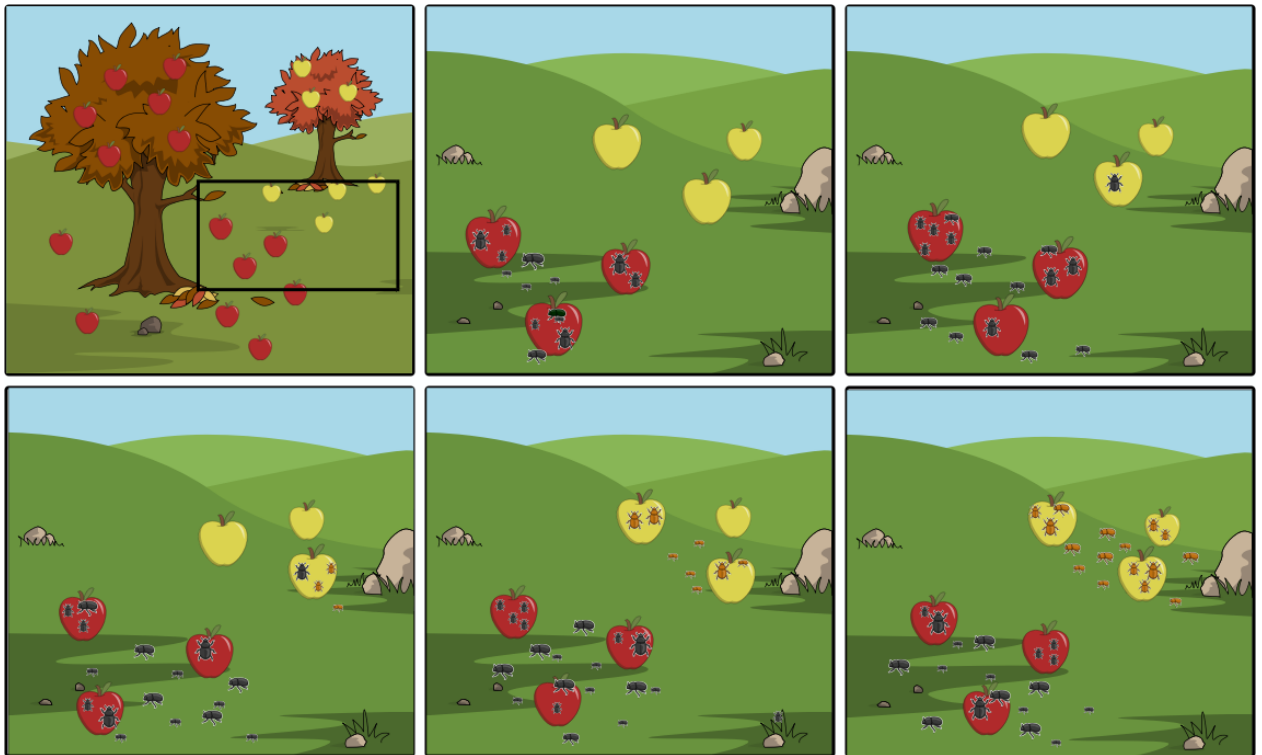
Dawkins R (1978) Replicator Selection and the Extended Phenotype. *Zeitschrift für Tierpsychologie*, **47**, 61-76.

Dobzhansky TG (1937) *Genetics and the Origin of Species*, Columbia University Press.

- Fisher R (1930) *The Genetical Theory of Natural Selection*, Oxford: Clarendon Press.
- Gould SJ (1977) *Ontogeny and Phylogeny*, Harvard University Press.
- Gould SJ, Lewontin RC (1979) The spandrels of San Marco and the Panglossian paradigm: a critique of the adaptationist programme. *Proceedings of the Royal Society of London B: Biological Sciences*, **205**, 581-598.
- Haldane J (1924) A mathematical theory of natural and artificial selection, part I. *Transactions of the Cambridge Philosophical Society*, **23**, 19-41.
- Huxley J (1942) *Evolution: the Modern Synthesis*, George Allen and Unwin.
- Jablonka E, Raz G (2009) Transgenerational epigenetic inheritance: prevalence, mechanisms, and implications for the study of heredity and evolution. *The Quarterly Review of Biology*, **84**, 131-176.
- Jacob F (1977) Evolution and tinkering. *Science*, **196**, 1161-1166.
- Keeling PJ, Palmer JD (2008) Horizontal gene transfer in eukaryotic evolution. *Nature Reviews Genetics*, **9**, 605.
- Koonin EV (2009) Towards a postmodern synthesis of evolutionary biology. *Cell Cycle*, **8**, 799-800.
- Lewontin R (1964) The interaction of selection and linkage. I. General considerations; heterotic models. *Genetics*, **49**, 49.
- MacArthur R, Wilson E (1967) *The Theory of Island Biogeography*, Princeton University Press, New Jersey.
- Mallet J (2007) Hybrid speciation. *Nature*, **446**, 279-283.
- Margulis L, Fester R (1991) *Symbiosis as a Source of Evolutionary Innovation: speciation and morphogenesis*, MIT Press.
- Mayr E (1942) *Systematics and the Origin of Species from the Viewpoint of a Zoologist*, Columbia University Press.
- Mendel G (1865) Versuche über Pflanzenhybriden. *Verhandlungen des naturforschenden Vereines in Brünn*, **IV**, 3-47.
- Mereschkowsky C (1910) Theorie der zwei Plasmaarten als Grundlage der Symbiogenesis, einer neuen Lehre von der Entstehung der Organismen. *Biologisches Centralblatt*, **30**, 278-288.
- Odling-Smee F (1988) Niche-constructing phenotypes. In *The Role of Behavior in Evolution* (ed Plotkin H), pp. 73-132. Cambridge, MA: The MIT Press.
- Ohno S (1970) *Evolution by Gene Duplication*, Springer-Verlag, New York.

- Pigliucci M (2007) Do we need an extended evolutionary synthesis? *Evolution: International Journal of Organic Evolution*, **61**, 2743-2749.
- Pigliucci M, Finkelman L (2014) The extended (evolutionary) synthesis debate: where science meets philosophy. *BioScience*, **64**, 511-516.
- Simpson GG (1944) *Tempo and Mode in Evolution*, Columbia University Press.
- Smith JM (1978) *The Evolution of Sex*, Cambridge University Press, Cambridge New York.
- Smith JM, Burian R, Kauffman S, Alberch P, Campbell J, Goodwin B, Lande R, Raup D, Wolpert L (1985) Developmental constraints and evolution: a perspective from the Mountain Lake conference on development and evolution. *The Quarterly Review of Biology*, **60**, 265-287.
- Stebbins GL (1959) The role of hybridization in evolution. *Proceedings of the American Philosophical Society*, **103**, 231-251.
- Stebbins GL (1966) *Processes of Organic Evolution*, Prentice Hall.
- Via S, Lande R (1985) Genotype-environment interaction and the evolution of phenotypic plasticity. *Evolution*, **39**, 505-522.
- Wagner GP, Altenberg L (1996) Perspective: complex adaptations and the evolution of evolvability. *Evolution*, **50**, 967-976.
- Wallace AR (1871) *Contributions to the Theory of Natural Selection*, Macmillan.
- Wilson DS, Sober E (1994) Reintroducing group selection to the human behavioral sciences. *Behavioral and Brain Sciences*, **17**, 585-608.
- Wilson EO (1975) *Sociobiology: The New Synthesis*, Harvard University Press.
- Wright S (1942) Statistical genetics and evolution. *Bulletin of the American Mathematical Society*, **48**, 223-246.

GENERAL INTRODUCTION



SPECIATION

Speciation is the evolutionary process by which populations diverge to become distinct species. The term was coined in phylogenetics to differentiate the splitting of lineages (*i.e.* cladogenesis) in contrast to the phyletic evolution within a lineage (*i.e.* anagenesis) (Cook, 1906). Although species are recognized as natural kinds (*i.e.* real independent entities; Mayr, 1988) there is no consensus on the delimitation of the species concept (Wilkins, 2009). In line with Natural Selection theory, the most widely employed definition for species is that of the Biological Species Concept (Mayr, 1942), in which a species consists of populations of organisms that can reproduce with one another, but are reproductively isolated from other populations (Dobzhansky, 1937). This leads to various geographic modes of speciation based on the extent to which populations are isolated from each other (Fitzpatrick et al., 2009). The most straightforward mode of population divergence comes from the origination of a [partial (*i.e.* parapatric speciation) or complete (*i.e.* allopatric and peripatric speciation)] geographical barrier, which consequently fragments a population's habitat, and limits gene flow between the resulting subpopulations and promotes their genetic divergence via differential selective pressures. However, it is rarer for a population to diverge within the same geographical area (*i.e.* sympatric speciation) since the persistence of gene flow without secondary contact would require the evolution of strong reproductive barriers during sister species formation (Slatkin, 1987). Even with this condition, it is hard to determine whether a population has diverged in sympatry [under the Biological Species Concept] because incomplete lineage sorting can lead to the creation of viable hybrids between recently diverged species (Joly et al., 2009).

SYMPATRIC SISTER SPECIES & 'ECOLOGICAL SPECIATION'

Sympatric speciation can lead to the observation of syntopic sister species that coexist in space and time without outcompeting each other. Their existence contradicts the traditional belief that geographic barriers to dispersal are necessary for speciation, but does not contradict the fact that gene flow prevents divergence (Slatkin, 1987). However, it is possible that environmental induction can have the same effect as a physical barrier, and it is important to recognize that environmentally induced barriers to interbreeding can have equivalent effects on gene flow as physical barriers. Furthermore, natural selection

can overcome the homogenizing processes of gene flow and recombination, and produce divergent lineages without the precondition of an extrinsic barrier (Fitzpatrick et al., 2009). With this in mind, the established conditions for sympatric speciation are: (1) the existence of strong combined effects between disruptive selection and non-random mating, (2) a strong association between genes affecting fitness and those affecting non-random mating, (3) high levels of genetic variation, and (4) minimal costs for mate choice (Gavrilets, 2005).

On the other hand, ecological speciation makes reference to the situation when barriers to gene flow (*e.g.* reproductive isolation) evolve between populations as a result of ecologically-induced divergent selection. Thus, it involves three main components: (1) an ecological source of divergent selection, (2) a form of reproductive isolation, and (3) a genetic mechanism linking the two (Rundle & Nosil, 2005). Sources of divergent selection and reproductive isolation are numerous, and divergent selection on genes affecting ecological traits can be transmitted directly via pleiotropy (Cheverud, 1996) or indirectly via linkage disequilibrium (Lewontin, 1963) to genes causing reproductive isolation.

CASE STUDIES

In various model organisms, ecological speciation has been linked to adaptive radiation; *i.e.* the evolution of ecological and phenotypic diversity within a rapidly diverging lineage, typically due to the colonization of a new environment and the evolution of a “key innovative trait” that opens new ecological niches and/or paths of evolution (Schluter, 2000). Radiations of ecologically and morphologically differentiated sympatric species are believed to have been produced by the ecological divergence (aka ecological barriers) between populations together with the acquisition of reproductive isolation in a process of ecological speciation (Rundell & Price, 2009). In the current tome I examine the phenotypic evolution of two groups of ecologically distinct vertebrate syntopic sister species thought to have evolved in sympatry: Lake Victoria modern haplochromine cichlids (Cichlidae) and Malagasy mantellid anurans (Mantellidae: Mantellinae).

East African cichlids are one of the classical textbook model organisms alongside Darwin’s Galapagos finches and the Caribbean *Anolis* lizards for adaptive radiation and

ecological speciation, whereas Malagasy mantellid frogs constitute a non-model group for which there is currently building up a large body of literature due to their interesting evolutionary history. Both groups exhibit high amounts of phenotypic and genetic variation for their clades, and show high levels of ecomorphological specialization in large part due to the presence of clade-unique key innovative traits: the pharyngeal jaws in cichlids and femoral glands in mantellids. The differences between the processes governing their adaptive radiations are interesting in an evolutionary context because they belong to different vertebrate taxa under different ecological and sexual pressures. Comparison between the selective processes influencing their evolution can shed light on how sympatric speciation progresses in different vertebrate clades and clarify the underlying processes that may apply to other taxa. In addition to the former, these groups suppose an excellent case to investigate these matters because (1) they belong to different orders of the same subphylum: Vertebrata, (2) they both have undergone a process of adaptive radiation at different time scales, (3) the species of both co-occur in a relatively small geographic area in consequence eliminating the influence of vicariance processes, and (4) in both, species have differentiated in sympatry, leaving out the processes of dispersion, migration, and secondary contact, therefore concentrating adaptive variation on morphological rather than genetic traits.

NON-DESTRUCTIVE MORPHOMETRIC METHODS

Traditionally, morphological studies involved the damaging (*e.g.* anatomical dissections) and/or destruction (*e.g.* clearing and staining or 2D/3D reconstruction from microtome slices) of a sample to obtain the osteological and anatomical data of a specimen, thus preventing its preservation for future studies. Even so, these techniques provide priceless information on the morphology and biomechanical structure of a species, making their use worthwhile. However, certain species can be more difficult to obtain than others, and for rare species there may not be any more known individuals. In these cases, the preservation of the sample is essential to the conservation of the knowledge of the species; this is especially true for non-model organisms and museum specimens. Present-day, we count on various technologies that allow us to obtain the same anatomical information albeit with an added time of digital post-processing, but in exchange, these technologies allow maintaining the sample intact, conserving its use for future studies and the potential new technologies that may arise.

In the current tome I make extensive use of several of these technologies, predominantly of that of computed tomography (CT). This technique is similar to that of the microtome, however it does not section the sample physically, but uses X-rays to reconstruct a volumetric density map of sections of the sample in all three spatial planes. The density histogram is subsequently rendered into a volume, which can later be exported as a polygon surface. Given the natural density of an organism's organs, certain tissues will give predetermined density values depending on the input parameters (*e.g.* voltage and amperage) of the CT-scan. To facilitate visualization of the different materials in the volume render, certain staining techniques can be applied to give specific tissues more density and increase the contrast between different types of tissues in the sample. In the current tome I employ a combination of a reversible (*i.e.* IKI; Gignac & Kley, 2014) and a translucent (*i.e.* PMA; Pauwels et al., 2013) staining chemical to enhance the contrast between the muscles and other tissues in the mantellid hindleg. These techniques allow for the continued preservation of the samples in view of the scarcity of these specimens and the difficulty of their re-collection.

In addition to advances in obtaining the morphological data, there have also been modern advances in their analysis. The most significant breakthrough in morphometric studies this century could well be the development of the statistical framework of Geometric Morphometrics (Zelditch et al., 2004; Adams et al., 2013). Said simply, this method treats shape as a multivariate variable defined in as many dimensions as landmarks used to delimitate it in two- or three-dimensions. Shape variation can then be visualized as a deformation grid of the original landmark configuration (Thompson, 1942). This method, as powerful and precise as it may be, still requires anatomical and/or functional homology between corresponding landmarks across the different specimens in an analysis for its biological interpretation. In most cases this is normally not a problem [*e.g.* cichlid external morphology], however structural homology is difficult to determine when comparing phylogenetically-distant taxa or featureless anatomical structures [such as smooth long bones or the cranial vault]. This was the case for the mantellid pelvis; however I was able to successfully apply to this biomechanically-relevant featureless structure a recently-developed landmark-free method within the Geometric Morphometrics framework: the Generalized Procrustes Surface Analysis (Pomidor et al., 2016).

MORPHOLOGY, PERFORMANCE, AND FITNESS

The first response of an organism to its environment is phenotypic. Thus, the progress of phenotypic evolution precedes that of the genotype (*e.g.* genetic assimilation) in an individual and determines whether a population potentially adapts to a certain ecological niche through recurrent morphological specialization. The observation of phenotypic divergence between (sub)populations, however, does not necessarily imply that morphological changes are functionally/evolutionary adaptive; Natural selection acts upon phenotypes and produces immediate phenotypic effects within a generation that can be measured without recourse to heredity. In contrast, the evolutionary response to selection depends on genetic variation passed down from one generation to the next. Upon making this distinction between phenotypic selection and the evolutionary response to selection, the possibility arises in multivariate selection theory to measure selection in natural populations by the changes it originates in the means, variances, and covariances of morphological traits (Lande & Arnold, 1983). This task is simplified by breaking it into two parts: (1) measurement of the effects of morphological variation on fitness and (2) measurement of the effects of performance on fitness (Arnold, 1983). The performance gradient represents the effect of morphological variation in a trait on some [biomechanical] aspect of performance, whereas the fitness gradient represents the effect of [biomechanical] performance on fitness.

THESIS STRUCTURE

My intention in the current tome was to be the first to achieve the sufficient information to implement Arnold's (1983) methodology and measure the strength of selection through the relationship between morphological variation, biomechanics [or performance], and heredity during the speciation process. Unfortunately, I was not able to collect all the necessary data on the same taxon to carry out these calculations, but in my pursuit of this feat, I have examined the methodology and gathered the information for each step separately, and paved the way for its prospective execution in the future. In this view, I divide my thesis in three sections:

SECTION I

Lake Victoria cichlids

The adaptive radiation of East African cichlids constitutes the most species-rich and fastest of all vertebrate taxa, the most recent of which has occurred in the modern haplochromines of Lake Victoria in less than 15000 years (Verheyen et al., 2003; Stager & Johnson, 2008). In the first chapter of my thesis I follow the development of morphological specialization in two *Haplochromis* sister species from Lake Victoria during ontogeny to their trophic niche. In chapter two, I also consider their lab-reared interspecific hybrid to determine the influence of the process of hybridization on their morphological specialization. In these works I applied 2D geometric morphometrics on standardized pictures following an unbending procedure to correct for parallax.

SECTION II

Malagasy mantellids

The Mantellidae represents the most species-rich and ecologically diverse anuran family endemic to the islands of Madagascar and Mayotte (Glaw & Vences, 2007). The relatively recent (6-8 Mya) oceanic dispersal of Mantellinae member *Blommersia wittei* from mainland Madagascar to Mayotte has led to the syntopic radiation of two species on the Comorian island (Vences et al., 2003; Crottini et al., 2012). In chapter three of my thesis I describe the external morphology and ecological reproductive niche of the two *Blommersia* species on Mayotte. In chapter four I elaborate the complete osteological description of the species on Mayotte undergoing a process of gigantism. Lastly, in chapter five I focus on the musculoskeletal anatomy of the *Blommersia* locomotor system. For these works I applied micro-CT scans combined with tissue staining techniques.

SECTION III

Wood frog locomotor biomechanics

Wood frogs exhibit one of the most extreme freeze tolerance mechanisms in vertebrates (Storey & Storey, 1988). In chapter six I examine the biomechanical performance in this species before and after a freeze/thaw cycle, with special focus on the hindleg musculature implicated in thrust production during jumping and swimming locomotion.

REFERENCES

- Adams DC, Rohlf FJ, Slice DE (2013) A field comes of age: geometric morphometrics in the 21st century. *Hystrix*, **24**, 7.
- Arnold SJ (1983) Morphology, performance and fitness. *American Zoologist*, **23**, 347-361.
- Cheverud JM (1996) Developmental integration and the evolution of pleiotropy. *American Zoologist*, **36**, 44-50.
- Cook O (1906) Factors of species-formation. *Science*, **23**, 506-507.
- Crottini A, Madsen O, Poux C, Strauß A, Vieites DR, Vences M (2012) Vertebrate time-tree elucidates the biogeographic pattern of a major biotic change around the K–T boundary in Madagascar. *Proceedings of the National Academy of Sciences*, **109**, 5358-5363.
- Dobzhansky TG (1937) *Genetics and the Origin of Species*, Columbia University Press.
- Fitzpatrick B, Fordyce J, Gavrilets S (2009) Pattern, process and geographic modes of speciation. *Journal of Evolutionary Biology*, **22**, 2342-2347.
- Gavrilets S, Vose A (2005) Dynamic patterns of adaptive radiation. *Proceedings of the National Academy of Sciences*, **102**, 18040-18045.
- Gignac PM, Kley NJ (2014) Iodine-enhanced micro-CT imaging: methodological refinements for the study of the soft-tissue anatomy of post-embryonic vertebrates. *Journal of Experimental Zoology Part B: Molecular and Developmental Evolution*, **322**, 166-176.
- Glaw F, Vences M (2007) *A Field Guide to the Amphibians and Reptiles of Madagascar*, Vences & Glaw.
- Joly S, McLenachan PA, Lockhart PJ (2009) A statistical approach for distinguishing hybridization and incomplete lineage sorting. *The American Naturalist*, **174**, E54-E70.
- Lande R, Arnold SJ (1983) The measurement of selection on correlated characters. *Evolution*, **37**, 1210-1226.
- Mayr E (1942) *Systematics and the Origin of Species from the Viewpoint of a Zoologist*, Columbia University Press.
- Mayr E (1988) *Toward a New Philosophy of Biology: observations of an evolutionist*, Harvard University Press.
- Pauwels E, Van Loo D, Cornillie P, Brabant L, Van Hoorebeke L (2013) An exploratory study of contrast agents for soft tissue visualization by means of high resolution X-ray computed tomography imaging. *Journal of Microscopy*, **250**, 21-31.

- Pomidor BJ, Makedonska J, Slice DE (2016) A landmark-free method for three-dimensional shape analysis. *PLoS One*, **11**, e0150368.
- Rundell RJ, Price TD (2009) Adaptive radiation, non-adaptive radiation, ecological speciation and non-ecological speciation. *Trends in Ecology & Evolution*, **24**, 394-399.
- Rundle HD, Nosil P (2005) Ecological speciation. *Ecology Letters*, **8**, 336-352.
- Schluter D (2000) *The Ecology of Adaptive Radiation*, OUP Oxford.
- Slatkin M (1987) Gene flow and the geographic structure of natural populations. *Science*, **236**, 787-792.
- Stager J, Johnson T (2008) The late Pleistocene desiccation of Lake Victoria and the origin of its endemic biota. *Hydrobiologia*, **596**, 5-16.
- Storey KB, Storey JM (1988) Freeze tolerance in animals. *Physiological Reviews*, **68**, 27-84.
- Thompson DaW (1942) *On Growth and Form*.
- Vences M, Vieites DR, Glaw F, Brinkmann H, Kosuch J, Veith M, Meyer A (2003) Multiple overseas dispersal in amphibians. *Proceedings of the Royal Society of London B: Biological Sciences*, **270**, 2435-2442.
- Verheyen E, Salzburger W, Snoeks J, Meyer A (2003) Origin of the superflock of cichlid fishes from Lake Victoria, East Africa. *Science*, **300**, 325-329.
- Wilkins JS (2009) *Species: a history of the idea*, University of California Press.
- Zelditch ML, Swiderski DL, Sheets HD (2004) *Geometric Morphometrics for Biologists: a primer*, Elsevier Academic Press, New York.

OBJECTIVES

The main objective of this thesis is to develop a methodological framework with the sufficient discriminatory power to characterize phenotypic differences between sister species pairs that potentially are involved in their ecomorphological divergence, by applying non-destructive methods that allow a continued preservation of the samples.

I strive to achieve this goal in two disparate vertebrate tetrapod species pairs that have undergone a process of adaptive radiation in sympatry, each with their distinctive phylogenetic history and methodological particularities: (a) model Lake Victoria modern haplochromine cichlids, and (b) non-model Malagasy mantellids. I predict that contrasting between the two vertebrate classes will potentially allow to make more generalized inferences on the selective pressures underlying the speciation process.

In each section additional (sub)objectives are presented that build towards the accomplishment of the main objective:

SECTION I

1. Validate a methodology that can discriminate subtle morphological differences.
- 2- Track the phenotypic changes throughout ontogeny between two syntopic Lake Victoria haplochromine sister species pertaining to different trophic guilds, and discuss the functional implications of the observed shape variation at each ontogenetic stage.
3. Evaluate the ontogenetic shape variation of the interspecific hybrid between our Lake Victoria haplochromines at each ontogenetic stage, and discuss the ecomorphological implications of the hybrid's shape variation in the context of the hybrid origin of East African cichlid species flocks.

SECTION II

4. Assess the ecological differentiation between the two *Blommersia* sister species that have diverged on the Comorian island of Mayotte due to both external and reproductive morphology.
5. Develop a methodology to observe the internal anatomy of samples submerged in alcohol without the destruction or deterioration of the samples.
6. Elaborate the complete osteological description of a *Blommersia* species to identify osteological functional adaptations and serve as a model for future comparative studies on functional morphology in mantellids.
7. Visualize the musculoskeletal anatomy of *Blommersia* species and locate phylogenetically-relevant phenotypic variation in biomechanical traits that potentially influence known differences in species' dispersal.

SECTION III

8. Test rapid jump and swim biomechanical performance focusing on the hindleg musculature implicated in thrust production.

DIRECTOR'S REPORT

The PhD candidate Javier Hilario Santos Santos presents his thesis entitled “Ecomorphological discrimination of vertebrate sister species with recent phylogenetic divergence using novel non-destructive morphometric methods”.

The director of the thesis, Dr. David Vieites Rodríguez, informs that this doctoral thesis is composed of six manuscripts of pronounced quality in the format of scientific articles. All the Chapters have been published or will be submitted soon to international scientific journals pertaining to the first quartiles in their respective fields of the Science Citation Index. Below is detailed the scientific contribution of the candidate in each of the manuscripts, as well as the impact factor according to the ISI Journal Citation Reports for the year 2017 of the journals where they have been published or will be submitted:

1. Divergent ontogenies of trophic morphology in two closely related haplochromine cichlids

Javier H. Santos-Santos, Leen Audenaert, Erik Verheyen, Dominique Adriaens

Journal of Morphology, 2015 (<https://doi.org/10.1002/jmor.20385>).

Impact Factor: 1.711

- The candidate performed the geometric morphometric analyses; and prepared the manuscript.

2. Ontogenetic body shape development in a non-natural Lake Victoria haplochromine hybrid

Javier H. Santos-Santos, Leen Audenaert, Erik Verheyen, Dominique Adriaens

Biological Journal of the Linnean Society, 2012 (BJLS-2415), to be resubmitted.

Impact Factor: 2.532

- The candidate performed the geometric morphometric analyses; and prepared the manuscript.

3. Hidden in plain sight: two new species of the genus *Blommersia* from the oceanic island of Mayotte

David R. Vieites, Sandra Nieto Román, Marcos Peso Fernández, Javier H. Santos-Santos

Zookeys, to be submitted.

Impact Factor: 1.079

- The candidate participated in the collection of the animals and species recognition.

4. Descriptive skeletal anatomy of *Blommersia alexi* sp. nov.

Javier H. Santos-Santos, Mireia Guinovart-Castán, Dominique Adriaens, David R. Vieites

Journal of Anatomy, to be submitted.

Impact Factor: 2.479

- The candidate processed computed tomography data and performed the visual interpretation and description of the anatomical data; and prepared the manuscript.

5. Morphological variation in *Blommersia* pelvic shape coincides with muscular architecture and parallels genus phylogenetic evolution

Javier H. Santos-Santos, Mireia Guinovart-Castán, Barbara De Kegel, Dominique Adriaens, David R. Vieites

Journal of Anatomy, to be submitted.

Impact Factor: 2.479

- The candidate developed the soft-tissue contrast staining protocol for computed tomography and performed the Generalized Procrustes Surface Analyses; and prepared the manuscript.

6. Kinematic performance and muscle activation patterns during post-freeze locomotion in wood frogs (*Rana sylvatica*)

Javier H. Santos-Santos, Brett M. Culbert, Emily M. Standen

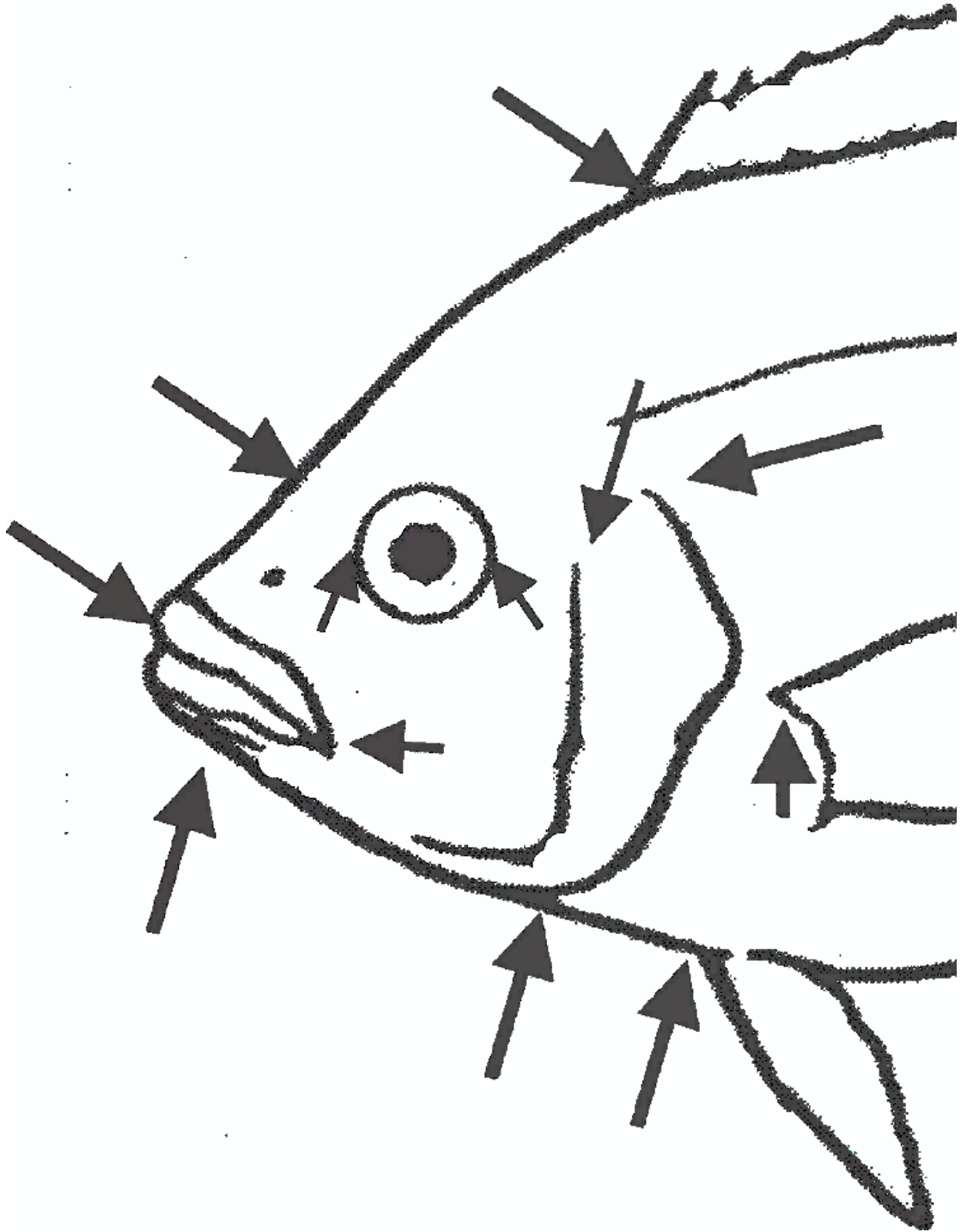
Canadian Journal of Zoology, 2018 (<https://doi.org/10.1139/cjz-2017-0240>).
Impact Factor (2016): 1.347

- The candidate participated in animal collection, designed the experimental setup, and performed the biomechanical experiments and their corresponding statistical analysis; and prepared the manuscript.

Dr. David Vieites Rodríguez

Museo Nacional de Ciencias Naturales,
Consejo Superior de Investigaciones Científicas

SECTION I



Lake Victoria Cichlids

CHAPTER 1

Divergent ontogenies of trophic morphology in two closely related haplochromine cichlids

Javier H. Santos-Santos^{1,2}, Leen Audenaert³, Erik Verheyen^{3,4}, Dominique Adriaens¹

¹ *Evolutionary Morphology of Vertebrates, Ghent University, K.L. Ledeganckstraat 35, B-9000 Gent, Belgium*

² *Integrative Biogeography and Global Change Group, Museo Nacional de Ciencias Naturales, Consejo Superior de Investigaciones Científicas (MNCN-CSIC), 28006 Madrid, Spain*

³ *Department of Vertebrates, Royal Belgian Institute of Natural Sciences, Vautierstraat 29, B-1000 Brussels, Belgium*

⁴ *Evolutionary Ecology Group, Biology Department, University of Antwerp, Belgium*

ABSTRACT

Fish develop morphological specializations in their trophic and locomotor systems as a result of varying functional demands in response to environmental pressures at different life stages. These specializations should maximize particular performances in specialists, adapting them to their trophic and habitat niches at each ontogenetic stage. As differential growth rates of the structural components comprised in the head are likely to be linked to the diet of a fish throughout its development, we investigated the ontogenetic development of two haplochromine cichlid species belonging to different trophic guilds. We employed geometric morphometric techniques to evaluate whether starting from morphologically similar fry they diverge into phenotypes that characterize trophic guilds and locomotor types. Our examination of overall body shape shows that certain specialized morphological features are already present in fry, whereas other traits diverge through ontogeny due to differences in species-specific allometric variation. Allometric shape variation was found to be more relevant for the biter specialist than for the sucker morphotype. Our results confirm that phenotypic changes during ontogeny can be linked to dietary and habitat shifts in these fish. Furthermore, evidence for an integrated development of trophic and locomotor specializations in morphology was observed.

KEYWORDS: adaptive radiation; allometry; functional morphology; ontogeny; cichlids.

INTRODUCTION

Cichlids are an excellent multidisciplinary model to investigate morphological evolution considering functional morphology, ecological speciation, phenotypic plasticity, and convergent morphotypes. In this context, East African cichlids exhibit a large array of ecotypes in relation to selective pressures on foraging performance and/or behavior, occupying a large range of habitats and trophic niches (Fryer & Iles, 1972; Liem & Osse, 1975; Van Oijen et al., 1981; Witte, 1981; Hoogerhoud et al., 1983; Witte & Van Oijen, 1990). In part, the characterization of these ecotypes is based upon the functional pressures on their internal and external anatomy, which interrelate with environmental factors that stimulate the expression of genetic and plastic responses in their morphology (Sage & Selander, 1975). In accordance, these functional pressures change ontogenetically (Osse, 1990; Zengeya et al., 2007), parallel to dietary and niche shifts that many of these species experience (Galis & De Jong, 1988; Goldshmidt et al., 1990; Galis, 1993). This results in a progressive modification of the locomotor and trophic apparatus' morphology, making them more efficient towards a species-specific diet and habitat during ontogeny (Adriaens et al., 2001; Holzman et al., 2008).

Trophic specialization is reflected in an array of internal and external morphologies that can be situated along a biting/sucking functional continuum (Albertson & Kocher, 2006). This has led to the description of numerous trophic guilds (Greenwood, 1974). In the constructional sense, cichlid morphology can be divided into different functional apparatuses that are integrated spatially. It has been documented that certain morphological specializations in locomotor anatomical structures reiteratively correspond to specific trophic guilds, advocating a connection between the development of locomotor and trophic specializations in cichlid fish (Barel, 1983).

Of the functional systems known in cichlids, their oral apparatus is one of the best documented. It generally reflects a trade-off between two mechanically different functions involved in food acquisition: sucking and biting. Mechanically speaking, a fish jaw consists of two opposing lever systems, one for jaw opening and the other for jaw closing (Albertson & Kocher, 2006). The magnitude of how the lever system transmits force or speed is calculated by two ratios that are determined from the insertions of the interopercular mandibular ligament and adductor mandibulae muscle, respectively, at the mandibular articulation. The first characterizes jaw opening, and is the ratio of the

retroarticular process (opening in-lever) and the length to the rostral (tooth) tip of the lower jaw (out-lever). The second ratio is calculated as the ratio between the length from the tip of the coronoid process (closing in-lever) and the length of the out-lever, and characterizes jaw closing. These ratios reflect the mechanical advantage of the system. A low mechanical advantage predicts rapid jaw rotation, characteristic of sucking species, while a high mechanical advantage predicts powerful jaw rotation, characteristic of biting species.

Feeding performance is influenced by locomotor ability in labrid fish (Higham, 2007a; Collar et al., 2008). Integration of locomotor behavior and feeding kinematics in centrarchid fish (Higham, 2007b) and cichlids (Higham et al., 2006) has led to the prediction that physiological, behavioral, and morphological aspects implicated in these functions co-evolve in fish. More recently, certain locomotor morphotypes have been associated to substrate type (Hulsey et al., 2013; Takeda et al., 2013), which is known to be correlated with diet (Winemiller et al., 1995; Genner et al., 1999; Kassam et al., 2004; Arbour & López-Fernández, 2013). In general, four locomotor types have been related to body shape for fish (Webb, 1982): 1) fast steady swimming, 2) unsteady time-dependent swimming, 3) unsteady acceleration plus turning swimming, and 4) place-bound maneuverability. Following this classification, zooplanktivores would require steady swimming, which is characterized by an efficient anterior streamline provided by a relatively narrow head and high postcranial body; and benthic oral-shelling molluscivores would require place-bound maneuverability, which is characterized by round dorsal head profiles and a relatively deep body at the height of the paired fins (Barel, 1983).

Whether this integration of trophic and locomotor specializations is already present in fry morphology or develops later during ontogeny has not been documented yet. Here, we survey the morphological variation throughout the ontogeny of two haplochromine cichlids belonging to different trophic guilds to observe at what developmental moment species develop morphological specializations belonging to their respective trophic and locomotor ecological niches. Furthermore, we will discuss the functional implications of morphological specialization at different stages in ontogeny as predicted from literature.

The haplochromine species flock of Lake Victoria, the youngest of the African rift lakes, has led to the appearance of ~300 endemic species in the last 200,000 years (Fryer & Iles, 1972; Elmer et al., 2009). Species have occupied basically every available niche and food

resource, taking on a wide variety of morphotypes specific to the functional demands imposed by their particular environments (Rainey & Travisano, 1998). Within these, *Haplochromis piceatus* and *H. fischeri* are two syntopic endemic species from Lake Victoria (*i.e.* Mwanza Gulf). These two species are specialized feeders located on opposite sides of the sucking/biting functional axis, with adult head and body shape features representative of their respective trophic guilds: *H. piceatus* is a pelagic zooplanktivore (fast and steady swimmer) and specialized in suction feeding (Barel, 1983; Goldschmidt et al., 1990), and *H. fischeri* is a benthivorous, oral-shelling molluscivore (place bound maneuverer) specialized in forceful biting (Greenwood, 1981 in: Katunzi, 1983). As such, they form an excellent case for comparing shape differentiation reflecting morphological specializations during the different stages of ontogeny since they belong to different trophic guilds along the sucking/biting functional axis (Albertson & Kocher, 2001). However, the amount of shape variation that corresponds to genetic factors or to plastic factors cannot be accounted for since genetic relationships within the endemic Lake Victoria superflock are still under discussion (Meyer, 1993; Verheyen et al., 2003; Wagner et al., 2012).

To analyze shape variation reflecting morphological specializations, morphological features implicated in feeding and locomotion must be identified and quantified, taking into account the homology of structures in both the head and body (Kershbaumer & Sturmbauer, 2011). Since Lake Victoria cichlids are known to exhibit low morphological variation albeit with important consequences for their ecology (Van Oijen et al, 1981), we expect that morphological specializations will become more pronounced in later stages of ontogeny given that functional requirements during larval stages are more similar (Moser, 1981).

MATERIALS & METHODS

Specimens

The *Haplochromis piceatus* (Greenwood & Gee, 1969) and *Haplochromis fischeri* [Seegers, 2008; formerly *H. sauvagei* (Pfeffer, 1896)] specimens that founded the aquarium population stock used in this study were collected at the Mwanza Gulf in southern Lake Victoria and shipped to the Haplochromis Ecology Survey Team (HEST) (Van Oijen et al., 1981) laboratory at the University of Leiden during the 1980's. Since

then they have been tank bred and reared for 29 generations. In the aquarium facility of the Royal Belgium Institute of Natural Sciences specimens were fed “ad libitum” with commercial fish food (JBL Novostick and Hikari Cichlid Excel pellets) and a weekly complement of frozen *Tubifex* and *Daphnia*. Carcasses were fixated in 80% non-denaturalized ethanol after an overdose of MS-222. A total of 34 specimens of *H. piceatus* and 37 specimens of *H. fischeri* were used. The samples for each species comprised an ontogenetic series with individuals that had already absorbed their yolk sac, spanning from 1 - 11.5cm standard length (SL) (Table 1). In order to account for the influence of domestication on shape, three type specimens from Lake Victoria, Tanzania were included for *H. piceatus* (RMNH 62769) and two for *H. fischeri* (formerly *H. sauvagei*; RMNH 70426), provided by the NCB Naturalis (the Netherlands Centre for Biodiversity, National Museum of Natural history and Research Center on Biodiversity in Leiden, The Netherlands).

Table 1. Sampling design with the number of individuals per species and species’ size class.

Species	Individuals	I	II	III
<i>H. piceatus</i>	34	9	14	11
<i>H. fischeri</i>	37	10	11	16
TOTAL	71	19	25	27

Size classes are designated based on intervals of standard length (SL): ‘I’ (1-4 cm SL), ‘II’ (4-8 cm SL), and ‘III’ (>8 cm SL).

Specimens were photographed with a Nikon D70 digital reflex camera using a Sigma 105mm macro lens at five megapixels resolution. Fish were placed on a 20x15cm dissection board with a white paper background equipped with a scale bar. Specimens were centered to avoid optical distortion of the images at the lens borders (Arnqvist & Martensson, 1998). When needed, pins were placed in the tail and/or pectoral fin region to minimize unnatural bending of certain structures due to the fixation process.

To match the observed ontogenetic morphological changes to ecological data found in literature specimens of both species were pooled into three size classes (1-4 cm SL, 4-8 cm SL, ≥ 8 cm SL). We use size as a proxy for age, which has its pros and cons (Godfrey & Sutherland, 1995), but whose use has been justified before in ontogenetic studies (Zelditch et al., 2000). These size limits were established based on earlier work on

ontogenetic development in African cichlids (Van Oijen et al., 1981; Witte, 1981; Hoogerhoud et al., 1983; Goldschmidt et al., 1990; Witte et al., 1990). Maternal mouthbrooding care stops when fry reach an approximate length of 1 cm SL, and these experience an increase of 4 cm SL during their first year (Witte, 1981). Witte et al. (1990) noted changes in habitat, diet, and morphology at an approximate length of 7 cm SL and observed an increased growth (1cm) of tank-bred specimens relative to wild individuals of the same species (*H. piceatus*). Adjusting our data to these observations, size ranges have been defined as ‘I’ (1-4 cm SL), ‘II’ (4-8 cm SL), and ‘III’ (>8 cm SL).

Morphological Data Acquisition

To analyze shape variation in head and body morphology, 32 homologous landmarks (LMs) (Fig. 1) were digitized: 13 in the head region, 11 outlining the exterior and denoting the base of the fins, two for the pectoral fin, and six indicating the lateral line and central longitudinal axis. The landmarks denoting the longitudinal axis were not included in the shape analysis, but were used as reference to apply the unbending procedure in TPS Util v1.38 (Rohlf, 2006a), in this way circumventing shape variation caused by unnatural bending during the fixation process.

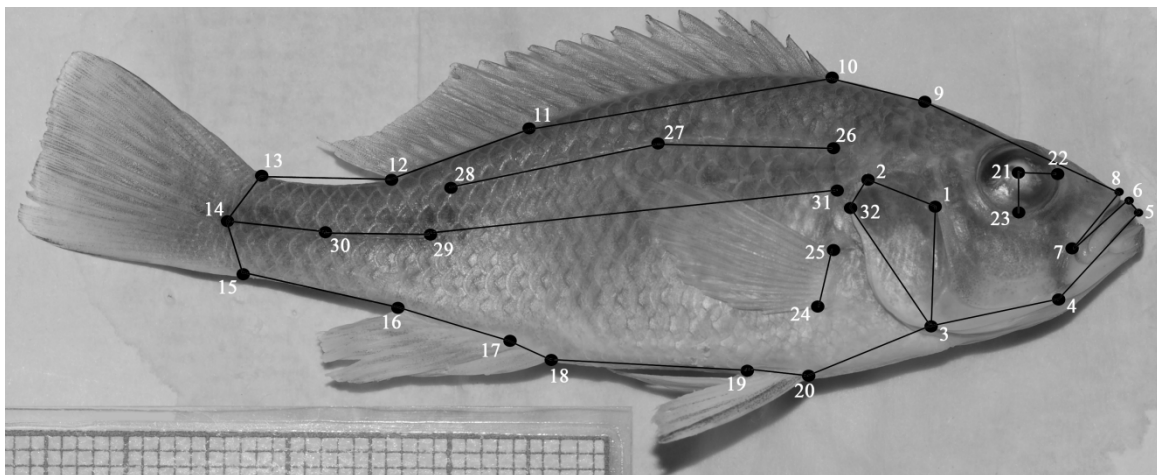


Fig. 1. Landmarks digitized. Landmarks 1-25 and 32 were used for the morphological analysis. Landmarks 8, 14, and 26-31 were used for the unbending procedure. Landmark definitions are explained in the text.

The following LMs were used for the shape analysis: **LM1:** dorso-caudal tip of the preopercular bone; **LM2:** dorsal origin of the opercular slit; **LM3:** ventral intersection point between opercular and interopercular bone; **LM4:** caudal tip of lower jaw at the level of retroarticular process; **LM5:** inferior rostral tip of the upper jaw; **LM6:** superior

rostral tip of upper jaw at the intersection between premaxillary and upper lip; **LM7**: dorso-caudal bending point of the upper lip tissue at the extremity of the lip fissure; **LM8**: unbending landmark: anterior margin of rostral tip of the rostrum; **LM9**: dorso-caudal margin of the supraoccipital crest; **LM10**: base of dorsal fin leading edge; **LM11**: posterior end of the base of the last spinous dorsal fin ray; **LM12**: base of dorsal fin trailing edge; **LM13**: base of caudal fin at the dorsal edge; **LM14**: unbending landmark: caudal end of lateral line in caudal fin peduncle; **LM15**: base of caudal fin at the ventral edge; **LM16**: base of anal fin trailing edge; **LM17**: posterior end of the base of the last spinous anal fin ray; **LM18**: base of anal fin leading edge; **LM19**: base of pelvic fin trailing edge; **LM20**: base of pelvic fin leading edge; **LM21**: center of the orbit; **LM22**: anterior-most point of the orbital margin; **LM23**: ventral-most point of the orbital margin; **LM24**: base of ventral edge of the pectoral fin; **LM25**: base of dorsal edge of the pectoral fin; **LM32**: point of maximum curvature at dorso-caudal side of the operculum.

Landmark coordinates were digitized on the photographs using TPS Dig2 v2.10 (Rohlf, 2006b). Digitization error (3.3%) (1 ind./size class * 2 species * 3 replicas) and orientation error (6.3%) (5 inds. * 2 species * 3 replicas) in the sample were quantified according to the protocol: <http://www.fun-morph.ugent.be/Miscel/Methodology/Morphometrics.pdf>.

In order to incorporate variation in head width in the analysis (as biter morphotypes tend to have wider heads), two measurements were taken on the head using an electronic caliper (0.1 mm accuracy). ‘Snout width’ was measured at the height of the posterior extremity of the gape (LM7) and ‘head width’ was measured at the level of the preopercular bone (LM1). In addition, standard length and interlandmark distances (calculated in Past v1.81 (Hammer et al., 2001)) were included as variables in the regression analysis.

Analysis of Shape

Shape data was analyzed statistically by means of Geometric Morphometrics (Zelditch et al., 2004). The correlation between Procrustes and tangent distances between specimens was tested using TPS Small v1.2 (Rohlf, 2003). A Principal Component Analysis (PCA) was performed on shape variables in MorphoJ v1.05b (Klingenberg, 2011) to search for the axes that maximize shape variation within the ontogenetic sample. Multivariate

analysis of variance (MANOVA) was performed on shape variables in IBM SPSS Statistics v19 (SPSS, Inc.) to test for significant differences between species' ontogenetic trajectories. Ontogenetic growth vectors were calculated and their directions and lengths compared. To estimate the range of angles between growth vectors, the residuals from the regression of shape on size (CS and lnCS) were paired with predicted shape values and bootstrapped (2500 iterations) with replacement in IMP-VecCompare8 (Sheets, 2003-2014) to obtain significance values under the null hypothesis of parallel vectors. Ontogenetic growth vector lengths were calculated as Procrustes distances in IMP-Regress8 (Sheets, 2003-2014) using as a reference the consensus shape from the twelve smallest specimens (*i.e.* the six smallest specimens of each species). These distances were then regressed on size (lnCS) for each sample, and the slopes' mean, confidence intervals (95%), and p-values calculated through a Monte Carlo resampling procedure (1000 iterations) with replacement (Zelditch et al., 2004) using the PopTools v3.2 (Hood, 2011) plugin in Microsoft Excel 2010. Next, the common allometric trajectory was calculated for both species and a novel PCA performed on the residuals to extract species-specific allometric shape variation. Shape changes are visualized by means of the deformation-based thin-plate spline interpolating function (Bookstein, 1991; Bookstein et al., 1996) and illustrated as wireframe grids.

To discern what structures were developing divergently at each ontogenetic stage and whether or not their development was correlated with size(lnCS), an ANOVA was performed to test for differences between group means in log-transformed biometric variables (SL, snout width, head width, and interlandmark distances). Afterwards, variables were corrected for size (lnCS) to eliminate ontogenetic size variation using General Linear Models (GLM) in IBM SPSS Statistics v19 (SPSS, Inc.). To explore the differences between factor levels in GLM models with two categorical variables (*i.e.* SPECIES and SIZE_CLASS), in the absence of post-hoc significance tests when the homogeneity of slopes assumption is violated, we compared the estimated marginal means plots. The level of statistical significance was set at a p-value < 0.05. The Bonferroni and Tamhane's T^2 (when variables present unequal error variances across groups) adjustment for multiple comparisons were applied where necessary.

RESULTS

Ontogenetic Shape Trajectories

A MANCOVA was performed on shape variables using ‘size’ (lnCS) as the covariate to test the null hypothesis of isometric growth and remove the effect of size differences between individuals within the ontogenetic series (Table 2). Again Wilk’s λ resulted significantly greater than expected by chance, indicating that species differ in their ontogenetic shape trajectories irrespective of differences in size. The multivariate distribution parameter was also significant for lnCS, leading us to reject the null hypothesis of isometric growth. This means that shape is allometric, so that it changes as a function of size. The interaction effect ‘species*lnCS’ also resulted significant, which violates the homogeneity of slopes assumption in the MANCOVA. However, in biological terms this implies that each species has a different allometric trajectory in the shared ontogenetic shape space. ‘Size’ explains a larger proportion of the variance (~10%) in the model than ‘species’ in view of the partial ETA squared values (ETA = 0.994 (size) vs 0.864 (species)). In units of Procrustes distance (d^2) this corresponds to 0.072 vs. 0.057 of 0.155, respectively.

Table 2. Multivariate analysis of covariance results for size-dependent shape variables.

Effect		value	F	sig.	partial ETA squared
intersection	Pillai’s Trace	.993	59.895	.000	.993
	Wilk’s λ	.007	59.895	.000	.993
	Hotelling’s Trace	143.747	59.895	.000	.993
	Roy’s Major Root	143.747	59.895	.000	.993
species	Pillai’s Trace	.864	2.650	.010	.864
	Wilk’s λ	.136	2.650	.010	.864
	Hotelling’s Trace	6.360	2.650	.010	.864
	Roy’s Major Root	6.360	2.650	.010	.864
lnCS	Pillai’s Trace	.994	64.365	.000	.994
	Wilk’s λ	.006	64.365	.000	.994
	Hotelling’s Trace	154.476	64.365	.000	.994
	Roy’s Major Root	154.476	64.365	.000	.994
species*lnCS	Pillai’s Trace	.894	3.509	.002	.894
	Wilk’s λ	.106	3.509	.002	.894
	Hotelling’s Trace	8.421	3.509	.002	.894
	Roy’s Major Root	8.421	3.509	.002	.894

Design: Intersection + species + lnCS + species * lnCS.

All effects in the model had significance values under $p < 0.05$. Partial ETA squared values reflect the relative contribution of each effect in explaining the total variance in the model.

The magnitude of the difference between species' ontogenetic shape trajectories was tested under the null hypothesis of parallel directions in the shared morphospace. The angle between species' ontogenetic vectors is of 34.4°, and the 95th percentile of the ranges of the within-species angles are 30.7° for *H. piceatus* and 24.2° for *H. fischeri*. The interspecific angle exceeds both within-species ranges, so we can conclude that the two species differ significantly in the direction of their ontogenies of shape.

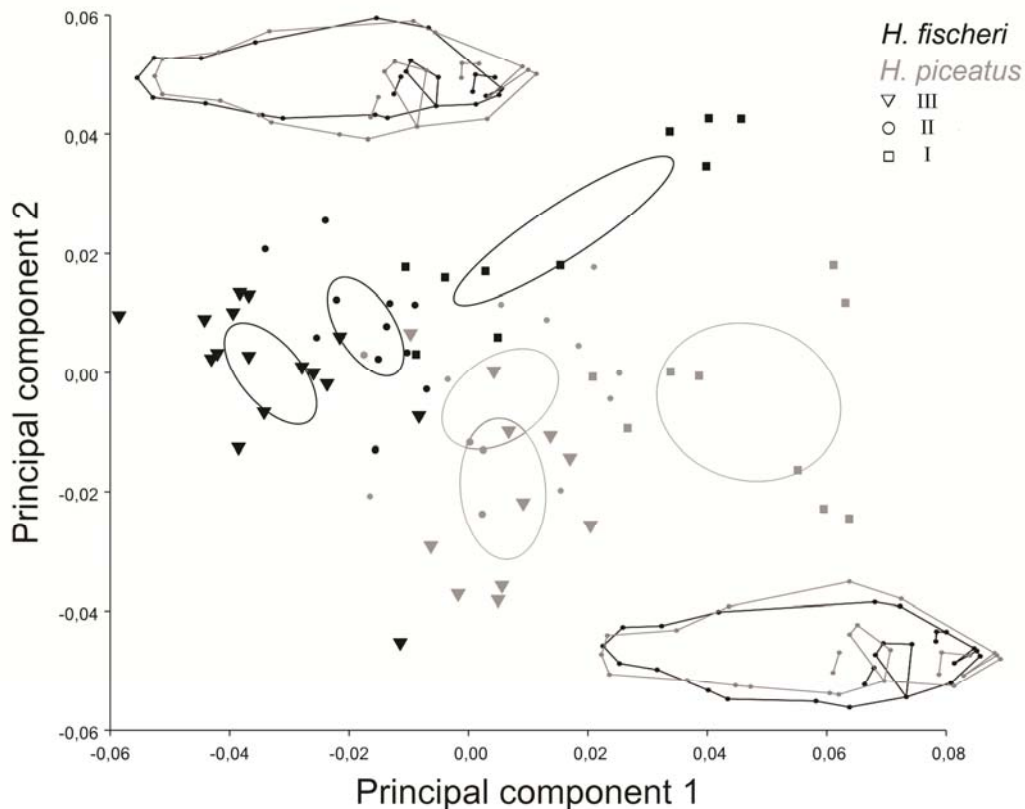


Fig. 2. PCA scatterplot showing the first two principal components. PC1 explains 37% of the total ontogenetic variation, and PC2 15%. Species samples are divided into three groups defined by size class. Confidence ellipses denote 90% mean value intervals for groups. Wireframe deformation grids are included to illustrate the shape variation ranging from -0.1 to 0.1 units in PC value from the consensus configuration for each axis. The black outline approximates shape variation for the biter morphotype (more negative PC1 values and more positive PC2 values), while the grey outline for the sucker morphotype (more positive PC1 values and more negative PC2 values) for each axis.

To test for differences in the ontogenetic rate of amount of shape variation relative to increase in size between species, we calculated the Procrustes distance from each specimen to a consensus configuration calculated using the 6 smallest specimens of each species (1-2cm SL). The Procrustes distances were plotted on size (CS) and the slope of the regression bootstrapped (1000 iterations) to obtain the confidence intervals for each

species (*H. piceatus*: 0.0024-0.0042; *H. fischeri*: 0.0026-0.0039). No significant differences were observed between species in the length of their ontogenetic vectors.

Ontogenetic Shape Variation

The PCA analysis maximized between individual shape differences, revealing two trends in the shared ontogenetic morphospace: PC1 (37%) shape variation reflects similar shape changes for both species in relation with size increase, while PC2 (15%) reflects a component of shape variation that discriminates species (Fig. 2). Since PC1 shape variation is frequently considered a size axis in geometric morphometric studies, we calculated how much of PC1 and PC2 shape variation are correlated with size in our sample by regression. We observed that 64% ($p < 0.0001$) of PC1 shape variation is predicted by size, while 17% ($p < 0.0001$) is predicted for PC2.

Shape changes associated with the PC1 axis from smaller to larger individuals (positive to negative values) (Fig. 2) involve *i*) a relatively shorter head, snout and oral jaws, *ii*) a dorsally shifted and reduced orbit, *iii*) a relatively longer ascending arm of the preopercular and larger opercular area, *iv*) a relatively deeper body and straightening of the dorsal outline, *v*) a rostral displacement and inclination of the pectoral fin, and *vi*) a steeply angled transition from the caudal peduncle towards the anal fin.

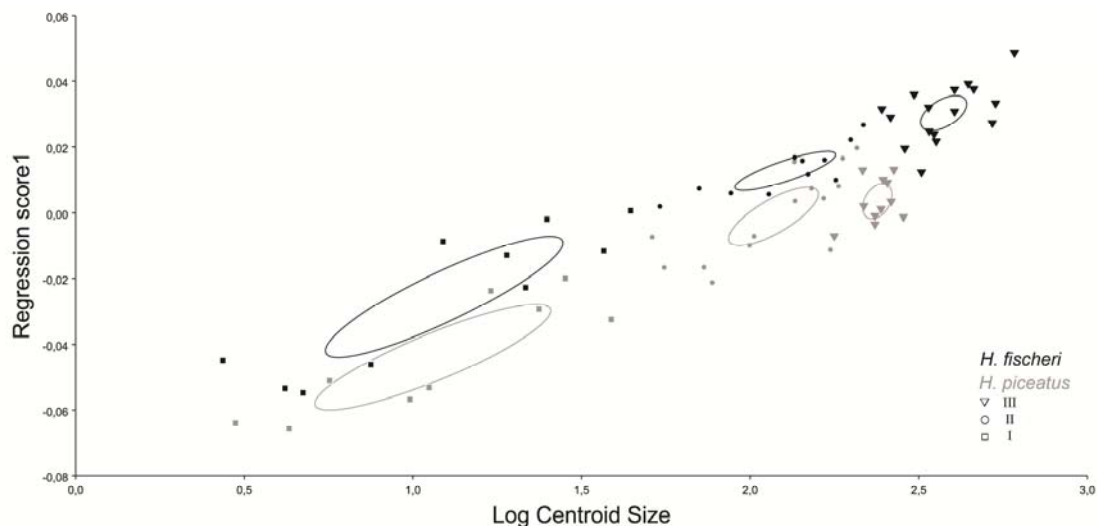


Fig. 3. A plot of the regression scores of ontogenetic shape on size (lnCS). Confidence ellipses denote 90% mean value intervals for species' size classes.

Shape changes associated with the PC2 axis from positive (*H. fischeri*) to negative (*H. piceatus*) values (Fig. 2) reflect *i*) a proportionally deeper head and cheek depth, *ii*) relatively longer snout, oral jaws and ascending arm of the preopercular, *iii*) a steeper angled transition from the neurocranium towards the dorsal fin, *iv*) a relatively deeper anterior body with a steeper angled transition towards the caudal peduncle, and *v*) a relatively shorter caudal peduncle.

Allometric Shape Variation

The multivariate regression of shape on size revealed that 28% ($p < 0.0001$) of ontogenetic shape variation is explained by size (Fig. 3). This allometric shape variation from positive to negative values is similar to PC1 shape variation, but differs in that *i*) there is no relative shortening of the head, *ii*) the leading edge of the dorsal fin shifts more dorso-rostrally, *iii*) there is no relative change in the inclination of the dorsal outline of the caudal peduncle, and *iv*) the bases of the leading edges of the anal and pelvic fins display a less important ventral shift.

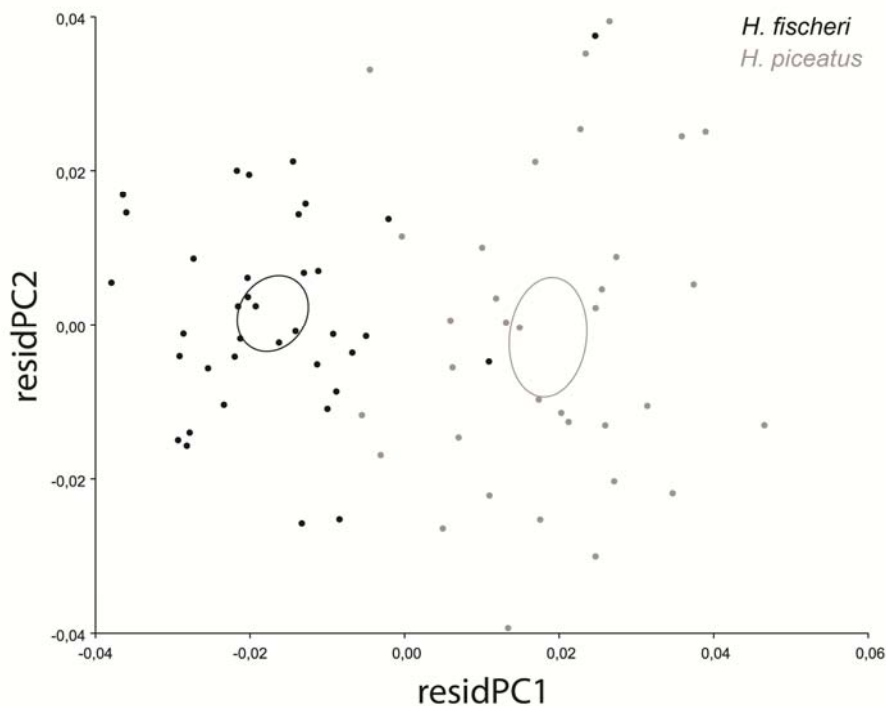


Fig. 4. PCA scatterplot of ontogenetic shape variation described by the residuals of the multivariate regression of shape on size (lnCS). residPC1 explains 30% of the total variation. A clear separation between species can be observed along the residPC1 axis. *H. piceatus* (grey) individuals are located on the positive values, and *H. fischeri* (black) individuals are located on the negative values. Ellipses denote the species' 90% mean confidence intervals.

Deriving from the significant interaction effect between species and size in the MANCOVA that indicated different allometries of shape between species, we regressed species' allometries separately, but within the same Procrustes superimposition. For *H. piceatus* 28% of shape variation could be predicted by size and 42% for *H. fischeri*. The interspecific angle between them was of 35° ($p < 0.0001$). To test for allometric shape variation discriminating species we performed a new PCA on the residuals from the shared allometric regression to maximize shape differences between individuals. Species were clearly discriminated (Wilk's $\lambda = 0.031$; $F = 14.333$; $p < 0.001$; $\text{ETA} = 0.969$) along residPC1 (30%) (Fig. 4); *Haplochromis piceatus* individuals have positive residPC1 scores, while *H. fischeri* individuals have negative ones (with two exceptions). residPC1 axis shape variation predicted 34% of PC1 shape variation (with vectors at an angle of 40°) and 48% of PC2 (with vectors at an angle of 55°).

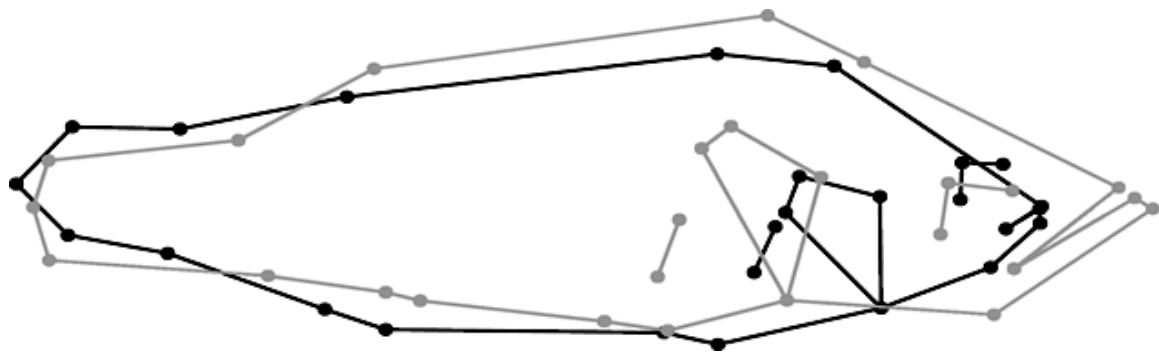


Fig. 5. Wireframe deformation grid of residPC1. The grey outline (*H. piceatus*) defines a change in the PC score of 0.1, and the black outline (*H. fischeri*) a change in the PC score of -0.1 from the consensus configuration.

Shape changes described by the residPC1 axis (Fig. 5) from *H. fischeri* to *H. piceatus* comprise *i*) a significant increase in head length, oral jaw length, snout height, and body height, *ii*) a more terminal positioned mouth, *iii*) a dorso-rostral shift of the origin of the first soft and hard dorsal fin rays, creating a steep transition towards the dorsal caudal peduncle, *iv*) a caudal shift of the pectoral fin, *v*) and a dorso-rostral shift of the origin of the first soft and hard anal fin rays, resulting in a steep transition towards the ventral caudal peduncle.

Biometric Variables

Interlandmark distances were chosen from the landmark configuration considering that they covered anatomical structures known to be implicated in sucking/biting performance and/or in other functions (Fig. 6). The linear measurements employed are defined in Table 3. All variables were transformed to their natural logarithm to linearize allometric relationships for regression analysis (Mascaro et al., 2013). A preliminary GLM was performed using $\ln CS$ as covariable to test what variables were correlated with an increase in size (Table 4). Variables not correlated with an increase in size were OpW, GH, LJ, PDA, BH, AF2, and PcF-PvF. It is noteworthy to mention that CS did not show significant differences between species, indicating a similar growth rate (as quantity of shape change per increase in size) (Fig. S1).

To observe what variables differed between species, a distinct ANOVA with SPECIES as the categorical variable was performed for each variable to avoid correlation interactions between variables in a multivariate GLM model (Table 4). Species had significantly different means for the variables BL, OpW, GH, HL, HH, and AF2. Since species samples consist of an ontogenetic series, an ANCOVA was performed to correct for size ($\ln CS$). Additionally, the variables SL, HW, LJ, ChD, SnL, PDA, and PcF-PvF resulted significant, however violating the homogeneity of slopes assumption (except for SL). This indicates that the relationship between these variables and the covariate differ between species, suggesting different ontogenetic trends of these variables for each species.

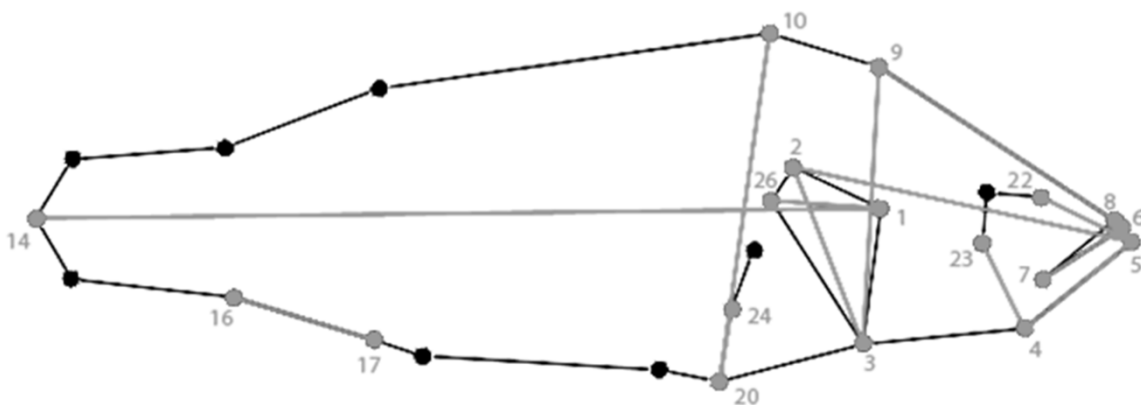


Fig. 6. Illustration of the wireframe used to describe body shape. Interlandmark distances calculated from the landmark configuration (in grey) constitute the variables used in the regression analysis that are described in Table 3.

To observe differences in our biometric variables between size classes through ontogeny, ANOVA was performed as before with SIZE_CLASS as the categorical variable (Table 4). Size classes presented significantly different means for the variables CS, SL, SW, HW, BL, HL, ChD, SnL, and NL. However, after correcting for differences in size (lnCS) through ANCOVA, only the variables HW, HH, BH, and PcF-PvF resulted significantly different between size classes. Of these, only BH violated the homogeneity of slopes assumption, suggesting a change in the ontogenetic trend of this variable at a determined size range for both species.

Table 3. Definition of the interlandmark distances used in the regression analyses.

Variable	Landmarks	Definition	Apparatus
SL		Standard length	
CS		Centroid size	
HW		Head width	trophic
SW		Snout width	trophic
HH	LMs 3—9	Head height	trophic
NL	LMs 8—9	Neurocranium length	locomotor
HL	LMs 2—5	Head length	trophic
SnL	LMs 5—22	Snout length	trophic
ChD	LMs 4—23	Cheek depth	trophic
LJ	LMs 4—5	Lower jaw length	trophic
PDA	LMs 6—7	Premaxilla dentigerous arm length	trophic
GH	LMs 2—3	Gill height	respiratory, trophic (Osse, 1990)
BH	LMs 10—20	Body height	locomotor
BL	LMs 1—14	Body length	locomotor
AF2	LMs 16—17	Soft anal fin region	locomotor
PcF-PvF	LMs 20—24	Interpectoral-pelvic fin distance	locomotor
OpW	LMs 1—26	Opercular width	respiratory, trophic (Osse, 1990)

Interlandmark distances were calculated in Past v1.81 (Hammer et al., 2001).

To further elucidate differences between species' ontogenetic series in biometric variables, a GLM was performed including both SPECIES and SIZE_CLASS as categorical variables in the model (Table 4). Once again, size correction was executed. Size classes had significantly different means for the variables SL, SW, HW, HL, LJ, ChD, SnL, PDA, and PcF-PvF. All of them violated the homogeneity of slopes assumption indicating differences in variable values between species, depending on the size range of individuals during ontogeny. Estimated marginal means plots were

generated to estimate the timing of these ontogenetic shifts in variable values between species' size categories (Fig. 7).

Table 4. Results of the GLM analyses on interlandmark distance variables.

Variable	InCS	species	size_class	species*size_class
SL	*	*		*†
HW	*	*†	*	*†
SW	*			*†
HH	*	*	*	
HL	*	*		*†
SnL	*	*†		*†
ChD	*	*†		*†
LJ		*†		*†
PDA		*†		*†
GH		*		
BH			*†	
BL	*	*		
AF2		*		
PcF-PvF		*†	*	*†
OpW		*		

Each column represents a separate GLM model with its corresponding categorical variable(s). (*) denotes a significant effect between the dependent variable and the covariate/categorical variable in each column. (†) denotes the violation of the homogeneity of slopes assumption for a dependent variable in each column. [For more explanation see the *Biometric Variables* section in Materials & Methods.]

DISCUSSION

Evolution of Morphological Allometry

Shape variation associated to a common allometric trajectory and that from species-specific allometry were examined separately to observe what shape changes were correlated solely to a common allometric trajectory from those that involved species-specific development (Fig. 5). Species-specific allometric shape variation accounted for a larger percentage of the shape variation within the ontogenetic sample (30%) than the common allometric component (28%). Both allometric components contribute to the shape differences associated to our PC1 and PC2 axes that maximize individual differences (Fig. 2), and an interaction between them in ontogenetic shape space is patent. Together they predict 98% (64% and 34%) of PC1 shape variation and 65% (17% and 48%) for PC2.

Allometric changes discriminating our species coincide with shape variation associated to their respective locomotor and trophic specializations, similar to what has been observed

in other Lake Victoria specialists (Bouton et al., 1999). Since species did not display differences in relative growth rates, allometric differences in biometric variables between species must improve some species-specific function at a certain moment in ontogeny (Pelabon et al., 2014). In a constructional context, this may be achieved by different spatial arrangements of the respective apparatuses between species and/or size classes (Strauss, 1984; Barel et al., 1989; Liem, 1991; Barel, 1993) originated by the reallocation of resources to meet functional demands at different ontogenetic moments (Ruehl & DeWitt, 2005; Taborsky, 2006; Von Bertalanffy, 1957). This seems to be the case with the oral jaws and the interpectoral-pelvic fin length (Table 4). In relation to the recent literature on cichlid shape divergence along the benthic-limnetic axis (Hulsey et al., 2013; Takeda et al., 2013), the sucker morphotype apparently may be allocating more resources to increase in body length along the anterior-posterior axis during ontogeny, while the biter morphotype to increase lengths along the dorso-ventral axis and head width.

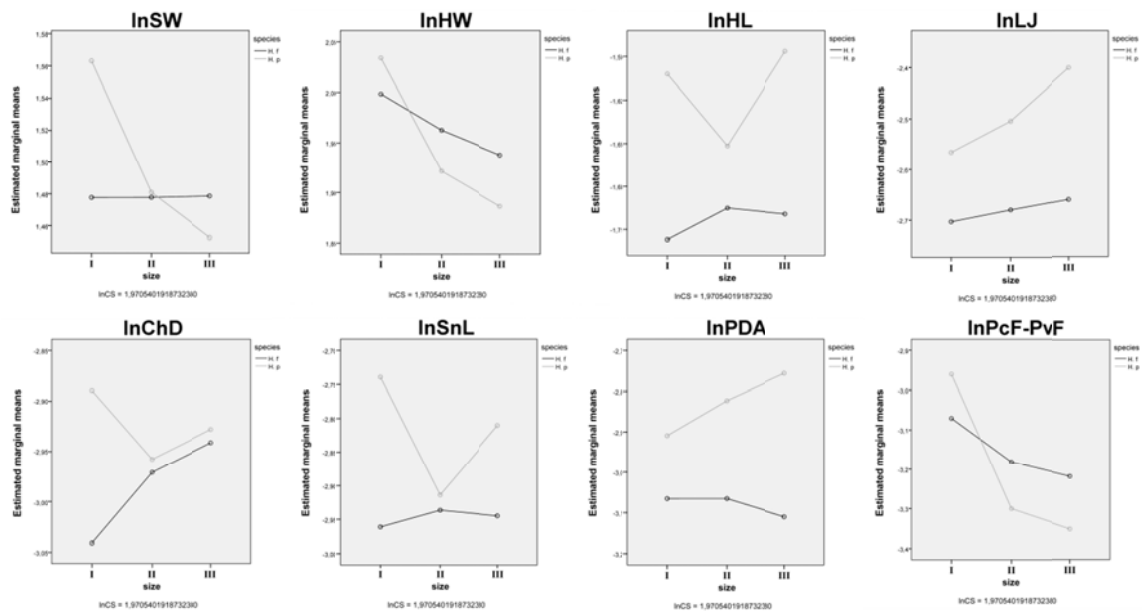


Fig. 7. Estimated marginal means for variables that have a significant SPECIES*SIZE_CLASS interaction effect, and that violate the homogeneity of slopes assumption. The horizontal axes denote size classes and individual lines represent each species (black: *H. fischeri*, grey: *H. piceatus*). Line segments that are parallel indicate that there is no interaction between the categorical variables at that ontogenetic interval. Estimated marginal means were calculated at the covariable value of $\ln CS = 1.97$.

We expected that species' shape differences would become more pronounced through ontogeny starting out from morphologically similar fry. We found that even though larvae were morphologically very similar, they already displayed differences in morphological characters uncorrelated with size that are implicated in trophic/respiratory (gill height and

opercular width), a larger size of the gill arches enlarges the volume of the buccal cavity during suction feeding (Osse, 1990), and locomotor functions (soft anal fin region length). The former variables had larger values in the sucker morphotype, whereas the latter was larger in the biter morphotype. Hence, functionally relevant morphological differentiation between species is already present at the beginning of ontogeny for these characters, but is later magnified due to species-specific allometries that arise at specific moments in ontogeny (size classes). This implies that the developmental program of morphological specializations is decoupled in modular genetic programs throughout ontogeny, which may allow for phenotypic plastic adjustments at each ontogenetic stage (Atchley, 1984). In view of the morphologic (Barel et al., 1977) and genetic irresolution (Elmer et al., 2009; Wagner et al., 2012) of the Lake Victoria *Haplochromis* genus (including the species studied), we lack the phylogenetic framework to make any conclusions on the divergence in the evolutionary direction of species' allometric trajectories. Nonetheless, the most recent common ancestor of the entire Lake Victoria Region haplochromine species flock was estimated to have existed at 4.5 million years ago (Elmer et al., 2009).

Trophic and Locomotor Functional Significance of Shape Variation

Species-specific allometric shape variation discriminating species (Fig. 5) agrees with similar comparisons relating to convergent sucker and biter morphotypes in all three East African Lake cichlid assemblages (Young et al., 2009): elongate bodies are typical of planktivorous suction feeders, whereas deep bodies with short down-turned heads are associated with diets comprised of harder prey items.

The functional implications of morphological specializations that facilitate more powerful biting have been evaluated in cichlids before (Barel, 1983; Van Leeuwen & Spoor, 1987; Galis, 1992; Bouton et al., 1998). It is agreed that in molluscivores, the jaw apparatus is more adapted to forceful biting. To this we have to add the intraspecific differences in muscle recruitment and possible patterns of jaw movement (Liem, 1978; Galis, 1992). However, intraspecific shape variation due to phenotypic plastic adaptations to diet items (Bouton et al., 1999) can be ignored in our results because species were fed the same food regime. The pattern of morphological variation observed in *H. fischeri* in overall body shape predicts certain internal anatomical variation (Sanderson, 1990). In the head, the

ample dorso-caudal shift of the eye and the substantial increase in length of the ascending arm of the preopercular bone and in height of the suspensorium, enlarges the space in this region, providing a larger insertion area and available volume for the adductor mandibulae muscle implicated in forceful biting (Barel, 1983). In the oral jaw lever system, we observe a relative increase in length of the coronoid process (closing in-lever) relative to the lower jaw (out-lever), which grants a higher mechanical advantage to the system (Albertson & Kocher, 2006). Both of these changes mechanically lead to a progressively stronger biting force (Bouton et al., 2002), which can thus be expected in *H. fischeri*.

In the constructional context (Barel et al., 1989), the development of structures implicated in the trophic core functions of biting and sucking (Barel, 1983) is also constrained by that of adjacent apparatuses. All these apparatuses (oral jaw apparatus, expansion apparatus, gill apparatus, and locomotor apparatus) share spatial demands, resulting in morphological constraints reflected in functional trade-offs. The different arrangements between apparatuses determine the range of form-features allowed architectonically. Based on these arrangements, Barel (1983) identified associated morphologies between the oral jaw apparatus and remaining apparatuses that either optimize one core trophic function or the other.

The head shape of *H. fischeri* has a more rounded profile resulting from the rostral-ventral shift of the anterior edge of the dorsal fin. The rostral-ventral shift of the leading edges of the anal and pelvic fins create a flat ventral margin, which is complementary to this shape of the head profile in providing rotation maneuverability characteristic of benthic feeders (Aleyev, 1977). In more recent investigations (Drucker & Lauder, 2001; Chadwell & Ashley-Ross, 2012), functional studies of locomotor specialization have revealed certain aspects of fin development that were also apparent in our results. Differences in the soft anal fin region length affect the generation/resistance of hydrodynamic forces during swimming. This is because the posterior region of the anal fin is functionally decoupled from the anterior region and provides roll and/or yaw stability while generating additional thrust forces during slow turning maneuvers (Chadwell & Ashley-Ross, 2012). The development of these locomotor specializations associated with the biter trophic morphotype advocate a certain integration of feeding and locomotor functions (Collar et al., 2008; Franchini et al., in press), although it may just be

a species-specific pattern. However, preliminary tests of shape covariation between head and postcranial body landmark configurations for this species display shape changes related to trophic and associated locomotor specializations with PLS2 paired axis explaining 15% of the total shape covariation between modules, supporting the former outcome (pers. obs.).

The relative elongation of the lower jaw (out-lever) in our *H. piceatus* sample results in a smaller mechanical advantage and consequently in an improved kinematic efficiency. The dorsal shift at the ventral intersection point between opercular and interopercular bone alters the inclination of the head occasioning an upturned mouth characteristic of pelagic feeders. The increase in size of the snout and increasing horizontal dorso-ventral orientation of the ventral head profile provide a more rectangular lateral head profile that when expanded results in a larger and more cylindrical buccal cavity with an increased buccal volume characteristic of suction feeders (Barel, 1983; Muller & Osse, 1984).

Associated changes in the locomotor apparatus are an efficient anterior streamline and a minimum body area reflected in relatively small widths and depths in outer head shape. In the constructional context, the increase in body height and the caudal displacement of the pectoral fin in *H. piceatus* leave more space adjacent to the head for the epaxial and hypaxial musculature, which coincides with the necessity of an increased need of power for head expansion in slow-swimming suckers (Barel, 1983; Wainwright et al., 2001; Carroll et al., 2004). In accordance with *H. fischeri*, the development of these locomotor specializations associated to the sucker morphotype advocate a certain integration of feeding and locomotor functions in Lake Victoria haplochromines.

Ecomorphological Implications of Morphological Specialization

The existence of differences between species in biometric variables correlated with size that are implicated in trophic and locomotor function advocate a benefit of increased growth considering that fish mortality is usually an inverse function of size (Galis & De Jong, 1988). Growths of characters in the head are especially important for food uptake. In the biter morphotype, the increase in head width allows individuals to feed upon larger prey items through ontogeny. Such a functional ontogenetic shift has been put forward for *H. fischeri* (Katunzi, 1983), and our observations corroborate that morphological

specializations produced by its species-specific allometry facilitate a behavioral food-partitioning between individuals of different ontogenetic stages based on prey size in this species (Katunzi, 1983; Ferry-Graham et al., 2002). However, this is not the case for the sucker morphotype since Galis and De Jong (1988) observed during its ontogeny by means of optimal foraging models equal *Chaoborus* prey uptake and decreasing uptake of *Daphnia* prey with increasing size. We observed that variables in the head implicated in trophic specialization in this species do not begin to increase significantly in length until size class II, suggesting that a relatively larger buccal volume isn't a constraint in food uptake until size class III, which coincides with the optimal foraging model of Galis & De Jong (1988). And on the contrary, oral jaw length increases in value through all of ontogeny, continuously potentiating suction feeding (kinematic efficiency and jaw protrusion) as *H. piceatus* individuals get bigger.

The benefits of increased growth in size class II are less obvious in view of biometric variables implicated in locomotor performance. Both body height and interpectoral-pelvic fin length display a similar increase in value at this size class for both species (*H. piceatus* displaying higher absolute values), but neither were correlated with size. The increase in interpectoral-pelvic fin length for the size class II biter morphotype results in enhanced maneuvering capacities and force generation at the pectoral girdle (Drucker & Lauder, 2002). This morphological specialization can be linked to an ontogenetic habitat shift towards deeper waters (Goldschmidt et al., 1990) where larger forces are necessary for benthic locomotion due to higher pressures. Similarly, the dorsal head profile at size class II becomes higher and more rounded which in addition to the flat ventral outline provided by the increase in interpectoral-pelvic fin length, provides an adaptation to pitch over the bottom more effectively (Aleyev, 1977). These observations in our biter morphotype advocate an integrated development of the trophic and locomotor apparatus through ontogeny due to changing functional demands (Higham, 2007).

The development of locomotor specializations described by an efficient streamline in the sucker morphotype due to increased values in their body height and interpectoral-pelvic fin length is also more pronounced at size class II. However, body length displayed a significantly increased growth rate at size class I for this species. These observations support that morphogenetic programs are decoupled at different ontogenetic stages (Atchley, 1984), and coincide with the ontogenetic niche shift this species undergoes

from shallow littoral nurseries to deeper waters when becoming III since predator avoidance and prey capture depend more on speed in pelagic waters (Witte, 1981; Goldschmidt et al., 1990).

In the context of the adaptive radiation of East African cichlids, more ecological studies surrounding the biomechanics of the ontogenetic dietary and niche shifts that the two species studied undergo are necessary to evaluate whether the here observed morphological differentiation corresponds directly to differences in performance that can influence their survival at different moments in ontogeny. Although the species are syntopic in Lake Victoria, they shouldn't compete with one another since they have different depth distributions (Van Oijen et al., 1981; Goldschmidt et al., 1990), and differences in breeding strategies concerning timing, spawning, and brooding sites that are likely to contribute to the partitioning of resources (Goldschmidt & Witte, 1990). Thus that the ontogenetic patterns of morphological specialization observed should be more the product of independent selective pressures for each species. The integration during ontogeny of shape variation patterns involving morphological features implicated in trophic and locomotor specializations does not agree with a three stage model of adaptive radiation in which habitat and trophic niche adaptation are considered independent of one another (Streelman & Danley, 2003), but puts forward an integration of these two stages in the adaptive radiation process.

ACKNOWLEDGMENTS

We thank the Haplochromis Ecology Survey Team (HEST), the University of Leiden, and the Naturalis (Leiden) for supplying the stock of *H. piceatus* and *H. fischeri* specimens that was used as a starting point for our own breeding experiments and for providing the type specimens used in this investigation. J.H.S-S. was supported by an Erasmus studies exchange grant between the University of Salamanca and the University of Ghent. Research was funded by the Research Foundation Flanders (projects 1.1.A72.10.N.00 and 3G014911), and Belgian Science Policy project MO/36/013.

REFERENCES

- Adriaens D, Aerts P, Verraes W (2001) Ontogenetic shift in mouth opening mechanisms in a catfish (Clariidae, Siluriformes): a response to increasing functional demands. *Journal of Morphology*, **247**, 197-216.
- Albertson R, Kocher T (2006) Genetic and developmental basis of cichlid trophic diversity. *Heredity*, **97**, 211-221.
- Albertson RC, Kocher TD (2001) Assessing morphological differences in an adaptive trait: a landmark-based morphometric approach. *Journal of Experimental Zoology*, **289**, 385-403.
- Aleyev Y (1977) *Nekton*, Dr. W. Junk B.V. Publishers, The Hague, Netherlands.
- Arbour JH, Lopez-Fernandez H (2013) Ecological variation in South American geophagine cichlids arose during an early burst of adaptive morphological and functional evolution. *Proceedings of the Royal Society of London B: Biological Sciences*, **280**, 20130849.
- Arnqvist G, Martensson T (1998) Measurement error in geometric morphometrics: empirical strategies to assess and reduce its impact on measures of shape. *Acta Zoologica Academiae Scientiarum Hungaricae*, **44**, 73-96.
- Atchley WR (1984) Ontogeny, timing of development, and genetic variance-covariances structure. *The American Naturalist*, **123**, 519-540.
- Barel C (1983) Towards a constructional morphology of cichlid fishes (Teleostei, Perciformes). *Netherlands Journal of Zoology*, **33**, 357-424.
- Barel CDN (1993) Concepts of an architectonic approach to transformation morphology. *Acta Biotheoretica*, **41**, 345-381.
- Barel C, Anker GC, Witte F, Hoogerhoud R, Goldschmidt T (1989) Constructional constraint and its ecomorphological implications. *Acta Morphologica Neerlando-Scandinavica*, **27**, 83-109.
- Barel C, Van Oijen M, Witte F, Witte-Maas EL (1977) An introduction to the taxonomy and morphology of the haplochromine Cichlidae from Lake Victoria. *Netherlands Journal of Zoology*, **27**, 333-380.
- Bookstein F (1991) *Morphometric Tools for Landmark Data. Geometry and Biology*, Cambridge University Press.
- Bookstein F, Marcus L, Corti M, Loy A, Naylor G, Slice D (1996) *Advances in Morphometrics*, Plenum Press, New York.
- Bouton N, De Viser J, Barel CDN (2002) Correlating head shape with ecological variables in rock-dwelling haplochromines (Teleostei: Cichlidae) from Lake Victoria. *Biological Journal of the Linnean Society*, **76**, 39-48.

Bouton N, Van Alphen JJ, Schenk A, Seehausen O (1999) Local adaptations in populations of rock-dwelling haplochromines from southern Lake Victoria. *Proceedings of the Royal Society B: Biological Sciences*, **266**, 355-360.

Bouton N, Van Os N, Witte F (1998) Feeding performance of Lake Victoria rock cichlids: testing predictions from morphology. *Journal of Fish Biology*, **53**, 118-127.

Carroll AM, Wainwright PC, Huskey SH, Collar DC, Turingan RG (2004) Morphology predicts suction feeding performance in centrarchid fishes. *Journal of Experimental Biology*, **207**, 3873-3881.

Collar DC, Wainwright PC, Alfaro ME (2008) Integrated diversification of locomotion and feeding in labrid fishes. *Biology Letters*, **4**, 84-86.

Chadwell BA, Ashley-Ross MA (2012) Musculoskeletal morphology and regionalization within the dorsal and anal fins of bluegill sunfish (*Lepomis macrochirus*). *Journal of Morphology*, **273**, 405-422.

Drucker EG, Lauder GV (2001) Wake dynamics and fluid forces of turning maneuvers in sunfish. *Journal of Experimental Biology*, **204**, 431-442.

Elmer KR, Reggio C, Wirth T, Verheyen E, Salzburger W, Meyer A (2009) Pleistocene desiccation in East Africa bottlenecked but did not extirpate the adaptive radiation of Lake Victoria haplochromine cichlid fishes. *Proceedings of the National Academy of Sciences*, **106**, 13404-13409.

Ferry-Graham LA, Bolnick DI, Wainwright PC (2002) Using functional morphology to examine the ecology and evolution of specialization. *Integrative and Comparative Biology*, **42**, 265-277.

Fryer G, Iles T (1972) *The Cichlid Fishes of the Great Lakes of Africa: their biology and distribution*, Oliver and Boyd, Edinburgh.

Galis F (1992) A model for biting in the pharyngeal jaws of cichlid fish *Haplochromis piceatus*. *Journal of Theoretical Biology*, **155**, 343-368.

Galis F (1993) Morphological constraints on behaviour through ontogeny: the importance of developmental constraints. *Marine & Freshwater Behaviour & Physiology*, **23**, 119-135.

Galis F, De Jong P (1988) Optimal foraging and ontogeny; food selection by *Haplochromis piceatus*. *Oecologia*, **75**, 175-184.

Genner MJ, Turner GF, Hawkins SJ (1999) Foraging of rocky habitat cichlid fishes in Lake Malawi: coexistence through niche partitioning? *Oecologia*, **121**, 283-292.

Godfrey LR, Sutherland MR (1995) Flawed inference: why size-based tests of heterochronic processes do not work. *Journal of Theoretical Biology*, **172**, 43-61.

Goldschmidt T, Witte F (1990) Reproductive strategies of zooplanktivorous haplochromine cichlids (Pisces) from Lake Victoria before the Nile perch boom. *Oikos*, **58**, 356-368.

Goldschmidt T, Witte F, De Visser J (1990) Ecological segregation in zooplanktivorous haplochromine species (Pisces: Cichlidae) from Lake Victoria. *Oikos*, **58**, 343-355.

Greenwood PH (1974) The cichlid fishes of Lake Victoria, East Africa: the biology and evolution of a species flock. *Bulletin of the British Museum of Natural History (Zool.)*, **6**, 1-134.

Greenwood PH (1981) *The Haplochromine Fishes of the East African Lakes*, Kraus Publications.

Hammer Ř, Harper D, Ryan P (2001) PAST: Paleontological statistics software package for education and data analysis. *Paleontologia Electronica*, **4**, 9.

Higham TE (2007a) The integration of locomotion and prey capture in vertebrates: morphology, behavior, and performance. *Integrative and Comparative Biology*, **47**, 82-95.

Higham TE (2007b) Feeding, fins, and braking maneuvers: locomotion during prey capture in centrarchid fishes. *Journal of Experimental Biology*, **210**, 107-117.

Higham T, Hulsey C, Řičan O, Carroll A (2007) Feeding with speed: prey capture evolution in cichlids. *Journal of Evolutionary Biology*, **20**, 70-78.

Holzman R, Collar DC, Day SW, Bishop KL, Wainwright PC (2008) Scaling of suction-induced flows in bluegill: morphological and kinematic predictors for the ontogeny of feeding performance. *Journal of Experimental Biology*, **211**, 2658-2668.

Hoogerhoud RJC, Witte F, Barel CDN (1983) The ecological differentiation of two closely resembling haplochromine species from Lake Victoria. *Netherlands Journal of Zoology*, **33**, 283-305.

Hood, GM (2011) PopTools version 3.2.5. <http://www.poptools.org>.

Hulsey C, Roberts R, Loh YH, Rupp M, Streelman J (2013) Lake Malawi cichlid evolution along a benthic/limnetic axis. *Ecology and Evolution*, **3**, 2262-2272.

Kassam D, Adams DC, Yamaoka K (2004) Functional significance of variation in trophic morphology within feeding microhabitat-differentiated cichlid species in Lake Malawi. *Animal Biology*, **54**, 77-90.

Katunzi EF (1983) Seasonal variation in the food of a molluscivorous cichlid *Haplochromis sauvagei* Pfeffer 1896. *Netherlands Journal of Zoology*, **33**, 337-341.

Kerschbaumer M, Sturmbauer C (2011) The utility of geometric morphometrics to elucidate pathways of cichlid fish evolution. *International Journal of Evolutionary Biology*, **2011**, 290245.

- Klingenberg CP (1998) Heterochrony and allometry: the analysis of evolutionary change in ontogeny. *Biological Reviews of the Cambridge Philosophical Society*, **73**, 79-123.
- Klingenberg CP (2011) MorphoJ: an integrated software package for geometric morphometrics. *Molecular Ecology Resources*, **11**, 353-357.
- Liem KF (1978) Modulatory multiplicity in the functional repertoire of the feeding mechanism in cichlid fishes. I. Piscivores. *Journal of Morphology*, **158**, 323-360.
- Liem KF (1991) A functional approach to the development of the head of teleosts: implications on constructional morphology and constraints. In *Constructional Morphology and Evolution*, pp. 231-249. Springer, Berlin, Heidelberg.
- Liem KF, Osse J (1975) Biological versatility, evolution, and food resource exploitation in African cichlid fishes. *American Zoologist*, **15**, 427-454.
- Mascaro J, Litton CM, Hughes RF, Uowolo A, Schnitzer SA (2013) Is logarithmic transformation necessary in allometry? Ten, one-hundred, one-thousand-times yes. *Biological Journal of the Linnean Society*, **111**, 230-233.
- Meyer A (1993) Phylogenetic relationships and evolutionary processes in East African cichlid fishes. *Trends in Ecology & Evolution*, **8**, 279-284.
- Moser HG (1981) Morphological and functional aspects of marine fish larvae. In *Marine Fish Larvae: morphology, ecology, and relation to fisheries*, pp. 89-131. University of Washington Press.
- Muller M, Osse JWM (1984) Hydrodynamics of suction feeding in fish. *Transactions of the Zoological Society of London*, **37**, 51-135.
- Osse JWM (1990) Form changes in fish larvae in relation to changing demands of function. *Netherlands Journal of Zoology*, **40**, 362-385.
- Pélabon C, Firmat C, Bolstad GH, Voje KL, Houle D, Cassara J, Rouzic AL, Hansen TF (2014) Evolution of morphological allometry. *Annals of the New York Academy of Sciences*, **1320**, 58-75.
- Rainey PB, Travisano M (1998) Adaptive radiation in a heterogeneous environment. *Nature*, **394**, 69-72.
- Rohlf F (2003) tpsSmall, version 1.20. Department of Ecology and Evolution, State University of New York at Stony Brook.
- Rohlf F (2006a) tpsDig, version 2.10. Department of Ecology and Evolution, State University of New York, Stony Brook.
- Rohlf F (2006b) tpsUtil, version 1.38. Department of Ecology and Evolution State University of New York at Stony Brook.

Ruehl CB, DeWitt TJ (2005) Trophic plasticity and fine-grained resource variation in populations of western mosquitofish. *Evolutionary Ecology Research*, **7**, 801-819.

Sage RD, Selander RK (1975) Trophic radiation through polymorphism in cichlid fishes. *Proceedings of the National Academy of Sciences*, **72**, 4669-4673.

Sanderson SL (1990) Versatility and specialization in labrid fishes: ecomorphological implications. *Oecologia*, **84**, 272-279.

Sheets HD (2003-2014) IMP8 Software Series. sheets@canisius.edu. <http://www.canisius.edu/~sheets/morphsoft.html>.

Strauss RE (1984) Allometry and functional feeding morphology in haplochromine cichlids. In *Evolution of Fish Species Flocks* (eds Echelle AA, Kornfield I), pp. 217-229. University of Maine: Orono Press.

Streelman JT, Danley PD (2003) The stages of vertebrate evolutionary radiation. *Trends in Ecology & Evolution*, **18**, 126-131.

Taborsky B (2006) The influence of juvenile and adult environments on life-history trajectories. *Proceedings of the Royal Society of London B: Biological Sciences*, **273**, 741-750.

Takeda M, Kusumi J, Mizoiri S, Aibara M, Mzighani SI, Sato T, Terai Y, Okada N, Tachida H (2013) Genetic Structure of Pelagic and Littoral Cichlid Fishes from Lake Victoria. *PLoS One*, **8**, e74088.

Van Leeuwen JL, Spoor CW (1987) Biting force in cichlids. A discussion of the planar model of Barel. *Netherlands Journal of Zoology*, **37**, 307-314.

Van Oijen M, Witte F, Witte-Maas E (1981) An introduction to ecological and taxonomic investigations on the haplochromine cichlids from the Mwanza Gulf of Lake Victoria. *Netherlands Journal of Zoology*, **31**, 149-174.

Verheyen E, Salzburger W, Snoeks J, Meyer A (2003) Origin of the superflock of cichlid fishes from Lake Victoria, East Africa. *Science*, **300**, 325-329.

Von Bertalanffy L (1957) Quantitative laws in metabolism and growth. *The Quarterly Review of Biology*, **32**, 217-231.

Wagner CE, Keller I, Wittwer S, Selz OM, Mwaiko S, Greuter L, Sivasundar A, Seehausen O (2012) Genome-wide RAD sequence data provide unprecedented resolution of species boundaries and relationships in the Lake Victoria cichlid adaptive radiation. *Molecular Ecology*, **22**, 787-798.

Wainwright PC, Ferry-Graham LA, Waltzek TB, Carroll AM, Hulsey CD, Grubich JR (2001) Evaluating the use of ram and suction during prey capture by cichlid fishes. *Journal of Experimental Biology*, **204**, 3039-3051.

- Webb PW (1982) Locomotor patterns in the evolution of actinopterygian fishes. *American Zoologist*, **22**, 329-342.
- Winemiller KO, Kelso-Winemiller LC, Brenkert AL (1995) Ecomorphological diversification and convergence in fluvial cichlid fishes. *Environmental Biology of Fishes*, **44**, 235-261.
- Witte F (1981) Initial results of the ecological survey of the haplochromine cichlid fishes from the Mwanza Gulf of Lake Victoria (Tanzania): breeding patterns, trophic and species distribution, with recommendations for commercial trawl-fishery. *Netherlands Journal of Zoology*, **31**, 175-202.
- Witte F, Barel C, Hoogerhoud R (1990) Phenotypic plasticity of anatomical structures and its ecomorphological significance. *Netherlands Journal of Zoology*, **40**, 278-298.
- Witte F, Van Oijen MJP (1990) Taxonomy, ecology and fishery of Lake Victoria haplochromine trophic groups. *Zoologischer Verhandelingen*, **262**, 1-47.
- Young KA, Snoeks J, Seehausen O (2009) Morphological diversity and the roles of contingency, chance and determinism in African cichlid radiations. *PLoS One*, **4**, e4740.
- Zelditch ML, Sheets HD, Fink WL (2000) Spatiotemporal reorganization of growth rates in the evolution of ontogeny. *Evolution*, **54**, 1363-1371.
- Zelditch ML, Swiderski DL, Sheets HD (2004) *Geometric Morphometrics for Biologists: a primer*, Elsevier Academic Press, New York.
- Zengeya TA, Marshall BE (2007) Trophic interrelationships amongst cichlid fishes in a tropical African reservoir (Lake Chivero, Zimbabwe). *Hydrobiologia*, **592**, 175-182.

SUPPLEMENTARY MATERIAL

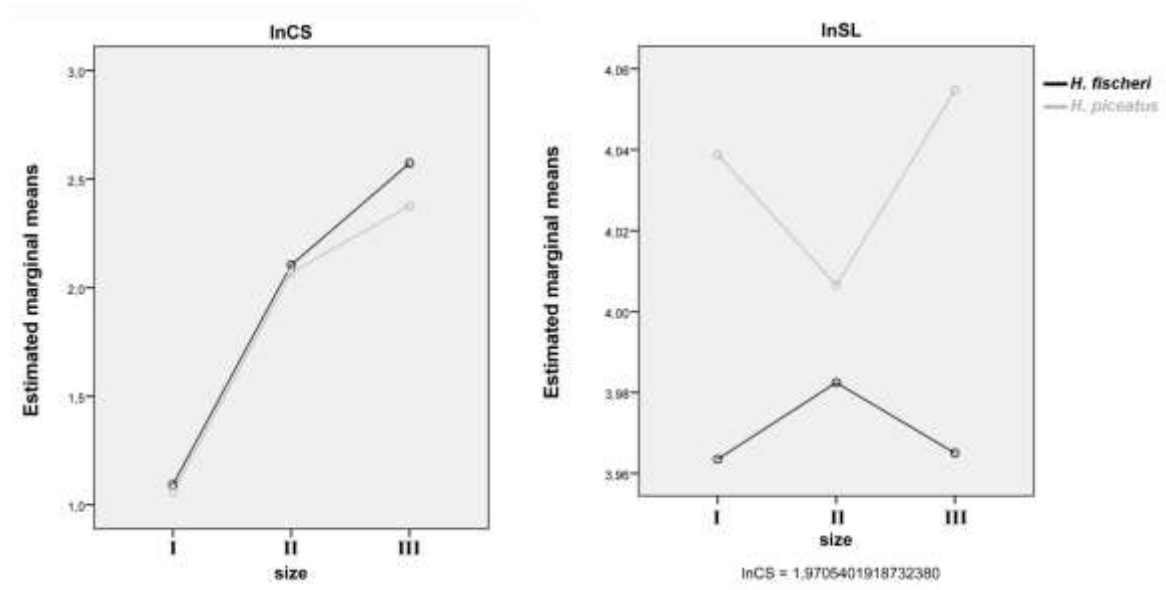


Fig. S1. Estimated marginal means of covariates (SL corrected by lnCS). The horizontal axes denote size classes and individual lines represent each species (black: *H. fischeri*, grey: *H. piceatus*). Line segments that are parallel indicate that there is no interaction between the categorical variables at that ontogenetic interval.

CHAPTER 2

Ontogenetic body shape development in a non-natural Lake Victoria haplochromine hybrid

Javier H. Santos-Santos^{1,2}, Leen Audenaert³, Erik Verheyen^{3,4}, Dominique Adriaens¹

¹ *Evolutionary Morphology of Vertebrates, Ghent University, K.L. Ledeganckstraat 35, B-9000 Gent, Belgium*

² *Integrative Biogeography and Global Change Group, Museo Nacional de Ciencias Naturales, Consejo Superior de Investigaciones Científicas (MNCN-CSIC), 28006 Madrid, Spain*

³ *Department of Vertebrates, Royal Belgian Institute of Natural Sciences, Vautierstraat 29, B-1000 Brussels, Belgium*

⁴ *Evolutionary Ecology Group, Biology Department, University of Antwerp, Belgium*

ABSTRACT

Hybridization has reiteratively been shown to prove an important mechanism in generating the raw phenotypic variation for selection to act upon in the East African cichlid adaptive radiations. However, evidence for the most part comes from studies on genetics and/or adult morphology. In the current study we track changes in external body shape in a Lake Victoria hybrid throughout its post-hatch ontogeny in relation to known parental species' trophic and locomotor morphological specializations. We observed an extensive phenotypic intermediacy of the hybrid throughout all ontogenetic size categories, albeit with the expression of several transgressive traits. Analyses of allometric shape variation and species-specific ontogenetic allometry revealed an interaction between the two morphogenetic programs that changed depending on size category. In size category III the hybrid potentially resides in an area of the allometric morphospace unoccupied by either parental. Between-group principal component analysis on body shapes across size categories revealed axes of shape variation exclusive to the hybrid in size categories I and II. We discuss our findings with a review of the recent literature concerning the hybrid origin of the Lake Victoria cichlid adaptive radiation and that of other cichlid faunas.

KEYWORDS: adaptive radiation; allometry; body shape; cichlid; functional morphology; hybridization; ontogeny; phenotypic plasticity, species-specific allometry.

INTRODUCTION

The adaptive radiations of East African cichlids have produced the most speciose vertebrate assemblages on the planet. It is assumed that cichlid fish from Lake Tanganyika migrated via intermediate riverine ancestors to the other African watersheds (Salzburger et al., 2005; Koblmüller et al., 2008; Loh et al., 2012; Schwarzer et al., 2012) [and even back again (Meyer et al., 2015)]. Colonization of the different basins by these generalist ancestors led to ecological specialization and several events of explosive speciation, being the most prominent those of Lakes Malawi and Victoria (Seehausen et al., 2003; Seehausen, 2006). The adaptive radiation in Lake Victoria gave rise to the monophyletic lineage of modern haplochromines (*i.e.* *Haplochromis*). While its phylogenetic relationships to other tribes are well resolved, recent analyses have still failed to resolve its resolution at the species level (Wagner et al., 2012; Takahashi & Sota, 2016; but see Keller et al., 2013). A main reason for this is the presence of extensive introgressive hybridization within the Cichlidae (Salzburger et al., 2002) and consequent incomplete lineage sorting (Loh et al., 2012), which is more pronounced in more recently diverged lineages. With this in mind, the Lake Victoria Region Superflock (LVRS) is estimated to have started to diversify 100-200k years ago (Verheyen et al., 2003), while the Lake Victoria adaptive radiation consisting of ~500 endemic species is believed to have originated in less than 15000 years (Stager & Johnson, 2008).

The vast range of morphological and functional diversity East African cichlids exhibit is remarkable for the estimated time of origin for each species flock (Salzburger et al., 2005; Schwarzer et al., 2012). It is highly improbable that this amount of variation could have been generated through natural selection alone within this timeframe and reiterative convergent morphologies of ecologically-equivalent species between lakes (Rüber & Adams, 2001; Albertson & Kocher, 2006; Young et al., 2009) advocates shared standing genetic variation and the retention of ancestral polymorphism (Moran & Kornfield, 1993; Meier et al., 2018). Although body shape in cichlids appears to be determined to a large extent genetically (Husemann et al., 2017), it can respond to selection immediately through plasticity within the lifetime of an individual (Bouton et al., 2002; Magalhaes et al., 2009; Schneider et al., 2014) and end up becoming an adaptation through genetic assimilation (Schneider & Meyer, 2017). Accordingly, the explosive radiation of East African cichlids is attributed in large part to polymorphism in trophic morphology and

male nuptial coloration patterns (Fryer & Iles, 1972; Sage & Selander, 1975; Seehausen et al., 2008; Salzburger, 2009; Hulsey et al., 2015), ergo, hybridization in East African cichlids appears to have facilitated rapid adaptive radiation by means of recombination and sorting of admixture-derived polymorphisms through divergent and sexual selection (Keller et al., 2013; Malinsky et al., 2015), coinciding with the ecological opportunity provided by the paleogeographic history of the African Great Lakes and Rift Valley (Seehausen, 2002; Schwarzer et al., 2012; Wagner et al., 2012).

Hybridization has been reiteratively shown to be an evolutionary mechanism promoting the generation of genetic diversity, functional novelty, and speciation in cichlids (McElroy & Kornfield, 1993; Rieseberg et al., 1999; Smith et al., 2003; Seehausen, 2004; Parnell et al., 2008; Keller et al., 2013; Meier et al., 2018). Introgression of traits involved in adaptation and reproductive isolation between closely related species/lineages in sympatry results in mosaic haplotypes that can lead to the formation of novel phenotypes in hybrid zones (Heaney & Timm, 1985; Auffrey et al., 1996; Chiba, 2005). This may result in intermediate or transgressive phenotypes due to the additive effects of morphogenetic genes (*e.g.* quantitative trait loci (QTL)) (Albertson & Kocher, 2006; Hansen & Houle, 2008). While transgressive segregation generates hybrid phenotypic traits that exceed the range observed in the parental species, functional novelty in the hybrid phenotype can also result from the many-to-one mapping of form to function (Wainwright et al., 2005; Parnell et al., 2008; Martinez & Sparks, 2017). Although the latter has proven to be a significant driver of phenotypic variation in cichlids (Barel, 1983), there are also constructional (Hulsey et al., 2007) and genetic (Albertson & Kocher, 2005) constraints on the potential structural combinations permitted in a form-function system (Young et al., 2009). All things considered, whether or not the novel hybrid morphotypes achieve an adequate fitness and survive in nature depends on various factors: *e.g.* anthropogenic (Stauffer et al., 1996; Witte et al., 2008), biomechanical (McGee et al., 2015), ecological/environmental (Robinson & Wilson, 1994), genetic (Stelkens et al., 2015), geographical (Sturmbauer et al., 2005), biological invasions (Boyer et al., 2008; Roy et al., 2015), sexual (Svensson et al., 2017), and spatial (Lowe et al., 2015).

In the current manuscript we explore the influence of hybridization on an additional aspect of cichlid evolution. Utilizing a lab-reared interspecific hybrid of two sympatric

haplochromine species from Lake Victoria with known contrasting trophic specializations [(*Haplochromis fischeri* (biter) and *Haplochromis piceatus* (sucker)) (Santos-Santos et al., 2015)], we examine body shape variation during ontogeny in relationship to trophic and locomotor specialization. Although morphological variation in external shape cannot account for function directly, significant morphological differences in external structures can serve as a proxy to define internal structures that are known to be implicated in functional systems, giving insights where future studies should focus on to understand the anatomical and functional patterns underlying the observed shape variation in overall body shape and potentially leading to the design of more precise biomechanical models for future studies (Higham et al., 2016). Since ontogenetic morphological variation has never been studied in a cichlid hybrid, our results add a novel aspect to understanding hybridization in cichlid fish.

MATERIALS & METHODS

Specimens

The material and size categories used of both parental species (*H. fischeri* and *H. piceatus*) this study are the same as for Santos-Santos et al., 2015. All hybrid specimens are viable F2 single cross hybrids originating from two nests, each obtained from *H. piceatus* females and a single *H. fischeri* male. The hybrid status of the offspring was confirmed using microsatellite markers that allowed to unambiguously distinguish specimens of both species in the breeding experiment at the Royal Belgium Institute of Natural Sciences (data not shown). A total of 35 hybrid specimens [12, 19, and 4 for size category I, II, and III, respectively], 37 specimens of *H. fischeri*, and 34 specimens of *H. piceatus* were used for this study. Species samples and that of the hybrid will be referred to as operational taxonomical units (OTU's) in the remaining text.

Data Acquisition and Shape Analysis

The acquisition of landmark data (Fig. 1), error testing, and unbending procedure for Geometric Morphometric (GMM) analysis of body shape were the same as described in Santos-Santos et al., 2015. The correlation between Procrustes distances and tangent distances between specimens was tested using TPS Small v1.34 (Rohlf, 2017). Resulting magnitudes and lengths of shape variation from GMM analysis are expressed as units of

Procrustes distance (Pd). Shape change is visualized by means of the deformation-based thin-plate spline interpolating function (Bookstein, 1991; 1996) and illustrated as wireframe grids.

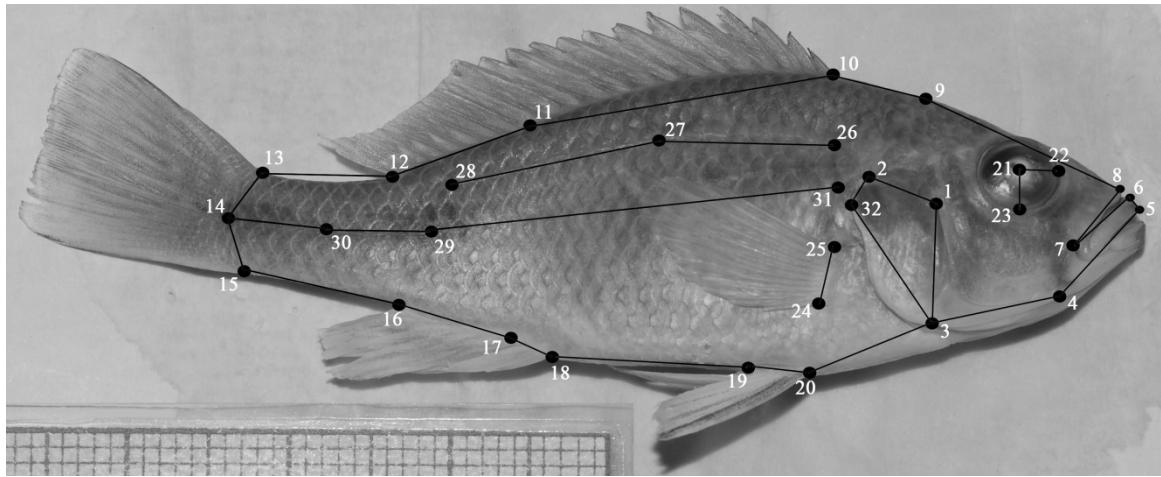


Fig. 1. Photograph of a size category III hybrid specimen illustrating digitized landmarks. Landmarks 1-25 and 32 were used to evaluate body shape; remaining landmarks were used in the unbending procedure. Detailed landmark anatomical descriptions are found in Santos-Santos et al., 2015.

First, to observe the range of shape differences between individuals we performed a Principal Component Analysis (PCA) on the three OTU sample in MorphoJ v1.06d (Klingenberg, 2011). To determine whether there were significant shape differences between grouping variables (*i.e.* OTU and size_category) we performed a full factorial Multivariate Analysis of Variance (MANOVA) on the resulting PCscores in IBM SPSS Statistics v23 (SPSS). Significance ($p < 0.05$) was determined using Wilk's λ and the effect size estimated by means of the partial eta-squared (η^2_p). Then, to determine whether or not OTU's presented differences in their allometric trajectories, a Procrustes ANOVA/Regression (Klingenberg & McIntyre, 1998) with residual randomization permutation procedures (RRPP; Collyer & Adams, 2018) was performed on shape variables using centroid size (lnCS) as the covariate, OTU as the grouping factor, and including a nested size category effect in R v3.5.1 statistical software (<https://www.R-project.org>) within the package *geomorph* v3.0.7 (Adams et al., 2018). Subsequently, the allometric vector for each OTU size category was calculated and the angles between them tested by means of a bootstrap procedure (10000 iterations) with an associated p-value in MorphoJ. Allometric rates of shape variation (Zelditch et al., 2004) were determined by calculating the Procrustes distance between the aligned specimens and the smallest configuration for each size category sample in tpsSmall v1.2 (Rohlf, 2003). A resampling

procedure with replacement was performed for each sample, and a Monte Carlo simulation (1000 iterations) performed to calculate the mean and 95% confidence intervals for the Procrustes distance travelled at each ontogenetic size category using the PopTools v3.2 (Hood, 2011) plugin in Microsoft Excel 2010. We next performed for each size category separately a Multivariate Regression of shape on size (lnCS), and a between-group PCA (bwgPCA; Mitteroecker & Bookstein, 2011) was performed on the residuals to visualize differences in OTU-specific allometric shape variation in MorphoJ. Group consensus configurations were calculated in tpsRelw v1.69 (Rohlf, 2017). Finally, to compare the dynamic differences in shape change attributes (*i.e.* path length, orientation, and quantity) between OTU's during ontogeny, we performed Phenotypic Trajectory Analysis (PTA; Adams & Collyer, 2009; Collyer & Adams, 2013) on aligned shape variables in *geomorph*. Trajectory points were determined by size categories and trajectory attributes assessed via RRPP with an associated z-score that defines the effect size (Adams & Collyer, 2016). PTA was performed on both ontogenetic and OTU-specific allometric shapes.

In addition to analyzing ontogenetic patterns of shape variation in overall body shape, we measured additional biometric variables to track their changes between OTU's during ontogeny. Standard length (SL), snout width (SW), and head width (HW) were measured with a caliper, while snout length (SnL), cheek depth (ChD), head length (HL), head height (HH), neurocranium length (NL), lower jaw length (LJ), premaxilla dentigerous arm length (PDA), gill height (GH), opercular width (OpW), interpectoral-pelvic fin distance (PcF-PvF), soft anal fin length (AF2), body height (BH), and body length (BL) were obtained from interlandmark distances in Past v2.08b (Hammer & Harper, 2001). All biometric variables were transformed to their natural logarithms before analysis. Statistical analyses follow that in Santos-Santos et al., 2015.

RESULTS

Principal Component Analysis

The first two Principal Components (PC's) explained 49% of the between-individual shape variation [35%, 14%, respectively] (Fig. 2). The MANOVA on PCscores resulted significant for OTU ($\lambda = 0.012$; $p < 0.001$; $\eta^2p = 0.89$), size category ($\lambda = 0.047$; $p < 0.001$; $\eta^2p = 0.78$), and their interaction effect ($\lambda = 0.036$; $p = 0.014$; $\eta^2p = 0.56$).

Allometry Analyses

The Procrustes ANOVA on allometric trajectories (Fig. 3) revealed non-parallel slopes in shape space ($p < 0.001$; $z = 5.4$) between OTU's ($p < 0.001$; $z = 8.3$), size categories ($p < 0.001$; $z = 4.6$), and OTU-size category groups ($p < 0.001$; $z = 4.8$). All factors covaried significantly with size ($\ln CS$; $p < 0.001$; $z = 7.9$).

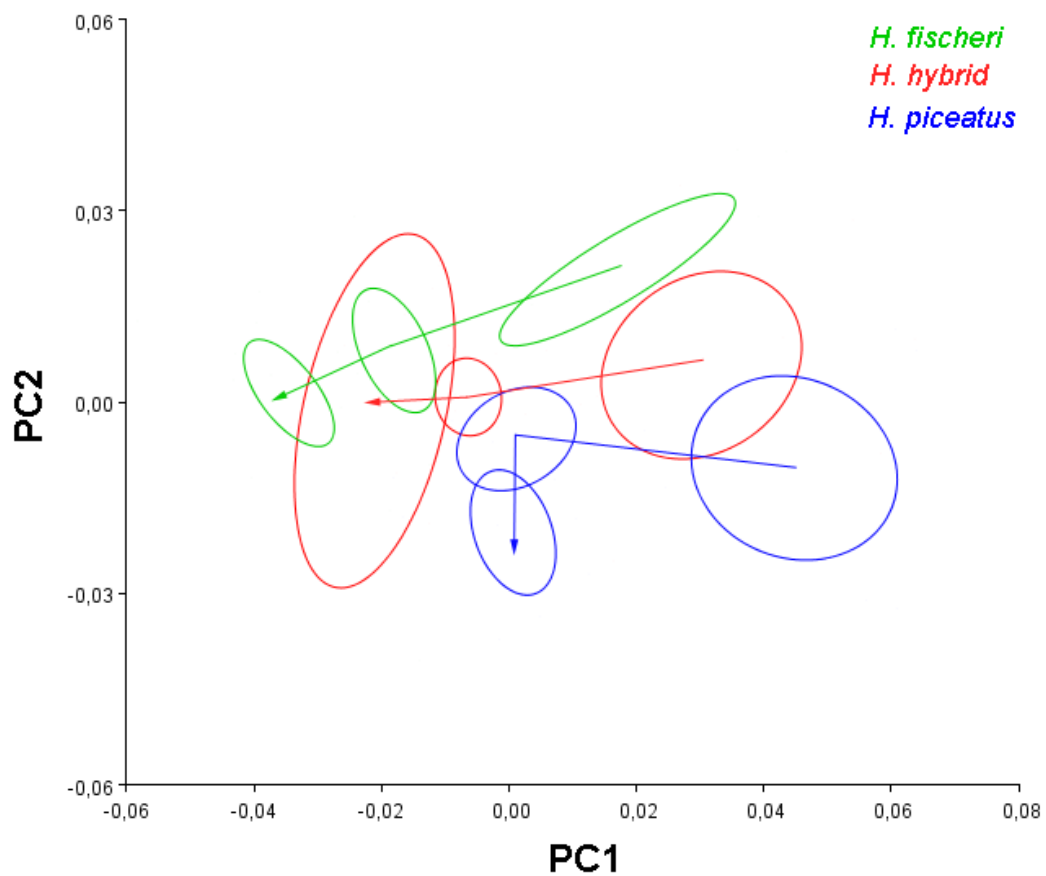


Fig. 2. Scatterplot of the first two principal components from the PCA on the three OTU sample. Confidence ellipses denote 90% mean value intervals for OTU-size category groups. Arrows point towards size category III.

Allometry accounted for 29% ($p < 0.0001$) of total shape variation in the three OTU sample. In the combined-OTU size category I, allometry accounted for 21% ($p < 0.001$) of total shape variation [$H.f.$ = 47% ($p = 0.0015$); $H.h.$ = 27% ($p < 0.001$); $H.p.$ = 26% ($p = 0.0223$)]. All OTU groups displayed significant differences in the angles between their allometric trajectories for this size category [$H.f. - H.h.$ = 39° ($p < 0.0001$); $H.p. - H.h.$ =

46° ($p < 0.0001$); $H.f. - H.p. = 62^\circ$, $p = 0.0003$]. In the combined-OTU size category II, allometry accounted for 9% ($p = 0.0004$) of total shape variation [$H.f. = 16\%$ ($p = 0.1388$); $H.h. = 15\%$ ($p = 0.0009$); $H.p. = 18\%$ ($p = 0.0309$)]. Allometric vector angles were significantly different between the hybrid and both its parental species for this size category [$H.f. - H.h. = 72^\circ$ ($p = 0.0133$); $H.p. - H.h. = 46^\circ$ ($p < 0.0001$); $H.f. - H.p. = 87^\circ$ ($p = 0.3736$)]. In the combined-OTU size category III, allometry accounted for 21% ($p < 0.0001$) of total shape variation [$H.f. = 8\%$ ($p = 0.2901$); $H.h. = 46\%$ ($p = 0.2489$); $H.p. = 6\%$ ($p = 0.6900$)]. Allometric vector angles were significantly different between the parental species for this size category [$H.f. - H.h. = 80^\circ$ ($p = 0.1202$); $H.p. - H.h. = 86^\circ$ ($p = 0.3226$); $H.f. - H.p. = 73^\circ$ ($p = 0.0227$)].

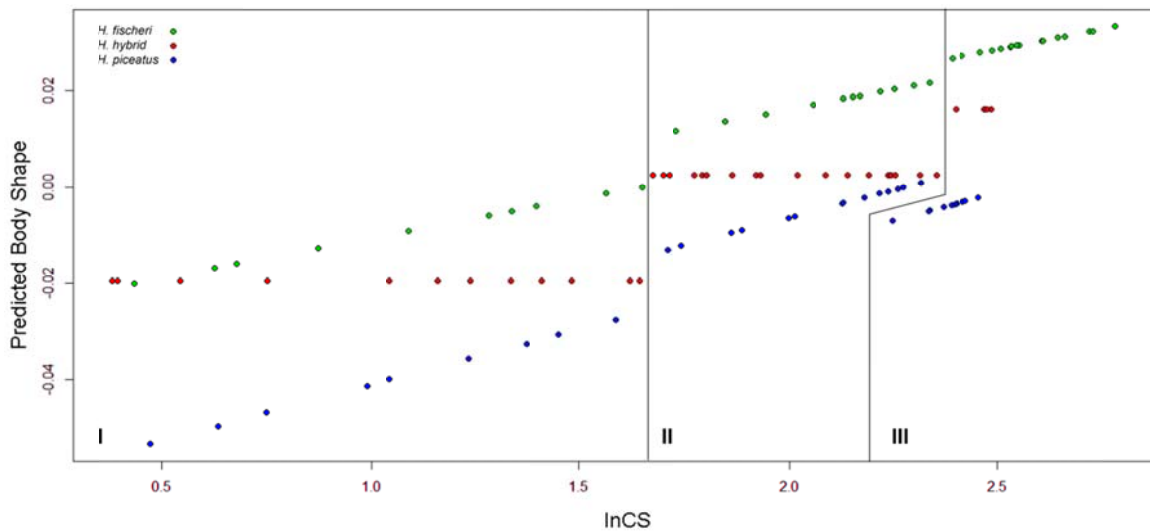


Fig. 3. Predicted values for body shape from OTU-size category-specific regressions versus lnCS.

The rates of response of shape per increment in size for each OTU and size category are shown in Table 1. Allometric rates of shape variation in size category I were similar across OTU's with *H. fischeri* displaying the steepest slope. In size category II, *H. piceatus* travelled a larger Pd from its consensus than did the hybrid, but with an inferior increase in lnCS. The hybrid travelled a shorter Procrustes distance than both parental species in size category III with *H. fischeri* displaying a considerably larger increase in SL.

Table 1. Allometric rates of shape variation for each OTU and size category.

Size category	OTU	Mean Pd	95% CI	$\Delta \ln CS$	slope	ΔSL (cm)
I	<i>H. fischeri</i>	0.0577	0.0492 – 0.0660	1.2134	0.0247	2.7
	H. hybrid	0.0623	0.0562 – 0.0678	1.2585	0.0185	2.9
	<i>H. piceatus</i>	0.0668	0.0575 – 0.0759	1.1129	0.0091	2.6
II	<i>H. fischeri</i>	0.0363	0.0309 – 0.0410	0.6034	0.0276	3.3
	H. hybrid	0.0322	0.0292 – 0.0354	0.6806	0.0107	3.7
	<i>H. piceatus</i>	0.0417	0.0378 – 0.0455	0.6071	0.0074	3.6
III	<i>H. fischeri</i>	0.0424	0.0380 – 0.0479	0.3932	0.0355	3.5
	H. hybrid	0.0297	0.0216 – 0.0375	0.0862	0.1625	0.9
	<i>H. piceatus</i>	0.0529	0.0447 – 0.0606	0.0601	0.0916	1.8

Values are given for the mean Procrustes distance (Pd) travelled within each size category; its 95% confidence intervals, its respective increment in size ($\ln CS$), the slope resulting from plotting the distance on size, and its respective increment in standard length (SL).

Size category OTU-specific Allometries

The size category I bwgPC1 (Fig. 4) explained 79% of the variance discriminating OTU's at that ontogenetic stage. Shape variation associated with the axis from negative (*H. fischeri*) to positive (*H. piceatus*) values involve *i*) a relative decrease in postcranial body length in favor of an increased head, snout, and oral jaw length, *ii*) a relative increase in snout height, *iii*) a relative caudal displacement of the pectoral and pelvic fins, *iv*) a relative increase in pelvic fin length, *v*) a relative shortening of the anal fin, *vi*) a relative lengthening and deepening of the caudal peduncle, and *vii*) a relative heightening of the body at the level of the last spinous dorsal fin ray.

The size category I bwgPC2 (21%) towards positive values (hybrid) illustrated (Fig. 5) *i*) a relatively shorter snout and more dorsally oriented gape, *ii*) a relatively extremely longer preopercular ascending arm length, *iii*) a relatively wider operculum, *iv*) a relative dorsal displacement of the pectoral fin's ventral edge, and *v*) a relatively more pronounced tapering of the postcranial body towards the caudal peduncle.

The size category II bwgPC1 (Fig. 6) explained 76% of the variance discriminating OTU's at that ontogenetic stage. Shape variation associated with this size category axis from negative (*H. fischeri*) to positive (*H. piceatus*) values involve *i*) a relative increase in the length of the snout and oral jaws, *ii*) a relative increase in gape size and height of the snout, *iii*) a relative ventral displacement of the eye, *iv*), a relative decrease in head height

and length of the ascending arm of the preopercular, *v*) a relative decrease in operculum width, *vi*) a relative posterior displacement of the pectoral fin and also dorsal of its dorsal edge, *vii*) a relative shrinkage of the body along its ventral outline, markedly at the leading edges of the pelvic and anal fins, *viii*) a relatively more rostral origin of the dorsal fin, *ix*) a relatively more rostral termination of the dorsal and anal fins, and *x*) a relatively longer caudal peduncle with a more level transition towards the anal fin and a steeper transition towards the dorsal fin.

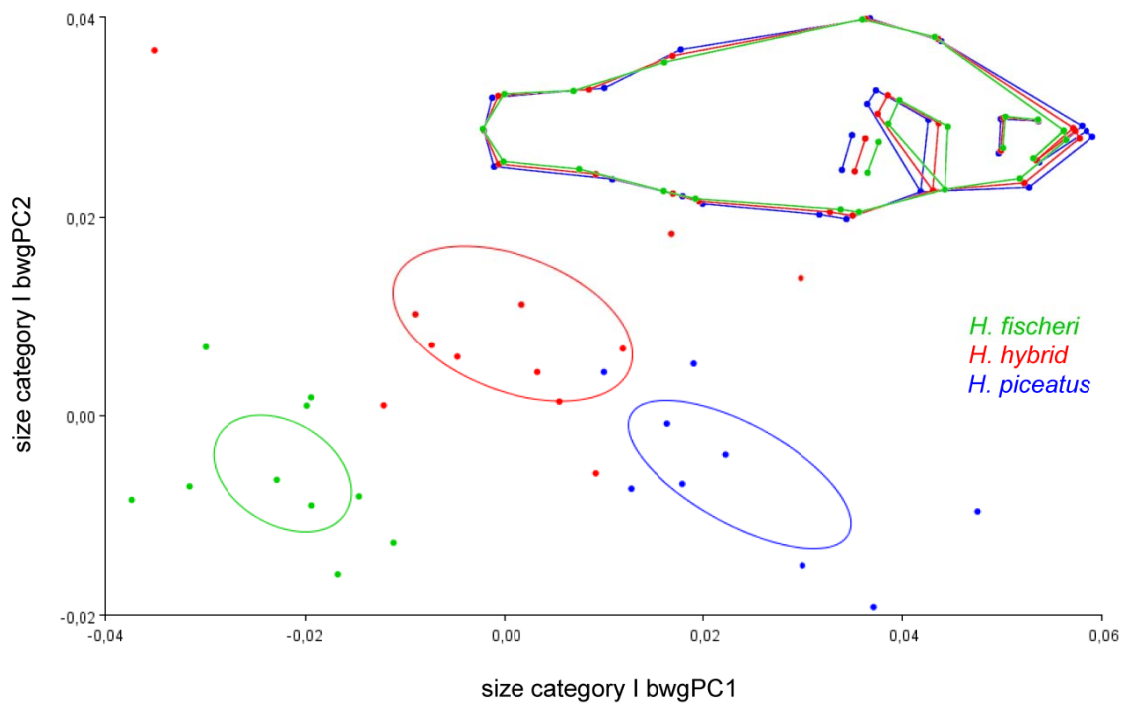


Fig. 4. Between-group Principal Component Analysis scatterplot for size category I individuals. The wireframe illustrates bwgPC1 body shape corresponding to each OTU relative from the size category I consensus. Confidence ellipses denote 90% mean value intervals for OTU groups.

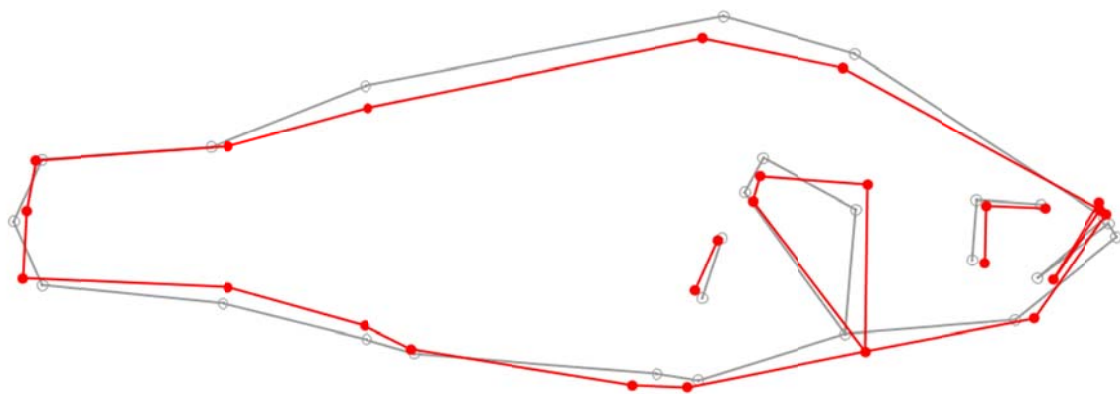


Fig. 5. Wireframe illustrating size category I bwgPC2 body shape variation. The red outline corresponds to a change in the bwgPC2 score of 0.05 from the category I consensus (grey outline).

The size category II bwgPC2 (24%) towards negative values (hybrid) illustrated (Fig. 7) *i*) a relatively smaller snout in both height and length, *ii*) a relative caudal displacement of the ventral margin of the ascending arm of the preopercular, *iii*) a relative increase in head and body height, *iv*) a relative increase in length of the pelvic fin, and *v*) a relative flattening of the body's ventral outline due to the ventral displacement of the pelvic fin's trailing edge.

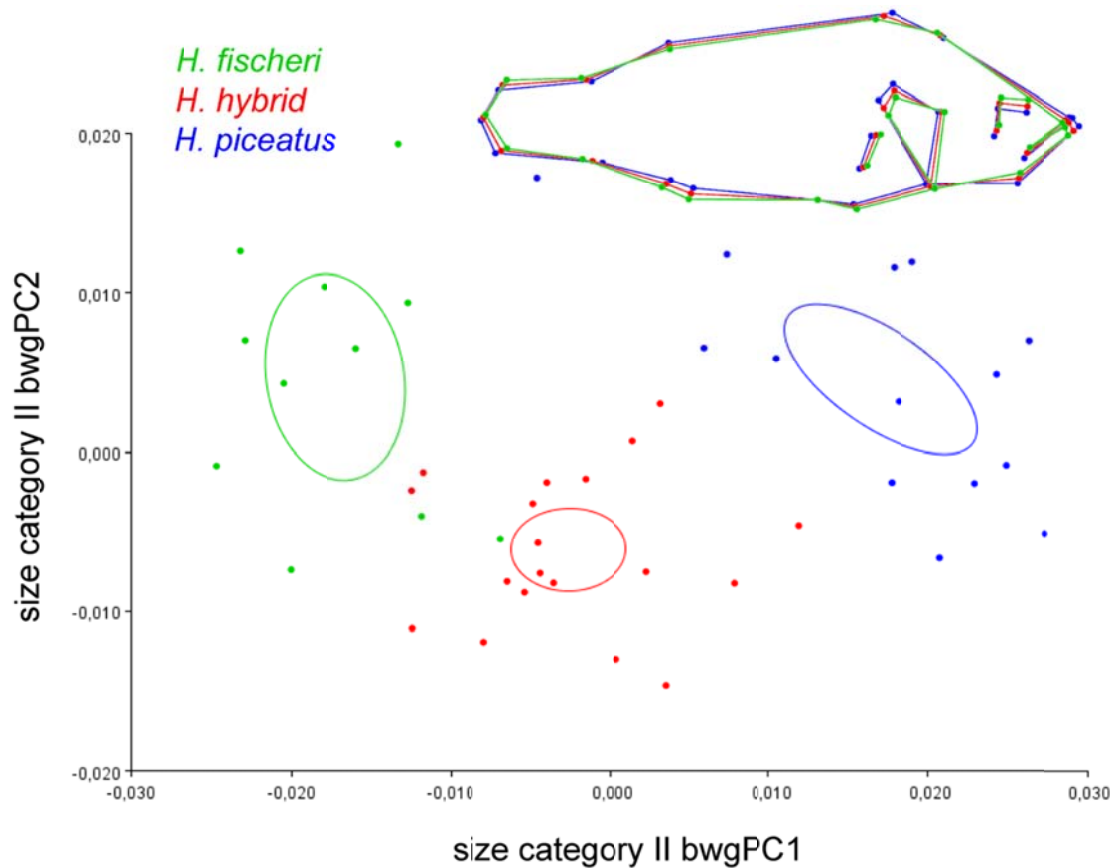


Fig. 6. Between-group Principal Component Analysis scatterplot for size category II individuals. The wireframe illustrates bwgPC1 body shape corresponding to each OTU relative from the size category II consensus. Confidence ellipses denote 90% mean value intervals for OTU groups.

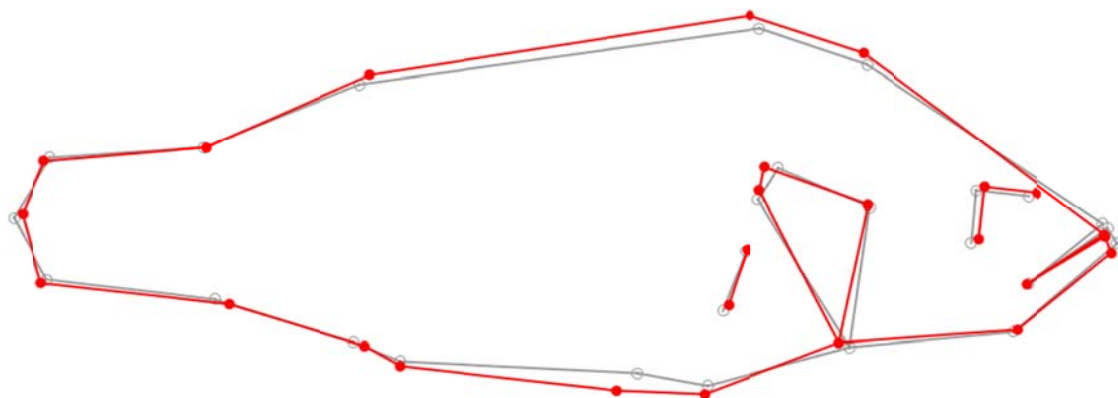


Fig. 7. Wireframe illustrating size category II bwgPC2 body shape variation. The red outline corresponds to a change in the bwgPC2 score of 0.03 from the category II consensus (grey outline).

The size category III bwgPC1 (Fig. 8) explained 59% of the variance discriminating OTU's at that ontogenetic stage. Shape changes associated with this size category axis from negative (*H. fischeri*) to positive (*H. piceatus*) values are similar to those described by size category II bwgPC1, albeit smaller in magnitude and with their own particularities: *i*) gape size does not present a relative increase in size, *ii*) relative decrease in head height and preopercular ascending arm length occur to a lesser extent, *iii*) operculum width does not decrease relatively, *iv*) the dorsal edge of the pectoral fin does not present a relative dorsal displacement, and *v*) the transition from the dorso-caudal margin of the supraoccipital crest to the leading edge of the dorsal fin becomes relatively much more steeper.

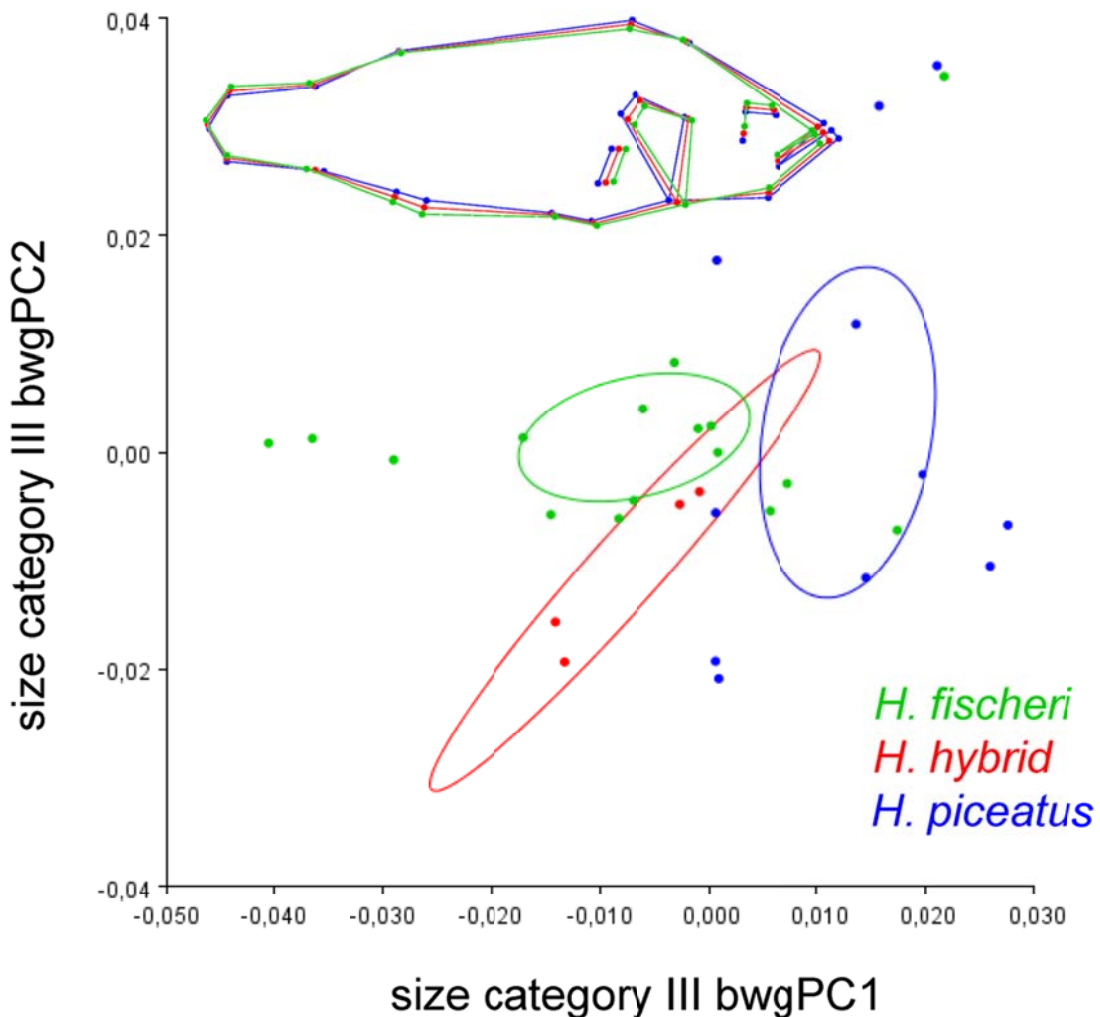


Fig. 8. Between-group Principal Component Analysis scatterplot for size category III individuals. The wireframe illustrates bwgPC1 body shape corresponding to each OTU relative from the size category III consensus. Confidence ellipses denote 90% mean value intervals for OTU groups.

Phenotypic Trajectory Analysis

All factors in the PTA on shape variables were highly significant ($p < 0.001$) in the MANOVA model; size category presented the highest z-score ($z = 8.3$) followed by OTU (6.6) and the interaction term size category*OTU (4.0). Ontogenetic shape trajectories (Fig. 9 left) revealed similar absolute path distances between OTU's [Pd *H. hybrid* = 0.0610; Pd *H. fischeri* = 0.0611; Pd *H. piceatus* = 0.0705], however the parental species displayed significantly different angles (37.5° ; $p = 0.001$) and quantities of shape variation ($\Delta Pd = 0.2792$; $p = 0.026$).

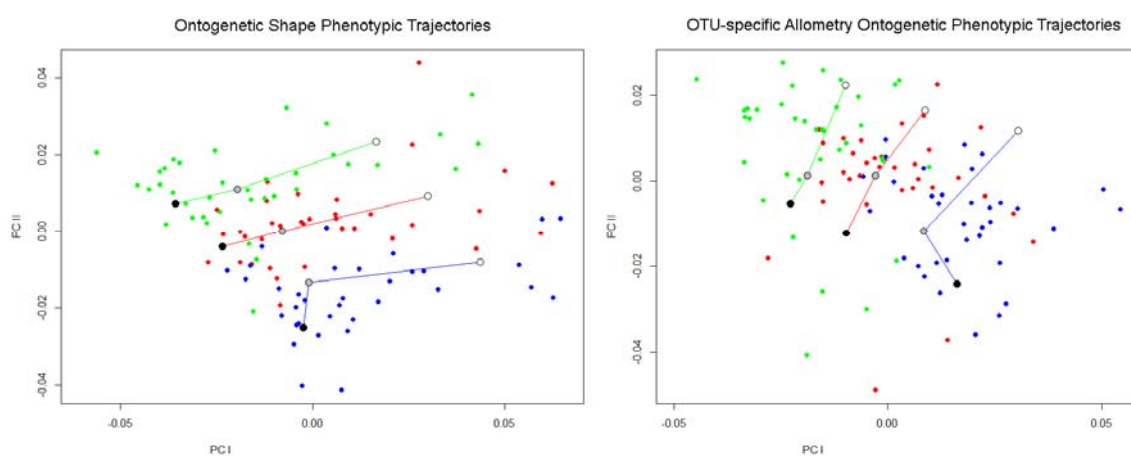


Fig. 9. Phenotypic Trajectory Analysis scatterplots for (left) ontogenetic shapes and (right) OTU- specific allometric shape. Open circle: size category I; Grey circle: size category II; Black circle: size category III.

All factors in the PTA on OTU-specific allometries were highly significant ($p < 0.001$) in the MANCOVA model; OTU presented the highest z-score ($z = 8.6$) followed by lnCS (7.9), the interaction term size category*OTU (4.9), and size category (4.8). Ontogenetic OTU-specific allometric trajectories (Fig. 9 right) revealed significant differences in absolute path distance between the parental species (Pd *H. fischeri* = 0.0413; Pd *H. piceatus* = 0.0606; $p = 0.015$) and between the hybrid and the sucker morphotype (Pd *H. hybrid* = 0.0422; $p = 0.035$), trajectory angles were again different between parental species (51.8° ; $p = 0.011$), but all OTU's displayed a similar quantity of shape variation.

DISCUSSION

Hybrid Ontogenetic Shape Development

The *Haplochromis* hybrid displayed an intermediate morphology throughout ontogeny along the main axis of each aspect of shape variation (*i.e.* ontogenetic, allometric, and

OTU-specific allometry). Our results reflect this clearly for size categories I and II, however for size category III we are aware that the hybrid sample size is relatively lower and advise caution in making conclusive inferences. In any case, at this ontogenetic size category the parental species show an increase in shape divergence proper of their morphological specializations, and our hybrid sample's shape appears to, overall, follow more closely that of the biter morphotype. In the PTA on ontogenetic shape (Fig. 9 left) the hybrid displayed a similar path distance, angle, and quantity of shape variation as either parental species; however the PTA on OTU-specific allometric shape variation (Fig. 9 right) discovered differences in path distance between the sucker morphotype and that of the hybrid and biter. Although parental species presented similar quantities of shape change in OTU-specific phenotypic trajectories, the sucker morphotype travels a larger distance during size category II and makes a change in angle at size category III, potentially indicating a metamorphic phase associated to a change in its nutrition source or trophic behavior at that life stage (Galis & De Jong, 1988; Galis, 1993; Santos-Santos et al., 2015).

Comparison of the OTU allometric trajectories (Fig. 3) for size categories I and II shows the hybrid to start out with an initial shape similar to that of the smallest biter morphotype, however it then presents an isometric growth pattern terminating at the largest shape of the sucker morphotype for each corresponding size category. At size category III however, the hybrid occupies a vacant area of the allometric morphospace since suckers alter their allometric trajectory at this size category and the trajectory of size category II hybrids differed significantly from that of both parental species. In nature this could potentially lead to an ontogenetic 'morphological release' in the hybrid, incrementing its ecological opportunity if shape variation patterns translate into differences in ecological/functional performance. Looking at Figs. 3 & S3 it appears that the hybrid will continue to occupy a vacant area of the allometric morphospace throughout its remaining ontogeny, however as we mentioned before, the hybrid size category III sample is too small to make any conclusions.

In the axes of morphospace that maximize between-individual ontogenetic variation (Fig. 2), the hybrid is located in the regions in-between parental species' size category groups. While this region appears to be more constrained at size category II, it presents an extensive area at size category I. Since these axes (*i.e.* PC1 and PC2) describe shape

changes with relevant consequences in trophic and associated locomotor function (see Santos-Santos et al., 2015); the hybrid's intermediate morphology can be expected to be able to explore the functionality of both morphotypes, and consequently may provide the hybrid in a fluctuating environment with a wider range of preadaptive phenotypes during early ontogeny. Such stochastic environmental conditions may have occurred during the Pleistocene water level fluctuations in Lake Victoria and surrounding water basins (Sturmbauer et al., 2001; Verheyen et al., 2003; Elmer et al., 2009), creating a potential situation for hybrid populations to exploit arising novel ecological niches.

The shape changes described by the axes of between-individual variation coincide to a large degree with those described by the axes of between-group variation. Size category I bwgPCA shape variation highlights increased growth of structures in an antero-posterior direction, while size category II bwgPCA shape variation highlights increased growth of structures in a dorso-ventral direction. Alternatively, size category III bwgPCA shape variation illustrates changes in the body outline to better streamline species to the locomotor needs of their position in the water column (Barel, 1983 in Santos-Santos et al., 2015). Although bwgPC1's explained most of the variation between OTU size categories (~80%), it is relevant to indicate that the hybrid diverges in shape from its parental species along bwgPC2 for size categories I and II (Figs. 4 & 5). Were this separation not so evident would make it difficult to consider shape variation along these axes biologically meaningful, however these shape differences (Figs. S1 & S2) confer the hybrid with a unique region of morphospace to exploit during these ontogenetic stages. Whether or not this potential shape variation conveys a biomechanical and/or adaptive advantage is difficult to tell from morphological description alone, but the possession of plasticity at structures relevant in trophic and locomotor function may confer opportunism in a fluctuating environment during early life stages when mortality rates are highest (Sage & Selander, 1975; Galis & De Jong, 1988).

Hybridization and Allometry

Conclusions on how hybridization has promoted adaptive phenotypic divergence have always been done comparing the species and hybrid populations at an adult life stage, during embryogenesis, or by means of comparison of mitochondrial and/or nuclear DNA sequences to elucidate their relationships (*op. cit.*). There are few studies (Watanabe et

al., 1985; Galis, 1993) that have followed the phenotypic development of a hybrid fish through its post-hatch ontogeny. In our study we observe interplay between the parental species' ontogenetic allometric and species-specific allometric morphogenetic programs, reflecting that morphogenesis in our OTU's is decoupled into distinctive modular genetic programs at each ontogenetic stage (Atchley, 1984; Santos-Santos et al., 2015; Navon et al., 2017). Initial morphological differences are magnified and held constant up to size category II by means of allometric shape change (Fig. 3), and then species diverge radically due to species-specific allometric shape development (Fig. 9 right). In addition, we observe differential significance of mean values for biometric variables before and after size correction. Evolutionary allometric trajectories are considered relatively invariant and to have low evolvability (Pélabon et al., 2014). If we consider the Lake Victoria cichlid flock to originate from a pelagic riverine ancestor (Loh et al., 2012), then it is most probable that the benthic biter morphotype is the derived condition (Franchini et al., 2014). It follows then that in the case of hybridization between both lineages, the benthic haplotype would be more conservative and be expressed more dominantly in the phenotype. This scenario fits with our results, however another scenario is possible in which the pelagic morphotype may be the more-derived condition. Since the Lake Victoria flock's ancestral population underwent several episodes of intra-generic introgressive hybridization (Keller et al., 2013), there exists the possibility that epigenetic factors activated in the derived benthic haplotype the expression of the pelagic ancestor's morphotype. In either case, we should consider *H. piceatus*' allometric trajectory to result from natural selection for functional optimization (Pélabon et al., 2014) in light of our results on allometric rates of shape change. *H. piceatus* travelled the furthest Pd in shape space, albeit with the smallest associated increase in size (Table 1). This reallocation of resources preferentially to species-specific allometry rather than to growth may be a response to reduce syntopic/sympatric resource-competition (Robinson et al., 1993). Nonetheless, ontogenetic allometry does not only result from the differential growth of body parts, but also because of the differences in the timing of their development (Meyer, 1987; Witte et al., 1990). However, we cannot make any speculations on the directionality of potential differences in ontogenetic timing (Table 2) without knowledge on the phylogenetic relationship between our species.

Table 2. Results of the GLM analyses on interlandmark distance variables.

Variable	InCS	OTU	size category	OTU*size category
SL	*	*†		*†
HW	*		*†	*†
SW	*			*†
HH	*		*	
HL	*	*		
SnL	*	*		
ChD	*			
LJ	*	*†		
PDA		*†		*†
GH		*		
BH			*†	
BL	*	*		
AF2		*		
PcF-PvF		*†		*†
OpW	*	*		

Each column represents a separate GLM model with its corresponding categorical variable(s). * Denotes a significant effect between the dependent variable and the covariate (*i.e.* centroid size)/categorical variable in each column. † Denotes the violation of the homogeneity of slopes assumption for a dependent variable in each column. [More information in Santos-Santos et al., 2015.]

Hybridization and Functional Morphology

The manifestation in the hybrid of a mosaic of parental characters and uniquely expressed traits coincides with that observed in other investigations with hybridized fish (West & Hester, 1966; Crapon de Caprona & Fritzs, 1984; Campton, 1987; Smith et al., 2003; Nolte & Sheets, 2005; Mallet, 2007). Hybrid intermediacy in phenotypic characters is consistent with an additive polygenic model of their genetic control (McElroy & Kornfield, 1993; Albertson et al., 2003); whereas transgressive phenotypic characters have been considered as evidence of genetic introgression and/or that a component of dominance or epistasis is involved in their expression (Hubbs, 1955; Valentin et al., 2002). Our F2 hybrid individuals presented an intermediate morphology along the main axes of shape variation in functionally-relevant trophic and locomotor structures, therefore we can assume that the *Haplochromis* parental species present low genetic differentiation (Stelkens & Seehausen, 2009). However, our hybrid displayed secondary axes of shape variation towards unoccupied areas of the shared morphospace and a transgressive phenotype for SW and PcF-PvF during ontogenetic size category II, and for NL in II and III (Fig. 10). The presence of transgressive phenotypic characters in an interspecific hybrid increases the phenotypic variance upon which natural selection can

work upon, potentially facilitating ecological speciation to novel selection pressures (Keller et al., 2013; Husemann et al., 2017; Kagawa & Takimoto, 2018). However, it is also known that genetic architecture limits transgression in structures that have evolved under strong directional selection, such as the cichlid lower jaw (Albertson & Kocher, 2005). Intermediate combinations of these structures may result in a less-than-intermediate performance of the hybrid relative to its parental species in functional traits (McGee et al., 2015). Nevertheless, a mosaic phenotype in the hybrid, although overall intermediate relative to its parental species, may also be the result of a relaxation between existing genetic and morphological covariance structures, consequently reducing evolutionary constraint to the production of novel combinations of phenotypic traits (Selz et al., 2014; Martinez & Sparks, 2017). In these cases, functional transgression in the hybrid can occur without the requirement of transgressive morphology (Parnell et al., 2008), and hybrid intermediacy does not necessarily result in a decrease of the hybrid's fitness (McElroy & Kornfield, 1993; Van der Sluijs et al., 2008; tkint et al., 2012).

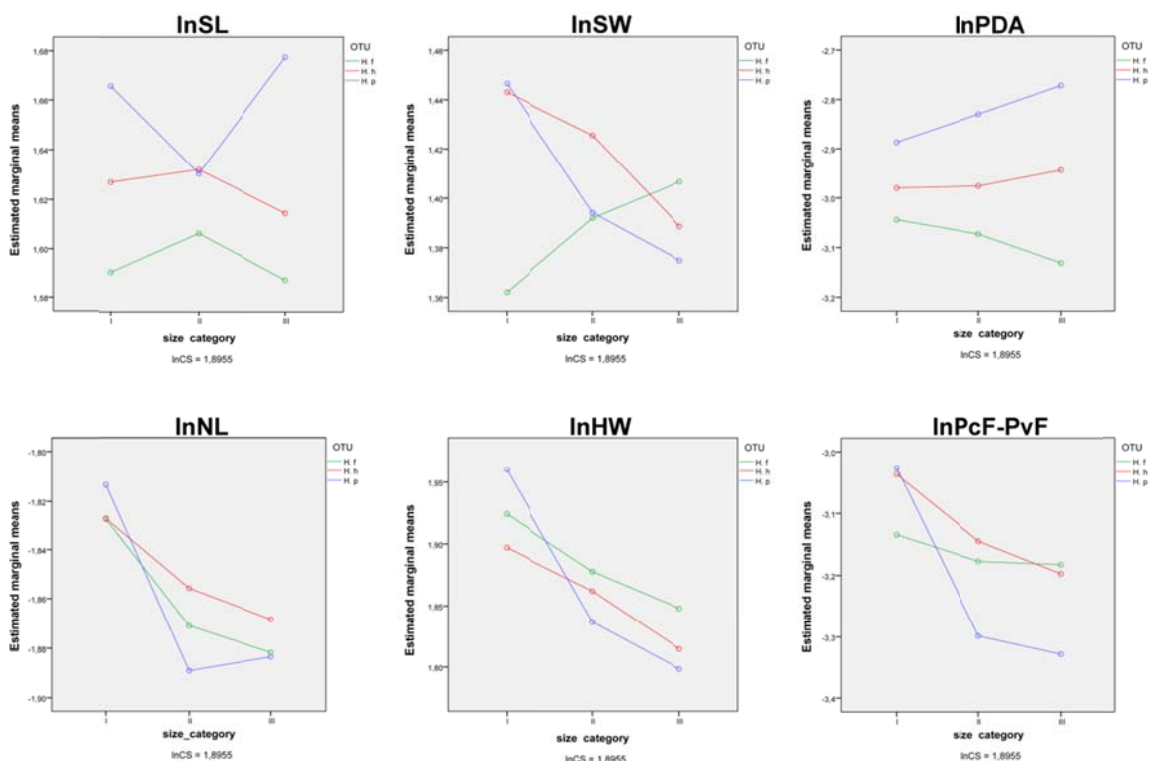


Fig. 10. Estimated marginal means of variables with a significant OTU*size category interaction effect, and, that violate the homogeneity of slopes assumption. NL was not significant, but represents a transgressive character in the hybrid. The horizontal axes denote size categories and individual lines represent each OTU (green: *H. fischeri*; red: hybrid; blue: *H. piceatus*). Line segments that are parallel indicate that there is no interaction between the categorical variables at that ontogenetic interval. Estimated marginal means were calculated at the covariable value of $\ln CS = 1.895$.

Although we do track external body shape change in our hybrid throughout ontogeny, we cannot account for potential phenotypic plastic variation because our OTU's were fed the same food regime and tank-reared in a similar environment. If the phenotypic intermediacy of our hybrid that results from a mosaic of parental features is the result of relaxed morphological covariance structures (see above), the potentiality for the hybrid to exhibit phenotypic plasticity at each ontogenetic stage must be extremely higher than either parental species (Wagner & Altenberg, 1996; Hansen & Houle, 2008). What we are observing then is a many-to-one mapping of the hybrid's phenotype producing numerous intermediate combinations that match the same functional requirements as the parental species in the rearing-tanks. However, if the hybrids occurred naturally this potential transgressive range of morphological variation could confer an adaptive advantage in a fluctuating environment due to the benefits of phenotypic plasticity for ecological opportunity (Wimberger, 1994; Skúlason & Smith, 1995; Swanson et al., 2003). That this has been the case for Lake Victoria hybrids seems plausible in view of the continuous range of variation between extreme morphotypes present in 'modern haplochromines' (Elmer et al., 2009; Keller et al., 2013). The hybrids' more extensive morphospace coverage, which includes part of its specialized parentals' ranges, and their unique combination of morphological features may provide them with a larger pool of possible phenotypes that could result in a broader functional range in feeding (Liem & Osse, 1975; Ferry-Graham et al., 2002) and/or locomotion (Webb, 1982) capacities, and consequently behaviors (Higham, 2007), potentially giving them a selective advantage over the parental species in unstable environmental conditions (McElroy & Kornfield, 1993). Later, the persistence in sympatry of incipient hybrid populations could have been favored by resource-partitioning between the different OTU's of the ecological community (Skúlason & Smith, 1995; Genner et al., 1999; Ferry-Graham et al., 2002; Kassam et al., 2003), and niche-overlap further avoided by cichlid philopatric and low dispersal behaviors, which have been seen to maintain species composition within the different microhabitats of each African lake constant (Witte, 1981).

ACKNOWLEDGEMENTS

We thank the Haplochromis Ecology Survey Team (HEST), the University of Leiden, and the Naturalis (Leiden) for supplying the stock of *H. piceatus* and *H. fischeri* specimens that was used as a starting point for our own breeding experiments and for providing the

type specimens used in this investigation. J.H.S-S. was supported by an Erasmus studies exchange grant between the University of Salamanca and the University of Ghent. Research was funded by the Research Foundation Flanders (projects 1.1.A72.10.N.00 and 3G014911), and Belgian Science Policy project MO/36/013.

REFERENCES

Adams D, Collyer ML, Kaliontzopoulou A (2018) Geomorph: software for geometric morphometric analyses. *R package version 3.0.7*, <https://cran.r-project.org/package=geomorph>.

Adams DC, Collyer ML (2009) A general framework for the analysis of phenotypic trajectories in evolutionary studies. *Evolution: International Journal of Organic Evolution*, **63**, 1143-1154.

Adams DC, Collyer ML (2016) On the comparison of the strength of morphological integration across morphometric datasets. *Evolution*, **70**, 2623-2631.

Albertson R, Kocher T (2006) Genetic and developmental basis of cichlid trophic diversity. *Heredity*, **97**, 211.

Albertson RC, Kocher TD (2005) Genetic architecture sets limits on transgressive segregation in hybrid cichlid fishes. *Evolution*, **59**, 686-690.

Albertson RC, Streelman JT, Kocher TD (2003) Genetic basis of adaptive shape differences in the cichlid head. *Journal of Heredity*, **94**, 291-301.

Atchley WR (1984) Ontogeny, timing of development, and genetic variance-covariances structure. *The American Naturalist*, **123**, 519-540.

Auffray JC, Alibert P, Latieule C, Dod B (1996) Relative warp analysis of skull shape across the hybrid zone of the house mouse (*Mus musculus*) in Denmark. *Journal of Zoology*, **240**, 441-455.

Barel C (1983) Towards a constructional morphology of cichlid fishes (Teleostei, Perciformes). *Netherlands Journal of Zoology*, **33**, 357-424.

Bookstein F (1991) *Morphometric Tools for Landmark Data. Geometry and Biology*, Cambridge University Press.

Bookstein FL (1996) Combining the tools of geometric morphometrics. In *Advances in Morphometrics* (eds Marcus L, Corti M, Loy A, Naylor G, Slice DE), pp. 131-151. New York: Plenum Press.

Bouton N, Witte F, Van Alphen JJ (2002) Experimental evidence for adaptive phenotypic plasticity in a rock-dwelling cichlid fish from Lake Victoria. *Biological Journal of the Linnean Society*, **77**, 185-192.

Boyer MC, Muhlfeld CC, Allendorf FW (2008) Rainbow trout (*Oncorhynchus mykiss*) invasion and the spread of hybridization with native westslope cutthroat trout (*Oncorhynchus clarkii lewisi*). *Canadian Journal of Fisheries and Aquatic Sciences*, **65**, 658-669.

Campton D (1987) Natural hybridization and introgression in fishes: methods of detection and interpretation. In *Population Genetics and Fishery Management* (eds Ryman N, Utter F), pp. 161-192. Seattle: University of Washington Press.

Chiba S (2005) Appearance of morphological novelty in a hybrid zone between two species of land snail. *Evolution*, **59**, 1712-1720.

Collyer ML, Adams DC (2013) Phenotypic trajectory analysis: comparison of shape change patterns in evolution and ecology. *Hystrix*, **24**, 75.

Collyer ML, Adams DC (2018) RRPP: An R package for fitting linear models to high-dimensional data using residual randomization. *Methods in Ecology and Evolution*, **9**, 1772-1779.

Crapon de Caprona M, Fritsch B (1984) Interspecific fertile hybrids of haplochromine Cichlidae (Teleostei) and their possible importance for speciation. *Netherlands Journal of Zoology*, **34**, 503-538.

Elmer KR, Reggio C, Wirth T, Verheyen E, Salzburger W, Meyer A (2009) Pleistocene desiccation in East Africa bottlenecked but did not extirpate the adaptive radiation of Lake Victoria haplochromine cichlid fishes. *Proceedings of the National Academy of Sciences*, **106**, 13404-13409.

Ferry-Graham LA, Bolnick DI, Wainwright PC (2002) Using functional morphology to examine the ecology and evolution of specialization. *Integrative and Comparative Biology*, **42**, 265-277.

Franchini P, Fruciano C, Spreitzer ML, Jones JC, Elmer KR, Henning F, Meyer A (2014) Genomic architecture of ecologically divergent body shape in a pair of sympatric crater lake cichlid fishes. *Molecular Ecology*, **23**, 1828-1845.

Fryer G, Iles T (1972) *The Cichlid Fishes of the Great Lakes of Africa: their biology and distribution*, Oliver and Boyd, Edinburgh.

Galis F (1993) Interactions between the pharyngeal jaw apparatus, feeding behaviour, and ontogeny in the cichlid fish, *Haplochromis piceatus*: a study of morphological constraints in evolutionary ecology. *Journal of Experimental Zoology*, **267**, 137-154.

Galis F, De Jong P (1988) Optimal foraging and ontogeny; food selection by *Haplochromis piceatus*. *Oecologia*, **75**, 175-184.

Genner MJ, Turner GF, Hawkins SJ (1999) Foraging of rocky habitat cichlid fishes in Lake Malawi: coexistence through niche partitioning? *Oecologia*, **121**, 283-292.

- Hammer \check{R} , Harper D, Ryan P (2001) PAST: Paleontological statistics software package for education and data analysis. *Paleontologia Electronica*, **4**, 9.
- Hansen TF, Houle D (2008) Measuring and comparing evolvability and constraint in multivariate characters. *Journal of Evolutionary Biology*, **21**, 1201-1219.
- Heaney LR, Timm RM (1985) Morphology, genetics, and ecology of pocket gophers (genus *Geomys*) in a narrow hybrid zone. *Biological Journal of the Linnean Society*, **25**, 301-317.
- Higham TE (2007) The integration of locomotion and prey capture in vertebrates: morphology, behavior, and performance. *Integrative and Comparative Biology*, **47**, 82-95.
- Higham TE, Rogers SM, Langerhans RB, Jamniczky HA, Lauder GV, Stewart WJ, Martin CH, Reznick DN (2016) Speciation through the lens of biomechanics: locomotion, prey capture and reproductive isolation. *Proceedings of the Royal Society of London B: Biological Sciences*, **283**, 20161294.
- Hubbs CL (1955) Hybridization between fish species in nature. *Systematic Zoology*, **4**, 1-20.
- Hulsey CD, García-De León FJ, Meyer A (2015) Sexual dimorphism in a trophically polymorphic cichlid fish? *Journal of Morphology*, **276**, 1448-1454.
- Hulsey CD, Mims M, Streebman J (2007) Do constructional constraints influence cichlid craniofacial diversification? *Proceedings of the Royal Society of London B: Biological Sciences*, **274**, 1867-1875.
- Husemann M, Tobler M, McCauley C, Ding B, Danley PD (2017) Body shape differences in a pair of closely related Malawi cichlids and their hybrids: Effects of genetic variation, phenotypic plasticity, and transgressive segregation. *Ecology and Evolution*, **7**, 4336-4346.
- Kagawa K, Takimoto G (2018) Hybridization can promote adaptive radiation by means of transgressive segregation. *Ecology Letters*, **21**, 264-274.
- Kassam DD, Adams DC, Hori M, Yamaoka K (2003) Morphometric analysis on ecomorphologically equivalent cichlid species from Lakes Malawi and Tanganyika. *Journal of Zoology*, **260**, 153-157.
- Keller I, Wagner C, Greuter L, Mwaiko S, Selz O, Sivasundar A, Wittwer S, Seehausen O (2013) Population genomic signatures of divergent adaptation, gene flow and hybrid speciation in the rapid radiation of Lake Victoria cichlid fishes. *Molecular Ecology*, **22**, 2848-2863.
- Klingenberg CP (2011) MorphoJ: an integrated software package for geometric morphometrics. *Molecular Ecology Resources*, **11**, 353-357.

- Klingenberg CP, McIntyre GS (1998) Geometric morphometrics of developmental instability: analyzing patterns of fluctuating asymmetry with Procrustes methods. *Evolution*, **52**, 1363-1375.
- Koblmüller S, Schliewen UK, Duftner N, Sefc KM, Katongo C, Sturmbauer C (2008) Age and spread of the haplochromine cichlid fishes in Africa. *Molecular Phylogenetics and Evolution*, **49**, 153-169.
- Liem KF, Osse J (1975) Biological versatility, evolution, and food resource exploitation in African cichlid fishes. *American Zoologist*, **15**, 427-454.
- Loh Y-HE, Bezault E, Muenzel FM, Roberts RB, Swofford R, Barluenga M, Kidd CE, Howe AE, Di Palma F, Lindblad-Toh K (2012) Origins of shared genetic variation in African cichlids. *Molecular Biology and Evolution*, **30**, 906-917.
- Lowe WH, Muhlfeld CC, Allendorf FW (2015) Spatial sorting promotes the spread of maladaptive hybridization. *Trends in Ecology & Evolution*, **30**, 456-462.
- Magalhaes I, Mwaiko S, Schneider M, Seehausen O (2009) Divergent selection and phenotypic plasticity during incipient speciation in Lake Victoria cichlid fish. *Journal of Evolutionary Biology*, **22**, 260-274.
- Malinsky M, Challis RJ, Tyers AM, Schiffels S, Terai Y, Ngatunga BP, Miska EA, Durbin R, Genner MJ, Turner GF (2015) Genomic islands of speciation separate cichlid ecomorphs in an East African crater lake. *Science*, **350**, 1493-1498.
- Mallet J (2007) Hybrid speciation. *Nature*, **446**, 279-283.
- Martinez CM, Sparks JS (2017) Malagasy cichlids differentially limit impacts of body shape evolution on oral jaw functional morphology. *Evolution*, **71**, 2219-2229.
- McElroy DM, Kornfield I (1993) Novel jaw morphology in hybrids between *Pseudotropheus zebra* and *Labeotropheus fuelleborni* (Teleostei: Cichlidae) from Lake Malawi, Africa. *Copeia*, **1993**, 933-945.
- McGee MD, Reustle JW, Oufiero CE, Wainwright PC (2015) Intermediate kinematics produce inferior feeding performance in a classic case of natural hybridization. *The American Naturalist*, **186**, 807-814.
- Meier JI, Marques DA, Wagner CE, Excoffier L, Seehausen O (2018) Genomics of parallel ecological speciation in Lake Victoria cichlids. *Molecular Biology and Evolution*, **35**, 1489-1506.
- Meyer A (1987) Phenotypic plasticity and heterochrony in *Cichlasoma managuense* (Pisces, Cichlidae) and their implications for speciation in cichlid fishes. *Evolution*, **41**, 1357-1369.
- Meyer BS, Indermaur A, Ehrensperger X, Egger B, Banyankimbona G, Snoeks J, Salzburger W (2015) Back to Tanganyika: a case of recent trans-species-flock dispersal in East African haplochromine cichlid fishes. *Royal Society open science*, **2**, 140498.

- Mitteroecker P, Bookstein F (2011) Linear discrimination, ordination, and the visualization of selection gradients in modern morphometrics. *Evolutionary Biology*, **38**, 100-114.
- Moran P, Kornfield I (1993) Retention of an ancestral polymorphism in the Mbuna species flock (Teleostei: Cichlidae) of Lake Malawi. *Molecular Biology and Evolution*, **10**, 1015-1029.
- Navon D, Olearczyk N, Albertson RC (2017) Genetic and developmental basis for fin shape variation in African cichlid fishes. *Molecular Ecology*, **26**, 291-303.
- Nolte AW, Sheets HD (2005) Shape based assignment tests suggest transgressive phenotypes in natural sculpin hybrids (Teleostei, Scorpaeniformes, Cottidae). *Frontiers in Zoology*, **2**, 11.
- Parnell NF, Hulsey CD, Streelman JT (2008) Hybridization produces novelty when the mapping of form to function is many to one. *BMC Evolutionary Biology*, **8**, 122.
- Pélabon C, Firmat C, Bolstad GH, Voje KL, Houle D, Cassara J, Rouzic AL, Hansen TF. 2014 (2014) Evolution of morphological allometry. *Annals of the New York Academy of Sciences*, **1320**, 58-75.
- Rieseberg LH, Archer MA, Wayne RK (1999) Transgressive segregation, adaptation and speciation. *Heredity*, **83**, 363-372.
- Robinson BW, Wilson DS (1994) Character release and displacement in fishes: a neglected literature. *The American Naturalist*, **144**, 596-627.
- Robinson BW, Wilson DS, Margosian AS, Lotito PT (1993) Ecological and morphological differentiation of pumpkinseed sunfish in lakes without bluegill sunfish. *Evolutionary Ecology*, **7**, 451-464.
- Roy D, Lucek K, Walter RP, Seehausen O (2015) Hybrid 'superswarm' leads to rapid divergence and establishment of populations during a biological invasion. *Molecular Ecology*, **24**, 5394-5411.
- Rüber L, Adams D (2001) Evolutionary convergence of body shape and trophic morphology in cichlids from Lake Tanganyika. *Journal of Evolutionary Biology*, **14**, 325-332.
- Sage RD, Selander RK (1975) Trophic radiation through polymorphism in cichlid fishes. *Proceedings of the National Academy of Sciences*, **72**, 4669-4673.
- Salzburger W (2009) The interaction of sexually and naturally selected traits in the adaptive radiations of cichlid fishes. *Molecular Ecology*, **18**, 169-185.
- Salzburger W, Baric S, Sturmbauer C (2002) Speciation via introgressive hybridization in East African cichlids? *Molecular Ecology*, **11**, 619-625.

Salzburger W, Mack T, Verheyen E, Meyer A (2005) Out of Tanganyika: genesis, explosive speciation, key-innovations and phylogeography of the haplochromine cichlid fishes. *BMC Evolutionary Biology*, **5**, 17.

Santos-Santos JH, Audenaert L, Verheyen E, Adriaens D (2015) Divergent ontogenies of trophic morphology in two closely related haplochromine cichlids. *Journal of Morphology*, **276**, 860-871.

Schneider RF, Li Y, Meyer A, Gunter HM (2014) Regulatory gene networks that shape the development of adaptive phenotypic plasticity in a cichlid fish. *Molecular Ecology*, **23**, 4511-4526.

Schneider RF, Meyer A (2017) How plasticity, genetic assimilation and cryptic genetic variation may contribute to adaptive radiations. *Molecular Ecology*, **26**, 330-350.

Schwarzer J, Swartz ER, Vreven E, Snoeks J, Cotterill FPD, Misof B, Schliewen UK (2012) Repeated trans-watershed hybridization among haplochromine cichlids (Cichlidae) was triggered by Neogene landscape evolution. *Proceedings of the Royal Society of London B: Biological Sciences*, **279**, 4389-4398.

Seehausen O (2002) Patterns in fish radiation are compatible with Pleistocene desiccation of Lake Victoria and 14 600 year history for its cichlid species flock. *Proceedings of the Royal Society of London B: Biological Sciences*, **269**, 491-497.

Seehausen O (2004) Hybridization and adaptive radiation. *Trends in Ecology & Evolution*, **19**, 198-207.

Seehausen O (2006) African cichlid fish: a model system in adaptive radiation research. *Proceedings of the Royal Society of London B: Biological Sciences*, **273**, 1987-1998.

Seehausen O, Koetsier E, Schneider MV, Chapman LJ, Chapman CA, Knight ME, Turner GF, van Alphen JJ, Bills R (2003) Nuclear markers reveal unexpected genetic variation and a Congolese-Nilotic origin of the Lake Victoria cichlid species flock. *Proceedings of the Royal Society of London B: Biological Sciences*, **270**, 129-137.

Seehausen O, Terai Y, Magalhaes IS, Carleton KL, Mrosso HD, Miyagi R, Van Der Sluijs I, Schneider MV, Maan ME, Tachida H (2008) Speciation through sensory drive in cichlid fish. *Nature*, **455**, 620-627.

Selz O, Lucek K, Young KA, Seehausen O (2014) Relaxed trait covariance in interspecific cichlid hybrids predicts morphological diversity in adaptive radiations. *Journal of Evolutionary Biology*, **27**, 11-24.

Skúlason S, Smith TB (1995) Resource polymorphisms in vertebrates. *Trends in Ecology & Evolution*, **10**, 366-370.

Smith PF, Konings A, Kornfield I (2003) Hybrid origin of a cichlid population in Lake Malawi: implications for genetic variation and species diversity. *Molecular Ecology*, **12**, 2497-2504.

Stager J, Johnson T (2008) The late Pleistocene desiccation of Lake Victoria and the origin of its endemic biota. *Hydrobiologia*, **596**, 5-16.

Stauffer Jr JR, Bowers NJ, Kocher TD, McKaye KR (1996) Evidence of hybridization between *Cynotilapia afra* and *Pseudotropheus zebra* (Teleostei: Cichlidae) following an intralacustrine translocation in Lake Malawi. *Copeia*, **1996**, 203-208.

Stelkens R, Seehausen O (2009) Genetic distance between species predicts novel trait expression in their hybrids. *Evolution: International Journal of Organic Evolution*, **63**, 884-897.

Stelkens RB, Schmid C, Seehausen O (2015) Hybrid breakdown in cichlid fish. *PLoS One*, **10**, e0127207.

Sturmbauer C, Baric S, Salzburger W, Rüber L, Verheyen E (2001) Lake level fluctuations synchronize genetic divergences of cichlid fishes in African lakes. *Molecular Biology and Evolution*, **18**, 144-154.

Sturmbauer C, Koblmüller S, Sefc KM, Duftner N (2005) Phylogeographic history of the genus *Tropheus*, a lineage of rock-dwelling cichlid fishes endemic to Lake Tanganyika. *Hydrobiologia*, **542**, 335-366.

Svensson O, Woodhouse K, Van Oosterhout C, Smith A, Turner GF, Seehausen O (2017) The genetics of mate preferences in hybrids between two young and sympatric Lake Victoria cichlid species. *Proc. R. Soc. B*, **284**, 20162332.

Swanson BO, Gibb AC, Marks JC, Hendrickson DA (2003) Trophic polymorphism and behavioral differences decrease intraspecific competition in a cichlid, *Herichthys minckleyi*. *Ecology*, **84**, 1441-1446.

Takahashi T, Sota T (2016) A robust phylogeny among major lineages of the East African cichlids. *Molecular Phylogenetics and Evolution*, **100**, 234-242.

Tkint T, Verheyen E, De Kegel B, Helsen P, Adriaens D (2012) Dealing with food and eggs in mouthbrooding cichlids: structural and functional trade-offs in fitness related traits. *PLoS One*, **7**, e31117.

Valentin A, Sévigny JM, Chanut JP (2002) Geometric morphometrics reveals body shape differences between sympatric redfish *Sebastes mentella*, *Sebastes fassatus* and their hybrids in the Gulf of St Lawrence. *Journal of Fish Biology*, **60**, 857-875.

Van Der Sluijs I, Van Dooren TJ, Seehausen O, Van Alphen J (2008) A test of fitness consequences of hybridization in sibling species of Lake Victoria cichlid fish. *Journal of Evolutionary Biology*, **21**, 480-491.

Verheyen E, Salzburger W, Snoeks J, Meyer A (2003) Origin of the superflock of cichlid fishes from Lake Victoria, East Africa. *Science*, **300**, 325-329.

Wagner CE, Harmon LJ, Seehausen O (2012) Ecological opportunity and sexual selection together predict adaptive radiation. *Nature*, **487**, 366-370.

- Wagner GP, Altenberg L (1996) Perspective: complex adaptations and the evolution of evolvability. *Evolution*, **50**, 967-976.
- Wainwright PC, Alfaro ME, Bolnick DI, Hulsey CD (2005) Many-to-one mapping of form to function: a general principle in organismal design? *Integrative and Comparative Biology*, **45**, 256-262.
- Watanabe WO, Kuo C-M, Huang M-C (1985) The ontogeny of salinity tolerance in the tilapia *Oreochromis aureus*, *O. niloticus*, and an *O. mossambicus* × *O. niloticus* hybrid, spawned and reared in freshwater. *Aquaculture*, **47**, 353-367.
- Webb PW (1982) Locomotor patterns in the evolution of actinopterygian fishes. *American Zoologist*, **22**, 329-342.
- West JL, Hester FE (1966) Intergeneric hybridization of centrarchids. *Transactions of the American Fisheries Society*, **95**, 280-288.
- Wimberger PH (1994) Trophic polymorphisms, plasticity, and speciation in vertebrates. In *Theory and Application of Fish Feeding Ecology* (eds Stouder D, Fresh K, Feller R). Columbia, SC: University of South Carolina Press.
- Witte F (1981) Initial results of the ecological survey of the haplochromine cichlid fishes from the Mwanza Gulf of Lake Victoria (Tanzania): breeding patterns, trophic and species distribution, with recommendations for commercial trawl-fishery. *Netherlands Journal of Zoology*, **31**, 175-202.
- Witte F, Barel C, Hoogerhoud R (1990) Phenotypic plasticity of anatomical structures and its ecomorphological significance. *Netherlands Journal of Zoology*, **40**, 278-298.
- Witte F, Welten M, Heemskerk M, van der Stap I, Ham L, Rutjes H, Wanink J (2008) Major morphological changes in a Lake Victoria cichlid fish within two decades. *Biological Journal of the Linnean Society*, **94**, 41-52.
- Young KA, Snoeks J, Seehausen O (2009) Morphological diversity and the roles of contingency, chance and determinism in African cichlid radiations. *PLoS One*, **4**, e4740.
- Zelditch ML, Swiderski DL, Sheets HD (2004) *Geometric Morphometrics for Biologists: a primer*, Elsevier Academic Press, New York.

SECTION II



Malagasy Mantellids

CHAPTER 3

Hidden in plain sight: two new species of the genus *Blommersia* from the oceanic island of Mayotte

David R. Vieites¹, Sandra Nieto Román¹, Marcos Peso Fernández¹, Javier H. Santos-Santos^{1,2}

¹ *Integrative Biogeography and Global Change Group, Museo Nacional de Ciencias Naturales, Consejo Superior de Investigaciones Científicas (MNCN-CSIC), 28006 Madrid, Spain*

² *Department of Animal Biology, University of Barcelona, Avenida Diagonal 645, 08028, Barcelona, Spain.*

ABSTRACT

We describe two new species of frogs of the genus *Blommersia* from Mayotte, a volcanic island of the Comorian archipelago in the Indian Ocean. One of the new species of *Blommersia* was known from Mayotte and is pending formal taxonomic description, but during fieldwork we found a second new species in sympatry that was completely unnoticed until now. Genetic analyses of 16S rRNA show that they are sister species that evolved in Mayotte, and that their sister taxon is *Blommersia wittei* from Northwestern Madagascar. Both species show clear morphological differences in adults and tadpoles, as well as different life histories and ecologies that suggest a case of ecological speciation within Mayotte. We propose a Red List status of Vulnerable for *Blommersia alexi* **sp. nov.** and Critically Endangered for *Blommersia nataliae* **sp. nov.**

KEYWORDS: Anura, *Blommersia alexi* **sp. nov.**, *Blommersia nataliae* **sp. nov.**, Comoros, Madagascar, Mantellidae, new species.

INTRODUCTION

The Mantellidae is a hyperdiverse family of frogs mostly endemic to Madagascar (Glaw & Vences, 2006), with few representatives known from the Comorian island of Mayotte, an oceanic island separated from Madagascar from depths of more than 3000m. So far one undescribed species of the genus *Boophis* as well as one undescribed species of the genus *Blommersia* were known from Mayotte (Vences et al., 2003). In 2003 we showed that the ancestor of those two species colonized Mayotte by oceanic dispersal from Madagascar circa 6-8 Mya (Vences et al., 2003; Crottini et al., 2012).

The genus *Blommersia* comprises ten species of frogs and constitutes a monophyletic radiation with at least five undescribed, genetically divergent lineages that may warrant species status, suggesting that the genus is likely more diverse than currently known (Vieites et al., 2009). Species in this genus are of small size and terrestrial, occurring mainly in swamps, rice fields, paddy fields and other water bodies, which could be degraded, in open lands, as well as in dry and rain forests across Madagascar. They usually call during the night, showing distinct advertisement calls that are diagnostic of each species, and some species are morphologically very similar. Like some Malagasy microhylids of the genus *Stumpffia*, which are miniaturized frogs of SVL from ca. 10mm (*Stumpffia pygmaea*) to 25mm (*Stumpffia be*), *Blommersia* species tend to miniaturization with the smallest species having snout-vent lengths (SVL) around 14-16mm (*B. kely*, *B. sarotra*, *B. domerguei*) to ca. 25mm (*B. wittei*) (Glaw & Vences, 2007). This trend towards miniaturization makes them an interesting group to study diversification patterns and speciation mechanisms related to the evolution of body size.

In this context, the known undescribed species present on Mayotte offers an interesting opportunity to study morphological and life history evolution of a species that has evolved in isolation without the presence of other congeners for the last seven to 10 million years. From few available specimens collected at the beginning of the century, it seems that this species has a bigger body size than any other *Blommersia* from Madagascar. During recent fieldwork on the Comorian island of Mayotte to collect specimens of this *Blommersia* species, we discovered a second undescribed species of much smaller body size that occurs in syntopy. This raises several questions related to the origin and evolution of these two species. First, if they are sister species or if they are the result of two independent colonizations from Madagascar. And second, if they are sister

taxa, how did the morphological and ecological diversification process take place in isolation with empty niches available and without other potential frog competitors? In this paper we formally describe and name these two new species, presenting the first data on their morphology and, so far known, life history and ecology.

MATERIALS & METHODS

Specimens of the new species were located by tracking their calls during regular searches for localizing calling males, as well as visiting different types of water bodies in Mayotte. Although one of the new species calls during the night, the other does not and no calls were ever heard in breeding places during reproduction. Specimens were euthanized using chlorobutanol, fixed in 90% ethanol, and preserved in 70% ethanol. They are deposited at the Museo Nacional de Ciencias Naturales (MNCN), Madrid, Spain.

Morphological measurements were taken by D. Vieites, using a Vernier caliper, to the nearest 0.1mm (Table 1): SVL (snout-vent length), HW (head width), HL (head length), ED (horizontal eye diameter), END (eye-nostril distance), NSD (nostril-snout tip distance), NND (nostril-nostril distance), TD (horizontal tympanum diameter), HAL (hand length), FORL (forelimb length), HIL (hindlimb length), FOL (foot length), FOTL (foot length including tarsus), TIBL (tibia length), FGL (femoral gland length), FGW (femoral gland width), FGD (minimal femoral gland distance from each other), and RHL (relative hindlimb length: point reached by the tibiotarsal articulation when the hindlimb is appressed along the body). RHL is coded as follows: when the hindlimb is appressed along body the tibiotarsal articulation reaches the (1) anterior eye corner, (2) eye center, (3) between the eye and nostril, (4) nostril, (5) snout tip, (6) between the nostril and snout tip, and (7) passes the snout tip. Calls were recorded using a digital recorder, but were lost. Measurements of the type series of *B. wittei* were taken from Vences et al. (2010) and Pabijan et al. (2011).

Tissue samples of species were taken in the field and preserved in 99% ethanol. DNA was extracted and a fragment of 489bp of the mitochondrial 16S rRNA gene was amplified using primers 16S-AL and 16S-BH (see Vences et al., 2005). PCRs were performed in 25µL reactions using ca. 50ng genomic DNA, 10pmol of each primer, 15nmol of each dNTP, 50nmol additional MgCl₂, and the Taq PCR buffer (10mm Tris-HCl, pH 8.3,

Table 1. Measurements, locality, and field number information for the type series of *Blommerisia nataliae* sp. nov. and *B. alexi* sp. nov. Acronyms as in the text.

Species	Locality	Field number	Sex	SVL	HW	HL	TD	ED	END	NSD	NND	FORL	HAL	HIL	FOTL	FOL	TIBL	FGL	FGW	FGD	RHL
<i>B. alexi</i>	Mont Choungi	DRV_6835	F	29.3	10.7	12.0	2.4	4.0	2.8	1.9	3.7	21.2	8.8	61.0	26.0	16.7	18.3	-	-	-	7
<i>B. alexi</i>	Mont Combani	DRV_6848	F	26.0	9.1	10.1	2.4	3.5	2.7	1.9	3.3	19.7	7.8	52.0	22.5	13.8	15.9	-	-	-	7
<i>B. alexi</i>	Mont Combani	DRV_6805	F	29.1	10.1	11.6	2.1	4.1	2.5	2.0	3.2	21.9	8.9	56.0	24.8	16.5	17.0	-	-	-	7
<i>B. alexi</i>	Mont Sapere	DRV_6813	F	30.4	10.8	12.7	2.8	4.3	2.9	2.0	3.6	23.3	9.9	60.0	26.4	17.7	18.8	-	-	-	7
<i>B. alexi</i>	Mont Bénara	DRV_6831	M	25.5	9.8	9.0	2.6	3.6	2.5	1.8	3.0	21.1	8.2	48.0	22.2	14.3	14.8	4.6	1.7	-	7
<i>B. alexi</i>	Mont Bénara	DRV_6832	M	25.5	8.5	9.8	2.4	3.1	2.5	1.6	2.9	19.7	8.6	50.9	22.2	13.8	15.0	4.5	1.6	1.5	7
<i>B. alexi</i>	Mont Bénara	DRV_6833	M	27.5	9.1	10.2	2.1	3.4	2.7	1.8	3.0	19.3	8.1	52.6	23.0	14.7	16.4	4.9	1.7	-	7
<i>B. alexi</i>	Mont Bénara	DRV_6841	M	24.6	8.7	11.3	2.3	3.7	2.5	2.2	3.1	19.5	8.1	48.5	20.9	14.9	14.7	4.8	1.6	1.0	7
<i>B. alexi</i>	Mont Bénara	DRV_6838	M	25.5	8.8	9.3	2.8	3.2	2.6	1.9	3.0	17.5	7.5	48.7	22.5	14.8	13.7	5.0	1.6	-	7
<i>B. alexi</i>	Mont Bénara	DRV_6836	M	26.0	9.3	9.9	2.5	3.6	2.6	1.7	3.0	17.0	7.6	45.0	22.1	13.7	14.5	5.6	1.7	1.6	7
<i>B. alexi</i>	Mont Combani	DRV_6852	M	24.5	8.4	9.7	2.1	3.4	2.2	1.4	3.0	16.4	6.4	47.0	21.1	13.4	14.5	3.8	1.5	-	7
<i>B. alexi</i>	Mont Combani	DRV_6819	M	25.0	8.4	10.3	2.7	3.4	2.2	1.7	3.2	18.4	7.4	44.1	19.9	13.0	14.4	4.4	2.0	-	7
<i>B. alexi</i>	Mont Combani	DRV_6818	M	26.0	8.8	9.4	2.4	3.5	2.8	1.7	3.0	18.9	7.8	49.0	23.6	14.5	15.3	4.6	1.7	-	7
<i>B. alexi</i>	Mont Combani	DRV_6806	M	26.5	8.7	9.2	2.2	3.7	2.6	1.9	3.3	14.5	7.8	50.6	23.0	14.5	14.5	5.7	1.8	1.0	7
<i>B. alexi</i>	Mont Combani	DRV_6849	M	27.0	9.4	12.0	2.4	3.9	2.5	2.0	3.6	18.2	8.6	46.0	22.7	15.7	15.1	4.5	1.6	1.6	7
<i>B. alexi</i>	Mont Combani	DRV_6850	M	27.0	9.4	10.2	2.4	3.4	2.5	1.9	3.4	18.0	8.3	44.0	23.9	15.7	15.6	4.8	1.6	-	7
<i>B. alexi</i>	Mont Sapere	DRV_6807	M	29.0	9.7	10.9	2.4	3.9	2.5	2.2	3.5	20.4	8.5	49.6	21.9	14.2	16.1	5.3	2.0	1.1	7
<i>B. nataliae</i>	Mont Sapere	DRV_6854	F	19.6	7.4	7.2	1.7	2.9	2.0	1.6	2.7	13.8	5.5	35.8	15.6	10.3	11.1	-	-	-	3
<i>B. nataliae</i>	Mont Sapere	DRV_6855	F	19.8	7.7	8.1	1.9	2.9	2.0	1.7	2.9	14.7	6.0	37.0	16.5	11.2	11.3	-	-	-	3
<i>B. nataliae</i>	Mont Sapere	DRV_6869	F	20.0	8.1	8.6	1.6	2.6	2.0	2.0	2.8	14.1	6.0	37.0	15.5	10.4	11.7	-	-	-	4
<i>B. nataliae</i>	Mont Sapere	DRV_6868	F	22.0	7.0	8.8	1.4	2.9	1.8	1.6	2.8	14.1	5.8	38.4	16.78	10.7	11.7	-	-	-	3
<i>B. nataliae</i>	Mont Sapere	DRV_6808	F	23.0	7.3	8.7	1.5	2.4	2.1	1.8	2.9	15.2	6.2	38.4	17.6	11.6	12.2	-	-	-	4
<i>B. nataliae</i>	Mont Sapere	DRV_6862	M	17.9	5.9	7.0	1.4	2.5	1.7	1.3	2.6	11.4	5.0	32.8	14.5	8.8	10.0	2.0	1.2	2.6	5
<i>B. nataliae</i>	Mont Sapere	DRV_6857	M	18.4	6.9	7.5	1.6	2.6	1.9	1.4	2.4	13.0	5.4	31.1	14.0	8.5	9.9	2.4	1.3	-	3
<i>B. nataliae</i>	Mont Sapere	DRV_6861	M	18.4	7.3	7.8	1.7	2.3	2.0	1.6	2.5	14.3	5.6	35.2	16.2	10.1	10.9	2.6	1.2	-	5
<i>B. nataliae</i>	Mont Sapere	DRV_6859	M	18.5	6.5	7.1	1.5	2.2	1.8	1.2	2.2	13.6	5.7	34.8	15.7	10.4	10.6	2.0	1.1	-	5
<i>B. nataliae</i>	Mont Sapere	DRV_6867	M	18.6	6.3	7.5	1.5	2.8	2.0	1.4	2.4	13.9	5.4	32.9	14.9	9.7	10.3	3.0	1.8	2.3	3
<i>B. nataliae</i>	Mont Sapere	DRV_6863	M	19.0	6.6	7.7	1.9	2.7	2.2	1.5	2.4	14.1	5.8	38.2	16.6	10.5	11.4	2.6	1.1	-	5
<i>B. nataliae</i>	Mont Sapere	DRV_6860	M	20.5	6.8	7.4	1.5	2.9	1.9	1.5	2.6	13.4	5.5	36.8	16.5	9.9	11.7	2.7	1.1	2.7	4

50mm KCl, 1.1mm MgCl₂, and 0.01% gelatin) and 1U of standard Taq DNA polymerase. PCR conditions follow Vieites et al. (2006): an initial denaturation step at 94°C for 90s; 35 cycles at 94°C for 30s, annealing temperature two degrees below T_m of each primer for 45s, extension at 72°C for 60s; final extension of 10min at 72°C. PCR products were purified using spin columns in a robot prior to cycle sequencing. A 10µL sequencing reaction included 1–2µL of template, 1µL of sequencing buffer, 2µL of 2pmol primer, 1.8µL of ABI sequence mix (BigDye Terminator version 3.1 Sequencing Standard, Applied Biosystems) and 3.2–4.2µL of water. The sequence reaction was 33 cycles of 10s at 96° C, 10s at 50 °C and 4min at 60°C. These were subsequently resolved on a 3100 ABI automated sequencer. Sequences were aligned in Geneious v. 11.1.5 (<https://geneious.com>). For phylogenetic analyses we assembled a dataset of sequences for all *Blommersia* species available in Genbank. Maximum likelihood phylogenetic analysis was performed using the program RaxML (Stamatakis, 2014) with 1000 bootstrap replicates and the GTR model. *Mantella laevigata* and *Gephyromantis liber* were used as outgroups. Newly determined sequences were submitted to Genbank (accession numbers to be added upon manuscript acceptance).

RESULTS

Molecular phylogenetics

The recovered phylogenetic relationships between *Blommersia* species are shown in Fig. 1. We recovered four main clades within *Blommersia*: one constituted by *B. angolafa*, *B. grandisonae*, and two divergent undescribed lineages; the second one constituted by *B. sarotra* and *B. kely*, with two undescribed lineages resembling *B. sarotra*; a third clade constituted by *B. galani*, *B. dejongi*, *B. blommersae*, *B. variabilis*, and two divergent lineages; and a fourth clade constituted by *B. wittei*, an undescribed species resembling *B. wittei*, and the two new species from the Comoros. These two Comorian species are monophyletic and sister taxa, and are 4.6% divergent considering uncorrected pairwise distances. *B. nataliae* **sp. nov.** shows 34 substitutions with *B. wittei* that results in an uncorrected pairwise divergence of 7 %, and there are 31 substitutions between *B. alexi* **sp. nov.** and *B. wittei* that correspond to a 6.4% uncorrected pairwise distance.

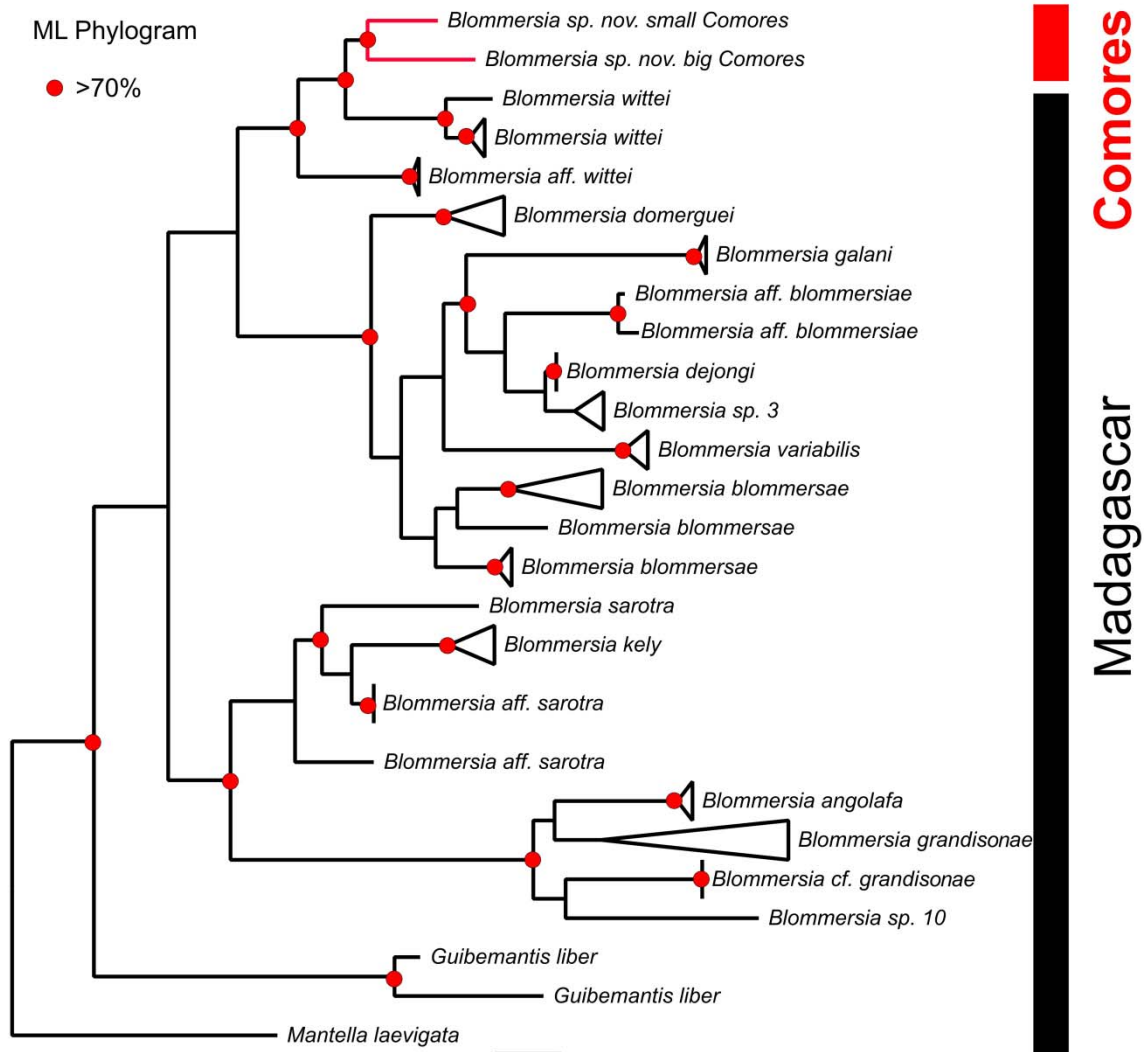


Fig. 1. Maximum Likelihood phylogram of 16S rRNA relationships within *Blommersia*. Nodes with Maximum Likelihood statistical support higher than 70% are shown in red.

Systematics

Blommersia nataliae **sp. nov.** and *B. alexi* **sp. nov.** (see descriptions below) can be distinguished from other *Blommersia* species, and between each other, by a combination of size, coloration, and several morphological traits: (1) the shape, position, and size of the femoral glands, (2) the presence or absence and shape of vomerine teeth, (3) tympanum size, (4) the extent to which lateral metatarsalia are fused or separated only by webbing and webbing formulae, (5) tongue shape, (6) relative hindlimb length, (7) tadpole morphology, and (8) size. *B. nataliae* coexists with its sister taxon *B. alexi* on the island of Mayotte and cannot be confused in the field with any Malagasy *Blommersia*.

Following an integrative taxonomic approach, morphological, genetic, life history, and biogeographic data support that *Blommersia nataliae* **sp. nov.** and *B. alexi* **sp. nov.** are true species under the evolutionary and biological species concepts. We therefore scientifically describe and name them here, providing a detailed description of adult morphology, intraspecific variation, and the first data on their life history and ecology.

***Blommersia nataliae* sp. nov.**



Fig. 2. Dorsolateral and ventral views of the *Blommersia nataliae* **sp. nov.** Holotype.

Holotype. DRV6867 (pending cataloging in the collection of the MNCN), adult male collected at the Mont Sapere, island of Mayotte, Comoros, -12.7656S, 45.1852E 500m a.s.l. in 2012 by D. Vieites and M. Peso Fernández.

Paratypes. females DRV6808, DRV6854-6855, DRV6868-6869; males DRV6857, DRV6859-DRV6863, collected at the Mont Sapere in 2012 by D. Vieites and M. Peso Fernández.

Etymology. Noun in the genitive case. D. Vieites and S. Nieto dedicate this species to their daughter Natalia Vieites Nieto, who has a birth mark resembling the beautiful conspicuous round moon-like brown spot characteristic of the species.

Diagnosis. Assigned to the genus *Blommersia* in the family Mantellidae and subfamily Mantellinae by a combination of (1) presence of femoral glands and absence of nuptial pads in males, (2) presence of intercalary elements between ultimate and penultimate phalanges of fingers and toes (verified by external examination and microCT scanning), (3) presence of a single subgular vocal sac in males, (4) small size (adult SVL < 30mm), and (5) molecular data. *B. nataliae* can be distinguished from the syntopic sister taxon *B. alexi* **sp. nov.** mainly by the shape and position of the femoral glands. In Fig. 3 we plotted the relative femoral gland length versus the relative distance between the inner edges of the femoral glands for both species and their sister taxon from Madagascar, *B. wittei*. *B. wittei* has an intermediate position between *B. nataliae* and *B. alexi* **sp. nov.**; where *B. nataliae* presents rounded and more shorter glands that are ca. two times more separated between each other than in *B. alexi* **sp. nov.** (median FGD 2.6 ± 0.2 mm vs. 1.3 ± 0.3 mm, respectively) and ca. half shorter (median FGL 2.6 ± 0.4 mm vs. 4.8 ± 0.5 mm) (see also Figs. 2 & 4). *B. nataliae* also differs from *B. alexi* **sp. nov.** in having inconspicuous vomerine teeth versus well developed and showing a V shape in *B. alexi* **sp. nov.**; the tongue is ovoid and not bifid, while in *B. alexi* **sp. nov.** and *B. wittei* it is bifid; the tympanum diameter is two thirds the size of the tympanum of *B. alexi* **sp. nov.** in both males and females, but of the same size as *B. wittei*. The hindlimbs are shorter than in *B. alexi* **sp. nov.** and the tibiotarsal articulation reaches between the eye and the nostril, while in *B. alexi* **sp. nov.** it passes well the snout tip when appressed along the body and in *B. wittei* it reaches the anterior eye corner. The inner metatarsal

tubercle is less distinct than in *B. alexi* **sp. nov.** or *B. wittei*, and the webbing formulae are different between the three species. The three species are differentiated from other *Blommersia* by having separated metatarsalia and presence vs. absence of vomerine teeth (except for *B. dejongi* and *B. variabilis* that also have vomerine teeth). The tadpole of *B. nataliae* shows a completely different morphology than any other *Blommersia* tadpole, but it will be described in detail elsewhere. The genetic data support that the new species is furthermore differentiated from all other species of *Blommersia* by a significant molecular genetic differentiation.

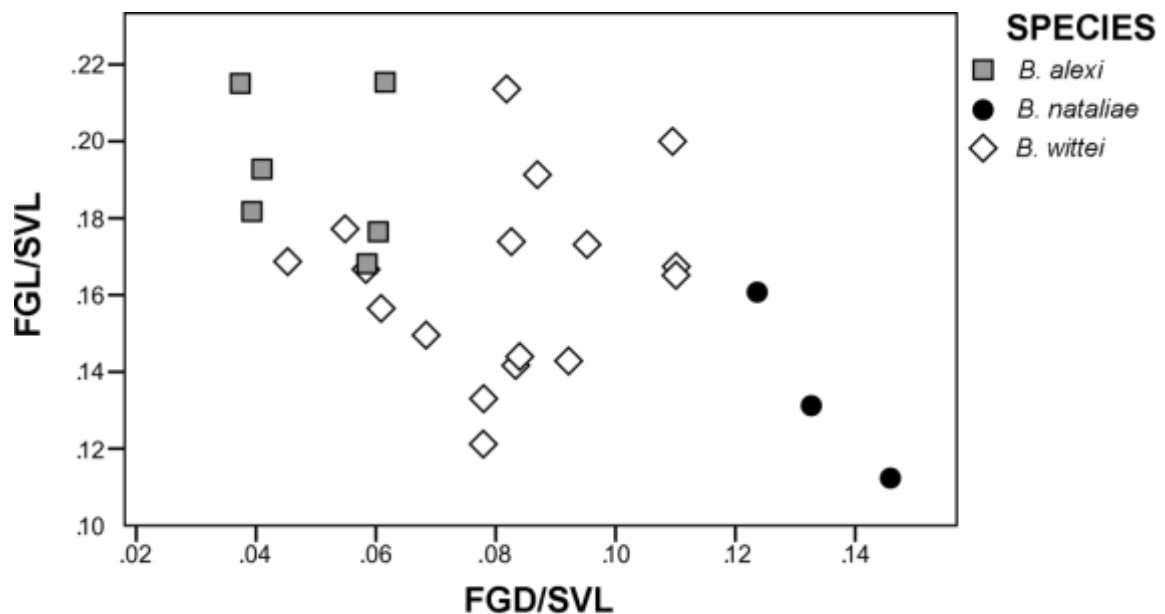


Fig. 3. Scatterplot of relative femoral gland length (FGL/SVL ratio) and relative distance between the inner edges of the femoral glands (FGD/SVL) in the two new species from Mayotte and their sister taxon *B. wittei* from Madagascar. Measurements are based on Table 1; and for *B. wittei* on Vences et al. (2010) and Pabijan et al. (2011). Note the intermediate position of *B. wittei* between *B. alexi* **sp. nov.** and *B. nataliae* **sp. nov.**

Description of the Holotype. Male specimen in good state of preservation. Part of left thigh lacking taken for genetic analyses. SVL = 18.6mm. The body is slender; the head is slightly longer than wide, but not wider than the body. Snout slightly pointed and rounded in lateral views with protuberant nostrils directed laterally, nearer to tip of snout than to eye; canthus rostralis indistinct and straight; loreal region straight; tympanum distinct and rounded; supratympanic fold present and slightly distinct behind the tympanum, but indistinct in its anterior part between the eye and the tympanum; tongue slender and ovoid, slightly notched posteriorly but not bifid; vomerine teeth present but very

inconspicuous and very small, hard to see, and not grouped or forming a particular shape; maxillary teeth rudimentary; choanae rounded. The arms are slender with distinct, single subarticular tubercles, the inner and outer metacarpal tubercles distinct, the fingers without webbing, and the relative length of the fingers is $1 < 2 < 4 < 3$ with the second finger shorter than the fourth one; terminal finger discs are enlarged and nuptial pads absent. Hindlimbs are relatively robust; the tibiotarsal articulation reaches between the eye and the nostril when the hindlimb is appressed along the body; the lateral metatarsalia are separated; the inner metatarsal tubercle is small and the outer distinct; toe discs are enlarged and the webbing between toes weakly developed [1(1), 2i(1.75), 2e(1), 3i(2.5), 3e(2), 4i/e(3), 5(1.5)]. The skin on the dorsal surface is smooth without folds or ridges. The ventral skin is uniformly smooth. Femoral glands are very distinct in life, as well as after ethanol preservation, in their external view.

Coloration of the Holotype. In life the overall color is creamy light brown with golden spots on the flanks, arms, and legs. It shows a thin yellowish line from the midpoint between the eyes to the vent. The legs are slightly darker brown and bands are visible. It shows a dark brown spot on the flanks and a characteristic larger moon-like spot on the back of each flank close to the pelvic region and the hindlimbs. It presents a facial mask from the snout, under the loreal region, to the tympanum. The loreal region, as well as the outer iris periphery, shows a thin golden-colored line. The pupil is black and the inner iris area dark brown, while the outer iris area is golden with dark reticulations. The throat is brownish. The belly is light brown with some whitish, silver, and gold spots. The femoral glands are oval in shape with a yellowish coloration and 9-10 circular internal rounded structures. After two years in preservative the back shows a creamy brown coloration that gets lighter towards the sides of the body, but the golden spots and dorsal line are lost. Ventral coloration is light brown without evident golden spots. The moon-like brown spot in the posterior part of the flanks is still evident, as well as the small ones on the flanks behind the arms. The femoral glands are whitish.

Variation. The measurements of the Holotype and paratypes are provided in Table 1. Sexual dimorphism is apparent in several characters: males present distinctive femoral glands, females are larger than males [males: median \pm SD SVL= 18.5 \pm 0.8mm (min-max=17.9-20.5); females: 20 \pm 1.5mm (min-max=19.6-23mm)]. The color pattern is rather

homogeneous, but females show an overall much creamier coloration than males, which are slightly darker. Both males and females show the characteristic brown rounded moon-like spot on the posterior flanks of the body, as well as some blotches on the lateral body sides behind the arms of variable size and shape. Vomerine teeth are more evident in specimen DRV6854, but only on one side of the vomer, and in DRV6855 and DRV6808 on both sides and more evident than in the Holotype. Female DRV6855 lacks the mole-like blotch in the posterior side of the body, but shows a large circular one behind the arms. Female DRV6808 shows a similar pattern, but with a smaller blotch. Female DRV6868 shows a constellation of small rounded to irregular dark blotches from behind the arms to the inguinal region.

Natural history. The species was found on the ground and in its breeding places: bamboo cut trunks filled with water. There, several males wait for the females to reproduce at night. No frogs were seen in the breeding places during the day. No call was ever heard during reproductive periods despite several attempts and leaving for two hours a digital recorder running at a breeding spot. The clutches are placed on the walls of the bamboo, but few eggs are fertilized. Females seem to deposit several unfertilized eggs in the water that can serve as food for the tadpoles. The tadpoles are white, semitransparent in the belly, and with an unique head morphology. They will be carefully studied and described elsewhere when more material is available. Few individuals can be seen during the day on the ground. No frogs were ever seen in other microhabitats like swamps, ponds, streams, or similar water bodies.

Distribution. Originally found in the slopes of Mont Sapere only where there is still forest present and big bamboo forests. In a 2015 expedition we also found it at Mont Bénara in forested places where there is less bamboo available, but we found several specimens. After several trips and visits around the whole main island of Mayotte we have not found it anywhere else and the habitat appears to be degraded for the species.

Conservation. The new species is only known from two localities and seems to be restricted to mountain areas where forest is still present, and bamboo. The area of occupancy is estimated to be less than 10km². There are bamboos also at lower elevations in degraded forests, but we never detected the species there. The distribution range is

extremely small, the habitat is increasingly degraded, the breeding places (bamboo broken trunks) not frequent, and the fact that the observed densities seem to be very low, suggest to consider the species as Critically Endangered in need of urgent conservation actions considering the ongoing degradation of forest habitats.

***Blommersia alexi* sp. nov.**



Fig. 4. Dorsolateral and ventral views of the *Blommersia alexi* sp. nov. Holotype.

Holotype. DRV6807 (to be catalogued in the collection of the MNCN), adult male collected at Mont Sapere in 2012 by D. Vieites and M. Peso Fernández.

Paratypes. females DRV6835 collected at Mont Choungi, DRV6805 and DRV6848 collected at Mont Combani, and DRV6813 collected at Mont Sapere; males DRV6831-6833, DRV6836, and DRV6838 collected at Mont Bénara, DRV6806, DRV6818-6819, DRV6849-6850, and DRV6852 collected at Mont Combani, and DRV6807 collected at Mont Sapere by D. Vieites and M. Peso Fernández.

Etymology. Noun in the genitive case. D. Vieites and S. Nieto dedicate this species to their son Alejandro (“Alex”) Vieites Nieto, for his dedication, enthusiasm, and help during fieldwork.

Diagnosis. Assigned to the genus *Blommersia* in the family Mantellidae and subfamily Mantellinae by a combination of (1) presence of femoral glands and absence of nuptial pads in males, (2) presence of intercalary elements between ultimate and penultimate phalanges of fingers and toes (verified by external examination and microCT scanning), (3) presence of a single subgular vocal sac in males, (4) small size (adult SVL < 30mm), and (5) molecular data. The differences with its sister taxon *B. nataliae* and with *B. wittei* are provided in the diagnosis section of *B. nataliae* above. The tadpole of *B. alexi* shows the typical tadpole morphology of a *Blommersia* tadpole and will be described elsewhere. The genetic data support that the new species is furthermore differentiated from all other species of *Blommersia* by a significant molecular genetic differentiation.

Description of the Holotype. Male specimen in good state of preservation. Part of left thigh lacking taken for genetic analyses. SVL = 29mm. The body is slender and the head is slightly longer than wide, but not wider than the body. The snout is pointed and rounded in lateral views with protuberant nostrils directed laterally, nearer to the tip of snout than to the eye; canthus rostralis indistinct and straight; loreal region straight; tympanum distinct and rounded; supratympanic fold present and slightly distinct behind the tympanum, but indistinct in its anterior part between the eye and the tympanum;

tongue ovoid and wide, clearly notched and bifid posteriorly with two evident separated rounded tissue elongations at the inner part of the tongue; vomerine teeth present and very distinct, grouped in two separated patches forming a V shape; maxillary teeth rudimentary; choanae rounded. The arms are slender with distinct, single subarticular tubercles; the inner metacarpal tubercles are distinct, the outer one present but less distinct; fingers are without webbing; relative length of the fingers is $1 < 2 < 4 < 3$, with the second finger shorter than the fourth one; terminal finger discs enlarged and nuptial pads absent. The hindlimbs are relatively robust; the tibiotarsal articulation passes the snout tip when the hindlimb is appressed along the body; lateral metatarsalia are separated; inner and outer metatarsal tubercles are distinct; toe discs are enlarged; webbing between the toes is weakly developed [1(1), 2i(1.75), 2e(0.75), 3i(2), 3e(1), 4i(2.3), 4e(2), 5(0.5)]. The skin on the dorsal surface is smooth without folds or ridges. The ventral skin is uniformly smooth. Femoral glands are very distinct in life, as well as after ethanol preservation, in their external view.

Coloration of the Holotype. In life the overall color is brown with darker brown areas on the back, flanks, arms, and legs. It shows a thin yellowish line from the midpoint between the eyes to the vent. In the legs and arms it presents darker brown bands. It presents a facial mask from the snout, under the loreal region, to the tympanum, but below the eye it is broken showing a light brownish coloration. The loreal region, as well as the outer iris periphery, shows a thin golden-colored line. The pupil is black and the inner iris area light brown, while the outer iris area is plain light golden. It presents an inverted V shaped mark behind the eyes of a slightly darker coloration than the back, as well as a darker bar between the eyes. The throat is brownish with some whitish spots below the lower mandible. The belly is light brown with some yellow-golden notches and a black central thin line. The femoral glands are elongated in shape with a dull yellowish coloration, being evident but not very distinct. After two years in preservative the back shows a dark brown coloration that gets lighter towards the sides of the body. Ventral coloration is light brown being the black thin line recognizable. The darker bars in legs and arms are distinguishable as well as the inverted V shape pattern behind the head, the dark bar between the eyes, and the dark facial mask.

Variation. The measurements of the paratypes are provided in Table 1. Sexual dimorphism is apparent in several characters: males present femoral glands, females are larger than males [males: median±SD SVL= 26±1.3mm (min-max=24.5-29mm); females: 29.2±0.8mm (min-max=26-30.4mm)]. Limbs are proportionally larger in females with FORL mean = 21.5mm [min-max=19.7-23.3mm] versus 18.4±1.8mm [min-max=14.5-21.1mm] and HIL mean 58.0±4.1mm [min-max=52-61mm] versus 48.2±13.5mm [min-max=44-52.6mm]. Some specimens show a dorsal white stripe and a well-defined band that goes from the tip of the snout to the vent (DRV6865). The color pattern is rather homogeneous, but females show a darker coloration than males. In preservative males tend to lose coloration, becoming dull light brown, whereas females retain a darker brown coloration in leg bands.

Natural history. It is present in the typical habitats for *Blommersia*: swamps, ponds, little brooks, roadside channels, and even water deposits, fountains or buckets, occurring in both forest habitats as well as in very degraded areas. Males are very active, calling at night everywhere. The breeding season can extend throughout the year as long as there is rain, as we observed clutches in spring and winter, although the main reproductive activity coincides with the rainy season. The males are very active in the breeding grounds, calling from leaves, shrubs, low branches of trees or rocks, sometimes with a frenetic activity. They were found calling in fountains of hotels during the night. They lay the clutches hanging above waterbodies as other mantellines, from where the tadpoles fall down into the water. Adults and juveniles are easily found during the day in forest leaf litter, road ditches, and sides of footpaths where the species is present.

Distribution. The species is common in the Northern side of the island, but less common in the Southern peninsula which is much drier and of lower elevation. It seems that it is rarer in lowlands, being very rare near the sea in most of the island, but common at higher elevations.

Conservation. The new species is only known from Mayotte where it is common and occupies degraded habitats as other *Blommersia* in Madagascar. The area of occupancy is less than 100km². Although the species could survive in degraded habitats, their primary habitat in the mountains is being degraded, which together with its small distribution

range suggests that the species can be listed as Vulnerable. The introduction of the chytrid fungus in Mayotte could decimate this species as well as *B. nataliae* in few years.

DISCUSSION

The Mantellidae was considered to be an endemic family of frogs to Madagascar where it is highly diverse with 223 species described so far. The presence of two species in Mayotte, a *Boophis* and a former *Mantidactylus* (now *Blommersia*) was known for a relatively long time, but these were considered recent introductions by humans. A 2003 work showed, however, that these represent different genetic lineages from Malagasy taxa (Vences et al. 2003), suggesting two independent oceanic colonizations of Mayotte by oceanic dispersal. Nobody was aware until now of the presence of a third species of mantellid on Mayotte, which raises interesting questions about their origin and evolution in isolation from the rest of congeners in Madagascar.

Oceanic islands offer unique opportunities to study the evolution of ecological and morphological characters as new colonizers can have few competitors and empty niches to exploit. In many cases, this leads to island radiations that show a wide range of ecological and morphological adaptations in small territories (*e.g.* Freed et al., 1987). There are not many cases of amphibian colonization of oceanic islands, being remarkable the case of the Guinean Gulf Islands where anurans and a caecilian were able to colonize from Africa (Measey et al., 2007; Bell et al., 2015a; 2015b), and the case of Mayotte. The existence of two species of *Blommersia* frogs in Mayotte that are sister taxa and evolved in complete isolation from other *Blommersia* species offers an unique model system and opportunity to study the process of speciation from different perspectives, including the genetic, morphological, and ecological ones.

From the external morphological point of view, and comparing with their sister taxon *B. wittei* from Madagascar, *B. nataliae* and *B. alexi* diverged in opposite directions. *B. wittei* shows intermediate measurements between the two in most characters, being a typical small *Blommersia* species. *B. alexi* has suffered a process of increase in body size, being the largest *Blommersia* species known so far. The overall aspect of *B. alexi* resembles more other Mantellinae genera from Madagascar than a typical *Blommersia*, being bigger, more robust, and darker in coloration with proportionally longer and more robust legs. *B.*

nataliae, on the contrary, has suffered a process towards miniaturization from their shared common ancestor, similar to other *Blommersia* species from Madagascar. We hypothesize that the ancestor of both species arrived to Mayotte and populations started to exploit empty ecological niches, as they do not compete with the undescribed *Boophis* present on the island. In the ecological component, divergence happened in the selection of breeding habitats, with *B. alexi* retaining the same ecology as *B. wittei*, but *B. nataliae* specializing to reproduce in bamboo trunks filled with water and maybe other cavities, leading to a specialized tadpole. Adaptation to different environments is also known from *Blommersia angolafa*, which is phytotelmic and reproduces in the water accumulated in fallen leaves (Andreone et al. 2010).

The different events of ecological release in Comorian species lead to their morphological divergence with an adult morphological pattern in *B. nataliae* that resembles other *Blommersia* from Madagascar that evolved towards miniaturization, whereas *B. alexi* seems to be undergoing a process of “gigantism”, occupying the morphological space of other genera present in Madagascar. This offers an unique opportunity to explore the mechanisms of their morphological evolution in isolation.

We have followed an integrative taxonomic approach by incorporating morphological, genetic, and life history data, which supports the species status of these two new taxa. The observed genetic divergence between them is above the values observed between other mantellid sister species (Vences et al., 2005; Vieites et al., 2009) and the morphological differences large. Both species have evolved in isolation and occur on a small island, being the actual range of *B. nataliae* very small. This, united to its particular breeding ecology and requirements for reproduction, the lack suitable areas for reproduction, and its apparent low density and small population size, suggest that this species is threatened. We propose a category of Critically Endangered following IUCN criteria, and predict that the species can disappear in parallel to the degradation of its environment if its remaining pockets of habitat are not well managed. *B. alexi* shows a different conservation situation since it can profit from degraded habitats, but it is more common in mountains and forested habitats. Consequently, the degradation its preferred environments can decrease its populations. The introduction of the chytrid fungus, which so far has not been reported on Mayotte, can easily lead the three amphibian species known on the island to extinction.

ACKNOWLEDGEMENTS

We are grateful to Nina Bernard and Isaac Pozo for their help in the field, and to M. Vences and F. Glaw for previous discussions about the origin and diversification of these frogs. We thank the Mayotte authorities for research permits. This work was supported by a Spanish Ministry of Science and Innovation grant (CGL2009-10198) to DRV.

REFERENCES

- Andreone F, Rosa GM, Noël J, Crottini A, Vences M, Raxworthy CJ (2010) Living within fallen palm leaves: the discovery of an unknown *Blommersia* (Mantellidae: Anura) reveals a new reproductive strategy in the amphibians of Madagascar. *Naturwissenschaften*, **97**, 525-543.
- Bell RC, Drewes RC, Zamudio KR (2015a) Reed frog diversification in the Gulf of Guinea: Overseas dispersal, the progression rule, and *in situ* speciation. *Evolution*, **69**, 904-915.
- Bell RC, Drewes RC, Channing A, Gvoždík V, Kielgast J, Lötters S, Stuart BL, Zamudio KR (2015b) Overseas dispersal of *Hyperolius* reed frogs from Central Africa to the oceanic islands of São Tomé and Príncipe. *Journal of Biogeography*, **42**, 65-75.
- Crottini A, Madsen O, Poux C, Strauß A, Vieites DR, Vences M (2012) Vertebrate time-tree elucidates the biogeographic pattern of a major biotic change around the K–T boundary in Madagascar. *Proceedings of the National Academy of Sciences*, **109**, 5358-5363.
- Freed LA, Conant S, Fleischer RC (1987) Evolutionary ecology and radiation of Hawaiian passerine birds. *Trends in Ecology & Evolution*, **2**, 196-203.
- Glaw F, Vences M (2006) Phylogeny and genus-level classification of mantellid frogs (Amphibia, Anura). *Organisms Diversity & Evolution*, **6**, 236-253.
- Glaw F, Vences M (2007) *A Field Guide to the Amphibians and Reptiles of Madagascar*, Vences & Glaw Verlag.
- Measey JG, Vences M, Drewes RC, Chiari Y, Melo M, Bourles B (2007) Freshwater paths across the ocean: molecular phylogeny of the frog *Ptychadena newtoni* gives insights into amphibian colonization of oceanic islands. *Journal of Biogeography*, **34**, 7-20.
- Pabijan M, Gehring P-S, Koehler J, Glaw F, Vences M (2011) A new microendemic frog species of the genus *Blommersia* (Anura: Mantellidae) from the East coast of Madagascar. *Zootaxa*, **2978**, 34-50.
- Stamatakis A (2014) RAxML version 8: a tool for phylogenetic analysis and post-analysis of large phylogenies. *Bioinformatics*, **30**, 1312-1313.

Vences M, Vieites DR, Glaw F, Brinkmann H, Kosuch J, Veith M, Meyer A (2003) Multiple overseas dispersal in amphibians. *Proceedings of the Royal Society of London B: Biological Sciences*, **270**, 2435-2442.

Vences M, Thomas M, Van der Meijden A, Chiari Y, Vieites DR (2005) Comparative performance of the 16S rRNA gene in DNA barcoding of amphibians. *Frontiers in Zoology*, **2**, 5.

Vences M, Köhler J, Pabijan M, Glaw F (2010) Two syntopic and microendemic new frogs of the genus *Blommersia* from the East coast of Madagascar. *African Journal of Herpetology*, **59**, 133-156.

Vieites DR, Chiari Y, Vences M, Andreone F, Rabemananjara F, Bora P, Nieto-Román S, Meyer A (2006) Mitochondrial evidence for distinct phylogeographic units in the endangered Malagasy poison frog *Mantella bernhardi*. *Molecular Ecology*, **15**, 1617-1625.

Vieites DR, Wollenberg KC, Andreone F, Köhler J, Glaw F, Vences M (2009) Vast underestimation of Madagascar's biodiversity evidenced by an integrative amphibian inventory. *Proceedings of the National Academy of Sciences*, **106**, 8267-8272.

CHAPTER 4

Descriptive skeletal anatomy of *Blommersia alexi* sp. nov.

Javier H. Santos-Santos^{1,2}, Mireia Guinovart-Castán¹, Dominique Adriaens³, David R. Vieites¹

¹ *Department of Biogeography and Global Change (BGC-MNCN-CSIC), Museo Nacional de Ciencias Naturales, C/José Gutiérrez Abascal 2, E-28006, Madrid, Spain.*

² *Department of Animal Biology, University of Barcelona, Avenida Diagonal 645, 08028, Barcelona, Spain.*

³ *Evolutionary Morphology of Vertebrates, Ghent University, K.L. Ledeganckstraat 35, B-9000 Gent, Belgium*

ABSTRACT

The Mantellinae subfamily of mantellids is the most species-rich and ecologically diverse of Malagasy frogs. These present an extensive adaptive radiation endemic to the islands of Madagascar and Comoros, of which the speciation processes and selective pressures are still unresolved. A main aspect of mantellid evolution involves the presence of a key innovative trait linked to the unique reproductive behavior of this group, which involves the development of femoral glands and a derived vomeronasal organ. In addition, previous studies point to size differentiation in playing an important role in species' dispersion and population ranges. Albeit the evidenced phenotypic variation in this taxon, up-to-date there still has not been an exhaustive morphological analysis of the anatomy of these anurans, much less in relation to internal structures. In the current study we present the first skeletal description of any mantellid species, employing for this labor a species of the genus *Blommersia* that is potentially undergoing a process of gigantism on the Comoros island of Mayotte. We describe with micrometer precision the intraspecific variation of the skeleton of this species utilizing non-destructive volume renderings of ten individuals and characterize the presence of sexual dimorphism and size covariation in skeletal structures. Notably, we found numerous signs of hyperossification, a novel structure exclusive as of yet to the genus *Blommersia*: the clavicular process, and the presence of several appendicular ossicles. Our findings suggest that skeletal phenotypic variation in this genus is linked to biomechanical function for reproduction and locomotion.

KEYWORDS: *Blommersia*, Mantellidae: Mantellinae, osteology.

INTRODUCTION

The Mantellidae represents the most species-rich and ecologically diverse anuran family endemic to the islands of Madagascar and Mayotte (Glaw & Vences, 2007). It is divided into three subfamilies: the semi-aquatic Mantellinae (Laurent, 1946), the terrestrial Laliostominae (Vences & Glaw, 2001), and the sizeable Boophinae (Vences & Glaw, 2001). Extensive work (Glaw & Vences, 2006; Vieites et al., 2009) has been carried out in view of resolving the biogeographic and phylogenetic relationships between taxonomic units to elucidate the evolutionary history of this relatively fast evolving lineage and shed light on the nature of the speciation processes that are in action. To this respect, variation in body size has been found to influence species' range sizes and biogeographic setting, linking smaller body sizes to higher clade diversity and geographically closer and more fragmented ranges (Wollenberg et al., 2011; Pabijan et al., 2012).

The Mantellidae family at the macroscale is phylogenetically nested within Asian frogs and its most recent common ancestor is estimated to have dispersed from this continent and colonized the island of Madagascar 76-87 Mya (Crottini et al., 2012; Samonds et al., 2013). In addition, there have been two more recent colonization events of oceanic dispersal from mainland Madagascar to the neighboring island of Mayotte, Comoros, 300km off the Northwest coast of Madagascar, regarding certain members of this family (*i.e.* Boophinae and Mantellinae) that are estimated to have occurred 6-8 Mya (Vences et al., 2003; Crottini et al., 2012). The Mantellinae colonization of Mayotte has led to the relatively rapid adaptive radiation of a *Blommersia wittei* (Vences et al., 2003) ancestor into two genetically distinct species that present differences in larvae, adult and femoral gland morphology, and preferred habitat (Chapter 3). These species, although highly syntopic, present different breeding ecologies and a large difference in size; one of them likely undergoing a process of gigantism on the island (Daugherty et al., 1993; Lomolino, 2005; Li et al., 2011). Most *Blommersia* species from Madagascar are small and there are even some cases miniaturization, however the larger species on Mayotte is ~30-35% bigger than its sister species. Both species have evolved in isolation on the island and have not competed with other frogs for resources or space, hence they have had the opportunity for an ecological, and potentially in parallel, morphological release, occupying part of the functional ecological and morphological spaces that are filled by other frog taxa in mainland Madagascar. This situation seems largely to be the case in

view of preliminary studies identifying phylogenetically-relevant morphological divergence in locomotor morphology between *Blommersia* species (Chapter 5).

Various morphological studies have been executed on anatomical subsystems of various species within the Mantellidae family: external morphology (*Blommersia* Vences et al., 2010; Pabijan et al., 2011; *Gephyromantis* Scherz et al., 2017a; *Guibemantis* Vences et al., 2015; *Mantidactylus* Vences et al., 2002; *Tysingymantis* Glaw et al., 2006), femoral glands (Vences et al., 2007; Altig, 2008), intercalary elements (Manzano et al., 2007), etc. However, in the current study we present the first full comprehensive skeletal description of a species within the Mantellidae, and at the same time introduce a species that is potentially undergoing a process of gigantism. We elaborate precise anatomical descriptions of all skeletal elements and define the level of intraspecific phenotypic variation (n=10) of highly variable elements. Anatomical descriptions are based on high-resolution rendered skeletons obtained from micro-CT (*i.e.* computed tomography) volume scans of individuals captured recently in Mayotte, Comoros. Approximations of non-calcified structures were inferred from additional CT-scans of stained specimens. Descriptions are made with elements referenced in a primary anterior (rostral) to posterior (caudal) axis and a secondary proximal (medial) to distal (lateral) axis. The main objective of this paper is to create a reference anatomy for future studies to compare other species within the same hyperdiverse family, Mantellinae subfamily, and *Blommersia* genus, and aid in the unravelling of the role of functional morphology in their speciation process and evolutionary history.

Anurans have a reduced number of cranial elements relative to other salamanders and caecilians and in accordance a simplified hyobranchial apparatus. Even so, they present an extensive anatomical diversity (6955+ species vs. ~715 salamanders and ~208 caecilians) and more elaborate sensory systems (*i.e.* olfactory and auditory), albeit with the exclusion of plethodontid salamanders (Madison, 1977). General characteristics of the anuran skull are that it is relatively broad, fenestrate (*i.e.* gymnokrotaphic), presents a poorly developed palate, reduced dentition, and that the jaw articulation (*i.e.* suspensorium) is located in the posterior limit of the skull (Duellman & Trueb, 1994). The auditory apparatus of anurans is also unique among vertebrates in that it contains a combination of structures that function in the transmission of both substrate vibrations and airborne waves (Hetherington & Lombard, 1982): the columella transmits vibrations

from the tympanic membrane to the inner ear, and the operculum transmits ground vibrations from the forelimbs to the inner ear.

MATERIALS & METHODS

A total of 10 (five male and five female) adult *B. alexi* **sp. nov.** individuals were retrieved from the collections at the National Museum of Natural History (MNCN-CSIC) Madrid, Spain (Table 1). Individuals were fixed with cotton and submerged in 70% ethanol within 50 mL polypropylene falcon tubes before CT-scanning in a Nikon XT H-160 system [reconstructed voxel size (μm) = 29.5-42 (isometric); X-ray (kV) = 53-56; X-ray (μA) = 172-188; Projections = 1800; voxels = 1008] at our internal Service of Non-destructive Techniques (MNCN-CSIC). The CT-scans were reconstructed with CT Pro 3D software and individual skeletons were volume rendered and visualized in Avizo [®] software. Additional CT-scans of stained specimens (Chapter 5) were performed to corroborate the position of non-calcified anatomical elements; these were performed with a custom setup at the Center for X-ray Tomography (UGCT) in collaboration with the Evolutionary Morphology of Vertebrates Lab of Ghent University, Belgium. The individual DRV6807 was chosen as the most representative individual for the species and was used as a reference for the generalized anatomical description.

Table 1. Data of the *Blommersia alexi* **sp. nov.** individuals used for the current study.

Field nº	Sex	Locality
DRV6805	F	Mont Combani
DRV6807	M	Mont Sapere
DRV6813	F	Mont Sapere
DRV6832	M	Mont Benara
DRV6833	M	Mont Benara
DRV6835	F	Mont Choungi
DRV6836	M	Mont Benara
DRV6841	M	Mont Benara
DRV6848	F	Mont Combani
DRV6851	F	Mont Combani

In addition, a total of 123 linear distances (Appendix S1) were measured on the rendered skeletons of all individuals to obtain the intraspecific range of variation of skeletal characters. Descriptive statistics were obtained and sexual dimorphism and size covariation evaluated through analysis of (co)variance ($\alpha = 0.05$) in IBM SPSS Statistics

for Windows, Version 24.0. We determined the snout-vent length (SVL) measurement that best covaried with skeletal linear distances by means of a univariate three-way analyses of covariance (ANCOVA), including all SVL measurements as covariates. Pelvis length (pelvL) was also explored as a covariate and included with the best resulting SVL covariate in univariate two-way ANCOVAs to determine which measurement covaried best with each skeletal linear distance.

RESULTS

Skull

There are two types of bone in the cranium: endochondral (*i.e.* develops from osteoblasts within cartilage) and dermal or membranous (*i.e.* develops intramembranously inside connective tissue) (Hall, 2005). The neurocranium represents an inverted T-shape box: the longitudinal branch going antero-posteriorly from the nasal to the auditory region, and each tip of the transversal branch ending at an auditory capsule (Fig. 1). As its name suggests, it protects the brain and adjacent sensory organs. The endochondral neurocranium is formed of five bones: the sphenethmoid, paired prootics, and paired exoccipitals.

Endochondral Neurocranium

Sphenethmoid

The sphenethmoid is an endochondral element that is ossified anteriorly, encircling the anterior part of the brain, contributing to the nasal capsule posterior walls, and forming the anterior margin of the optic foramen. Ossification extends further ventrolaterally (Fig. 2), creating a pair of small alae that penetrate the orbitonasal foramen slightly to either side of the parasphenoid. Ossification in the ventral region is exostosed (Duellman & Trueb, 1994), a sign of hyperossification evidenced by the presence of superficial sculpted patterns. Anteriorly it presents two bilaterally symmetric olfactory foramina that open to the internasal septum (Fig. 3). Posterodorsally the sphenethmoid separates medially forming the frontoparietal fontanelle, which is completely covered by the frontoparietals, except for its most-anterior tip, and extends dorsally slightly over half their length (Fig. 1).

Prootics and Exoccipitals

The prootics lie posterior to the sphenethmoid and expand laterally to cover the auditory capsules both anteriorly, forming the posterior margin of the optic foramen, and posterodorsally (Fig. 4). The prootics in *B. alexi* **sp. nov.** present signs of hyperossification evidenced in an exostosed surface and fusion with each other and with the exoccipitals to form a single massive element (*i.e.* otoccipital (Clack, 2001)). They unite dorsomedially at their most-posterior point, where they also fuse with the exoccipitals (Fig. 1). Each prootic presents anteriorly a large dorsal fenestra with a rostral-lateral extension that is discontinuous with the frontoparietal fontanelle. In addition, there is a diamond-shaped fenestra (*i.e.* otoccipital fenestra) between the prootics anterior to the dorsal union point of the otoccipital. The three fenestrae are completely covered by the frontoparietals, except for the posterior tip of the otoccipital fenestra. Below the protuberance at the posterolateral corner of the frontoparietal, the prootic presents two prominent epiotic eminences (Trueb, 1968b) that extend both antero- and postero-laterally (Figs. 1 & 4); the latter (*i.e.* opisthotic *sensu* Ecker, 1889) terminates in the prominentia ducti semicircularis posterioris (Laloy et al., 2013). This structure is narrowly separated from the antero-medial margin of the suprascapula.

The exoccipitals are fused completely ventrally and dorsally in a ring-like structure that unites dorsoanteriorly with the prootics, ventroanteriorly with the parasphenoid, flanks the foramen magnum, and forms the occipital condyles posteriorly (Fig. 3). Immediately anterior to each occipital condyle is a large circular foramen (*i.e.* foramen juglare) that corresponds to the exit of cranial nerves (CC.NN.) IX (glossopharyngeal) and X (vagus), which is separated laterally by a thin columella from another slightly more ovoid foramen located under the auditory capsule that corresponds to the exit of C.N. VIII (vestibulocochlear).

Auditory/Otic Capsules

The tympanic membrane in *B. alexi* **sp. nov.** is located at the level of the otic ramus of the squamosal bone. Below the posterior otic ramus of the squamosal lies the ossified portion (*i.e.* stylus) of the columella (*i.e.* middle ear) with an expanded proximal end (*i.e.* footplate), which articulates medially with the oval window (*i.e.* fenestra ovalis) membrane, anterior to the operculum (Fig. 4). Posterior and ventral covering the fenestra

ovalis lies the operculum, a lightly calcified cartilaginous element controlled by the m. opercularis. The Eustachian tubes, which connect the middle ear to the buccal cavity, exit the prootics at a posterolateral fenestra behind the articulation with the squamosal otic ramus. The inner ear is situated more medially within the auditory capsule and consists of a membranous labyrinth suspended within the otic capsule by loose connective tissue (Duellman & Trueb, 1994). The endolymphatic system (*i.e.* otic labyrinth) is suspended within the perilymphatic cistern, which connects with the perilymphatic sac within the neurocranium through two medial foramina (Fig. 3 & S1), one the round window (Duellman & Trueb, 1994), located anterior to that of the C.N. VIII (Simmons et al., 1992). The endolymphatic system in *B. alexi* **sp. nov.** consists of a large saccule divided by a central constriction that divides it into two compartments: the dorsal utriculus (semicircular canals) and the ventral sacculus (sensory epithelium). An endolymphatic duct leads from the sacculus to the endolymphatic torus surrounding the brain in the neurocranium (Dempster, 1930). The shape of the saccule compartments varied greatly between individuals, and due to the resolution of our CT-scans (~30µm) the identification of homologous structures at the nanoscale was not possible (but see Mason et al., 2015). However, there were some recurrent structures across individuals (Fig. S1): The shelf-like projection of the papilla amphibiorum recess was visible situated rostral-medially on the utriculus; in some individuals (*e.g.* DRV6807) another or another two round diverticula (the dorsal larger when both present) were visible extending medially from the amphibiorum recess (Richards, 2006). Medially at the level of the posterior perilymphatic duct and separated narrowly lateral to the sacculus lies the lagena (Duellman & Trueb, 1994), a saddle-shaped pouch with its seat oriented towards the sacculus. The endolymphatic system presents grooves that may correspond to the periotic canals of the perilymphatic system (Mason et al., 2015); the most common around its center circumference, and also frequent, dividing the utriculus roughly into left and right sections.

Nasal Capsule

Anurans have the most complex nasal capsule of all amphibians, consisting of an intricate arrangement of nasal sacs and ducts. *B. alexi* **sp. nov.** presents a calcified internasal septum (Trueb, 1968a; Laloy et al., 2013) that projects rostrally from the anterior sphenethmoid, taking on a rhomboid shape. Exostosed mineralization of this cartilaginous

element evidences hyperossification of the *B. alexi* **sp. nov.** skull once more (Figs. 1-3). The central region (*i.e.* septum nasi) presents the shape of a hollow rectangular prism invaded by spongy bone and is situated between the olfactory foramen of the sphenethmoid, extending forward to the level of the posteromedial margin of the nasals where it terminates in a slightly concave rectangular tip. From either dorsal corner of the septum nasi's tip, a calcified tectum nasi extends posterolaterally, terminating at the dorsal antero-lateral corners of the sphenethmoid. The anterior margin of the tectum nasi articulates with the nasals along $\frac{3}{4}$ its length on both sides. Narrowly separated, lateral, and ventral to the tectum nasi's posterior borders, the posterior region of the cup-shaped alary cartilages is calcified and fuses antero-medially with the ventral septum nasi at slightly over half its ventral-rostral length (Fig. 4). As a whole, the tectum nasi and alary cartilages serve as a roof and floor, respectively, to create a pair of large concavities (*i.e.* cavum principale; Trueb, 1968a) to either side of the septum nasi that ultimately lead to the olfactory foramen of the sphenethmoid. The palatine articulates with the ventral-lateral border of the alary cartilage, bracing the nasal capsule to the maxilla. The vomer's cup-shaped anterior segment constitutes the posterior nares, while the exterior anterior nares are located at the antero-lateral margin of the nasals (Reynolds, 1897).

Septomaxillae

The septomaxilla is a paired dermal bone above the maxilla and anterior to the vomer's rostral tip. In two individuals (*i.e.* DRV6835 and 6841) it was observed to contact the vomer. It presents the shape of a ventrolaterally oriented loop with a thickened ellipsoidal cap facing the maxilla (Trueb, 1968a) (Fig. 4). In several individuals (*e.g.* DRV6807, 6813, 6848) an unpaired dense spherical object of unknown nature was observed dorsal to the septomaxilla (Fig. 1).

Dorsal Dermal Neurocranium

Nasals

The nasal is a lightly ossified paired bone that lies dorsal of the nasal capsule and anterior to the ossified region of the sphenethmoid. It presents an extensive cartilaginous articulation with the center margin of the tectum nasi dorsal ridge. Posterolaterally the

nasal presents a more heavily ossified maxillary process (Duellman & Trueb, 1994) that terminates above the palatine and in line with the pars facialis of the maxilla (Fig. 2).

Frontoparietals

The anuran frontoparietal is derived from the fusion of the frontal and parietal elements present in other amphibians. It is a paired bone that originates dorsal to the sphenethmoid and extends posteriorly to slightly before the medial fusion of the prootics (Fig. 1). Additionally, in *B. alexi* **sp. nov.** it extends a short distance laterally above the anterior auditory capsule, covering about $\frac{1}{4}$ of the posterodorsal medial optic foramen (*i.e.* supraorbital flanges), which is yet another sign of hyperossification (Duellman & Trueb, 1994). The paired bones articulate at their medial margin, investing the entire dorsal roof of the neurocranium. At the posterolateral corner above the prootic it presents a dorsal odontoid protuberance presumably resulting again from hyperossification in *B. alexi* **sp. nov.** (Fig. 4).

Ventral Dermal Neurocranium

In *B. alexi* **sp. nov.** the ventral cartilaginous wall of the cranium is calcified. There are two bilaterally symmetric large foramina anterior to the posterior alae of the parasphenoid that correspond to the exit of CC.NN. V (trigeminal) and VII (facial) (Ecker, 1889; Reynolds, 1897). Slightly anterior and more medial to these is another pair of smaller foramina that correspond to the exit of C.N. VI (abducens). The orbitonasal foramen serves as an exit for CC.NN. II (optic nerve), III (oculomotor), and IV (trochlear) (Reynolds, 1897; Duellman & Trueb, 1994) (Fig. 3).

Vomers

The vomer (*i.e.* prevomer; Trueb, 1968a) is a paired bone located below the nasal capsule (Fig. 2). Its anterior segment resembles a shark's dorsal fin with an elongated leading edge (*i.e.* anterior portion; Maglia et al., 2007) and a cup-shaped trailing edge (*i.e.* prechoanal and postchoanal portions), whose base aligns almost parallel to the pars palatina of the maxilla. Along the leading edge before reaching the tip, the posterior segment branches off the anterior segment posteromedially via a peduncle. The posterior

segment (*i.e.* dentigerous portion) is cylindrical, covers a minimal part of the palate, and bears a dentigerous process $\frac{3}{4}$ its distal length below the nasal capsule. The dentigerous process bears ventrolaterally oriented vomerine teeth $\frac{3}{4}$ its distal length, as well as presenting vomerine teeth on its posterior tip, which terminates immediately posterior to the olfactory foramen of the sphenethmoid. The vomer does not present any visible osteological connection to either the premaxilla or the maxilla in *B. alexi* **sp. nov.** The septomaxilla is situated contiguous to the base of the vomer's leading edge above the maxilla.

Parasphenoid

The parasphenoid is an inverted T-shape bone that invests the braincase ventrally. The anterior ramus (*i.e.* cultriform process; Duellman & Trueb, 1994) extends from the medial posterior margin of the sphenethmoid to the prootic region, and the posterolateral alae cover the auditory capsules ventrally. In *B. alexi* **sp. nov.** the parasphenoid is less dense along its cultriform process; however it is hyperossified posteriorly fusing with the otoccipital posteroventrally (Fig. 2). *B. alexi* **sp. nov.** does not present parasphenoid odontoids.

Palatines

The palatine is a slim paired transverse element that braces the upper jaw against the neurocranium. Its medial end articulates laterally below the alary cartilages of the nasal capsule (Fig. 2), and its distal end widens and articulates with the medial lamina horizontalis of the maxilla immediately posterior to its pars facialis (Fig. 4). In *B. alexi* **sp. nov.** it is smooth and does not bear a serrate bony ridge.

Pterygoids

The pterygoid is a paired triradiate medial brace between the upper jaw, suspensorium, and neurocranium (Duellman & Trueb, 1994). It has the shape of an inverted “Y” laying laterally (Figs. 2 & 4). The anterior ramus presents a broad articulation with the maxilla and the ventral posterior ramus articulates laterally with the quadrate. The latter presents a caudal-ventrally oriented process at the ventroposterior edge of its medial surface (Fig. 3).

The anterior ramus is thicker along its dorsal edge, presenting a groove below its lateral margin that extends posteriorly to the base of the dorsal posterior ramus, investing the cartilaginous pterygoid process of the quadrate. The dorsal posterior ramus extends medially towards the lateral antero-ventral auditory capsule; however, it is not completely ossified; ossification extends along its leading edge about half the distance and its lateral face remains open like a saddle, embracing the cartilaginous pseudobasal process of the quadrate.

Lateral Dermal Neurocranium

Squamosal Bones

The squamosal in the lateral view looks like an anteriorly inclined “T” and participates in the suspension of the upper jaws from the skull (Fig. 4). The dorsal ramus (*i.e.* otic ramus) is oriented dorsomedially, articulating posteriorly with the dorsolateral margin of the prootic above the auditory capsule at a cartilaginous joint. The anterior otic ramus extends towards the maxilla a short distance, terminating in an acuminate tip at the level of the posterior margin of the orbitonasal foramen of the neurocranium. The ventral ramus (*i.e.* zygomatic ramus) extends ventroposteriorly at a slightly over 50-degree angle with the maxilla and articulates with the quadratojugal laterally and with the quadrate medially at its ventral end (Fig. 5). The medial surface of the zygomatic ramus presents a groove that continues into the posterior otic ramus, which invests the cartilaginous otic process of the quadrate.

Upper and Lower Jaws

Premaxillae

The premaxillae are located anteromedially in the head and are united syndesmotically medially to each other and laterally to the maxillae. The maxillae slightly overlap the premaxillae laterally. Each premaxilla is like a plate with a curved downward leading edge that bifurcates posteriorly in two acuminate branches. From the center of the leading edge a less dense vertical strut extends posterodorsally. Medially the bone presents a less dense circular fenestra. Traditionally the premaxilla is divided into three parts (Duellman & Trueb, 1994) (Fig. 3): the pars dentalis consists in the curved downward leading edge and bears a dental ridge; the pars palatina serves as the lingual shelf and consists in the

two posterior acuminate branches; and the alary process consists in a dorsal vertical strut that serves as a vertical abutment for the nasal capsule.

Maxillae

Each maxilla resembles a longitudinal plank following a parabolic curve in the anterior-posterior direction. It overlaps the premaxilla slightly anteriorly and articulates with the quadratojugal posteriorly. There is cylindrical process (*i.e.* lamina horizontalis; Blain & Arribas, 2017) along the midline of its medial surface that terminates caudally slightly anterior to the articulation with the quadratojugal and posterior to the articulation with the pterygoid (Fig. 3). This process expands medially from the bone's surface in the caudal-rostral direction immediately at the level of the pars facialis, creating a lingual shelf between the maxilla and its acuminate branch tip that terminates at the height of the septomaxilla (*i.e.* pars palatina). One individual (*i.e.* DRV6832) presented paired circlet processes on the lingual shelf at the level of the vomer's anterolateral tip. Anterior to the articulation with the palatine the maxilla's external margin presents a flat and wide triangular process (*i.e.* pars facialis) directed dorsally towards and at the level of the posterior tip of the nasal. The ventral border of the maxilla bears a dental ridge from its anterior tip to slightly before its articulation with the quadratojugal (*i.e.* pars dentalis).

Quadratojugals

The quadratojugals complete the upper jaw posteriorly. They articulate with the maxillae anteriorly and with the ventral-rostral margin of the zygomatic arch of the squamosals posteriorly in an upward curve (*i.e.* pars articularis) (Fig. 4).

Mentomeckelian Bones

The mentomeckelian bones are paired bones that form anteromedially in the Meckel's cartilage. They present a syndesmotomic union with each other medially and have the shape of cylindrical hooks that are oriented dorsally and face towards each other medially (Fig. 2). They present a short less dense acuminate process ventrolaterally, and dorsolaterally they articulate with the dentary (Fig. 3).

Dentaries

The dentary is a paired bone that covers the Meckel's cartilage anterolaterally. It articulates medially with the dorsolateral margin of the mentomeckelian bone and invests the dorsal region of the angulosplenic (Fig. 3). As in most anurans, in *B. alexi* **sp. nov.** the dentary bears no teeth and covers almost half the anterior length of the angulosplenic; both bones are solidly connected and their differentiation is inconspicuous.

Angulosplenic

The angulosplenic invests the ventrolateral, medial, and posterior regions of the Meckel's cartilage and is situated lateral to the ventral margin of the Mentomeckelian bone. It is an arcuate paired bone that extends antero-posteriorly, taking on a tight sigmoidal curve before its posterior articulation with the quadrate. In its caudal region, following the sigmoidal curve, there is a large groove along the midline of its lateral surface that opens up and flattens to terminate in an upward facing lobular plate, which embraces ventrally the quadratojugal-quadrate-pterygoid articulation of the suspensorium (Fig. 3). Along the dorsomedial border of its posterior curved region there is a crest that terminates in a curved upward odontoid process anterior to the quadratojugal-quadrate-pterygoid articulation. Prior to this odontoid process, a bony process extends posterolaterally from the crest's base supporting a large rounded head that curves downward towards a tiny acuminate process that protrudes from the dorsolateral border of the angulosplenic parallel to the odontoid process. The head of the bony process that extends from the crest is in line with an edge of the ossified cuboid quadrate (Fig. 5).

Suspensorium

Quadrates

The quadrate is the central element that suspends and braces the jaws to the skull and is majorly cartilaginous. Its pars articularis (Duellman & Trueb, 1994) presents perichondral ossification along its medial margin and buttresses the quadratojugal with the squamosal and the ventral-posterior ramus of the pterygoid at the mandibular articulation (Fig. 5). It is cuboid in shape.

Hyobranchial Apparatus

Anurans, along with plethodontid salamanders, have the most derived hyobranchial apparatus of all amphibians (Duellman & Trueb, 1994). The anuran hyoid consists of a central cartilaginous plate (*i.e.* hyoid plate) that constitutes the mouth floor and serves as an insertion site for the tongue muscles (*i.e.* m. hyoglossus). The hyoid plate bears several pairs of cartilaginous processes whose position and presence vary depending on the species (Duellman & Trueb, 1994). In *B. alexi* **sp. nov.** the hyoid plate (*i.e.* parahyoid) is very lightly calcified at its center with no obvious pattern across individuals (Fig. 6). This species presents two long and bony posteromedial processes whose anterior ends lay at the level of and dorsal to the anterior branch of the omosternum, each laying roughly on either side slightly before the omosternum's branching event. The posteromedial processes present an expanded anterior epiphysis and terminate as a truncated cylinder. Most individuals (excluding DRV6805, 6835, 6848) present a lateral crest on the posterior margin that terminates slightly before its posterior limit, and which displays varying degrees of development. They are flattened dorsoventrally and exhibit an upward inclination in the antero-posterior direction, terminating at the level slightly before the scapula-suprascapula articulation.

Pectoral Girdle

B. alexi **sp. nov.** presents a firmisternal pectoral girdle (Emerson, 1983) in that the epicoracoid cartilages lack horns and are fused medially; the sternum is fused to the pectoral arch and possesses relatively lengthier prezonal (*i.e.* omosternum) and postzonal (*i.e.* mesosternum) elements than in arcifery. In contrast to salamanders, anurans retain two dermal bones in the pectoral girdle, namely the clavicle and the cleithrum. Chondral elements include the scapula and the coracoid. Antero-posteriorly the prezonal elements include a cartilaginous episternum and an ossified omosternum; the postzonal elements consist in an ossified (meso)sternum and a cartilaginous xiphisternum (Duellman & Trueb, 1994).

Episternum

The episternum is an anterior cartilaginous extension of the omosternum that does not ossify. It enfolds the terminal end of the anterior branch of the omosternum and presents a rhomboid shape like a cranially-directed angled spade.

Omosternum

The omosternum is ossified into a style that bifurcates posterolaterally and articulates with both clavicles at a process along the first third of their proximal end, but never at their medial tip (Fig. 6). The length, width, and degree of ossification of the posterior branches of the omosternum vary across individuals (Table 2).

Mesosternum

The (meso)sternum is relatively lengthened compared to arciferal anurans and its shape depends on its level of ossification. The mesosternum is ossified into a stylus that articulates cranially with the medial ends of both coracoids at the epicoracoid cartilages (Fig. 6). It presents either of two configurations: a wide anterior end that tapers towards the center (*e.g.* 6807, 6805, 6832, 6833, 6835), or a bifurcated anterior end, presenting wider branches than those of the omosternum, in which each branch articulates anteriorly with one of the coracoids (*e.g.* DRV6813, 6836, 6841, 6848). One individual (*i.e.* DRV6851) presents a sternum with similar widths at the anterior and posterior ends that resembles an hourglass. The xiphisternum does not ossify and consists of a cordate expanded cartilage posterior to the mesosternum.

Clavicles

The clavicle is a paired, thin, and mostly straight bone that is flattened along its dorsoventral axis. It articulates with the procoracoid cartilage proximally, the coracoid ventrally, and with the scapula distally (Fig. 6). Ossification of the clavicle penetrates the procoracoid cartilage to various degrees depending on the individual. Its distal end widens cranially and its degree of ossification also varies across individuals (Table 2). The clavicle presents a yet undescribed process positioned cranially at its proximal end distal to the clavicle-coracoid articulation that appears to articulate with the posterior

branches of the omosternum and serve as an attachment site for several muscles (*i.e.* mm. deltoideus and coracoradialis) (Fig. 6).

Coracoids

The coracoid is a paired bone with a flattened proximal end and a rounded distal end. Its distal end articulates with the scapula at the glenoid cavity, whereas its proximal end articulates medially with the epicoracoid cartilage (Fig. 6). Ossification of its proximal end is variable and its shaft is smooth.

Scapulae

The scapula is a paired bone that presents a thin and flattened distal end that articulates laterally with the suprascapula. Its proximal end is bicapitate and consists of two bony arms that surround the head of the humerus; the anterior arm articulates with the clavicle, while the posterior with the coracoid.

Suprascapulae and Cleithrum

The suprascapula is a paired bone with varying degrees of ossification, albeit roughly $\frac{2}{3}$ of its surface. The bony leading edge of the suprascapula is denominated the cleithrum. Ossification invades the suprascapular cartilage through the cleithrum and extends towards the anterior medial edge, and posteriorly and medially, resembling a crab claw (Fig. 9). The anterior medial edge of the cleithrum is narrowly separated from the posterior epiotic eminence of the prootic, even making contact in some individuals (*e.g.* DRV6807; Fig. 1, DRV6835, 6848, 6851). At its distal end the suprascapula also presents varying levels of ossification and articulates at a cleft on the scapula.

Forelimb

Humerus

The humerus is the propodial element of the forelimb. The humerus head is round and slightly elongated. There is a large prominent cranial process at its proximal end denominated the deltoid crest (*i.e.* crista ventralis; Duellman & Trueb, 1994). The anterior ridge of the deltoid crest articulates medially with the humerus head, presenting a fenestra

directly below the articulation that initiates an intertubercular groove that extends distally below the deltoid crest to the lateral border of the humerus diaphysis (Fig. 6). The crista medialis is greatly reduced and limited to the proximal portion of the humerus immediately following the greater tubercle of the humerus head; otherwise the diaphysis is smooth. The diaphysis presents a slight sigmoidal curve that follows the line of the deltoid crest and ends at the distal lateral epicondyle.

Radioulna

The radioulna is the epipodial element of the anuran forelimb. The radio and ulna of tetrapods are fused into a single bone in anurans, although they can be differentiated at its distal end due to the presence of a groove (*i.e.* sulcus longitudinalis; Blain & Arribas, 2017). Proximally, the ulna articulates with the femur at the concave olecranon and the radio at the capitulum. Distally, the ulna articulates with the ulnare and the intermedium, while the radio articulates with the radiale and the centrale (Fig. 7).

Hand

Following Fabrezi & Alberch (1996), the hand consists of five mesopodial elements (*i.e.* ulnare, radiale, Element Y, distal carpal 543, and distal carpal 2), four metapodial elements (*i.e.* metacarpals), the prepollex, the phalanges, and intercalary cartilage elements. The ulnare articulates postaxially with the lateral border of the ulna's distal epiphysis. It has the shape of a laterally compressed square with two projections along its posterior margin, one dorsal, one ventral, and with another projection extending medially from its dorsoanterior border. Ventral to the ulnare lies the compound bone distal carpal 543. This bone articulates anteriorly with metacarpals IV-II and displays a lateral apophysis on its dorsoanterior border. Its ventrum extends below the metacarpals to constitute the palmar surface, which presents two points of contact: postaxially at the level between metacarpals IV-III and preaxially below metacarpal II. Above the latter, slightly lower, point of contact, distal carpal 543 presents a permeated tunnel in the antero-posterior axis, plausibly a remnant from the secondary fusion of embryonic distal carpal 3 into this compound bone (Fabrezi & Alberch, 1996). The radiale articulates preaxially with the posterior margin of the radio's distal epiphysis. It is cuboid in shape and presents two projections: one dorsomedially that contacts that of the ulnare, and

another ventromedially that articulates with the dorsal surface of distal carpal 543 at the level of the postaxial border of metacarpal II. The former results in the formation of two medial fenestrae between both carpals: a small dorsal one below the radioulna distal epiphysis and another larger ventral one that ends at the dorsal surface of distal carpal 543. Element Y (Shubin & Alberch, 1986) extends ventrolaterally from the radiale's posterior margin. This bone articulates medially with distal carpal 543, and distally along its dorsal margin with metacarpal I and along its ventral margin with the reduced distal carpal 2. Preaxially and dorsal to Element Y lies the prepollex. It appears to be composed of three elements, the most distal of which is a less dense elongated acuminate process. Distal carpal 2 articulates distally with metacarpal I, while the second segment of the prepollex articulates postaxially and only along its anterolateral border with this same element.

There are four Digits (I-IV), with the metacarpal of Digit I lacking the nuptial tubercle distinctive of anurans that perform amplexus (Altig, 2008). The phalangeal formula is 2-2-3-3 (Digits I-IV), Digit III being more elongated than the rest and Digit I shorter. Preaxial to Digit I is the prepollex, a rudiment in anurans from the reduction of a fifth Digit relative to other tetrapods. Between the terminal and subterminal phalanges there is an intercalary element that can be found in all Digits (of both hands and feet) believed to be related to the mechanical requirements of arboreal habits (Vences et al., 2003). It is fully mineralized, wedge-shaped, and presents biaxial articulations both distally with the subterminal phalange (sellaris type) and proximally with the terminal phalange (plane type) (Manzano et al., 2007). The terminal phalanges are differentiated from the other phalanges for lacking a terminal epiphysis; they are straight or slightly curved downward with a V-shaped tip, lack apophyses, and have an ellipsoidal proximal epiphysis (Manzano et al., 2007). The other phalanges are elongate and articulate at their proximal end with their corresponding Digit's metacarpal. Both the non-terminal phalanges and the metacarpals present a denser diaphysis than epiphysis (Fig. 8).

Vertebral Column

The vertebral column provides a rigid, but flexible, longitudinal brace for the support of the head and viscera and suspension of the appendicular skeleton, and additionally serves as a bony passage for the spinal cord (Fig. 9). It is composed of nine vertebrae [eight

presacrals (I-VIII) and the sacrum(IX)] and the urostyle (*i.e.* fused postsacrals; coccyx). Each vertebra is composed of a cylindrical bony body called the centrum that is oval in cross-section. Dorsal to the centrum passes the spinal cord within the vertebral foramen formed by the bony neural arches. These are non-imbricate, decrease slightly in height posteriorly, and join medially above the spinal cord in a blunt neural spine, or crest, which serves as a muscle and ligament attachment site. Some individuals present an incompletely ossified neural crest for presacral I (*e.g.* DRV6805, 6848). Each vertebra except the first bears two pairs of processes located dorsally on the neural arches for articulation with adjacent vertebrae: the prezygapophyses anteriorly and the postzygapophyses posteriorly. In addition, a pair of transverse processes (*i.e.* parapophyses, presacrals II and III; diapophyses, presacrals IV-VIII) emanate laterally from the neural arches; these are expanded in presacrals II-IV due to the attachment of musculature for suspension of the pectoral girdle and are absent in presacral I. The first postcranial vertebra (*i.e.* presacral I) is known as the atlas and is modified anteriorly to articulate with the skull, bearing two cup-shaped atlantal cotyles that form condyloid joints with the occipital condyles of the skull. Ribs are absent in *B. alexi* **sp. nov.**

In addition to the vertebral articulations, the successive monospondylous vertebral centra (Duellman & Trueb, 1994) articulate via condyloid joints. These articulations are displasiocoelus in *B. alexi* **sp. nov.**, meaning all articulations are procoelus (*i.e.* centrum concave anteriorly and intervertebral cartilage associated with the posterior end of each centrum; allows movement in two planes) except for that of the presacral VIII, which is amphicoelus (*i.e.* centrum terminally biconcave and separated by intervertebral cartilage that may or may not be independent of adjacent centra).

The centra of *B. alexi* **sp. nov.** do not fit perfectly into the categories for the developmental classification of anuran vertebral centra (*i.e.* ectochordal, holochordal, stegochordal: Griffiths, 1959; perichordal, epichordal: Mookerjee, 1931; Mookerjee & Das, 1939; Kluge & Farris, 1969; perichordal with chordacentral additions: Wake, 1970; Gardiner, 1983). The centra in this species are dorsoventrally depressed (characteristic of stegochordal and epichordal development) with a less dense core (probably a remnant of the notochord, or hypochord) towards its posterior end (characteristic of perichordal development). The hypochord remnants are absent in the atlas and increase in size caudally.

Presacral II

The transverse process is a parapophysis (as it is located relatively more ventrally on the neural arch). It is dorsoventrally flattened along its full length and its leading edge displays a slight ventro-dorsal inclination. It branches from the neural arch anterolaterally. Additionally, the transverse process is relatively shorter than in the rest of presacral vertebrae (Table 2). In two individuals (*i.e.* DRV6841, 6848) the neural crests of the atlas and presacral II are imbricate.

Presacral III

Presacral III displays the longest transverse processes of all vertebrae (Table 2). The transverse process is also a parapophysis, albeit it branches laterally from the neural arch lower than in presacral II. Additionally, its leading edge presents a steeper ventro-dorsal inclination relative to presacral II. The transverse process of presacral III displays the largest disparity of all vertebrae; there are three different characters that appear developed to different degrees depending on the individual and with no particular pattern (*e.g.* sexual dimorphism, symmetry, ...): (A) The development of a protuberance nearly $\frac{3}{4}$ the distal distance on the parapophysis' anterodorsal edge ranges from a small protuberance (*e.g.* DRV6807, 6851) to a large anteriorly directed process with a triangular profile (*e.g.* DRV6805, 6832). From the tip of this process the parapophysis flattens dorso-ventrally to its extreme in the lateral direction. (B) Another protuberance, displaying significantly less variation in size and position, is located on the posterodorsal edge of the parapophysis slightly more proximal than (a). (C) At the distal extremity of the parapophysis some individuals (*e.g.* DRV6813, 6833) present light calcifications that can contact ossified portions of the posterior suprascapula.

Presacral IV

Relative to presacrals II-III, presacral IV's transverse process is less dorso-ventrally flattened, and branches more dorsally on the neural arch (*i.e.* diapophysis) in a similar manner to the succeeding vertebrae (presacrals V-VIII). The diapophysis branches from the neural arch in a posterolateral direction and ends in a truncated cylinder. Its distal extremity is thickened to different degrees, more so posteriorly, depending on the individual.

Presacrals V, VI, VII, and VIII

The transverse processes of presacrals V-VII branch from the neural arch in a posterolateral direction, presenting a gradient of decreasing magnitude from presacral IV to presacral VII; the presacral VIII breaks this trend, branching once more slightly in an anterolateral direction. Unlike presacrals II-IV, the transverse processes of posterior presacrals V-VIII are not expanded but are narrower and rod-like in shape.

Sacral Vertebra

The sacrum is a single specialized vertebra from which the pelvic girdle is suspended (Fig. 10). It is located between the presacrals posteriorly and anterior to the urostyle, or coccyx. The sacrum bears a pair of prezygapophyses but lacks postzygapophyses. Its transverse processes are expanded resulting in the sacral diapophyses that articulate ventrolaterally with the ilia of the pelvic girdle. In *B. alexi* **sp. nov.** the sacral diapophyses are thick, rod-like, dorsoventrally compressed cylinders. These are located relatively more dorsally than in the rest of vertebrae nearly at the level of its neural crest, which leaves the anterior tip of the ilial shafts in line with the transverse processes of the presacral vertebra.

Urostyle

The urostyle is a long straight shaft that has a bicondylar articulation at its proximal end with the sacral vertebra (Fig. 10). It presents a dorsal urostylic crest that occupies slightly less than $\frac{2}{3}$ of its shaft (Table 2). The crest starts anteriorly at a large tubercle, which can be ossified to varying degrees depending on the individual, and progressively decreases in height in the caudal direction. Where the urostylic crest ends, the shaft reduces in density, flattens dorsoventrally, and continues until slightly before the caudal border of the ischium.

Pelvic Girdle

The pelvis comprises three paired elements that unite in a medial symphysis: the ilium, the ischium, and the pubis. The primary elements are the ilium and the ischium because in most anurans the pubis is reduced (Duellman & Trueb, 1994). The anterior half of the

pelvic wheel is formed by the expanded posterior portion of the ilium, whereas the posterior half is comprised by the ischium; the cartilaginous pubis is limited to its ventral portion, presenting varying degrees of ossification and fusion (Fig. 11).

Ilium

The ilial shafts articulate at their anterior end with the ventral sacral diapophyses (Fig. 10). In *B. alexi* **sp. nov.** this articulation is of type IIB (Emerson, 1982) or of the sagittal-hinge type (Reilly & Jorgensen, 2011). The configuration of the ilial-sacral articulation largely determines the locomotor mode of a species; the sagittal-hinge morphotype being characteristic of long-distance jumpers (*i.e.* >eight body lengths; Zug, 1978; Emerson, 1979) since it allows dorsoventral excursion of the pelvic girdle along the vertical plane. This morphotype in *B. alexi* **sp. nov.** is characterized by posterolaterally oriented round sacral diapophysis and well developed joint capsules at each ilial shaft articulation, presenting a narrow transverse ligament deep to the back musculature instead of a groove-like articulation characteristic of Emerson's (1982) type I. In some individuals (*e.g.* DRV6833, 6835, 6841), there are sesamoid bones within the ligament of the articulation that align with the tips of the sacral diapophyses. The length of the ilial shafts is relatively longer in saltatorial species.

The ilial shafts of *B. alexi* **sp. nov.** present large ilial crests along their full length, which originate anteriorly lateral to the ilial-sacral articulation and terminate at a well-developed lateral protuberance immediately before the ilium expands to form the anterior part of the acetabulum (Fig. 11). The crest increases in height posteriorly and presents two grooves: one medially along $\frac{3}{4}$ its length due to the medial curvature of the crest tip, and one laterally below the posterior protuberance that extends $\frac{1}{4}$ its length in the rostral direction. The posterior expansion of the ilium presents varying degrees of ossification depending on the individual. There are two concavities between the ilial shafts: one posterior to the acetabulum and another anterior to it that is relatively deeper (Fig. 10).

Ischium and Pubis

The ischium comprises the posterior half of the pelvic wheel and can vary considerably in shape due to the mechanical stresses exerted by the musculature in this area (Duellman &

Trueb, 1994). The pubis is mostly calcified in *B. alexi* **sp. nov.**, more densely posteriorly, and its articulations with the ischium and ilium are difficult to distinguish (Fig. 11). However, the presence of a bony plate, suggestive of an epipubis (*i.e.* chondrification of the linea alba; De Villiers, 1925; Rockova & Rocek, 2005), at the posterior border of the acetabulum may indicate its separation from the ischium. At the proposed articulation, the posterior origin of the plate presents two lateral processes that invade the acetabulum medially. The articulation of the ischium with the ilium is equally difficult to distinguish; however, we note a thickened bony cap on the tip of the posterior-most border of the pelvic wheel where other authors propose the location of this articulation (Ecker, 1889; Duellman & Trueb, 1994).

Hindlimb

Femur

The femur is the propodial element of the hindlimb. It is a long bone with a smooth diaphysis that presents a slight sigmoidal curve (Fig. 12). The femur head is round and articulates with the acetabulum of the pelvis (Fig. 11). At its epiphysis the bone widens and terminates in a truncated surface with two condyles (*i.e.* medial and lateral) that articulate with the tibiofibula.

Tibiofibula

The tibia and fibula are completely fused into a single bone (*i.e.* the tibiofibula) that comprises the epipodial element of the hindlimb. Its head presents two condyles with a thick bony ridge that crosses $\frac{3}{4}$ of their medial surface. The diaphysis is smooth and straight, presenting the nutrient foramen halfway along its length. Its epiphysis also presents two condyles, which articulate with the tibiale and fibulare.

Foot

The foot consists of six mesopodial elements (*i.e.* tibiale, fibulare, centrale, hallux-tarsal, and two distal tarsals), five metapodial elements (*i.e.* metatarsals), the prehallux, the phalanges, intercalary cartilage elements, and a heterotopic sesamoid (Hall, 2005). There

are five Digits (I-V) with relatively more elongated metapodial elements and phalanges than the hand. The phalangeal formula is 2-2-3-4-3 (Digits I-V).

Tibiale and Fibulare

The preaxial tibiale (aka astralagus) and postaxial fibulare (aka calcaneum) are mesopodial elements of the hindlimb that are extremely elongated relative to their homologues in other tetrapods. They are fused medially both proximally and distally at their epiphyses and metaphyses, and only a short distance along the most distal part of their smooth diaphyses. The tibiale presents a sesamoid bone (*i.e.* cartilago sesamoides; Nussbaum, 1982) on its proximal ventral epiphysis, and a pointed, medially-oriented apophysis on its distal epiphysis (Fig. 12).

Sole

Below the fibulare's distal epiphysis is an ovoid plantar (Ponssa et al., 2010) os sesamoides (Nussbaum, 1982). Its longitudinal axis lies in the proximal-distal direction and only its proximal margin is in contact with the fibulare (Fig. 12). Its distal border ends below and at the level of the separation of the proximal epiphyses of metatarsals V and IV. In addition, its distal segment presents preaxially either a rounded apophysis or an additional sesamoid bone (*e.g.* cartilago plantaris; Hoyos, 2003). The centrale (aka naviculare; Howes, 1888) articulates along its complete surface preaxially on the tibiale's distal epiphysis. It presents an extensive ventral apophysis below the tibiale that extends distally at its base, producing a sort of fulcrum. The centrale articulates postaxially with metatarsal I, and with the prehallux preaxially before the branching of its apophysis. Embryonic distal tarsals 2 and 3 fuse into a diagonally-oriented ellipsoidal bone along the preaxial-postaxial axis (*i.e.* cuboideum; Howes, 1888). The cuboideum's preaxial margin lies below metatarsal II, articulating with this element only at its dorsal margin (Fig. 12), whereas it articulates with metacarpal III along its complete distal postaxial margin. In between the dorsal segment of the centrale and the preaxial head of the cuboideum, lies the hallux-tarsal (Howes, 1888); a small nodule of calcified cartilage. The fused distal epiphyses of the tibiale and fibulare articulates preaxially with the cuboideum and postaxially with the metatarsals of Digits IV and V. The morphological characteristics of the intercalary elements in the foot are the same as those for the hand (see above).

ABBREVIATIONS

<i>a</i>	alae	<i>ff</i>	fontanelle/fenestra
<i>ant</i>	anterior	<i>med</i>	medial
<i>ap</i>	apophysis	<i>p</i>	process/protuberance
<i>c.</i>	cartilage	<i>pl</i>	plate
C.N.	cranial nerve	<i>pp</i>	pars
<i>cav</i>	cavity	<i>pst</i>	posterior
<i>cr</i>	crest/crista	<i>r</i>	ramus
<i>dor</i>	dorsal	<i>so.fl.</i>	supraorbital flange
<i>epio. e.</i>	epiotic eminence	<i>ven</i>	ventral
<i>f</i>	foramen	<i>zygo</i>	zygomatic
a.c.	alary cartilage	phy	parahyoid
agspl	angulosplenic	plym	perilymph
amph.r.	amphibiorum recess	preh	prehallux
at	atlas	prem	premaxilla
clei	cleithrum	prep	prepollex
clv	clavicle	prezyga	prezygapophysis
cntl	centrale	pro	prootic
col	columella	psph	parasphenoid
crc	coracoid	pstzyga	postzygapophysis
d	dentary	pltn	palatine
dcpl	distal carpal	ptyd	pterygoid
elym	endolymph	qdj	quadratojugal
E.t.	Eustachian tube	qu	quadrate
exo	exoccipital	rad	radius
fem	femur	radle	radiale
fp	frontoparietal	s.n.	septum nasi
hms	humerus	sc	scapula
hyob	hyobranchial	sph	sphenethmoid
int.el.	intercalary element	sptm	septomaxilla
lg	lagna	sq	squamosal
Mm.b.	Mentomeckelian bone	ssc	suprascapular
mterp	metacarpal	st	sternum
mttrl	metatarsal	t.n.	tectum nasi
mx	maxilla	t.ph.	terminal phalange
nas	nasal	uln	ulna
o.c.	otic capsule	ulne	ulnare
omst	omosternum	uro	urostyle
op	operculum	vom	vomer
oto	otoccipital		

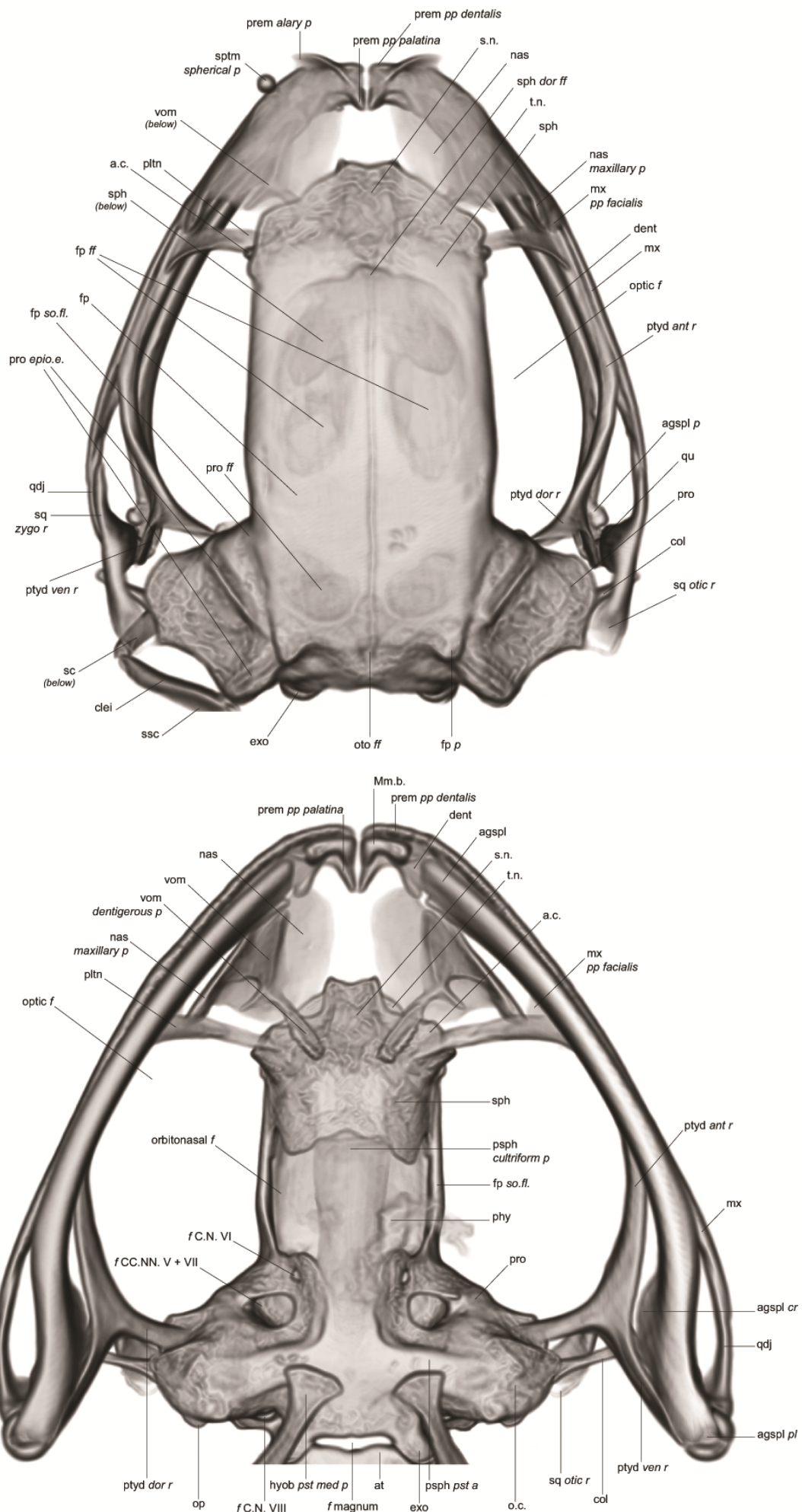


Fig. 1. Dorsal view of the *Blommersia alexi* sp. nov. skull [DRV6807 male; grey values: 12000-55500; volrenWhite and physics colormaps].

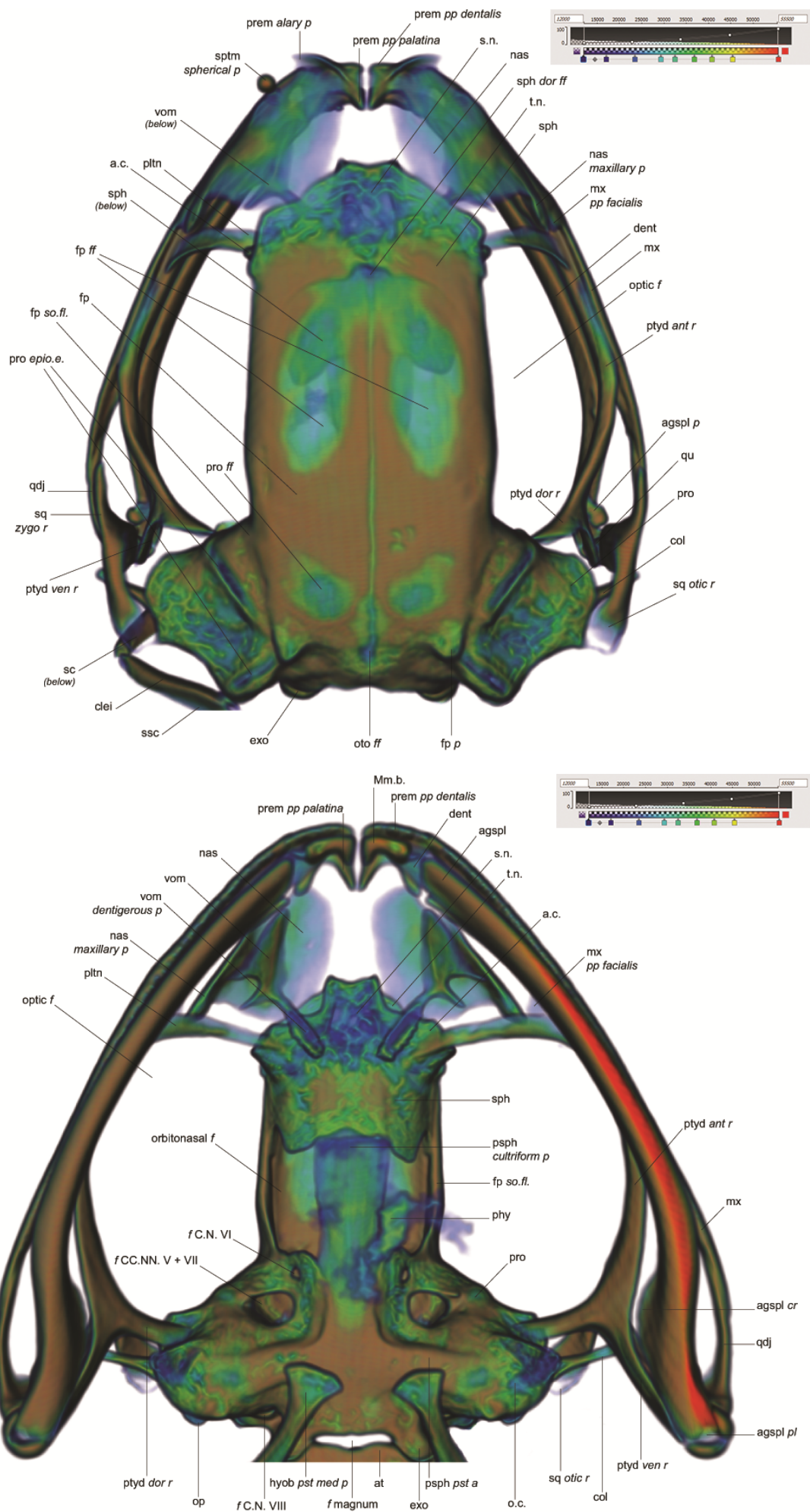


Fig. 2. Ventral view of the *Blommersia alexi* sp. nov. skull [DRV6807 male; grey values: 12000-55500; volrenWhite and physics colormaps].

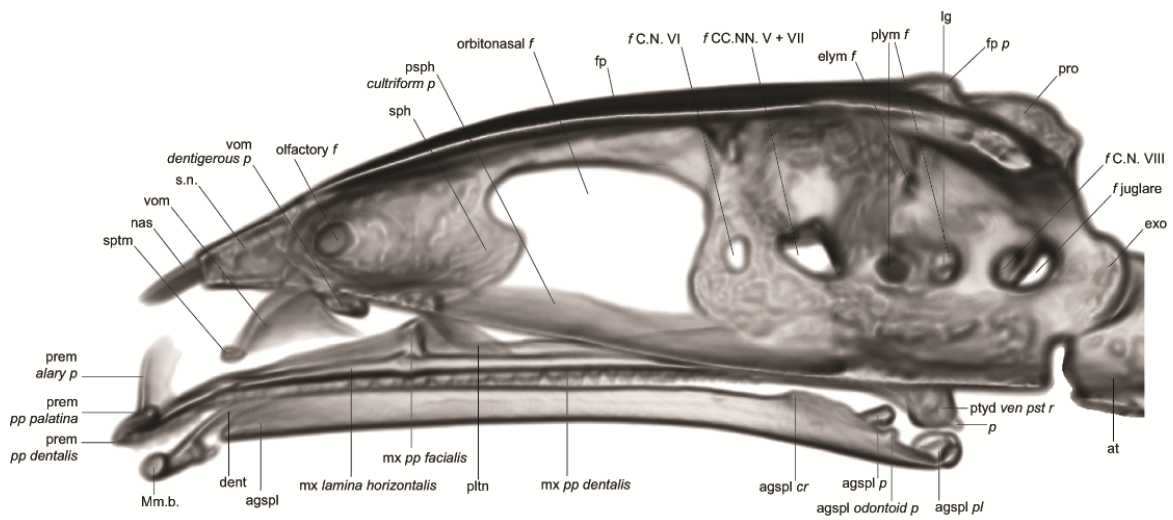
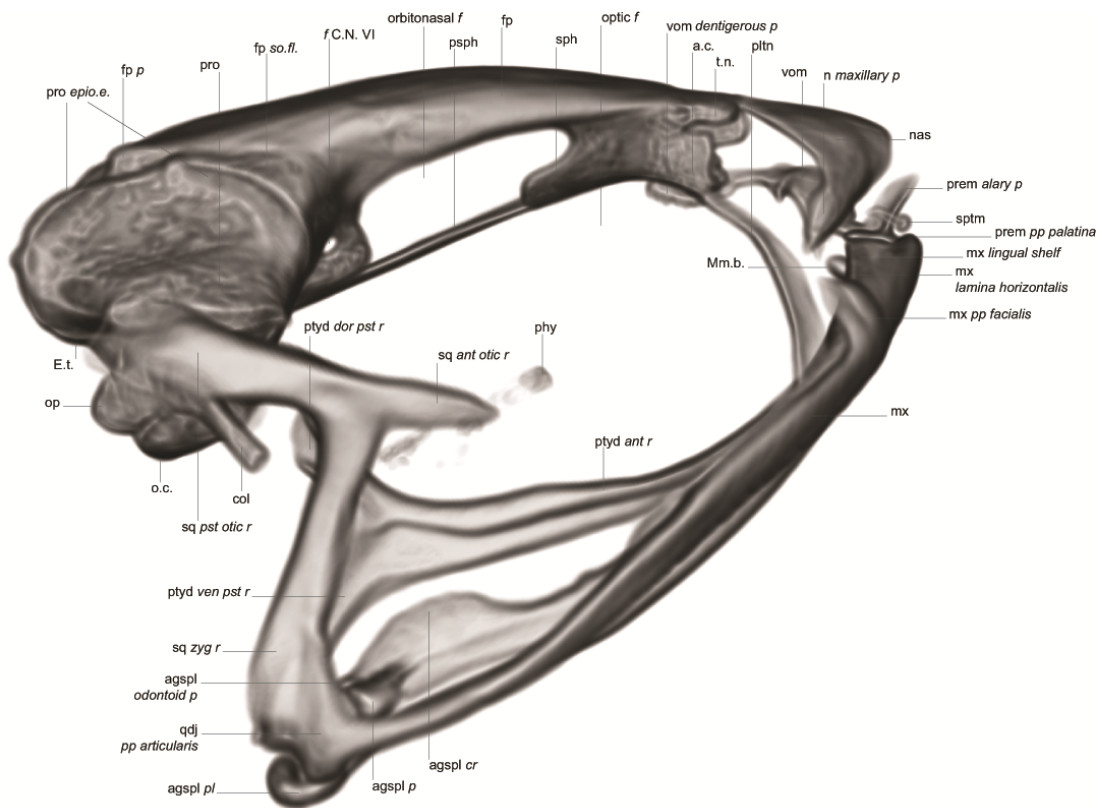


Fig. 3. Left sagittal plane, medial view of the right side of the *Blommersia alexi* sp. nov. skull [DRV6807 male; grey values: 12000-55500; volrenWhite and physics colormaps].



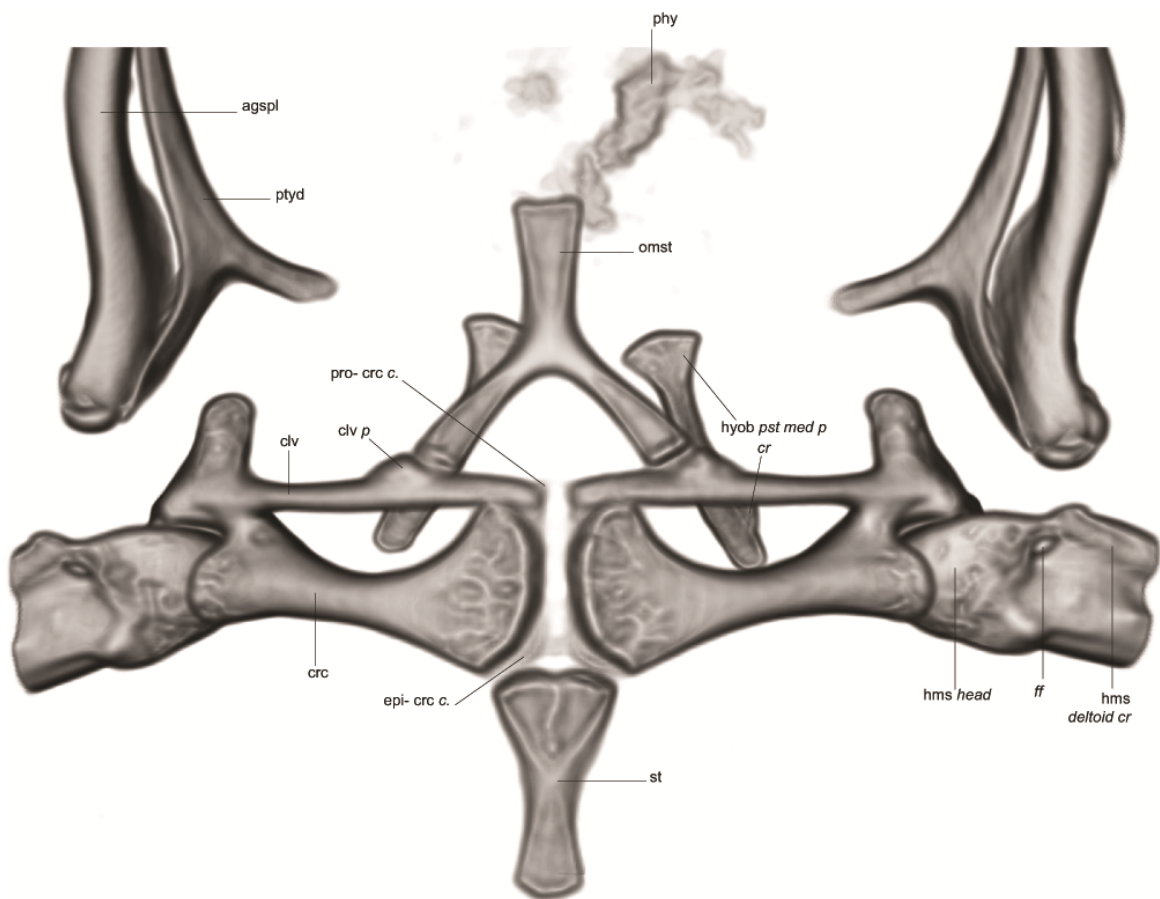
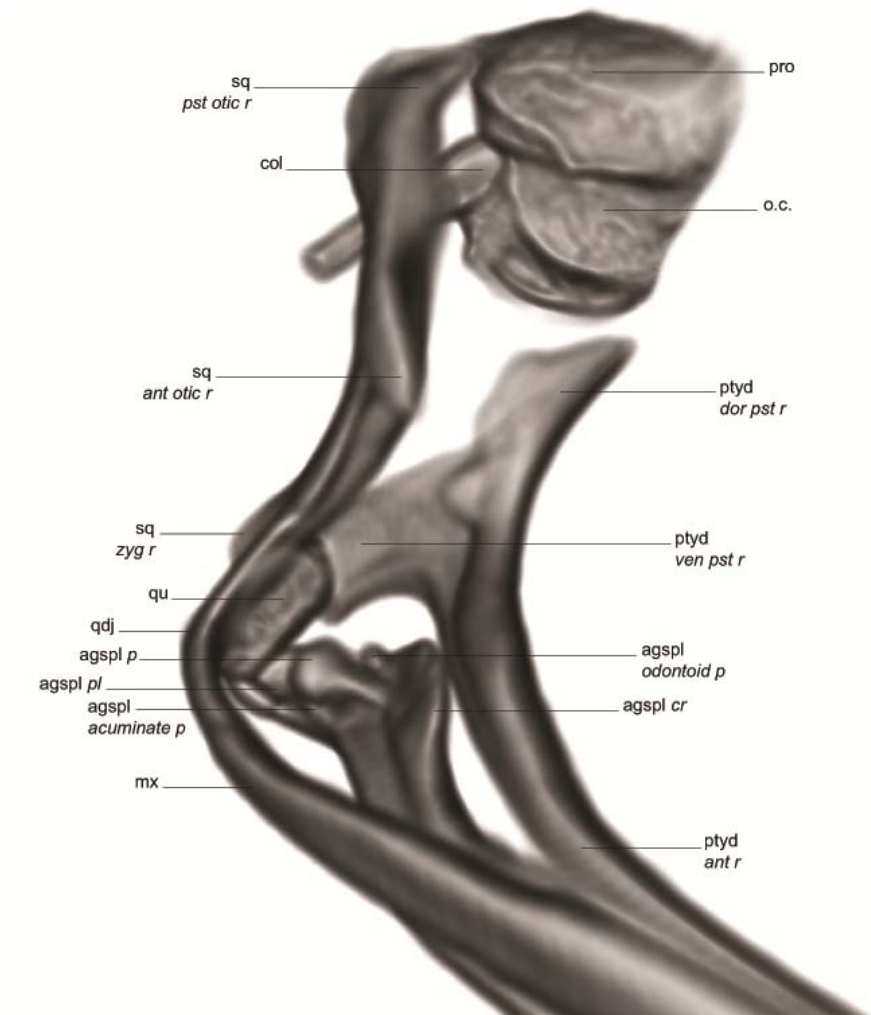


Fig. 5. Dorsal and internal view of the right *Blommersia alexi* sp. nov. suspensorium / jaw articulation [DRV6807 male; grey values: 12000-55500; volrenWhite and physics colormaps].

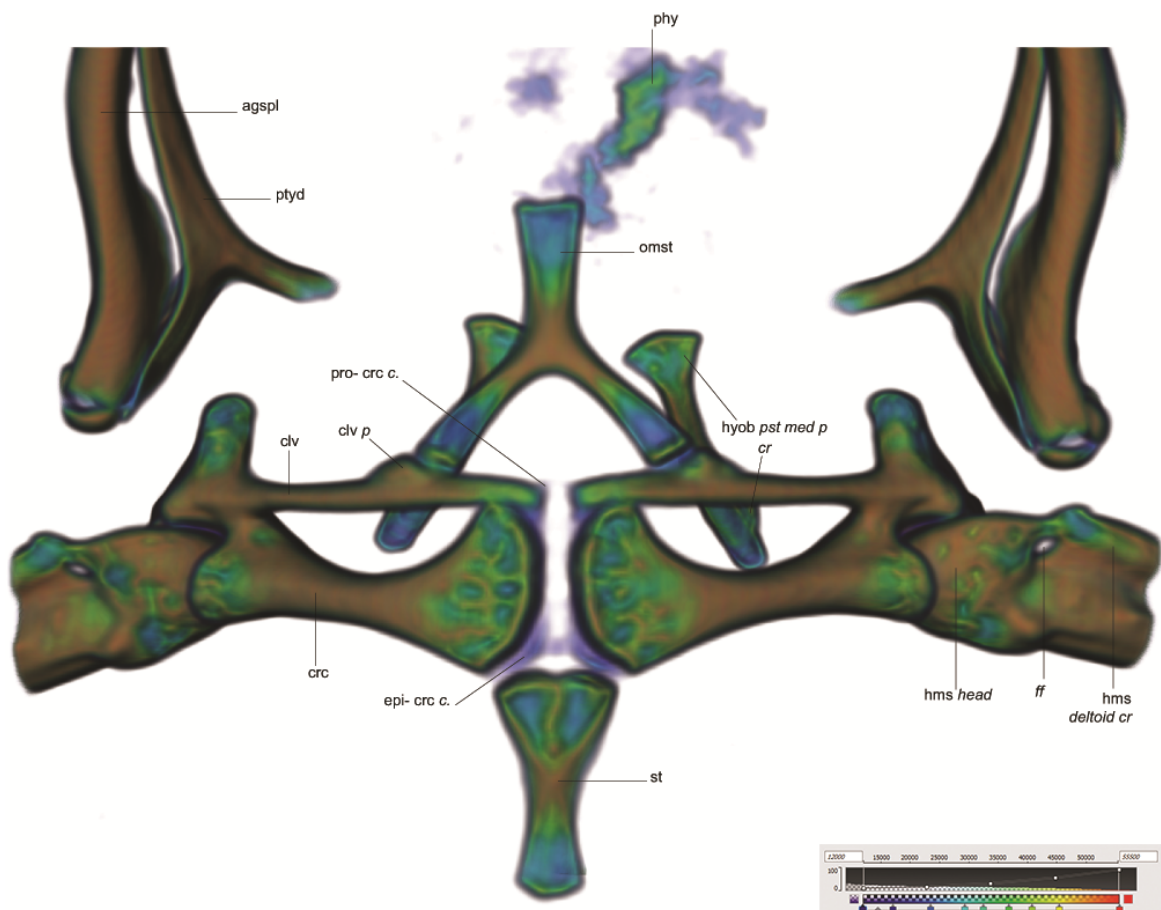
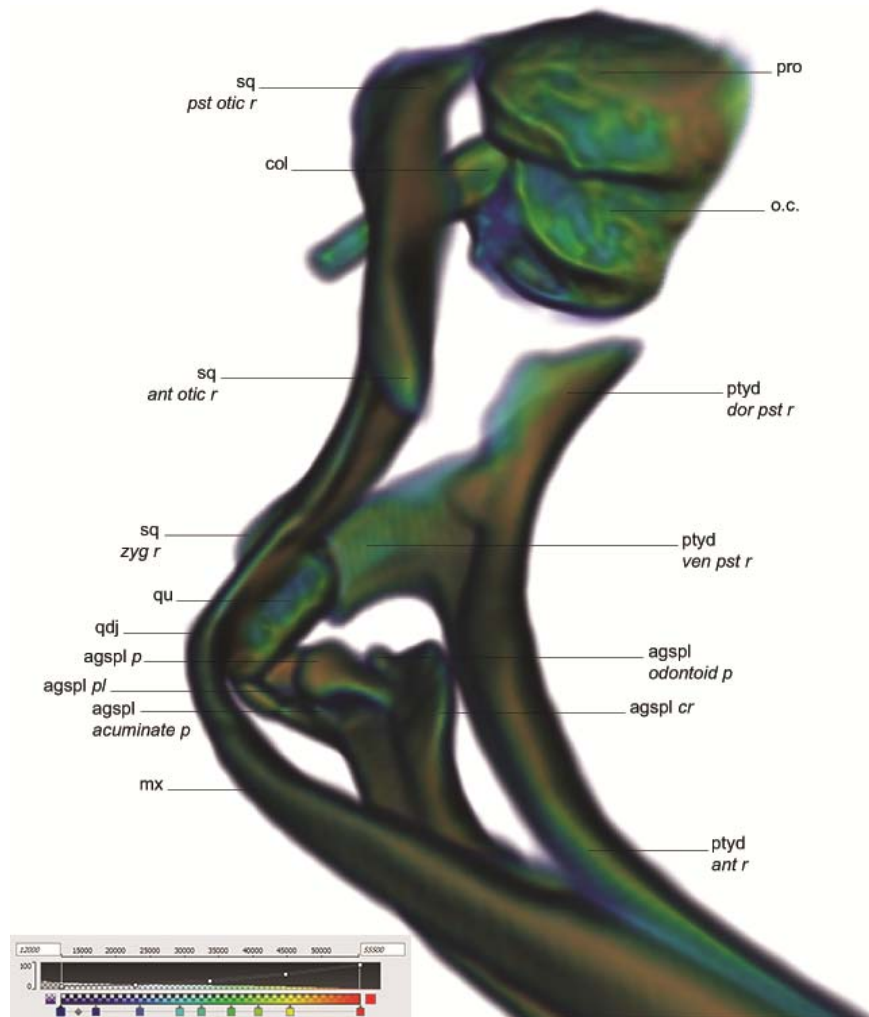


Fig. 6. Ventral view of the *Blommersia alexi* sp. nov. pectoral girdle. The dorsal coronal plane is clipped at the mandible to facilitate visualization [DRV6807 male; grey values: 12000-55500; volrenWhite and physics colormaps].

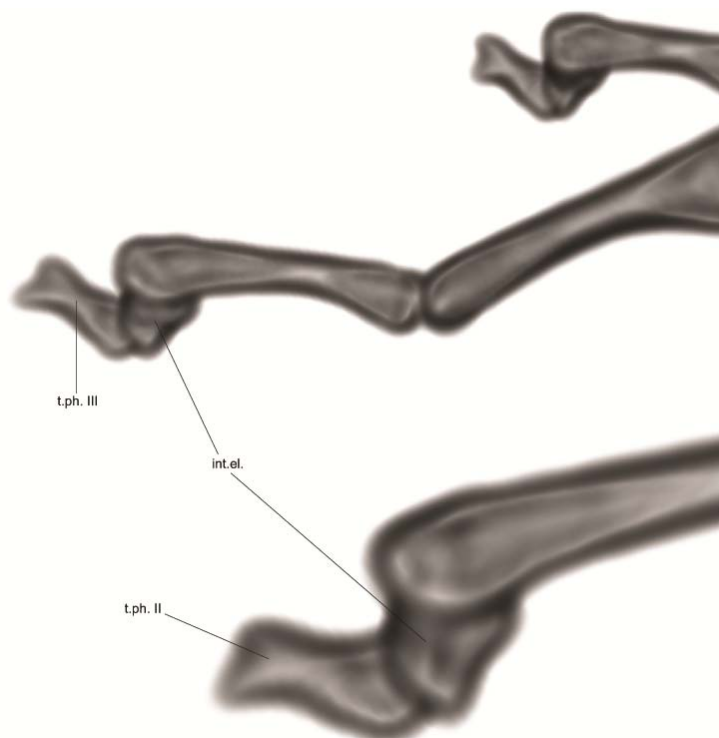
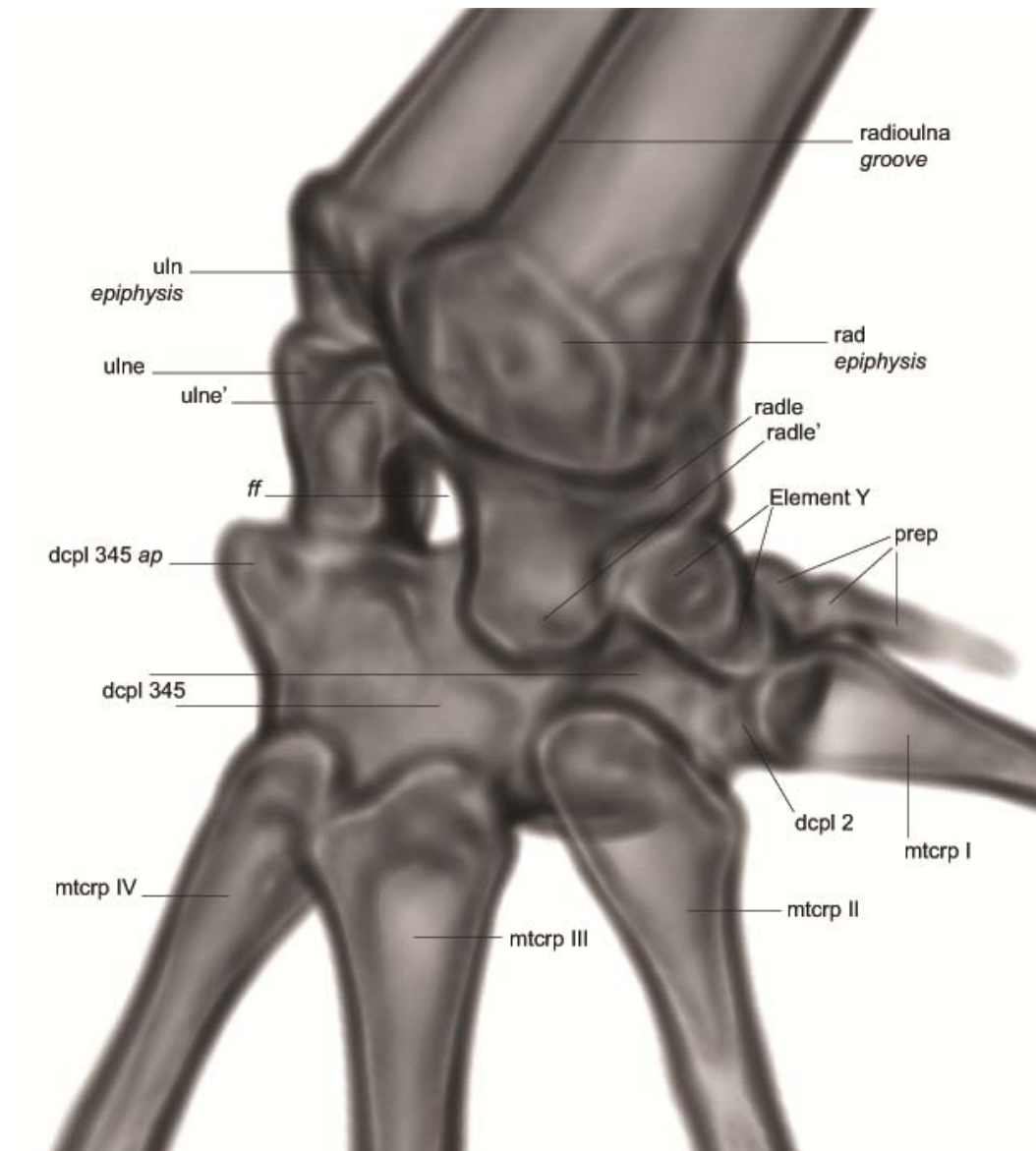


Fig. 7. Dorso-anterior view of the *Blommersia alexi* sp. nov. carpus. [DRV6836 male; grey values: 12000-55500; volrenWhite and physics* colormaps]. *This individual is relatively less developed than DRV6807, and as such is less densely ossified.

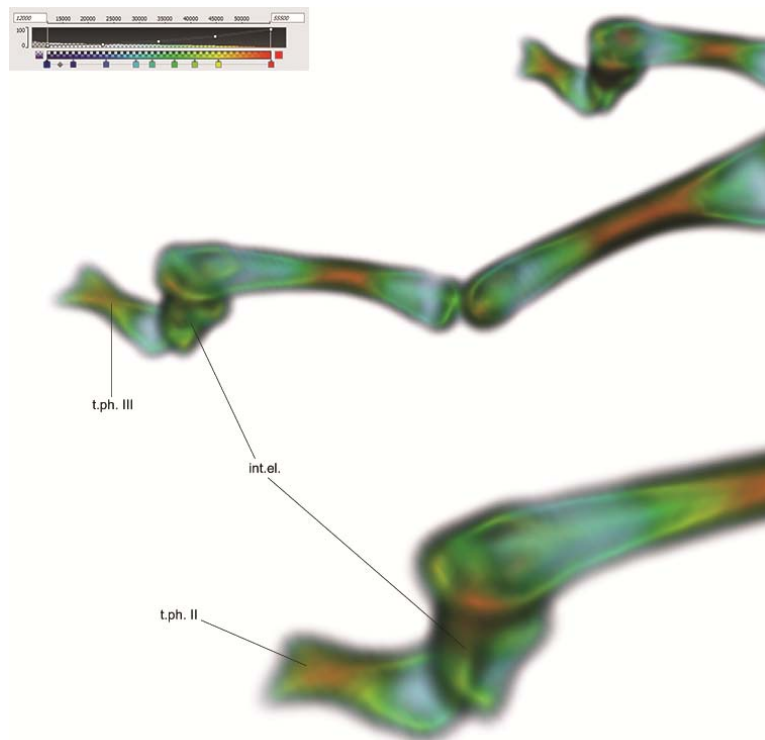
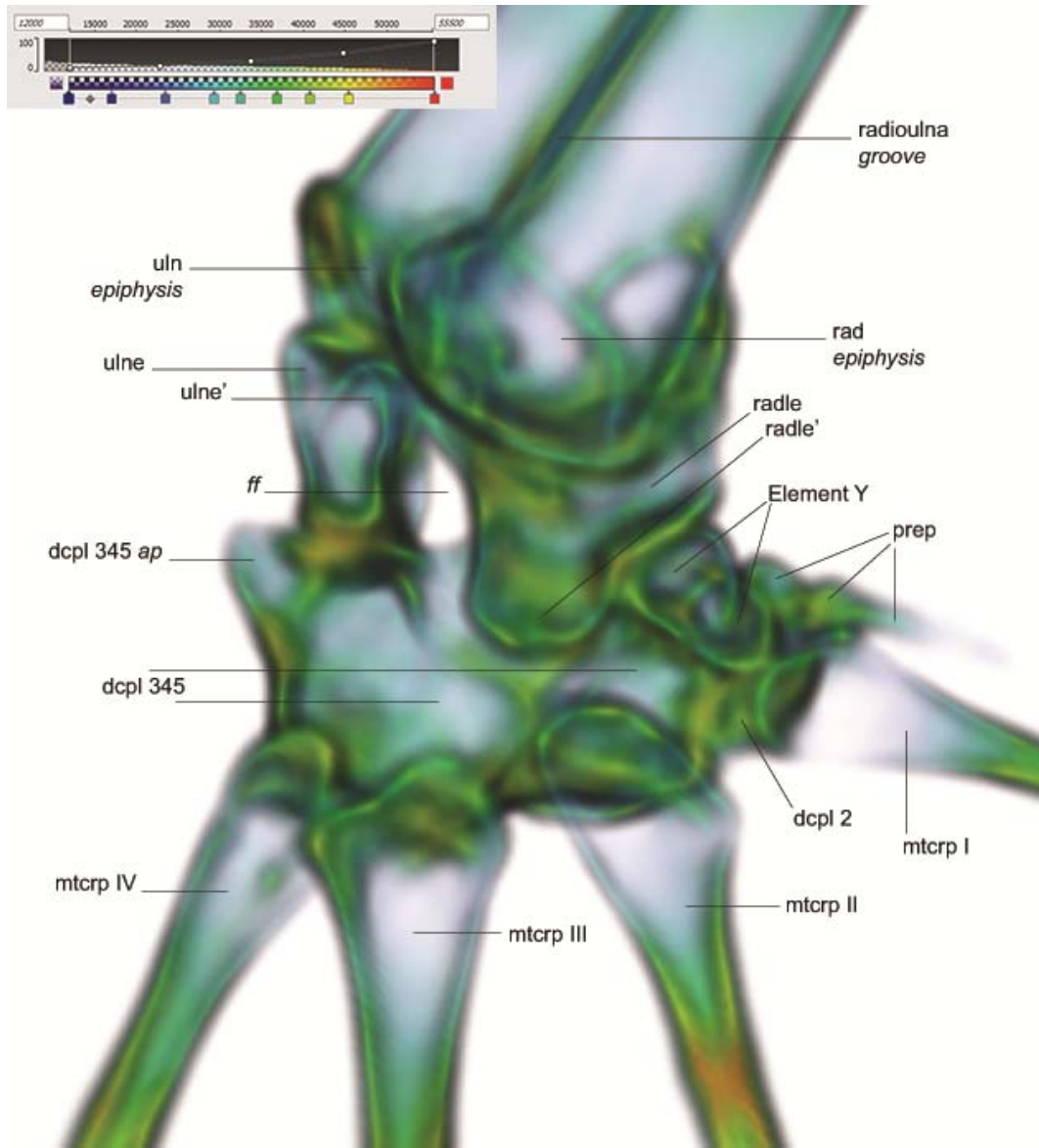


Fig. 8. Left sagittal plane, medial/preaxial view of the *Blommersia alexi* **sp. nov.** intercalary elements and terminal phalanges [DRV6807 male; grey values: 12000-55500; volrenWhite and physics colormaps].

Fig. 9. (A) Ventral view of the *Blommersia alexi* sp. nov. vertebral column. (B) Dorsal view of the *Blommersia alexi* sp. nov. vertebral column. The volumes are clipped anteriorly at the foramen magnum and posteriorly immediately before the sacrum [DRV6807 male; grey values: 12000-55500; volrenWhite and physics colormap].

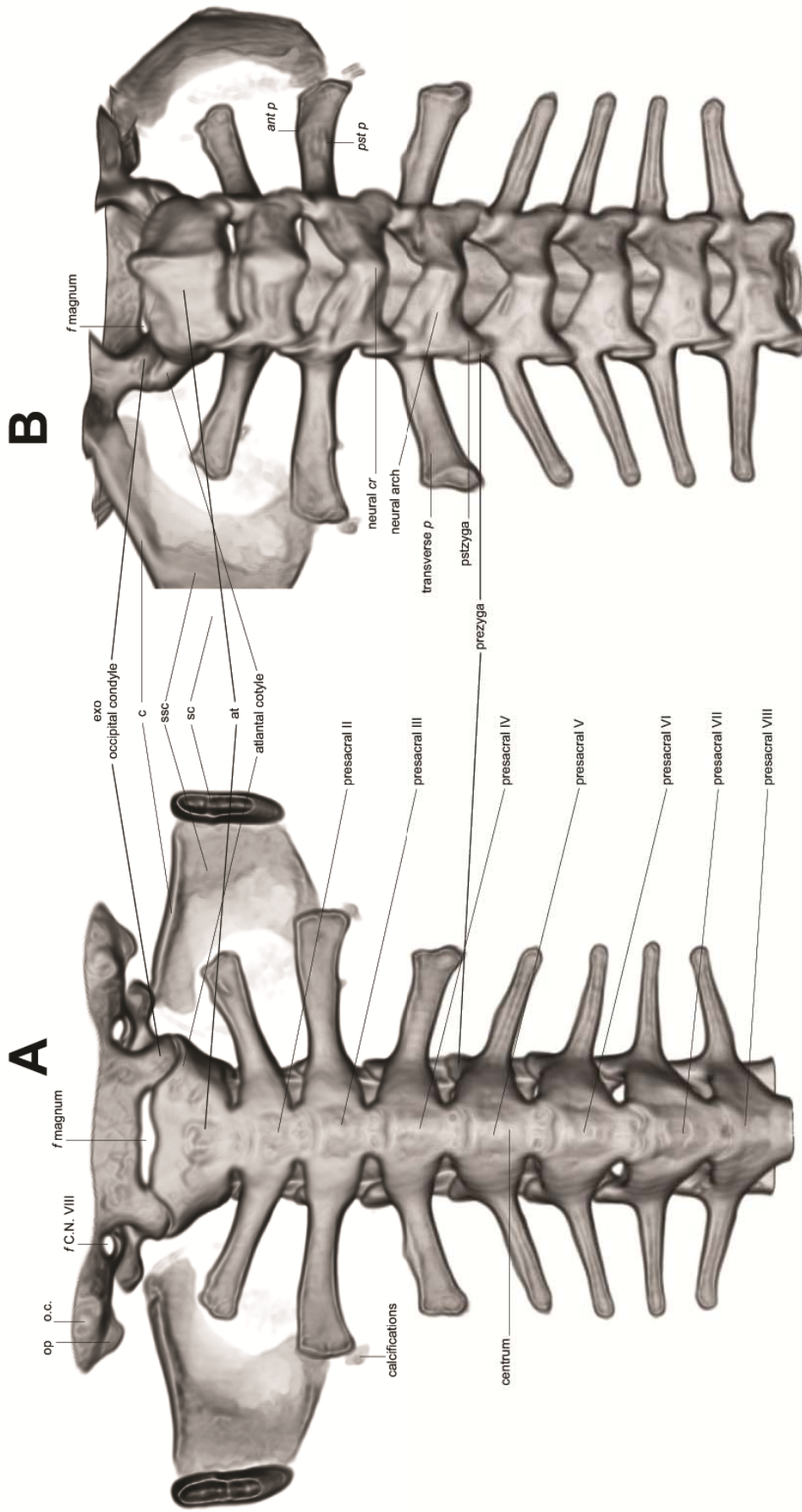
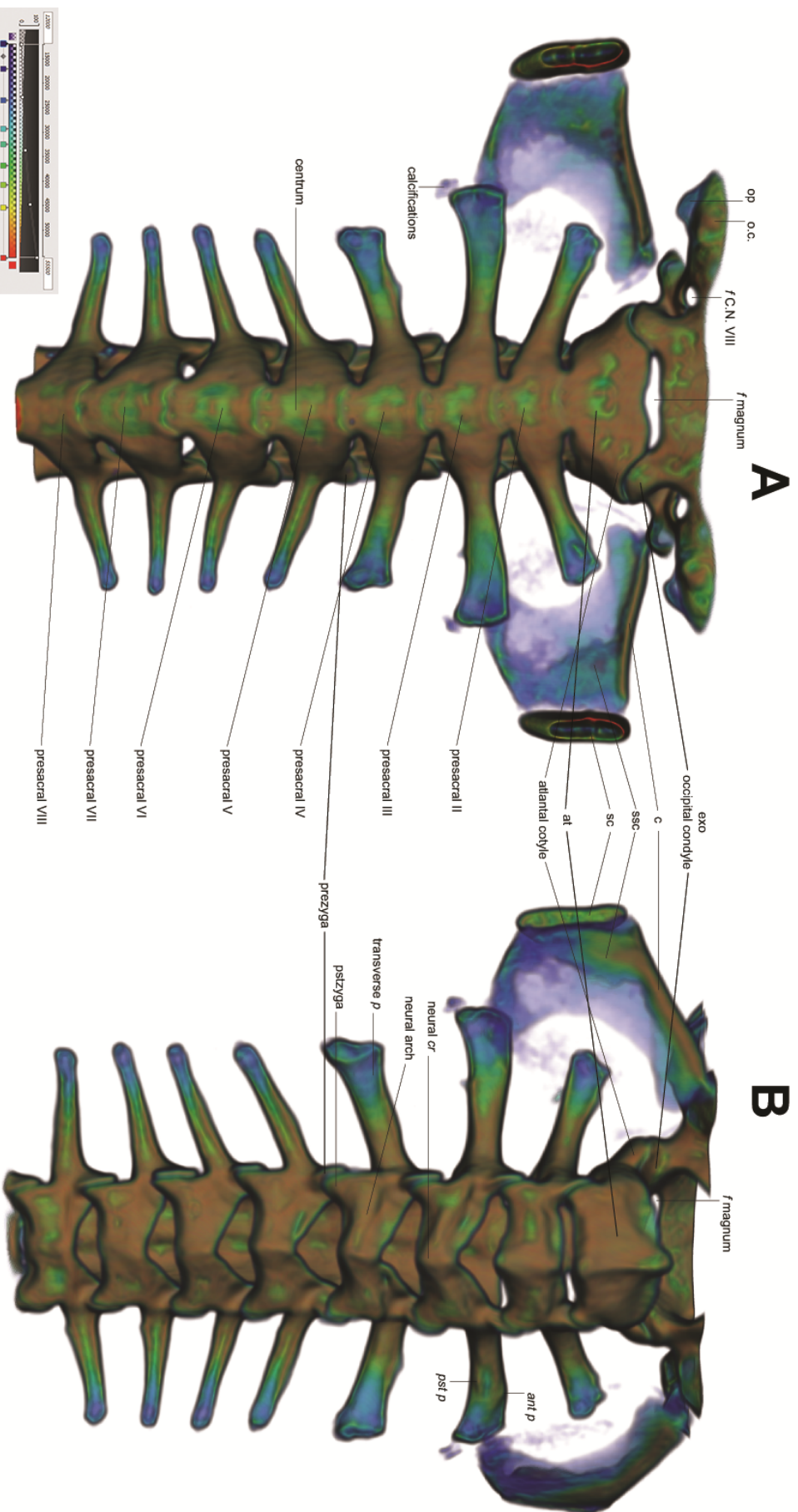


Fig. 9. (A) Ventral view of the *Blommerisia alexi* **sp. nov.** vertebral column. (B) Dorsal view of the *Blommerisia alexi* **sp. nov.** vertebral column. The volumes are clipped anteriorly at the foramen magnum and posteriorly immediately before the sacrum [DRV6807 male; grey values: 12000-55500, volrenWhite and physics colormap[s]].



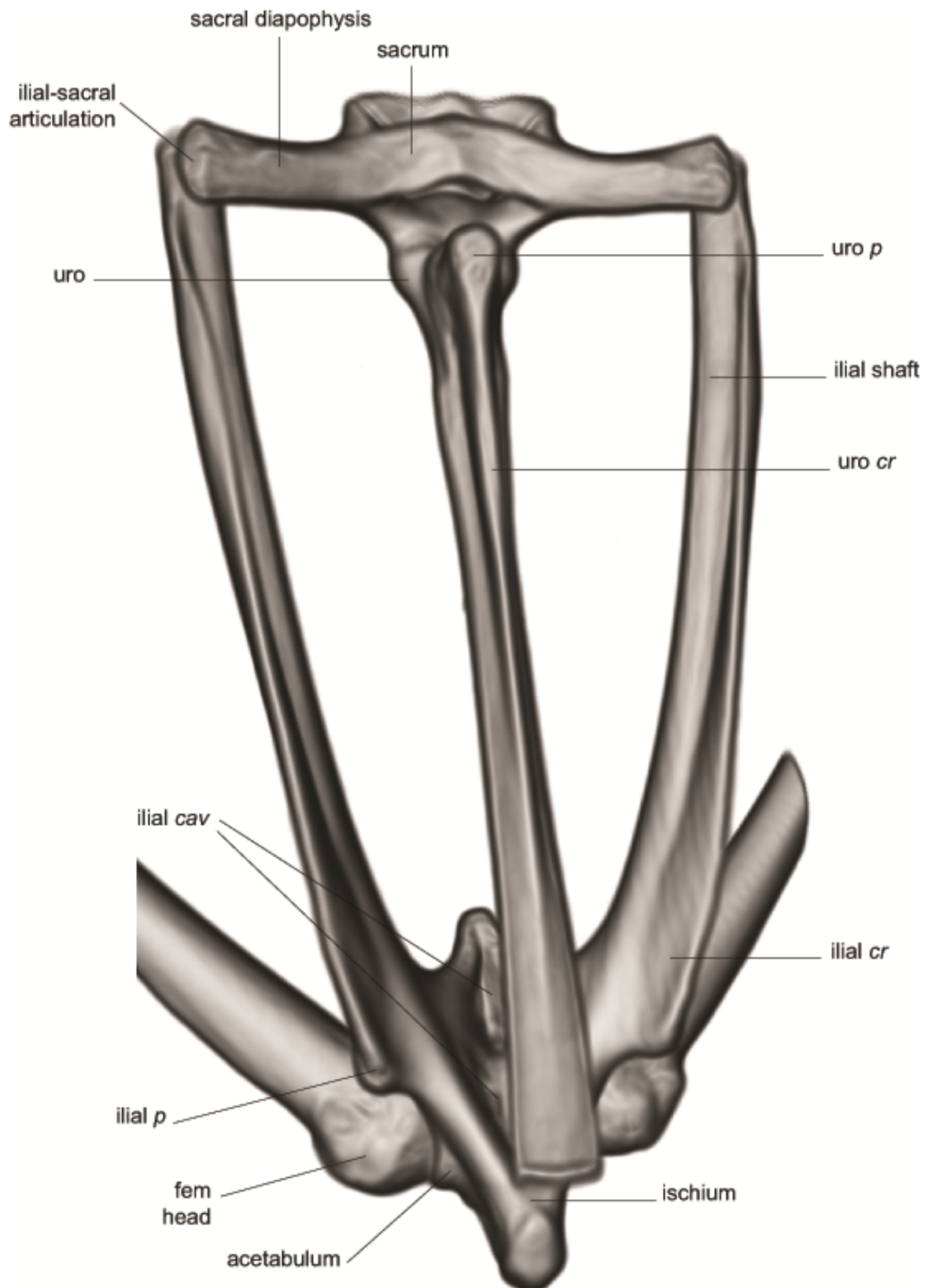


Fig. 10. Dorsal view of the *Blommersia alexi* sp. nov. pelvic girdle. The volume inclined slightly to the right and clipped anteriorly immediately after presacral VIII [DRV6807 male; grey values: 12000-55500; volrenWhite and physics colormaps].

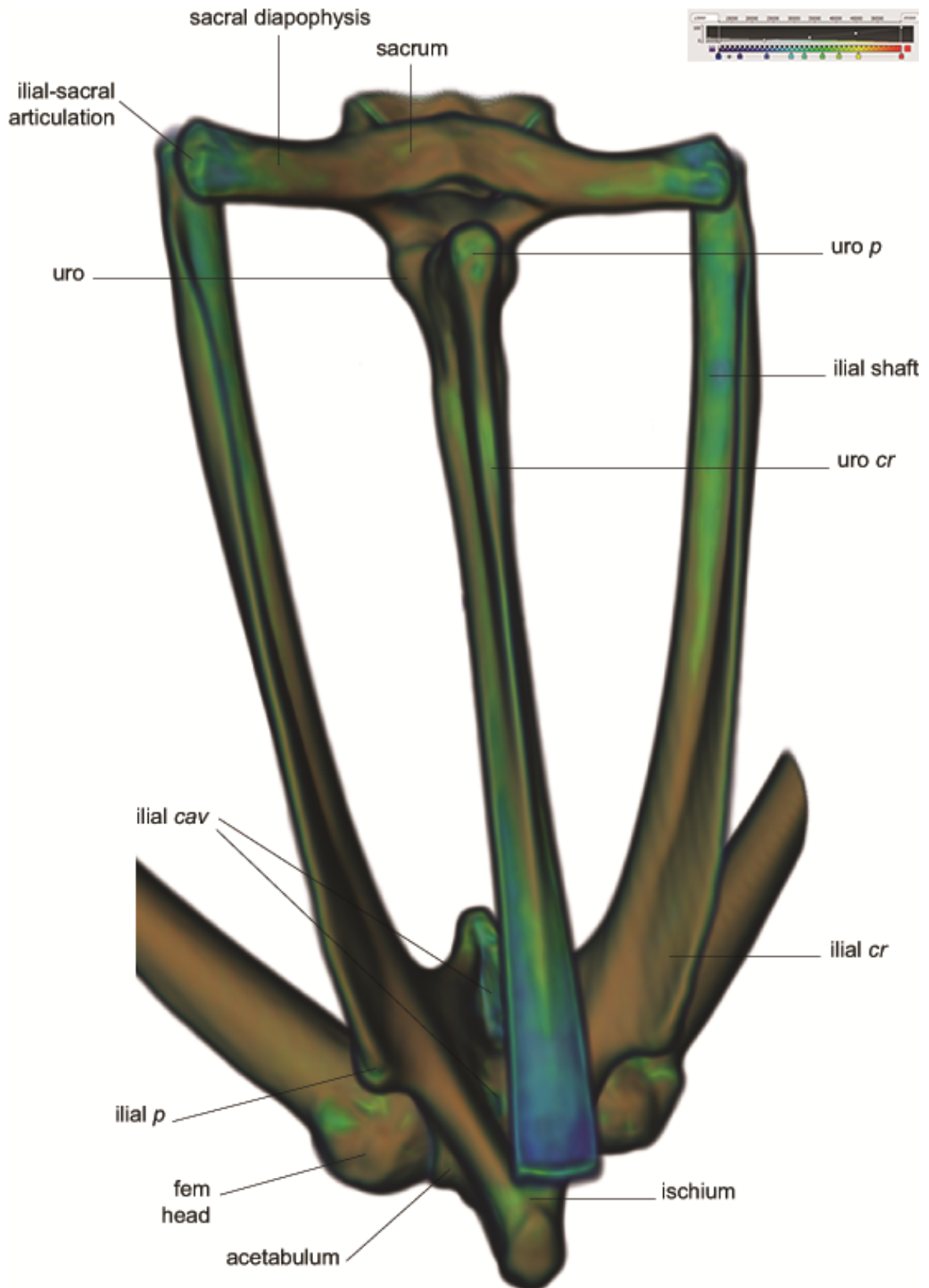


Fig. 10. Dorsal view of the *Blommersia alexi* **sp. nov.** pelvic girdle. The volume inclined slightly to the right and clipped anteriorly immediately after presacral VIII [DRV6807 male; grey values: 12000-55500; volrenWhite and physics colormaps].

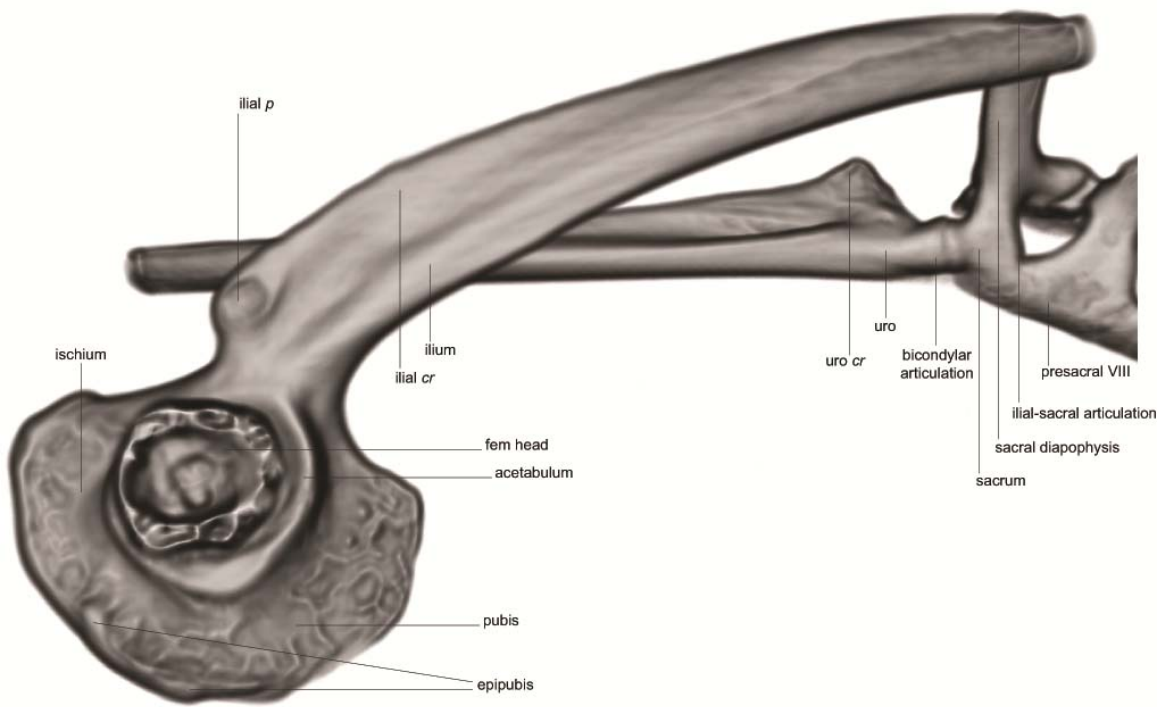
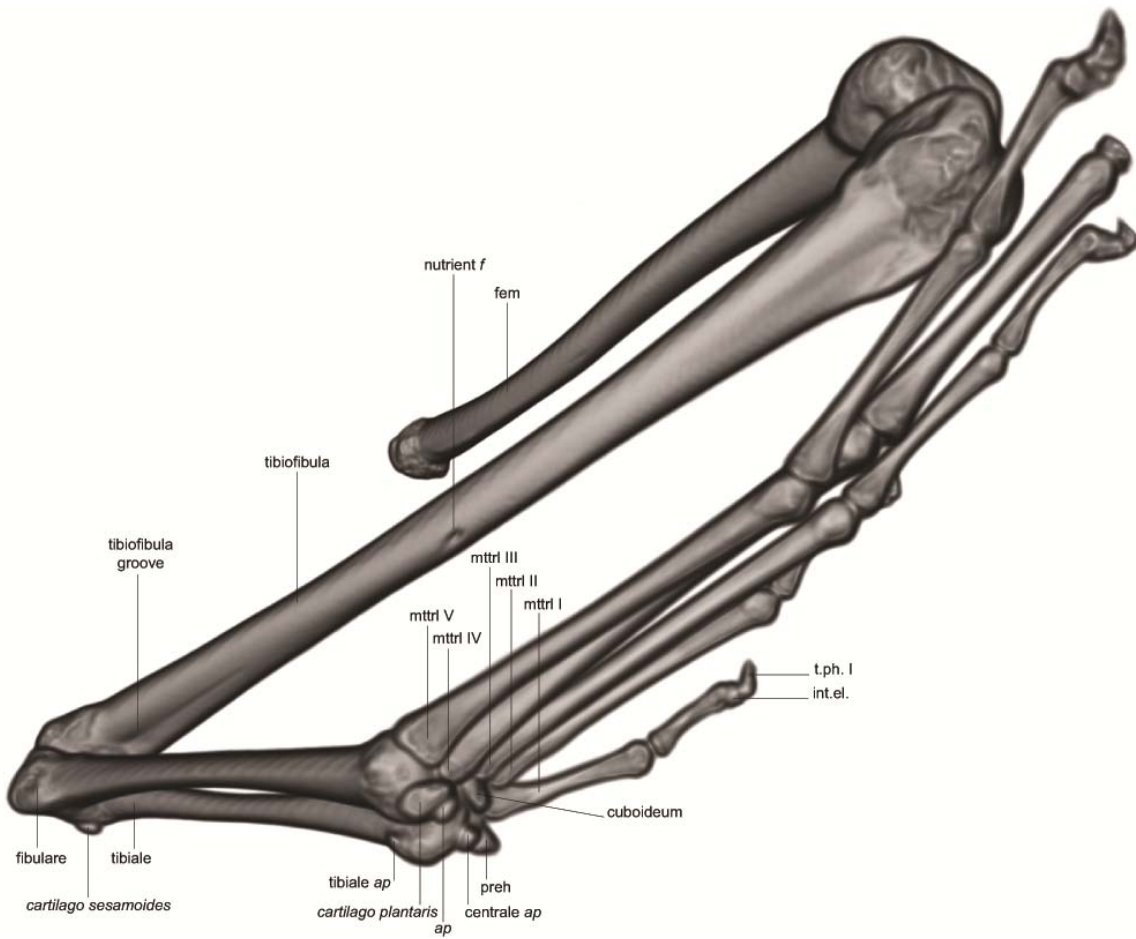


Fig. 11. Right lateral view of the *Blommersia alexi* sp. nov. pelvic girdle. The volume is clipped anteriorly at presacral VIII [DRV6807 male; grey values: 12000-55500; volrenWhite and physics colormaps].



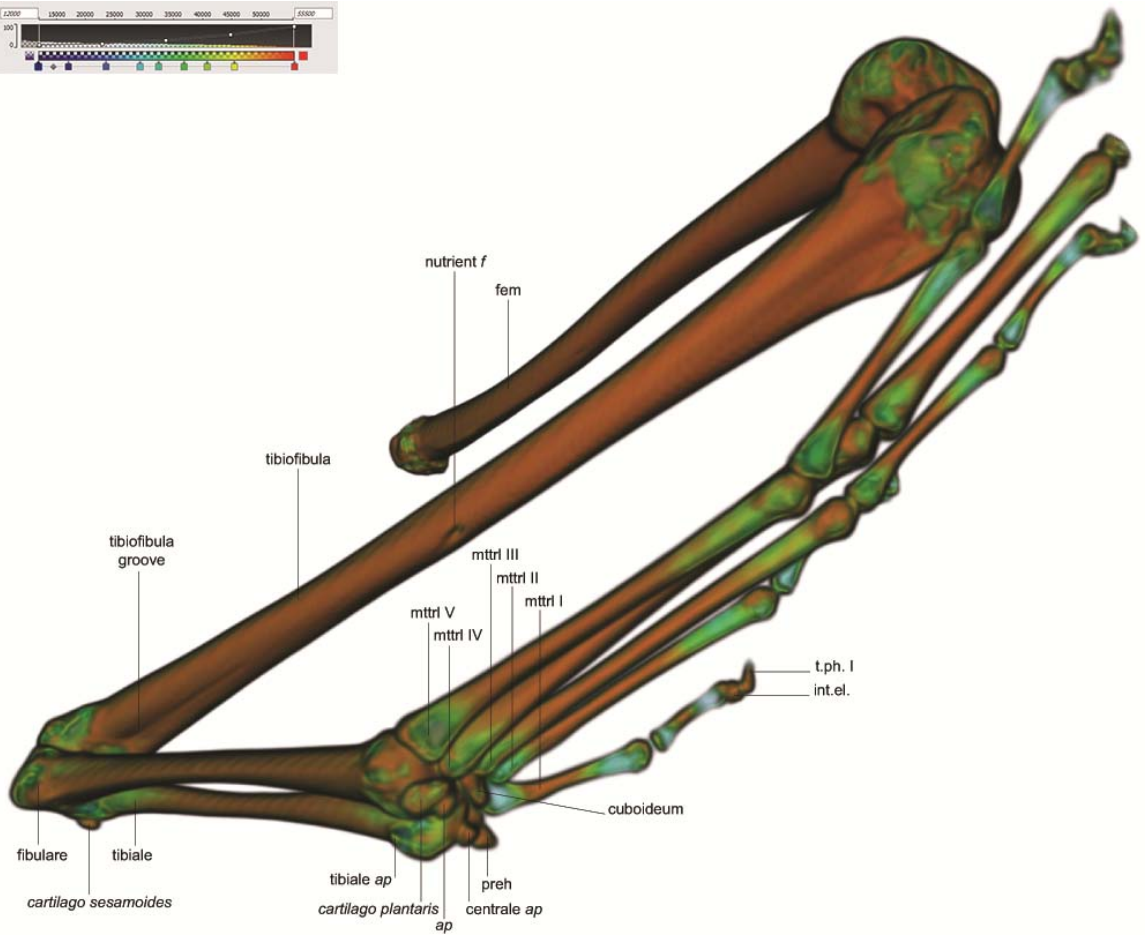
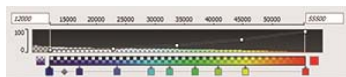
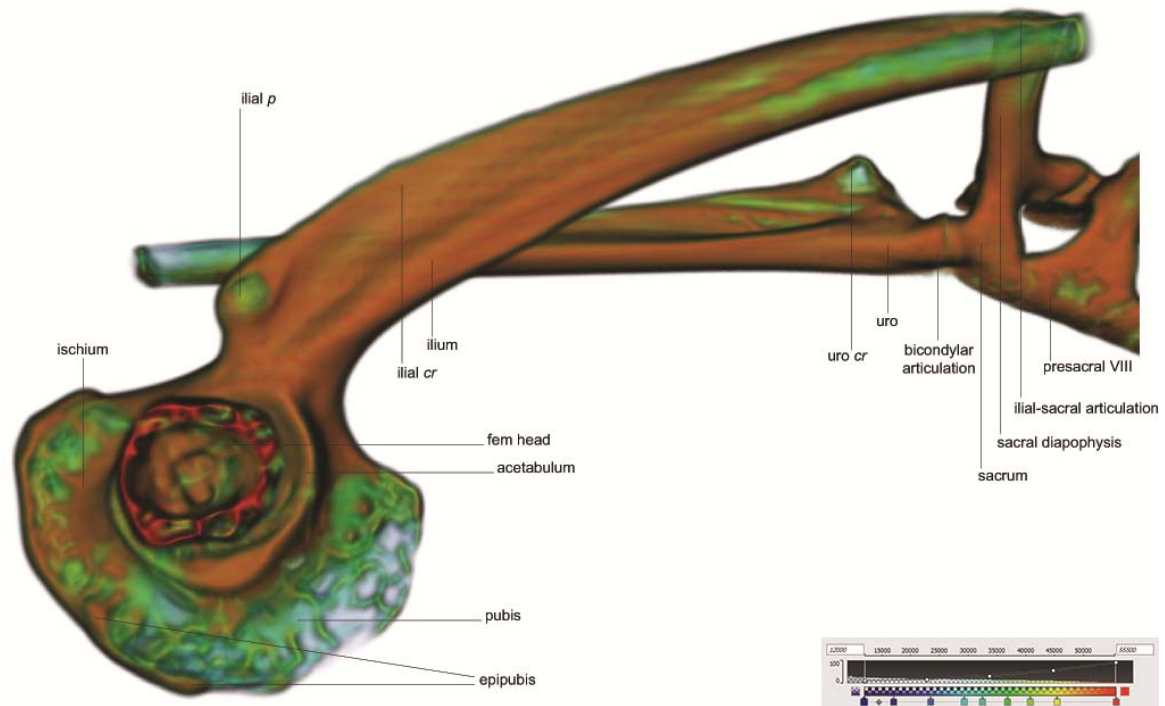


Fig. 12. Ventrolateral view of the right *Blommersia alexi* sp. nov. hindlimb [DRV6807 male; grey values: 12000-55500; volrenWhite and physics colormaps].

Table 2. Descriptive statistics and sexual dimorphism of the 123 skeletal measures taken on 10 specimens (five male / five female) of *Blommersia alexi* **sp. nov.** Measures are partitioned into anatomical regions to facilitate lecture: SVL, skull, pectoral girdle, forelimb, vertebral column, pelvic girdle, and hindlimb. Significant differences in mean length between males and females ($\alpha = 0.05$) are shown in bold. Abbreviations follow those indicated in the description of the measurements (Appendix S1).

(mm)	N	range	min	max	Sexual dimorphism	partial eta-squared	Median	Mean	sd	Asymmetry	Kurtosis
SVLext	10	5.88	24.50	30.38			27.25	27.34	2.0697	-.06	-1.39
	F	5			0.378	0.10		27.96	2.4016		
	M	5						26.73	1.7102		
SVLsk	10	6.26	23.81	30.07			25.40	26.19	2.3977	.83	-.86
	F	5			0.057	0.38		27.59	2.5957		
	M	5						24.79	1.1287		
SVLsum	10	6.39	27.00	33.39			28.38	29.55	2.6265	.44	-1.96
	F	5			0.190	0.20		30.68	2.8591		
	M	5						28.43	2.0457		
skullL	10	2.10	9.66	11.76			10.18	10.43	.7760	.75	-1.00
	F	5			0.021	0.51		10.96	.7450		
	M	5						9.91	.3371		
skullW	10	2.69	8.90	11.59			9.68	10.06	.9223	.65	-.98
	F	5			0.048	0.40		10.62	.9380		
	M	5						9.50	.5103		
oticsW	10	1.46	6.07	7.52			6.54	6.65	.4933	.94	-.01
	F	5			0.152	0.24		6.88	.5908		
	M	5						6.42	.2599		
colmL	10	.48	1.18	1.66			1.41	1.44	.1395	-.08	.15
	F	5			0.271	0.15		1.49	.1304		
	M	5						1.39	.1423		
pmaxH	10	.49	1.33	1.82			1.50	1.52	.1683	.87	-.25
	F	5			0.102	0.30		1.61	.2006		
	M	5						1.43	.0666		
pmaxW	10	.40	.88	1.28			1.02	1.05	.1314	.71	-.45
	F	5			0.027	0.48		1.14	.1279		
	M	5						.97	.0633		
pmaxD	10	.31	.84	1.15			1.00	1.01	.0882	-.50	.81
	F	5			0.049	0.40		1.07	.0717		
	M	5						.96	.0731		
MmblL	10	.38	.60	.98			.77	.79	.1093	.15	.14
	F	5			0.973	0.00		.79	.0901		
	M	5						.79	.1370		
maxL	10	2.51	9.18	11.69			9.87	10.11	.8783	1.10	.11
	F	5			0.037	0.44		10.66	.9177		
	M	5						9.56	.3621		
mandL	10	1.86	8.71	10.57			9.39	9.54	.6356	.61	-.61
	F	5			0.022	0.50		9.97	.5811		
	M	5						9.12	.3419		
nasL	10	.90	2.81	3.70			3.17	3.19	.2648	.53	.14
	F	5			0.014	0.55		3.37	.2149		
	M	5						3.00	.1553		
nasW	10	.49	1.42	1.91			1.67	1.68	.1509	.06	-.41
	F	5			0.901	0.00		1.68	.1423		
	M	5						1.67	.1757		
intnasW	6	.31	.80	1.11			.95	.97	.1094	-.24	-.13
	F	3			0.455	0.15		1.00	.0900		
	M	3						.93	.1322		
intnsptH	6	.41	1.19	1.60			1.34	1.39	.1705	.43	-1.76
	F	3			0.696	0.04		1.42	.1618		
	M	3						1.36	.2085		
sphH	10	.61	1.08	1.69			1.34	1.36	.1900	.48	-.28
	F	5			0.639	0.03		1.39	.2610		
	M	5						1.33	.1037		
sphW	10	.68	2.50	3.18			2.86	2.82	.2080	.02	-.53
	F	5			0.007	0.62		2.98	.1275		
	M	5						2.67	.1431		
frptL	10	1.02	5.06	6.08			5.44	5.48	.3383	.97	.36
	F	5			0.070	0.35		5.67	.3623		
	M	5						5.29	.1877		
frptW	10	.32	1.54	1.86			1.68	1.68	.0904	.46	.62
	F	5			0.258	0.16		1.71	.1012		
	M	5						1.64	.0727		
proH	10	.76	2.11	2.87			2.42	2.46	.2216	.51	.39
	F	5			0.452	0.07		2.52	.3035		
	M	5						2.41	.1018		

(mm)	N	range	min	max	Sexual dimorphism	partial eta-squared	Median	Mean	sd	Asymmetry	Kurtosis
exoL	10	.60	2.73	3.33			2.86	2.91	.1795	1.61	2.75
F	5				0.137	0.25		3.00	.2267		
M	5							2.82	.0515		
psphH	10	.73	3.16	3.88			3.48	3.52	.2438	.25	-.97
F	5				0.015	0.54		3.69	.2056		
M	5							3.35	.1372		
psphW	10	.84	4.15	4.99			4.66	4.63	.2598	-.50	-.29
F	5				0.551	0.05		4.68	.2166		
M	5							4.57	.3130		
vomH	10	.30	1.00	1.29			1.14	1.17	.1039	-.23	-1.12
F	5				0.094	0.31		1.22	.0739		
M	5							1.11	.1061		
vomW	10	.70	1.07	1.77			1.52	1.48	.2276	-.39	-.67
F	5				0.123	0.27		1.59	.1739		
M	5							1.37	.2341		
pltnL	10	1.05	2.61	3.65			2.99	3.02	.2991	.85	1.19
F	5				0.029	0.47		3.21	.2802		
M	5							2.83	.1688		
ptygdH	10	.92	1.68	2.60			1.93	2.01	.2573	1.29	2.33
F	5				0.027	0.48		2.18	.2592		
M	5							1.84	.1045		
ptygdW	10	1.64	4.84	6.48			5.59	5.59	.6036	.25	-1.11
F	5				0.036	0.44		5.97	.5141		
M	5							5.21	.4383		
squaH	10	1.02	2.44	3.45			2.77	2.80	.3014	1.29	1.48
F	5				0.079	0.34		2.97	.3383		
M	5							2.64	.1458		
squaW	10	1.05	2.45	3.51			2.83	2.89	.3322	1.02	.50
F	5				0.048	0.40		3.09	.3481		
M	5							2.69	.1637		
hyoL	10	.52	2.70	3.22			3.00	2.98	.1757	-.28	-1.04
F	5				0.498	0.06		3.02	.1998		
M	5							2.94	.1594		
omostH	10	.38	1.38	1.76			1.45	1.52	.1306	1.05	-.57
F	5				0.041	0.43		1.60	.1448		
M	5							1.43	.0320		
omostL	10	.42	1.28	1.70			1.40	1.43	.1280	1.09	.71
F	5				0.252	0.16		1.48	.1256		
M	5							1.39	.1233		
clavL	10	1.21	2.96	4.17			3.32	3.38	.3683	1.19	1.32
F	5				0.113	0.28		3.56	.4436		
M	5							3.19	.1474		
clav_pL	10	.49	.63	1.12			.73	.79	.1494	1.19	1.17
F	5				0.291	0.14		.84	.1801		
M	5							.74	.1041		
coraL	10	.92	2.68	3.60			2.98	3.05	.2605	.89	1.17
F	5				0.430	0.08		3.12	.3600		
M	5							2.98	.1045		
sterH	10	.74	1.28	2.02			1.63	1.63	.2651	.24	-1.14
F	5				0.127	0.27		1.76	.2554		
M	5							1.50	.2256		
sterWsup	10	.30	.88	1.17			.99	1.01	.0894	.56	-.13
F	5				0.079	0.34		1.06	.0909		
M	5							.96	.0606		
sterWmin	10	.36	.37	.73			.50	.50	.1086	.84	.67
F	5				0.144	0.25		.56	.1192		
M	5							.45	.0761		
sterWinf	10	.47	.42	.89			.58	.61	.1465	.74	.13
F	5				0.014	0.55		.71	.1286		
M	5							.51	.0706		
scapL	10	.85	3.08	3.93			3.41	3.48	.2965	.29	-1.38
F	5				0.334	0.12		3.57	.3817		
M	5							3.38	.1702		
cleilL	10	.80	2.61	3.40			2.78	2.86	.2499	1.32	1.37
F	5				0.488	0.06		2.92	.3402		
M	5							2.80	.1266		
supraH	10	.50	1.40	1.90			1.52	1.54	.1530	1.53	2.54
F	5				0.273	0.15		1.60	.2041		
M	5							1.49	.0568		
supraW	10	.88	1.94	2.82			2.22	2.26	.2886	.75	-.19
F	5				0.335	0.12		2.36	.3604		
M	5							2.17	.1889		

(mm)	N	range	min	max	Sexual dimorphism	partial eta-squared	Median	Mean	sd	Asymmetry	Kurtosis
humLcap	10	1.76	6.88	8.64			7.45	7.59	.5982	.76	-.79
	F	5			0.100	0.30		7.90	.7231		
	M	5						7.27	.1978		
humLtroc	10	1.78	6.94	8.72			7.49	7.62	.6147	.81	-.74
	F	5			0.086	0.32		7.95	.7281		
	M	5						7.29	.2103		
dltd_crH	10	.23	.45	.68			.53	.55	.0717	.71	-.26
	F	5			0.122	0.27		.58	.0697		
	M	5						.51	.0595		
dltd_crW	10	.87	1.86	2.73			2.01	2.18	.3373	.67	-1.36
	F	5			0.766	0.01		2.22	.4341		
	M	5						2.15	.2541		
radulnL	10	1.30	5.05	6.35			5.37	5.51	.4171	1.24	.69
	F	5			0.106	0.29		5.72	.5148		
	M	5						5.29	.1089		
mtcpl1	10	.82	1.99	2.81			2.30	2.32	.2341	.77	.93
	F	5			0.439	0.08		2.38	.3244		
	M	5						2.26	.0930		
mtcpl2	10	1.07	2.31	3.38			2.68	2.70	.3162	1.02	1.19
	F	5			0.485	0.06		2.77	.4334		
	M	5						2.62	.1515		
mtcpl3	10	.88	2.85	3.73			3.02	3.11	.2586	1.66	3.20
	F	5			0.246	0.16		3.21	.3395		
	M	5						3.01	.1029		
mtcpl4	10	.89	2.24	3.13			2.50	2.57	.2502	1.15	1.84
	F	5			0.387	0.09		2.65	.3533		
	M	5						2.50	.0518		
hand_ph1L1	10	.52	1.21	1.73			1.38	1.43	.1628	.57	-.49
	F	5			0.311	0.13		1.49	.2140		
	M	5						1.38	.0791		
hand_tph1L	10	.26	.50	.75			.62	.62	.0823	.46	-.21
	F	5			0.517	0.05		.64	.1118		
	M	5						.60	.0438		
hand_D1	10	1.59	3.70	5.29			4.35	4.38	.4643	.68	.39
	F	5			0.390	0.09		4.51	.6419		
	M	5						4.24	.1661		
hand_ph2L1	10	.55	1.55	2.10			1.80	1.79	.1671	.40	-.36
	F	5			0.475	0.07		1.83	.2246		
	M	5						1.75	.0907		
hand_tph2L	10	.27	.56	.82			.67	.68	.0830	.15	-.63
	F	5			0.573	0.04		.69	.1001		
	M	5						.66	.0695		
hand_D2	10	1.77	4.53	6.30			5.13	5.17	.5391	.90	.74
	F	5			0.473	0.07		5.30	.7354		
	M	5						5.04	.2641		
hand_ph3L1	10	.59	1.73	2.32			1.82	1.90	.1902	1.36	1.38
	F	5			0.201	0.20		1.98	.2422		
	M	5						1.82	.0827		
hand_ph3L2	9	.32	1.56	1.88			1.64	1.68	.1019	.96	.39
	F	4			0.033	0.50		1.75	.1035		
	M	5						1.62	.0483		
hand_tph3L	10	.20	.66	.86			.78	.77	.0563	-.34	.80
	F	5			0.657	0.03		.78	.0773		
	M	5						.76	.0311		
hand_D3	9	1.75	7.03	8.78			7.33	7.51	.5729	1.58	2.42
	F	4			0.070	0.40		7.89	.7039		
	M	5						7.20	.1606		
hand_ph4L1	10	.50	1.18	1.68			1.31	1.34	.1382	1.69	4.23
	F	5			0.457	0.07		1.37	.1852		
	M	5						1.30	.0749		
hand_ph4L2	10	.50	1.13	1.64			1.38	1.37	.1477	-.08	.26
	F	5			0.296	0.14		1.43	.1850		
	M	5						1.32	.0908		
hand_tph4L	10	.24	.65	.89			.75	.76	.0673	.15	.44
	F	5			0.945	0.00		.77	.0933		
	M	5						.76	.0385		
hand_D4	10	2.11	5.21	7.32			5.95	6.05	.5734	1.02	2.17
	F	5			0.406	0.09		6.21	.7880		
	M	5						5.89	.2324		

(mm)	N	range	min	max	Sexual dimorphism	partial eta-squared	Median	Mean	sd	Asymmetry	Kurtosis
column	10	2.73	7.74	10.47			8.35	8.70	.9767	.78	-.75
	F	5			0.255	0.16		9.07	1.2317		
	M	5						8.33	.5386		
atlasH	10	.38	.88	1.26			1.09	1.06	.1266	-.21	-.66
	F	5			0.240	0.17		1.11	.1441		
	M	5						1.01	.0963		
V2H	10	.22	.74	.96			.81	.83	.0769	.59	-1.14
	F	5			0.209	0.19		.86	.0942		
	M	5						.80	.0438		
V3H	10	.17	.87	1.05			.95	.95	.0596	.61	-.51
	F	5			0.453	0.07		.96	.0828		
	M	5						.93	.0236		
V4H	10	.33	.88	1.21			.95	.99	.1106	.88	-.03
	F	5			0.343	0.11		1.02	.1422		
	M	5						.95	.0647		
V5H	10	.50	.79	1.29			.97	1.00	.1549	.63	-.41
	F	5			0.501	0.06		1.04	.1947		
	M	5						.96	.1136		
V6H	10	.43	.90	1.33			1.06	1.07	.1487	.48	-.82
	F	5			0.623	0.03		1.10	.1960		
	M	5						1.05	.0989		
V7H	10	.48	.92	1.40			1.04	1.09	.1657	1.10	.04
	F	5			0.216	0.18		1.16	.2022		
	M	5						1.03	.0973		
V8H	10	.48	.76	1.24			.98	1.00	.1706	.21	-1.47
	F	5			0.147	0.24		1.08	.1787		
	M	5						.92	.1325		
sacrumH	10	.25	.58	.83			.69	.70	.0821	.16	-.96
	F	5			0.287	0.14		.73	.0993		
	M	5						.67	.0564		
V2_tpL	10	1.21	3.98	5.19			4.48	4.58	.4348	.47	-1.23
	F	5			0.493	0.06		4.68	.4978		
	M	5						4.48	.3896		
V3_tpL	10	1.41	5.36	6.78			5.81	5.91	.4793	.50	-.85
	F	5			0.131	0.26		6.14	.4940		
	M	5						5.68	.3713		
V4_tpL	10	1.45	4.65	6.11			4.97	5.20	.4978	.71	-.93
	F	5			0.215	0.19		5.41	.6095		
	M	5						5.00	.2879		
V5_tpL	10	1.16	4.63	5.79			5.00	5.11	.4534	.28	-1.92
	F	5			0.332	0.12		5.26	.5376		
	M	5						4.96	.3449		
V6_tpL	10	.93	4.74	5.67			5.05	5.15	.3901	.25	-2.06
	F	5			0.363	0.10		5.26	.4300		
	M	5						5.03	.3491		
V7_tpL	9	.93	4.62	5.55			5.11	5.06	.4058	.11	-2.13
	F	5			0.701	0.02		5.11	.4475		
	M	4						5.00	.4028		
V8_tpL	10	1.12	4.27	5.39			4.63	4.78	.4408	.25	-1.99
	F	5			0.476	0.07		4.89	.4585		
	M	5						4.67	.4454		
sacrum_tpL	10	1.74	3.47	5.21			4.28	4.43	.6165	-.07	-1.41
	F	5			0.167	0.22		4.71	.5889		
	M	5						4.16	.5631		

(mm)	N	range	min	max	Sexual dimorphism	partial eta-squared	Median	Mean	sd	Asymmetry	Kurtosis
uroL	10	2.10	7.41	9.51			7.88	8.14	.7067	.81	-.38
F	5				0.187	0.21		8.44	.8395		
M	5							7.83	.4326		
uroH	10	.38	1.33	1.71			1.39	1.47	.1540	.64	-1.61
F	5				0.110	0.29		1.55	.1748		
M	5							1.39	.0862		
uro_crL	10	1.87	3.89	5.76			4.86	4.89	.5031	-.30	1.20
F	5				0.075	0.34		4.61	.4577		
M	5							5.17	.4051		
uro_crH	10	.38	.85	1.22			.96	1.00	.1249	.63	-.74
F	5				0.185	0.21		1.05	.1473		
M	5							.94	.0780		
iiiL	10	2.07	7.38	9.45			7.95	8.21	.7354	.63	-1.13
F	5				0.097	0.31		8.59	.8214		
M	5							7.82	.4107		
pelvL	10	2.57	9.17	11.74			9.96	10.21	.8862	.67	-.96
F	5				0.103	0.30		10.67	1.0088		
M	5							9.76	.4731		
pelwL	9	1.16	3.28	4.44			3.52	3.69	.4066	1.22	.25
F	4				0.072	0.39		3.96	.5002		
M	5							3.47	.1169		
epipH	9	.60	1.74	2.34			1.89	1.95	.2297	1.18	.05
F	4				0.136	0.29		2.08	.2972		
M	5							1.85	.0941		
epipW	9	.33	.60	.92			.76	.76	.1097	-.15	-.81
F	4				0.067	0.40		.84	.0776		
M	5							.71	.0993		
femL	10	3.50	12.59	16.09			13.88	13.96	1.2775	.72	-.64
F	5				0.065	0.36		14.69	1.3972		
M	5							13.23	.6217		
tibfibL	10	4.27	14.58	18.85			16.11	16.22	1.5427	.54	-.94
F	5				0.100	0.30		17.03	1.6892		
M	5							15.42	.9421		
tibfiblL	10	1.84	7.58	9.42			8.16	8.29	.6216	.75	-.52
F	5				0.093	0.31		8.62	.7146		
M	5							7.96	.2947		
mttrs1	10	.73	1.90	2.63			2.13	2.14	.2259	1.03	1.43
F	5				0.662	0.03		2.17	.3037		
M	5							2.10	.1405		
mttrs2	10	1.28	3.64	4.92			4.01	4.07	.3789	1.36	2.16
F	5				0.209	0.19		4.22	.4891		
M	5							3.91	.1509		
mttrs3	10	1.40	4.81	6.21			5.23	5.31	.4189	1.17	1.39
F	5				0.237	0.17		5.47	.5367		
M	5							5.15	.1997		
mttrs4	10	1.36	5.75	7.10			6.07	6.21	.4721	1.07	.07
F	5				0.124	0.27		6.44	.5568		
M	5							5.97	.2370		
mttrs5	10	1.34	5.04	6.38			5.34	5.47	.4243	1.17	1.06
F	5				0.153	0.24		5.67	.5045		
M	5							5.27	.2330		

(mm)	N	range	min	max	Sexual dimorphism	partial eta-squared	Median	Mean	sd	Asymmetry	Kurtosis
foot_ph1L1	10	.50	.97	1.47			1.18	1.20	.1483	.32	-.13
F	5							1.23	.2025		
M	5				0.519	0.05		1.17	.0761		
foot_tph1L	10	.24	.39	.63			.49	.49	.0662	.65	1.24
F	5							.51	.0876		
M	5				0.383	0.10		.47	.0353		
foot_D1	10	1.46	3.26	4.72			3.80	3.82	.4315	.81	.86
F	5							3.91	.5827		
M	5				0.560	0.04		3.74	.2469		
foot_ph2L1	10	.67	1.65	2.32			1.75	1.83	.2101	1.59	2.59
F	5							1.91	.2795		
M	5				0.226	0.18		1.74	.0603		
foot_tph2L	10	.23	.49	.72			.56	.57	.0642	1.58	4.08
F	5							.59	.0836		
M	5				0.410	0.09		.55	.0386		
foot_D2	10	2.14	5.82	7.96			6.33	6.46	.6259	1.68	3.39
F	5							6.72	.8114		
M	5				0.210	0.19		6.20	.2383		
foot_ph3L1	10	.81	2.20	3.02			2.42	2.47	.2669	1.03	.41
F	5							2.60	.3258		
M	5				0.133	0.26		2.35	.1121		
foot_ph3L2	10	.50	1.50	2.01			1.59	1.65	.1619	1.32	1.48
F	5							1.72	.1994		
M	5				0.162	0.23		1.57	.0756		
foot_tph3L	10	.19	.52	.71			.59	.60	.0605	.96	.39
F	5							.62	.0814		
M	5				0.319	0.12		.58	.0245		
foot_D3	10	2.80	9.15	11.94			9.72	10.03	.8688	1.30	1.54
F	5							10.42	1.0907		
M	5				0.172	0.22		9.65	.3688		
foot_ph4L1	10	1.08	3.16	4.24			3.50	3.59	.3189	.89	.63
F	5							3.73	.3721		
M	5				0.154	0.24		3.44	.1902		
foot_ph4L2	10	.70	2.16	2.85			2.32	2.39	.2398	.98	-.23
F	5							2.49	.3107		
M	5				0.185	0.21		2.28	.0769		
foot_ph4L3	10	.51	1.57	2.08			1.71	1.77	.1878	.83	-.60
F	5							1.87	.2229		
M	5				0.097	0.31		1.67	.0728		
foot_tph4L	9	.17	.60	.77			.65	.67	.0629	.50	-1.12
F	4							.72	.0517		
M	5				0.017	0.58		.63	.0364		
foot_D4	9	3.54	13.50	17.05			14.05	14.69	1.2787	.94	-.35
F	4							15.55	1.4737		
M	5				0.063	0.41		14.00	.5484		
foot_ph5L1	10	.84	2.47	3.31			2.65	2.71	.2476	1.69	3.39
F	5							2.79	.3320		
M	5				0.343	0.11		2.63	.1103		
foot_ph5L2	10	.64	1.49	2.12			1.63	1.73	.2134	.77	-.76
F	5							1.84	.2376		
M	5				0.099	0.30		1.62	.1223		
foot_tph5L	9	.27	.48	.75			.61	.61	.0865	.23	-.20
F	4							.64	.1214		
M	5				0.364	0.12		.58	.0464		
foot_D5	9	2.95	9.58	12.53			10.07	10.47	.9583	1.48	1.67
F	4							10.92	1.2843		
M	5				0.229	0.20		10.11	.4846		

Table 3. Statistical results of one-way, two-way, and three-way analyses of covariance for the 123 skeletal measures taken on of *Blommersia alexi* sp. nov. Measures are partitioned into anatomical regions to facilitate lecture: SVL, skull, pectoral girdle, forelimb, vertebral column, pelvic girdle, and hindlimb. Significant results ($\alpha = 0.05$) are shown in bold. Abbreviations follow those indicated in the description of the measurements (Appendix S1).

	ANCOVAS						
	3-way			1-way	1-way	2-way	
	SVLext	SVLsk	SVLsum	SVLsk	pelvL	SVLsk	pelvL
SVLext	-	-	-	.002	.000	.374	.035
SVLsk	-	-	-	-	.000	-	-
SVLsum	-	-	-	.000	.000	.805	.132
skullL	.658	.009	.429	.000	.000	.035	.634
skullW	.840	.073	.365	.000	.000	.579	.057
oticsW	.276	.029	.381	.000	.000	.386	.377
colmL	.188	.740	.851	.008	.005	.965	.417
pmaxH	.013	.002	.009	.001	.001	.591	.449
pmaxW	.175	.012	.181	.000	.000	.393	.358
pmaxD	.087	.079	.139	.004	.005	.604	.686
MmbL	.500	.555	.699	.141	.770	.225	.422
maxL	.504	.000	.039	.000	.000	.007	.321
mandL	.150	.001	.062	.000	.000	.118	.640
nasL	.825	.381	.911	.004	.003	.945	.374
nasW	.058	.726	.493	.112	.660	.288	.537
intnasW	.349	.956	.297	.135	.264	.252	.154
intnsptH	.414	.720	.355	.434	.634	.297	.242
sphH	.796	.283	.761	.004	.009	.224	.717
sphW	.681	.768	.461	.023	.016	.965	.468
frptlL	.176	.010	.088	.001	.001	.485	.574
frptlW	.090	.875	.654	.044	.013	.200	.061
proH	.021	.007	.009	.024	.028	.626	.879
exoL	.342	.131	.708	.000	.000	.965	.135
psphH	.746	.198	.517	.049	.043	.919	.653
psphW	.006	.173	.030	.040	.020	.589	.250
vomH	.649	.928	.566	.424	.557	.493	.394
vomW	.454	.489	.545	.115	.067	.284	.529
pltnL	.787	.440	.727	.120	.068	.268	.502
ptygdH	.849	.136	.821	.002	.001	.816	.355
ptygdW	.658	.019	.608	.000	.000	.037	.896
squaH	.168	.011	.137	.000	.000	.172	.939
squaW	.936	.009	.301	.000	.005	.010	.103
hyoL	1.000	.864	.434	.007	.007	.706	.636

ANCOVAS							
	3-way			1-way	1-way	2-way	
	SVLext	SVLsk	SVLsum	SVLsk	pelvL	SVLsk	pelvL
omostH	.899	.228	.682	.001	.001	.600	.451
omostL	.578	.955	.265	.013	.018	.472	.997
clavL	.485	.587	.942	.005	.003	.932	.309
clav_pL	.794	.976	.227	.005	.002	.935	.299
coraL	.777	.497	.603	.001	.000	.909	.185
sterH	.307	.214	.338	.001	.004	.192	.760
sterWsup	.769	.275	.928	.016	.009	.863	.358
sterWmin	.407	.446	.532	.065	.028	.361	.148
sterWinf	.458	.358	.726	.074	.063	.574	.661
scapL	.881	.792	.310	.003	.003	.661	.574
cleiL	.323	.083	.307	.003	.003	.630	.605
supraH	.928	.667	.661	.019	.007	.527	.173
supraW	.521	.105	.901	.000	.000	.190	.878
humLcap	.136	.021	.528	.000	.000	.482	.083
humLtroc	.125	.009	.406	.000	.000	.362	.060
dltd_crH	.713	.172	.503	.030	.019	.867	.417
dltd_crW	.201	.498	.360	.094	.064	.411	.723
radulnL	.115	.005	.056	.000	.001	.364	.660
mtcpl1	.432	.195	.602	.003	.002	.758	.470
mtcpl2	.182	.084	.199	.005	.006	.573	.744
mtcpl3	.868	.210	.968	.008	.004	.889	.319
mtcpl4	.681	.225	.812	.003	.002	.934	.342
hand_ph1L1	.488	.270	.209	.000	.000	.398	.525
hand_tph1L	.932	.078	.633	.003	.010	.090	.394
hand_D1	.769	.157	.968	.001	.001	.650	.414
hand_ph2L1	.901	.242	.772	.001	.001	.317	.838
hand_tph2L	.685	.301	.960	.105	.141	.767	.486
hand_D2	.472	.131	.494	.003	.004	.852	.442
hand_ph3L1	.623	.110	.857	.000	.000	.507	.245
hand_ph3L2	.483	.029	.561	.000	.000	.050	.789
hand_tph3L	.631	.142	.835	.041	.059	.438	.811
hand_D3	.961	.111	.870	.001	.001	.476	.588
hand_ph4L1	.879	.233	.924	.016	.027	.363	.807
hand_ph4L2	.205	.287	.301	.008	.017	.233	.654
hand_tph4L	.681	.206	.532	.031	.041	.512	.947
hand_D4	.888	.202	.964	.004	.005	.853	.462

ANCOVAS							
	3-way			1-way	1-way	2-way	
	SVLext	SVLsk	SVLsum	SVLsk	pelvL	SVLsk	pelvL
column	.794	.711	.133	.000	.000	.914	.100
atlasH	.259	.369	.367	.018	.042	.171	.444
V2H	.850	.445	.467	.001	.002	.403	.803
V3H	.525	.584	.904	.017	.008	.718	.270
V4H	.685	.885	.241	.001	.000	.987	.200
V5H	.367	.361	.168	.007	.002	.618	.159
V6H	.784	.579	.127	.008	.005	.904	.329
V7H	.755	.330	.193	.027	.007	.262	.073
V8H	.450	.093	.529	.000	.000	.724	.045
sacrumH	.332	.151	.471	.002	.000	.340	.037
V2_tpL	.454	.846	.229	.009	.018	.291	.743
V3_tpL	.922	.175	.449	.000	.000	.220	.741
V4_tpL	.361	.257	.053	.000	.000	.472	.273
V5_tpL	.931	.673	.058	.000	.000	.916	.127
V6_tpL	.692	.385	.033	.002	.001	.820	.161
V7_tpL	.998	.119	.017	.012	.005	.658	.236
V8_tpL	.697	.045	.005	.005	.001	.686	.166
sacrum_tpL	.650	.700	.350	.001	.000	.898	.244
uroL	.267	.609	.371	.000	.000	.337	.013
uroH	.275	.019	.005	.000	.000	.313	.096
uro_crL	.672	.043	.084	.876	.860	.202	.203
uro_crH	.286	.330	.620	.000	.000	.208	.003
iiiL_lft	.668	.071	.263	.000	.000	.923	.002
pelvL	.175	.013	.963	.000	-	-	-
pelwL	.856	.019	.524	.000	.001	.062	.631
epipH	.345	.102	.312	.006	.009	.465	.888
epipW	.630	.480	.597	.211	.141	.366	.576

ANCOVAS							
	3-way			1-way	1-way	2-way	
	SVLext	SVLsk	SVLsum	SVLsk	pelvL	SVLsk	pelvL
femL	.196	.003	.123	.000	.000	.029	.632
tibfibL	.109	.007	.124	.000	.000	.133	.850
tibfiblL	.064	.007	.035	.001	.003	.281	.995
mttrsl1	.639	.234	.670	.009	.013	.445	.991
mttrsl2	.408	.076	.361	.002	.005	.216	.777
mttrsl3	.257	.032	.177	.002	.004	.239	.864
mttrsl4	.132	.002	.033	.000	.002	.126	.728
mttrsl5	.225	.022	.160	.001	.001	.360	.761
foot_ph1L1	.928	.130	.786	.003	.006	.282	.885
foot_tph1L	.681	.103	.857	.009	.021	.191	.550
foot_D1	.819	.158	.722	.004	.008	.890	.320
foot_ph2L1	.885	.198	.949	.001	.001	.723	.386
foot_tph2L	.711	.211	.910	.041	.710	.301	.603
foot_D2	.603	.085	.561	.001	.002	.987	.276
foot_ph3L1	.856	.278	.510	.001	.000	.951	.170
foot_ph3L2	.988	.046	.785	.000	.000	.449	.462
foot_tph3L	.661	.031	.694	.002	.007	.091	.438
foot_D3	.578	.038	.513	.000	.000	.684	.288
foot_ph4L1	.660	.108	.908	.000	.000	.819	.054
foot_ph4L2	.958	.134	.768	.000	.000	.871	.148
foot_ph4L3	.232	.002	.963	.000	.000	.032	.618
foot_tph4L	.905	.006	.217	.001	.005	.133	.649
foot_D4	.530	.012	.321	.000	.000	.560	.218
foot_ph5L1	.919	.383	.883	.006	.003	.879	.282
foot_ph5L2	.722	.012	.668	.000	.000	.162	.959
foot_tph5L	.116	.094	.388	.009	.029	.126	.406
foot_D5	.787	.068	.660	.001	.001	.576	.422

Intraspecific Variation and Statistical Analyses

A multivariate ANOVA on the 123 skeletal measures resulted in an overall sexual dimorphism in *B. alexi* **sp. nov.** (Pillai F = 2874.45; p = 0.014; partial eta-squared = 1), with females presenting larger values for all measured variables (Table 2). Between-subject effects showed sexual dimorphism in the following variables (Table 2): skull length, skull width, premaxilla width, premaxilla depth, maxilla length, mandible length, nasal length, sphenethmoid width, parasphenoid height, palatine length, pterygoid height and width, squamosal width, omosternum height, sternum inferior length, hand Digit III phalange 2 length, and foot Digit IV terminal phalange length.

Univariate three-way ANCOVAs including all three snout-vent measurements (*i.e.* SVL_{ext}, SVL_{sk}, SVL_{sum}) determined that the skeletal SVL measure was the best predictor, being the only significant covariable in most cases and presenting the lowest p-value when more than one covariable was significant (Table 3). One-way ANCOVAs showed that all variables covaried with SVL_{sk} and pelvL except mentomeckelian bone length, nasal width, inter-nasal width, internasal septum height, vomer height and width, palatine length, sternum inferior widths, deltoid crest width, hand Digit II terminal phalange length, urostyle crest length, and epipubis width. In addition, sternum minimum width did not covary with SVL_{sk}, and hand Digit III and foot Digit II terminal phalange lengths did not covary with pelvL (Table 3). Two-way ANCOVAs, including both SVL_{sk} and pelvL, resulted in SVL_{sk} showing significant covariation with skull length, maxilla length, pterygoid width, squamosal width, hand Digit III terminal phalange length, femur length, and foot Digit IV terminal phalange length; and with pelvL showing significant covariation with exterior snout-vent length, presacral VIII height, sacrum height, urostyle length, urostyle crest height, and ilial shaft length (Table 3).

DISCUSSION

B. alexi **sp. nov.** *Osteological Peculiarities*

There are many aspects of hyperdiverse tropical radiations for which we lack data that could help us to understand the patterns and processes related to species' diversification and speciation mechanics. These include detailed data on anatomical structures as well as phenotypic variation (*i.e.* intraspecific disparity), which have been key to define species since Linnaeus. However, despite that osteological and anatomical data have been at the

core of species descriptions in classical literature, for most species we currently only count on data of their external morphology (Vences et al., 2002; Glaw et al., 2006; Glaw & Vences, 2007). This is the case of the hyperdiverse family Mantellidae, where the majority of the recently described species mostly integrate external morphology, genetic data, and bioacoustics (Vieites et al., 2009; Vences et al., 2010; 2015; Scherz et al., 2017b), with few examples including internal structures in the skull like the presence or not of vomerine teeth or bone structures in hands or feet (Manzano et al., 2007; Kamermans & Vences, 2009). Here, we present the first detailed osteological description of a mantellid frog with two main purposes: (1) characterize the cranial and postcranial anatomy of a mantellid species with its intraspecific variation, and (2) provide a base for future studies on the comparative anatomy, phenotypic variation, and taxonomic relationships between the members of this family.

The genus *Blommersia* is constituted by 10 described species from Madagascar as well as two new species from Comoros. All species range from 14 to 30mm snout-vent length and are within the smaller-size of the mantellid frog spectrum. However, one of the species from the Comoros, the one described here, is larger than the rest and is likely undergoing a process of gigantism, which is commonly found in island taxa (Daugherty et al., 1993; Lomolino, 2005; Li et al., 2011). This makes it an interesting species to study its musculoskeletal system as a prior to comparative morphological analyses with other *Blommersia* and mantellid frogs. So far, there are no studies on the evolution of the musculoskeletal system in mantellids, neither of their jumping performance and kinematics, that directly links to dispersal capacity, habitat selection, and speciation. This lack of information precludes inferring conclusions about the relationships between their functional morphology and adaptive processes such as dispersion, size evolution, or phenotypic plasticity and adaptation to specific habitats. Postcranial morphology in anurans has been linked numerous times to a specific locomotor mode and/or habitat use (Zug, 1978; Emerson, 1979; 1982; Nauwelaerts et al., 2007; Reilly & Jorgensen, 2011; Soliz et al., 2016). A better understanding of the functional significance of skeletal traits could significantly improve the ecomorphological interpretation of the interactions between these characteristics and locomotor mode and/or habitat use (Arnold, 1983).

The clavicular process in *B. alexi* **sp. nov.** is located at the proximal end of the clavicle and articulates with the posterior branches of the omosternum (Fig. 6). This structure has

never been reported in any anuran species description (Emerson, 1988; Duellman & Trueb, 1994; Soliz et al., 2018); however some have suggested that the clavicle may be involved in impact absorption during landing (Emerson, 1984). In CT-scans of stained specimens (JHS-S pers. obs.) this process was observed to be embedded within the mm. deltoideus and coracoradialis, which flex the shoulder and elbow joint, respectively. Furthermore, we do not discard that the pectoral and forelimb musculature in *B. alexi* **sp. nov.** presents a more elaborate architecture than that of other frog taxa, involving supplementary musculotendon connections between the clavicular process and the humerus deltoid crest or other forelimb elements. However, we are working on a segmentation of the pectoral girdle's and forelimbs' muscular architecture in *B. alexi* **sp. nov.** to confirm this conjecture. At the moment we propose a completely different locomotor function to that of jump impact absorption for this structure in line with the unique reproductive behavior of Mantellinae frogs (Glaw & Vences, 2006), since the clavicular process was observed to be present in several more species within the genus *Blommersia* (e.g. *B. wittei*, *B. sarotra*, *B. grandisonae*, *B. domergui*, *B. blommersae*). Due to their distinctive reproductive behavior, Mantellinae frogs cling in parallel to leaves during fertilization. This position on the leaf surface does not involve the frog grasping a solid border to ascend with its forelimbs, thus we believe that the presence of the clavicular process provides some sort of biomechanical structural support for musculature involved in the adhesion of the frog to the leaf's surface. Until segmentation of the involved musculature is complete, we cannot make any inferences on the muscular mechanism involved since most studies on frog adhesion focus on the digit pads, which are also present in *B. alexi* **sp. nov.** (see below).

This species also presents several sesamoids (*i.e.* appendicular ossicles; Hall, 2007) and a heterotopic bone on the sole. The most extensive review of sesamoids in anurans (Ponssa et al., 2010) presents many missing data for the Mantellidae family to which we can now shed light with the inclusion of an additional genus (*i.e.* *Blommersia*). Of the sesamoids recognized by Ponssa et al. (2010) in Mantellidae, we confirm in *B. alexi* **sp. nov.** the presence of the cartilago sesamoides embedded in the m. plantaris profundus at the articulation of the tibiofibula with the tibiale. The presence of this sesamoid was thought to have phylogenetic relevance (Nussbaum, 1982); however this hypothesis has been put in doubt since Hoyos (2003). Other sesamoids observed in *B. alexi* **sp. nov.** that had not been confirmed for the family are those lateral to the sacral diapophyses and that on the

plantar surface of the foot. The latter is located where Hoyos (2003) considers is the cartilago plantaris, however in *B. alexi* **sp. nov.** this heterotopic element possesses an additional apophysis or associated os sesamoides (Fig. 12). Ponssa et al. (2010) describe three sesamoids that are osseous in the adult embedded in the plantar aponeurosis tendon that may correspond to those found in *B. alexi* **sp. nov.** Such skeletal elements have been reported in other anuran groups (Nussbaum, 1982; Hoyos, 2003) and are said to be biomechanically advantageous in that they maintain the shape of and strengthen tendons, as well as increase the mechanical advantage of force translation at articulations (Olson, 2000; Summer & Koob, 2002; Abdala et al., 2018). Other developmental studies have revealed that certain sesamoids differentiate before a mature tendon tissue is recognizable, thus dismissing their origination to be solely due to extrinsic factors such as mechanical loading. If we consider the categories of sesamoid distribution (*i.e.* omnipresent and fluctuating; Hall, 2007), these different circumstances relating to their presence suggests that the origin of phylogenetically ubiquitous sesamoids may be more linked to conservative genetic and developmental stimulus, while extrinsic factors may dominate over genetic ones more in those whose occurrence is irregular (Ponssa et al., 2010). The plantar sesamoid and those lateral to the sacral diapophyses are considered to be plesiomorphic in Anura, while the cartilago sesamoides a synapomorphy of the Neobatrachia (Ponssa et al., 2010). Given their occurrence in several additional *Blommersia* species with scarce differences [only in one *B. wittei* and one *B. domergui*], we deduce from that said beforehand that they provide some sort of locomotor advantage to the genus, however the developmental timing of shared sesamoids should be investigated further to make any conclusions in this context.

In addition to heterotopic elements, *B. alexi* **sp. nov.** presents two peculiar apophysis in the sole that may also have a locomotor function: a pointed apophysis on the tibiale's distal epiphysis (absent in lightly ossified DRV6848 and *B. blommersae*) and a fulcrum that extends ventrally from the centrale (Fig. 12). In a similar manner the palm distal carpal 543 presents a lateral apophysis and ventral expansions that result in two points of contact (Fig. 7). The sesamoid-traction epiphysis hypothesis (Parsons, 1904; Hall, 2007) defends that certain bony projections where tendons or ligaments insert develop independent of the limb itself, suggesting that these apophyses represent sesamoids that have been incorporated onto the long bones of the appendicular skeleton. This may most likely be the case for the tibiale's apophysis, and even for that of distal carpal 543. The

bony projections on the palmar and sole surface may serve as a fulcrum for better control and mechanical advantage during jumping locomotion (Biewener, 2003) analogous to the function hooves serve mountainous ungulates on steep slippery slopes.

In contrast, the presence of intercalary elements has been hypothesized to be related to arboreal habits, with distal phalanges, intercalary elements, muscles, and digit pads acting as integrated units to enhance climbing abilities (Burton, 2004). These are functionally integrated into a complex system, with distinctive morphostructural patterns between Hyloides and Ranoides (Manzano et al., 2007), related to different types of movements produced by a similar set of muscles and tendons. This system allows the angular movements necessary for the attachment and detachment of the adhesive digit pad (Hanna & Barnes, 1991). Kamermans & Vences (2009) found evidence for concerted evolution between climbing habits and bifurcated terminal phalanges, like those observed in *Blommersia*, as a result of this architecture allowing for two additional articulations that permit to move the digit without detaching the digit pad. These movements are produced by the action of the mm. extensores breves profundus and distalis, whose presence is variable in Mantellidae. We have not confirmed their presence in *B. alexi* **sp. nov.** as of date, however there is no obligatory correlation between the presence of intercalary elements or bifurcated terminal phalanges and climbing habits, existing several taxa, such as the mantellid genus *Aglyptodactylus*, that possess these elements and are completely terrestrial. As such, these elements appear to not cause any disadvantages to non-arboreal frogs and to not be under strong selective pressure. In *B. alexi* **sp. nov.** the intercalary elements are strongly mineralized and we suspect they aid the frogs during their reproduction when they exhibit arboreal habits. The intercalary element in anurans seems to be a morphological novelty that appeared early within the Neobatrachia and is interpreted as a synapomorphy for the Rhacophoroidea (Frost et al., 2006).

Otherwise, *B. alexi* **sp. nov.** presents several osteological peculiarities, the first of which jumps to view is its evident signs of hyperossification. Several regions of the skull (*i.e.* internasal septum, prootics, sphenethmoid, and parasphenoid) present dermal sculpting, or exostosis, that evidence this phenomenon and have been observed affecting the structure of the skull in different ways in other anuran genera (Duellman & Trueb, 1994). Other signs of hyperossification in dermal elements of *B. alexi* **sp. nov.** include the fusion of the prootics and exoccipitals into the otoccipital and the production of extensive

marginal flanges, such as that of frontoparietals' supraorbital flange or posterior protuberance (Fig. 1). Hyperossification is unrelated with the absolute size of a species (Duellman & Trueb, 1994), and accordingly we found differing levels of ontogenetic ossification across the 10 individuals of *B. alexi* **sp. nov.** in this study. The degree of ossification of several skeletal elements varied independently from size (*i.e.* SVL), sex, and each other, obfuscating the functional purpose of hyperossification in these structures and suggesting that their calcification may depend more on developmental cues rather than environmental. For example, the development of bony crests on the humerus have been associated to hypertrophied musculature in male frogs (Duellman & Trueb, 1994), however, in *B. alexi* **sp. nov.** the deltoid crest is not only well developed in females, but it also displays a continuation on the humerus head separated by a fenestra of varying size. This suggests that hyperossification does not play an important role in the musculoskeletal functional performance of these structures. Nevertheless, hyperossification of certain skeletal elements evokes the idea of structural compensation due to increasing individual size or improved mechanical performance at more developed stages. This is especially true for structures that serve as muscle attachment sites such as the bony crest on the hyobranchial's posteromedial processes or the level of development of diverse processes on the apophyses of presacral vertebrae II-IV. However, the asymmetry (DRV6832, 6835, 6841) in the degree of development of the latter observed in several individuals (*i.e.* DRV6832, 6835, 6841) seems to suggest that hyperossification of these skeletal structures does not alter their functional performance since an unsymmetrical musculoskeletal lever system would apparently result biomechanically unstable in a bilateral animal. This ambiguity in the role of the observed hyperossification still leaves unresolved the issue if this process has any [biomechanical] adaptive value in non-burrowing frogs other than that of water conservation due to exostosis (Ruibal & Shoemaker, 1984; Evans et al., 2014).

B. alexi **sp. nov.** *Osteological Intraspecific Variation*

An important factor to consider when describing the intraspecific variation of a species is to contrast across various individuals and cover as best as possible any potential group bias that may exist, such as sexual dimorphism or ontogenetic stage. The inclusion of 10 individuals of *B. alexi* **sp. nov.** for its description has allowed to discriminate the different status and directionality of ontogenetic ossification in several skeletal elements (*e.g.* skull,

vertebral diapophyses, and pelvic wheel), establish the ubiquity of appendicular ossicles, discriminate between individual artifacts and the general characteristics of the species, and determine what structures presented sexual dimorphism. Characterization of the observed intraspecific variation leads us to interpret the variables with positive values of asymmetry (>1 ; Table 2) to indicate skeletal structures in *B. alexi* **sp. nov.** that are under a continuous process of ontogenetic ossification since all sampled individuals are considered to be adults and annual cohort survival in anurans decreases with increasing age. In *B. alexi* **sp. nov.** we also observed an overall sexual dimorphism with females being relatively larger in all measurements (Table 2). However, univariate analyses show that this doesn't hold true for snout-vent length and that most sexually dimorphic characters are located in the head with the exception of the omosternum, sternum, and a couple of phalanges (Table 2). Increased size of the head in females may indicate an increased cranial volume and vomeronasal organ. This would be a logic evolutionary outcome in view of the transmission of volatile compounds from the males' femoral glands to the females' vomeronasal organ during courtship (Nowack & Vences, 2016; Nowack et al., 2017). Larger skeletal elements in the sternum and carpal/tarsal phalanges may likewise aid the female biomechanically in maintaining her vertical position during the reproductive act (Altig, 2008) by increasing muscle attachment area and potentially providing longer input levers relative to output levers.

The observation of sexual dimorphism distributed throughout the skeleton of *B. alexi* **sp. nov.** leads to test for size covariation of skeletal characteristics. The traditional length measurement in anurans has always been (exterior) snout-vent length, however the precision and repeatability of this measure is highly dependent on the observer. This is because the structure of the pelvic girdle in most anurans can compress under vertical load and their vertebral column is flexible, thus different measurement habits across observers can lead to obtain different values for the same individuals. With this in mind we tested three different snout-vent measurements to evaluate which one was a better predictor of size covariation. Our results (Table 3) indicate that the snout-vent length directly measured on the volume-rendered skeleton of the frog in its resting position is a better size covariate than either exterior snout-vent length or the summed skeletal snout-vent length (Appendix S1). That the SVL_{sum} measurement calculated by summing up the skeletal length distances of each anatomical region is a worse predictor than the SVL measured directly on the rendered skeleton, suggests that the "crouched" resting position

of *B. alexi* **sp. nov.** is correlated with size variation in the entire anatomy of a particular individual and may play a role in the allometric scaling of jumping performance in this species (Choi et al., 2000; Azizi & Roberts, 2010; Gillis, 2010). Another proposed length measurement for anurans that focuses on their locomotor function is that of pelvic length. When compared to skeletal snout-vent length, pelvic length presents very similar size covariation with skeletal elements (Table 3), however each covariable showed higher predictive power than the other in specific anatomical regions: skeletal snout-vent length was a better predictor of the skull and limb elements, while pelvic length was a better predictor of the elements of the vertebral column and pelvic girdle (Table 3). These observations in size covariation suggest that the anuran skeletal architecture is organized in modular developmental units. In this context, Soliz et al. (2017) determined that the girdles and vertebral column in hylids adjusted to different evolutionary modes of evolution that may well reflect a morphological continuum between locomotor modes (Fabrezi et al., 2017). This may also hold true for other anurans like *B. alexi* **sp. nov.** that we have described here, although further research including additional species of the genus is required to develop on this hypothesis.

Modern Methods in Anatomical Reconstructions

Despite that osteological data can be a substantial source for phylogenetically informative characters, the vast majority of phylogenies produced these days rely on genetic/genomic data. Nevertheless the availability and expansion of micro-CT is facilitating the generation of massive amounts of osteological data from vouchers deposited in Natural History collections (Reyes-Moya et al., *in review*), and it is likely to become more common as the technology further develops shortening CT generation times (Cole et al. 2018). In this view, there are currently several ongoing projects and open resources working together (Cross, 2017) to make osteological data across almost all vertebrate genera readily available for phylogenetic research. However, osteological data are sometimes hard to interpret and compare as they can be influenced by the age of the specimen (*i.e.* ontogeny), allometric and/or heterochronic processes, phenotypic plasticity in response to the local ecological niche, or because of the presence of homoplasy in a generated phylogenetic topology; in addition, some skeletal structures are more prone to be affected (*e.g.* the limbs and skull) than others. Despite of this, osteological data are

routinely used in paleontological studies to describe fossils and infer their phylogenetic relationships (Kluge & Farris, 1969; Hall, 2007; Laloy et al., 2013).

Another potential issue with osteological data generated from micro-CT is the processing and rendering of the CT-scans. Due to the differential ossification of skeletal structures and the small size of many frog species, the thresholds between ossified and non-ossified structures are usually hard to establish. This has caused discrepancies in the skeletal description when interpreting surface renders versus volume renders (Scherz et al., 2017c). The production of surface models requires the establishment of an isosurface density value for the rendering, and this threshold may not be the most adequate for the complete anatomy of the sample, creating artifacts and obfuscating the precise description of certain morphological structures. The generation of software tools that could allow to differentially surface render distinct modules of the volume and/or advances in the computational weighting of isosurfaces that could allow to equalize differences between those generated between different anatomical modules for their assemblage may lead in the future to more precise surface model interpretation. In contrast to isosurfaces that are generated based on a particular density value, volume rendering allows for a dynamic visualization of the model along a user-defined density curve with different options of transparency and coloration for predefined subranges of grey values. This allows exploring anatomical structures along their complete density gradient and to render tissues that correspond to different subranges of grey values within the sample differentially, in consequence increasing the contrast between them during visualization.

Density differentiation in the CT-scans of *B. alexi* **sp. nov.** allowed us to make some inferences on the development of the carpus (Fig. 7), whose nomenclature has been a controversial topic in anurans until the work of Fabrezi & Alberch (1996). They confirm the absence of centralia in the anuran carpus because these arise from the intermedium, and the intermedium in anurans has a dubious homology with that in other tetrapods because its embryonic origin is by segmentation off the ulnare rather than branching off the ulna. In *B. alexi* **sp. nov.** we observe a medial projection off the ulnare that corresponds to the embryonic structure Fabrezi (1992) designates to be homologous with the intermedium, or the ulnare'. We believe this structure is a chondrogenetic projection rather than a separate element in *B. alexi* **sp. nov.** in view of the existing large fenestrae in-between the ulnare and radiale in this species (Fig. 7). In the same way, distal carpal 5

is not a centrale since it arises from a single embryonic condensation. In *B. alexi* **sp. nov.** this element seems to segment twice, subsequently fusing primarily with distal carpal 4 and secondarily with distal carpal 3 as evidenced in the presence of a tunnel between both elements [distal carpal 54 and distal carpal 3] in the compound bone distal carpal 543 (Fabrezi & Alberch, 1996). The radiale in *B. alexi* **sp. nov.** also presents two projections (Fig. 7), indicating two independent embryonic cartilaginous condensations: the [posterior] radiale dorsomedially and the [anterior] radiale ventromedially (Fabrezi & Alberch, 1996). The latter is considered a new element characteristic of the hand ontogeny of some anuran species since the distal [posterior] end of the radiale gives rise to the Element Y and prepollex (Shubin & Alberch, 1986). The Element Y is a carpal element found exclusively in amphibians that arises from one to three embryonic condensations. In *B. alexi* **sp. nov.** this element appears to have originated from two independent embryonic chondrifications that fuse primarily later on (Fig. 7).

ACKNOWLEDGEMENTS

We would like to thank Barbara de Kegel from the Evolutionary Morphology of Vertebrates Lab at Ghent University for helping in the realization of the staining protocol, and the members of the UGCT that aided us in the CT processing of stained specimens. This research was funded by the Spanish Ministry of Economy and Competitiveness; grant number CGL2013-40924-P.

REFERENCES

- Abdala V, Ponssa ML, Tulli MJ, Fabre AC, Herrel A (2018) Frog tendon structure and its relationship with locomotor modes. *Journal of Morphology*, **279**, 895-903.
- Altig R (2008) Notes on the breeding biology of four species of mantellid frogs from Madagascar. *Tropical Zoology*, **21**, 187-194.
- Arnold SJ (1983) Morphology, performance and fitness. *American Zoologist*, **23**, 347-361.
- Azizi E, Roberts TJ (2010) Muscle performance during frog jumping: influence of elasticity on muscle operating lengths. *Proceedings of the Royal Society of London B: Biological Sciences*, **277**, 1523-1530.
- Biewener AA (2003) *Animal Locomotion*, Oxford University Press, Oxford.

- Blain HA, Arribas OJ (2017) A description of the skeletal morphology of *Rana pyrenaica* (Anura: Ranidae), with comments on functional morphology, ecological adaptation and relationships with other Iberian ranids. *Zootaxa*, **4319**, 510-530.
- Burton TC (2004) Muscles of the pes of hylid frogs. *Journal of Morphology*, **260**, 209-233.
- Choi I-H, Shim JH, Lee YS, Ricklefs RE (2000) Scaling of jumping performance in anuran amphibians. *Journal of Herpetology*, **2000**, 222-227.
- Clack J (2001) *The Otoccipital Region—Origin, Ontogeny and the Fish-Tetrapod Transition*, Systematics Association Symposium London.
- Cole JM, Symes DR, Lopes NC, Wood JC, Poder K, Alatabi S, Botchway SW, Foster PS, Gratton S, Johnson S, Kamperidis C (2018) High-resolution μ CT of a mouse embryo using a compact laser-driven X-ray betatron source. *Proceedings of the National Academy of Sciences*, **2018**, 201802314.
- Cross R (2017) The inside story on 20,000 vertebrates. *Science*, **357**, 742-743.
- Crottini A, Madsen O, Poux C, Strauß A, Vieites DR, Vences M (2012) Vertebrate time-tree elucidates the biogeographic pattern of a major biotic change around the K–T boundary in Madagascar. *Proceedings of the National Academy of Sciences*, **109**, 5358-5363.
- Daugherty CH, Gibbs GW, Hitchmough R (1993) Mega-island or micro-continent? New Zealand and its fauna. *Trends in Ecology & Evolution*, **8**, 437-442.
- De Villiers C (1925) On the development of the "epipubis" of *Xenopus*. *Annals of the Transvaal Museum*, **11**, 129-135.
- Dempster WT (1930) The morphology of the amphibian endolymphatic organ. *Journal of Morphology*, **50**, 71-126.
- Duellman WE, Trueb L (1994) *Biology of Amphibians*, JHU Press.
- Ecker A (1889) *The Anatomy of the Frog*, Clarendon Press.
- Emerson SB (1979) The ilio-sacral articulation in frogs: form and function. *Biological Journal of the Linnean Society*, **11**, 153-168.
- Emerson SB (1982) Frog postcranial morphology: identification of a functional complex. *Copeia*, 603-613.
- Emerson SB (1983) Functional analysis of frog pectoral girdles. The epicoracoid cartilages. *Journal of Zoology*, **201**, 293-308.
- Emerson SB (1984) Morphological variation in frog pectoral girdles: testing alternatives to a traditional adaptive explanation. *Evolution*, **38**, 376-388.

- Emerson SB (1988) Testing for historical patterns of change: a case study with frog pectoral girdles. *Paleobiology*, **14**, 174-186.
- Evans SE, Groenke JR, Jones ME, Turner AH, Krause DW (2014) New material of *Beelzebubo*, a hyperossified frog (Amphibia: Anura) from the Late Cretaceous of Madagascar. *PLoS One*, **9**, e87236.
- Fabrezi M (1992) El carpo de los anuros. *Alytes*, **10**, 1-29.
- Fabrezi M, Alberch P (1996) The carpal elements of anurans. *Herpetologica*, **1996**, 188-204.
- Fabrezi M, Goldberg J, Chuliver-Pereyra M (2017) Morphological Variation in Anuran Limbs: Constraints and Novelties. *Journal of Experimental Zoology Part B: Molecular and Developmental Evolution*, **328**, 546-574.
- Frost DR, Grant T, Faivovich J, Bain RH, Haas A, Haddad CF, De Sa RO, Channing A, Wilkinson M, Donnellan SC, Raxworthy CJ (2006) The amphibian tree of life. *Bulletin of the American Museum of Natural History*, **297**, 1-291.
- Gardiner BG (1983) Gnathostome vertebrae and the classification of the Amphibia. *Zoological Journal of the Linnean Society*, **79**, 1-59.
- Gillis GB (2010) Frog muscles start stretched. *Journal of Experimental Biology*, **213**, vi-vi.
- Glaw F, Hoegg S, Vences M (2006) Discovery of a new basal relict lineage of Madagascan frogs and its implications for mantellid evolution. *Zootaxa*, **1334**, 27-43.
- Glaw F, Vences M (2006) Phylogeny and genus-level classification of mantellid frogs (Amphibia, Anura). *Organisms Diversity & Evolution*, **6**, 236-253.
- Glaw F, Vences M (2007) *A Field Guide to the Amphibians and Reptiles of Madagascar*, Vences & Glaw.
- Griffiths I (1959) The phylogeny of *Sminthillus limbatus* and the status of the Brachycephalidae (Amphibia Salientia). *Journal of Zoology*, **132**, 457-487.
- Hall BK (2005) *Bones and Cartilage: Developmental and Evolutionary Skeletal Biology*, Academic Press.
- Hall BK (2007) *Fins into Limbs. Development, Transformation, and Evolution*, Chicago: The University of Chicago Press.
- Hanna G, Barnes JP (1991) Adhesion and detachment of the toe pads of tree frogs. *Journal of Experimental Biology*, **155**, 103-125.
- Hetherington TE, Lombard RE (1982) Biophysics of underwater hearing in anuran amphibians. *Journal of Experimental Biology*, **98**, 49-66.

- Howes GB (1888) On the carpus and tarsus of the Anura. *Journal of Zoology*, **56**, 141-182.
- Hoyos JM (2003) Additions to our knowledge of anuran sesamoids. *Herpetological Review*, **34**, 112.
- Kamermans M, Vences M (2009) Terminal phalanges in ranoid frogs: morphological diversity and evolutionary correlation with climbing habits. *Alytes*, **26**, 117.
- Kluge AG, Farris JS (1969) Quantitative phyletics and the evolution of anurans. *Systematic Biology*, **18**, 1-32.
- Laloy F, Rage JC, Evans SE, Boistel R, Lenoir N, Laurin M (2013) A re-interpretation of the Eocene anuran *Thaumastosaurus* based on microCT examination of a ‘mummified’ specimen. *PLoS One*, **8**, e74874.
- Laurent R (1946) Mises au point dans la taxonomie des ranides. *Revue de Zoologie et de Botanique Africaines*, **39**, 336-338.
- Li Y, Xu F, Guo Z, Liu X, Jin C, Wang Y, Wang S (2011) Reduced predator species richness drives the body gigantism of a frog species on the Zhoushan Archipelago in China. *Journal of Animal Ecology*, **80**, 171-182.
- Lomolino MV (2005) Body size evolution in insular vertebrates: generality of the island rule. *Journal of Biogeography*, **32**, 1683-1699.
- Madison DM (1977) Chemical Communication in Amphibians and Reptiles. In *Chemical Signals in Vertebrates*, pp. 135-168. Springer.
- Maglia AM, Pugener LA, Mueller JM (2007) Skeletal morphology and postmetamorphic ontogeny of *Acris crepitans* (Anura: Hylidae): a case of miniaturization in frogs. *Journal of Morphology*, **268**, 194-223.
- Manzano AS, Fabrezi M, Vences M (2007) Intercalary elements, treefrogs, and the early differentiation of a complex system in the Neobatrachia. *The Anatomical Record*, **290**, 1551-1567.
- Mason MJ, Segenhout JM, Cobo-Cuan A, Quiñones PM, van Dijk P (2015) The frog inner ear: picture perfect? *Journal of the Association for Research in Otolaryngology*, **16**, 171-188.
- Mookerjee HK (1931) IV. On the development of the vertebral column of Anura. *Philosophical Transactions of the Royal Society B*, **219**, 165-196.
- Mookerjee HK, Das SK (1939) Further investigation on the development of the vertebral column in Salientia (Anura). *Journal of Morphology*, **64**, 167-209.
- Nauwelaerts S, Ramsay J, Aerts P (2007) Morphological correlates of aquatic and terrestrial locomotion in a semi-aquatic frog, *Rana esculenta*: no evidence for a design conflict. *Journal of Anatomy*, **210**, 304-317.

- Nowack C, Peram P, Wenzel S, Rakotoarison A, Glaw F, Poth D, Schulz S, Vences M (2017) Volatile compound secretion coincides with modifications of the olfactory organ in mantellid frogs. *Journal of Zoology*, **303**, 72-81.
- Nowack C, Vences M (2016) Ontogenetic development of the derived olfactory system of the mantellid frog *Mantidactylus betsileanus*. *The Anatomical Record*, **299**, 943-950.
- Nussbaum RA (1982) Heterotopic bones in the hindlimbs of frogs of the families Pipidae, Ranidae and Sooglossidae. *Herpetologica*, **1982**, 312-320.
- Olson W (2000) Phylogeny, ontogeny, and function: extraskeletal bones in the tendons and joints of *Hymenochirus boettgeri* (Amphibia: Anura: Pipidae). *Zoology-Analysis of Complex Systems*, **103**, 15-24.
- Pabijan M, Gehring P-S, Koehler J, Glaw F, Vences M (2011) A new microendemic frog species of the genus *Blommersia* (Anura: Mantellidae) from the east coast of Madagascar. *Zootaxa*, **2978**, 34-50.
- Pabijan M, Wollenberg K, Vences M (2012) Small body size increases the regional differentiation of populations of tropical mantellid frogs (Anura: Mantellidae). *Journal of Evolutionary Biology*, **25**, 2310-2324.
- Parsons F (1904) Observations on traction epiphyses. *Journal of Anatomy and Physiology*, **38**, 248.
- Ponssa ML, Goldberg J, Abdala V (2010) Sesamoids in anurans: new data, old issues. *The Anatomical Record*, **293**, 1646-1668.
- Reilly SM, Jorgensen ME (2011) The evolution of jumping in frogs: morphological evidence for the basal anuran locomotor condition and the radiation of locomotor systems in crown group anurans. *Journal of Morphology*, **272**, 149-168.
- Reynolds SH (1897) *The Vertebrate Skeleton*, Cambridge University Press Warehouse, London.
- Richards CL (2006) Has the evolution of complexity in the amphibian papilla influenced anuran speciation rates? *Journal of Evolutionary Biology*, **19**, 1222-1230.
- Ročková H, Roček Z (2005) Development of the pelvis and posterior part of the vertebral column in the Anura. *Journal of Anatomy*, **206**, 17-35.
- Ruibal R, Shoemaker V (1984) Osteoderms in anurans. *Journal of Herpetology*, **1984**, 313-328.
- Samonds KE, Godfrey LR, Ali JR, Goodman SM, Vences M, Sutherland MR, Irwin MT, Krause DW (2013) Imperfect isolation: factors and filters shaping Madagascar's extant vertebrate fauna. *PLoS One*, **8**, e62086.
- Scherz MD, Hawlitschek O, Andreone F, Rakotoarison A, Vences M, Glaw F (2017c) A review of the taxonomy and osteology of the *Rhombophryne serratopalpebrosa* species

group (Anura: Microhylidae) from Madagascar, with comments on the value of volume rendering of micro-CT data to taxonomists. *Zootaxa*, **4273**, 301-340.

Scherz MD, Razafindraibe JH, Rakotoarison A, Dixit NM, Bletz MC, Glaw FR, Vences M (2017b) Yet another small brown frog from high altitude on the Marojejy Massif, northeastern Madagascar (Anura: Mantellidae). *Zootaxa*, **4347**, 572-582.

Scherz MD, Vences M, Borrell J, Ball L, Nomenjanahary DH, Parker D, Rakotondratsima M, Razafimandimby E, Starnes T, Rabearivony J, Glaw F (2017a) A new frog species of the subgenus *Asperomantis* (Anura, Mantellidae, Gephyromantis) from the Bealanana District of northern Madagascar. *Zoosystematics and Evolution*, **93**, 451.

Shubin NH, Alberch P (1986) A morphogenetic approach to the origin and basic organization of the tetrapod limb. In *Evolutionary Biology*, pp. 319-387. Springer.

Simmons D, Bertolotto C, Narins P (1992) Innervation of the amphibian and basilar papillae in the leopard frog: reconstructions of single labeled fibers. *Journal of Comparative Neurology*, **322**, 191-200.

Soliz M, Tulli MJ, Abdala V (2017) Osteological postcranial traits in hylid anurans indicate a morphological continuum between swimming and jumping locomotor modes. *Journal of Morphology*, **278**, 403-417.

Soliz MC, Ponssa ML, Abdala V (2018) Comparative anatomy and development of pectoral and pelvic girdles in hylid anurans. *Journal of Morphology*, **279**, 904-924.

Summers AP, Koob TJ (2002) The evolution of tendon—morphology and material properties. *Comparative Biochemistry and Physiology Part A: Molecular & Integrative Physiology*, **133**, 1159-1170.

Trueb L (1968a) Cranial osteology of the hylid frog, *Smilisca baudini*. *University of Kansas Publications, Museum of Natural History*, **18**, 11-35.

Trueb L (1968b) Variation in the tree frog *Hyla lancasteri*. *Copeia*, **1968**, 285-299.

Vences M, Andreone F, Glaw F, Mattioli F (2002) New dwarf species of *Mantidactylus* from northwestern Madagascar (Anura: Mantellidae). *Copeia*, **2002**, 1057-1062.

Vences M, Glaw F (2001) When molecules claim for taxonomic change: new proposals on the classification of Old World treefrogs. *Spixiana*, **24**, 85-92.

Vences M, Jovanovic O, Safarek G, Glaw F, Koehler J (2015) A new arboreal frog of the genus *Guibemantis* from the Southeast of Madagascar (Anura: Mantellidae). *Zootaxa*, **4059**, 569-580.

Vences M, Pabijan M, Kohler J, Glaw F (2010) Two syntopic and microendemic new frogs of the genus *Blommersia* from the East coast of Madagascar. *African Journal of Herpetology*, **59**, 133-156.

Vences M, Vieites DR, Glaw F, Brinkmann H, Kosuch J, Veith M, Meyer A (2003) Multiple overseas dispersal in amphibians. *Proceedings of the Royal Society of London B: Biological Sciences*, **270**, 2435-2442.

Vences M, Wahl-Boos G, Hoegg S, Glaw F, Spinelli Oliveira E, Meyer A, Perry S (2007) Molecular systematics of mantelline frogs from Madagascar and the evolution of their femoral glands. *Biological Journal of the Linnean Society*, **92**, 529-539.

Vieites DR, Wollenberg KC, Andreone F, Köhler J, Glaw F, Vences M (2009) Vast underestimation of Madagascar's biodiversity evidenced by an integrative amphibian inventory. *Proceedings of the National Academy of Sciences*, **106**, 8267-8272.

Wake D (1970) Aspects of vertebral evolution in the modern Amphibia. *Forma Functio*, **3**, 33-60.

Wollenberg KC, Vieites DR, Glaw F, Vences M (2011) Speciation in little: the role of range and body size in the diversification of Malagasy mantellid frogs. *BMC Evolutionary Biology*, **11**, 217.

Zug GR (1978) Anuran Locomotion—Structure and Function, 2: Jumping Performance of Semiaquatic, Terrestrial, and Arboreal Frogs. *Smithsonian Contributions to Zoology*, **276**.

SUPPLEMENTARY MATERIAL

Appendix S1. Measurements descriptions. All measurements were performed on the left side or paired element of the skeleton unless otherwise specified.

Snout-vent length external (SVL_{ext}): snout-vent length measured externally on the preserved specimen.

Snout-vent length skeletal (SVL_{sk}): in the right sagittal plane; distance from the cranial tip of the premaxilla to the caudal-most margin of the pelvis.

Summed Snout-vent length (SVL_{sum}): The sum of skull length (skullL), the column (column), and pelvis length (pelvL).

Skull length (skullL): in the ventral coronal plane; distance from the anterior margin of the left premaxilla to the caudal border of the left exoccipital.

Skull width (skullW): in the ventral coronal plane; maximum distance between the left and right jaw articulations.

Otic to Otic capsule distance (oticsW): in the ventral coronal plane; maximum transverse distance between the lateral margins of the left and right otic capsules.

Columella (colmL): distance along the columella's midline from its lateral tip to its medial articulation with the oval window.

Premaxilla height (pmaxH): in the left sagittal plane; distance from the premaxilla's antero-ventral margin (*i.e.* pars dentalis) to the dorsal tip of its alary process.

Premaxilla width (pmaxW): in the ventral coronal plane; distance between the medial and lateral tips of the premaxilla's pars palatina.

Premaxilla depth (pmaxD): in the ventral coronal plane; distance from the premaxilla's anterior medial margin to the caudal (medial) tip of its pars palatina.

Mentomeckelian bone length (MmbL): in the ventral coronal plane; distance along the Mentomeckelian bone's midline from its medial margin to its lateral margin.

Upper jaw length (maxL): distance along the upper jaw's surface from the antero-medial margin of the premaxilla to the caudal-most tip of the quadratojugal.

Lower jaw length (mandL): distance along the lower jaw's surface from the antero-medial margin of the Mentomeckelian bone to the caudal-most margin of the angulosplenic plate.

Nasal length (nasL): in the left sagittal plane; maximum distance along the nasal's lateral border from its cranial tip to the caudal termination of its maxillary process.

Nasal width (nasW): in the dorsal coronal plane; transverse distance from the left nasal's most-medial articulation point with the internasal septum to its lateral margin.

Inter-nasal width (intnasW): in the dorsal coronal plane; transverse distance between the medial calcified articulation points of the left and right nasals with the tectum nasi.

Internasal septum height (intnsptH): in the ventral coronal plane; distance from the left cranial margin of the internasal septum to the caudal tip of the left vomer (*i.e.* left olfactory foramen).

Sphenethmoid height (sphH): in the ventral coronal plane; distance from the left vomer's caudal tip (*i.e.* left olfactory foramen) to the caudal-most margin of the sphenethmoid's left lateral ala.

Sphenethmoid width (sphW): in the ventral coronal plane; distance from the caudal-most margin of the sphenethmoid's left lateral ala to the caudal-most margin of its right ala.

Frontoparietal length (frptlL): in the dorsal coronal plane; distance from the postero-lateral margin of the tectum nasi to the caudal tip of the posterior frontoparietal protuberance.

Frontoparietal width (frptlW): in the dorsal coronal plane; maximum distance between the left frontoparietal's medial and lateral margins.

Prootic height (proH): in the dorsal coronal plane; distance from the anterior border of the anterior epiotic eminence to the caudal-most margin of the prootic at the prominencia ducti semicircularis posterioris.

Exoccipital length (exoL): in the ventral coronal plane; transverse distance from the caudal-lateral border of the left exoccipital to that of the right exoccipital.

Parasphenoid height (psphH): in the ventral coronal plane; distance from the lateral intersection of the parasphenoid with the left ala of the sphenethmoid to the cranial margin of the origin of the parasphenoid's left posterolateral ala.

Parasphenoid width (psphW): in the ventral coronal plane; transverse distance from the anterior, lateral-most corner of the parasphenoid's left posterior ala to that of its right.

Vomer height (vomH): in the ventral coronal plane; distance from the caudal tip of the vomer's dentigerous process to its branching point with the postchoanal portion along its lateral edge.

Vomer width (vomW): in the ventral coronal plane; length of the antero-lateral margin of the vomer's anterior portion.

Palatine length (pltnL): distance along the palatine's caudal margin from its medial articulation with the alary cartilage to its lateral articulation with the maxilla.

Pterygoid height (ptygdH): in the right sagittal plane; distance from the tip of the left pterygoid's dorso-posterior ramus to the pterygoid's ventral margin along its ventral border.

Pterygoid width (ptygdW): in the right sagittal plane; distance along the left pterygoid's surface from its anterior-most articulation with the maxilla to its caudal-most tip at the jaw articulation.

Squamosal height (squaH): in the left sagittal plane; distance along the squamosal's zygomatic ramus midline from its ventro-caudal tip to the dorsal border of the squamosal's otic ramus

Squamosal width (squaW): in the left sagittal plane; distance along the squamosal's otic ramus midline from its anterior to posterior margins.

Hyoid bone length (hyoL): distance along the left hyoid's midline from its cranial tip to its caudal end.

Omosternum superior branch height (omostH): in the ventral coronal plane; distance along the omosternum's midline from its cranial edge to its caudal border at its posterior bifurcation.

Omosternum branch length (omostL): in the in the ventral coronal plane; distance along the left omosternum branch's midline from its articulation with the clavicular processes to the lateral border of the opposing branch's bifurcation.

Clavicle length (clavL): in the ventral coronal plane; distance along the clavicle's midline from its proximal articulation with the epicoracoid cartilage to its distal articulation with the scapula.

Distance to the clavicular process (clav_pL): in the ventral coronal plane; distance from the medial origin of the clavicle to the clavicular process.

Coracoid length (coraL): in the ventral coronal plane; distance along the coracoid's midline from its proximal articulation with the epicoracoid cartilage to its distal articulation with the humerus head in the glenoid cavity.

Sternum height (sterH): in the ventral coronal plane; distance along the sternum's midline from its cranial border to its caudal edge.

Sternum superior width (sterWsup): in the ventral coronal plane; maximum transverse distance between the sternum's anterior left and right lateral edges.

Sternum minimum width (sterWmin): in the ventral coronal plane; minimum transverse distance between the sternum's left and right lateral edges.

Sternum inferior width (sterWinf): in the ventral coronal plane; maximum transverse distance between the sternum's posterior left and right lateral edges.

Scapula length (scapL): distance from the scapula's ventral point of articulation with the humerus in the glenoid cavity to its caudal edge that articulates with the suprascapula.

Cleithrum length (cleiL): in the dorsal coronal plane; distance along the cranial edge of the suprascapula from its proximal border to its distal articulation with the scapula.

Suprascapula height (supraH): in the dorsal coronal plane; antero-posterior distance along the articulation with the scapula.

Suprascapular caudal-medial projection (supraW): in the dorsal coronal plane; distance from the postero-lateral articulation with the scapula to the most medial point of ossification.

Humerus length capitulum (humLcap): linear distance from the proximal end of the humerus head to the distal capitulum of the humerus (*i.e.* part of the epiphysis that articulates with the radius).

Humerus length trochlea (humLtroc): linear distance from the proximal end of the humerus head to the distal trochlea of the humerus (*i.e.* part of the epiphysis that articulates with the ulna).

Deltoid crest height (dltd_crH): in the ventral coronal plane; maximum height of the deltoid crest from its anterior edge to posterior base.

Deltoid crest width (dltd_crW): in the ventral coronal plane; distance from the proximal end of the base of the deltoid crest where it touches the humeral head to its distal end on the humerus.

Radioulna length (radulnL): distance from the proximal end of the olecranon (articulation with the humerus) to the distal end of the ulna (articulation with the carpals).

Metacarpal lengths (mtcplX): distance along the metacarpal's midline from its proximal end (articulation with the carpals) to its distal end (articulation with the phalanges).

Phalange lengths (hand_phXL/foot_phXL): distance along the phalange's midline from its proximal end to its distal end.

Terminal phalange lengths (hand_tphL/foot_tphL): distance from the terminal phalange's left proximal end to its left projection on its distal end.

Digit lengths (hand_DX/foot_DX): sum of the metacarpal/metatarsal length (mtcpl/mttrsl), phalange lengths (hand_phXL/foot_phXL), and terminal phalange length (hand_tphL/foot_tphL) for the same limb Digit.

Column (column): sum of all vertebral body heights.

Vertebral body heights (atlasH/VXH/sacrumH): in the ventral coronal plane; distance along the midline of the vertebra's centrum from its cranial border to its caudal margin.

Distances between vertebral transverse processes (VX_tpL/sacrum_tpL): in the ventral coronal plane; distance from the tip of the left transverse process to the tip of that of the right along their midline.

Urostyle length (uroL): in the left sagittal plane; distance along the urostyle's midline from its articulation with the sacral vertebra to its caudal tip.

Urostyle height (uroH): in the left sagittal plane; distance from the urostyle's dorsal border to its ventral border at its cranial tip.

Urostyle crest length (uro_crL): in the left sagittal plane; distance from the base of the cranial origin of the urostyle crest to its posterior end.

Urostyle crest height (uro_crH): in the left sagittal plane; maximum distance from the dorsal edge of the urostyle crest to its ventral edge.

Iliac shaft length (iliL): in the left sagittal plane; distance from the left iliac shaft's dorso-cranial tip at the iliac-sacral articulation to the caudal edge of the iliac protuberance immediately before the acetabulum.

Pelvis length (pelvL): in the left sagittal plane; maximum distance from the dorso-anterior tip of the iliac shaft to the most caudal border of the pelvic wheel at the ischium.

Pelvic wheel length (pelwL): in the left sagittal plane; maximum linear distance between the anterior and posterior edges of the pelvis.

Epipubis height (epipH): in the ventral coronal plane; distance along the epipubis' midline from its anterior edge to its posterior edge.

Epipubis width (epipW): in the ventral coronal plane; distance from epipubis' left lateral edge to its right lateral border.

Femur length (femL): distance along the femur's midline from its proximal end (articulation with the acetabulum) to its distal end (articulation with the tibiofibula).

Tibiofibula length (tibfibL): distance along the tibiofibula's midline from its proximal end (articulation with the femur) to its distal end (articulation with the tibiale and fibulare).

Tibiale and Fibulare length (tibfibL): distance along the fibulare's midline from its most proximal end (articulation with the tibiofibula) to its most distal end (articulation with the metatarsals).

Metatarsal lengths (mttrsIX): distance along the metatarsal's midline from its proximal end (articulation with the tarsals) to its distal end (articulation with the phalanges).

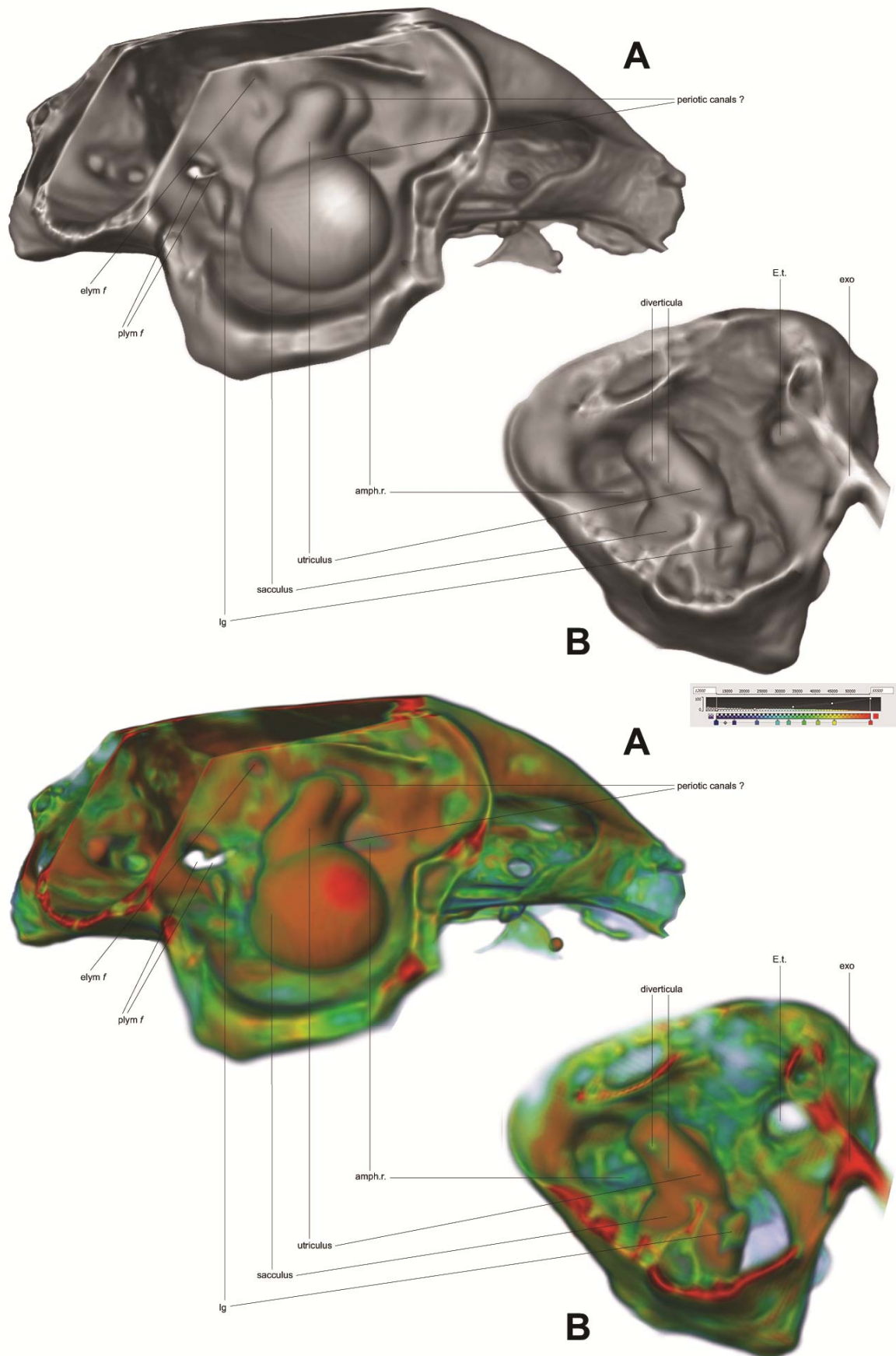


Fig. S1. (A) Right lateral view of the *Blommersia alexi* sp. nov. otic capsule. The cranium has been clipped laterally, posteriorly, and dorsally to facilitate visualization of the interior of the otic capsule. The anterior portion of the skull is clipped at the articulation of the palatine and alary cartilage (B) Corresponding left sagittal plane, medial view of the *Blommersia alexi* sp. nov. otic capsule. The volume has been clipped to facilitate visualization of the interior of the otic capsule [DRV6807 male; grey values: 12000-55500; volrenWhite and physics colormaps].

CHAPTER 5

Morphological variation in *Blommersia* pelvic shape coincides with muscular architecture and parallels genus phylogenetic evolution

Javier H. Santos-Santos^{1,2}, Mireia Guinovart-Castán¹, Barbara De Kegel³, Dominique Adriaens³, David R. Vieites¹

¹ *Department of Biogeography and Global Change (BGC-MNCN-CSIC), Museo Nacional de Ciencias Naturales, C/José Gutiérrez Abascal 2, E-28006, Madrid, Spain.*

² *Department of Animal Biology, University of Barcelona, Avenida Diagonal 645, 08028, Barcelona, Spain.*

³ *Evolutionary Morphology of Vertebrates, Ghent University, K.L. Ledeganckstraat 35, B-9000 Gent, Belgium*

ABSTRACT

Mantellids are a hyperdiverse group of frogs endemic to Madagascar, showing a large variation in morphology and ecological specialization that parallels their phylogenetic diversification. Among them, the genus *Blommersia* comprises several small species of small to miniature frogs, two of which occur in syntopy on the Comorian archipelago, which was colonized by their ancestor several millions of years ago in an event of transoceanic dispersal from Madagascar. They have evolved in isolation, which has supposed an evolutionary experiment of morphological and genetic divergence without competition. In mantellids, as well as in other amphibians, body size is correlated with dispersal capabilities and these may have allowed the colonization of new habitats in parallel to morphological divergence. Consequently, we hypothesized that variation in the *Blommersia* musculoskeletal anatomy implicated in locomotor performance would reflect potential differences between species in accordance to their diversification into different ecological niches and lifestyles. To tackle this question we focused on one of the main components of the anuran locomotor system: the pelvis. We compared the pelvic shape of seven *Blommersia* species, with special emphasis on the Comorian sister species pair and their Malagasy sister taxon. In addition, we mapped for the first time the insertion sites of the musculature on the *Blommersia* pelvis by means of a customized contrast staining technique prior to CT-scanning. Morphological distances resulting from the pelvic shape comparison between species correlated to a high extent with their 16S phylogenetic distances. In accordance, we discuss the observed patterns of pelvic shape variation and their relationship with size variation in the context of pelvic musculoskeletal architecture evolution in anurans and its potential interactions with locomotor function in the *Blommersia* genus.

KEYWORDS: *Blommersia*, computed tomography, contrast staining, musculoskeletal anatomy, pelvic shape.

INTRODUCTION

The role of adaptive radiations as generators of biodiversity is a main topic in evolutionary biology, albeit the mechanisms by which species diversify are still far from being completely understood. Accordingly extensive research has been carried out on the topic aiming to interpret the patterns and processes of speciation. Ecological, environmental, genetic, historical, functional, and reproductive factors have all been evoked to explain diversification in different situations. Even though all of these factors influence different aspects of organismal evolution, most of them have directly or indirectly contributed to shaping species' morphology and aided in their divergence.

Extant anurans are characterized for having a highly-derived musculoskeletal anatomy as a result of evolution to their bimodal lifestyle in both aquatic and terrestrial habitats (Handrigan & Wassersug, 2007; Gillis, 2010). Morphological specializations include a truncated axial skeleton, fused post-sacral vertebrae into an urostyle, elongated iliac shafts that articulate with the sacral diapophyses, fused pubis and ischium with the posterior ilium in a wheel-like acetabular structure, fused zeugopodian elements, and relatively long hindlimbs. Their specialized morphology is a clear reflection of a many-to-one mapping of form to function (Wainwright et al., 2005) in view of the large diversity of locomotor modes they have achieved with minimal changes to their *bauplan* (aka body plan), which has allowed them to colonize about every potential habitat (Duellman & Trueb, 1994). To this respect, there appears to be a strong relationship between the ilio-sacral and sacral-urostylic articulations and preferred locomotor mode in anurans (Emerson, 1982; Reilly & Jorgensen, 2011). The variation in articulation types confers, reduces, or transfers mobility, granting mechanical advantage to specific movements involved in each locomotor mode. For example, specialized long-distance jumpers have repeatedly evolved a sagittal-hinge type ilio-sacral articulation that restricts movement to the vertical (*i.e.* sagittal) plane, and a bicondylar sacro-urostylic joint that provides additional axial rigidity to lateral-bending behaviors. While these structural differences in skeletal elements have proven to largely predict locomotor mode, size differences and/or shape modifications in them can also alter the distribution, size, and properties of associated musculature influencing locomotor performance (Emerson, 1978; Zug, 1978; Emerson & De Jongh, 1980; James et al., 2007).

Jumping locomotion in basal anurans is believed to have evolved in response to escape predators on land, foraging, and/or increase dispersal capabilities (Gans & Parsons, 1966; Prikryl et al., 2009; Essner et al., 2010; Sigurdson et al., 2012; Lires et al., 2016). Throughout the evolution of the anuran *bauplan*, it is clear from that mentioned beforehand that pelvic morphology has played an important role in their functional diversification and geographic dispersal. Hence, we can expect that the selective pressures that have shaped this morphofunctional structure are still at work in extant species as they adapt to novel environments and different ecological pressures (Gomes et al., 2009; Hudson et al., 2016).

In Madagascar there are five endemic frog radiations with ~100% species endemism, of which the Mantellidae represent the largest adaptive radiation with 214 described species (amphibiaweb.org) and many more yet to be described (Vieites et al., 2009). Within these Malagasy radiations, the degree of morphological variation is large and its impact on species' diversification and distribution patterns of importance, but not yet fully understood. For example, it has been observed that body size influences species' range size and biogeographic setting in Madagascar, potentially influencing dispersal and speciation rates (Wollenberg et al., 2011; Pabijan et al., 2012). These processes are repercussive in species under processes of miniaturization, or nanism (Whittaker et al., 2007), which appears to be the trend in Malagasy mantellids and microhylids (Scherz et al., 2017a; 2017b). In these species, selective pressures have driven a reduction in their anatomy as an adaptive response to different ecological niches, although entailing strong biological constraints in order to maintain organ function at very small sizes. Up-to-date there are no studies concerning the impact of body size evolution on the musculoskeletal system of mantellids nor on its resulting influence on jumping performance, which can relate directly to their habitat selection, dispersal capability, and biogeographic speciation pattern.

The current study constitutes the first comparison within the Mantellidae of a functionally-relevant trait implicated in locomotor performance. We take advantage of a natural evolutionary experiment occurring on the Comorian archipelago, originated 6.5 Mya by the transoceanic dispersal of their most recent common ancestor from mainland Madagascar to Mayotte. This *Blommersia* ancestor diverged in sympatry on the island, producing two genetically-distinct syntopic sister species that differ in morphology and

breeding ecology (Chapter 3). More interestingly, one presents a trend of decreasing body size relative to its closest mainland sister taxon (*B. wittei*), while the other, one of increasing body size (Chapter 3). Given that the muscles implicated in locomotor mode and function insert on the pelvis, we hypothesize that differential adaptations to species' ecological niche will have generated divergent morphological variation in pelvic structure (Duncan & Turner, 1995). In addition, we search for any potential phylogenetic patterns in pelvic morphological variation by comparison between the Comorian sister species and their closest Malagasy relative, and between these and other Malagasy *Blommersia* representatives.

MATERIALS & METHODS

Specimens

A total of 41 frogs pertaining to seven phylogenetically-proximal *Blommersia* species (Table 1) were retrieved from the Vieites' Lab Collection (DRV) to be catalogued at the National Museum of Natural History, Madrid (MNCN-CSIC) and loaned from the herpetological collection of the Department of Animal Biology at the University of Antananarivo (UADBA). Individuals were selected based upon availability and anatomical integrity with the intention of covering the observable range of variation within each species, including male-female proportions and geographical locations. Most individuals were collected recently by the authors (JHS-S and DRV) in fieldwork excursions to Mayotte and Madagascar. Both Comorian sister species, *B. nataliae* **sp. nov.** and *B. alexi* **sp. nov.**, are pending formal taxonomic description (Chapter 3), and the complete skeletal description of *B. alexi* **sp. nov.** is pending publication (Chapter 4). Measurements of snout-vent length and hindlimb length were taken on all specimens with a caliper (0.1 mm).

Morphological Data Acquisition

In order to obtain the precise morphology of the pelvic skeleton without the destruction of the museum samples, specimens were fixed with cotton and submerged in 70% ethanol within 50 mL polypropylene falcon tubes before CT-scanning (*i.e.* computed tomography) in a Nikon XT H-160 system [reconstructed voxel size (μm) = 18-38 (isometric); X-ray (kV) = 53-58; X-ray (μA) = 169-188; Projections = 1800; voxels =

1008] at the internal Service of Non-destructive Techniques (MNCN-CSIC). The CT-scans were reconstructed with CT Pro 3D software and volumes rendered in VGStudio Max 2.2 © (Volume Graphics GmbH, VGL). Isosurfaces were determined through visual examination for each specimen by the same observer (MG-C) to best capture the density histogram of the skeletal structures that constitute the pelvis. Subsequently, bioinformatics segmentation of the pelvis was done manually by separating the head of the femur from the acetabulum and the sacral vertebra from the pelvis at the ilio-sacral articulation. The resulting segmentation was then extracted as a 3D polygon volumetric model (.ply). Polygon models were then post-processed in MeshLab (Cignoni et al., 2008). Computational error/noise in the models' point clouds were corrected as well as any incongruence in their triangulation. In addition, anatomically non-homologous structures (*e.g.* individual-unique bony hypertrophies) were removed from the models to standardize pelvic shape for intra- and inter-specific shape variation comparisons. Lastly, only the external surface of the volumetric model was kept for downstream analyses to further avoid anatomical non-homologies in the bone's internal structure. Final models ranged from 30 – 134k polygons (median = 52k).

To visualize hindlimb musculature and corroborate muscle insertion sites on the surface of the pelvis, additional Comorian specimens of both species were stained prior to CT-scanning to increase the images' contrast between tissue types (Table S1). We followed a custom protocol that is reversible in most part and does not cause damage to the rare samples in order to maintain their potential consultation unaltered for future reference. First samples were washed in running tap water for 8h prior to an initial staining in a 2.5% phosphomolibdic acid solution within a vacuum chamber for one week (Descamps et al., 2014). Later specimens were stained a second time in a 100% IKI [I2 1% ; KI 2%] solution for an additional 24h (Gignac & Kley, 2014). Subsequently excess iodine was washed during 8h and samples were submerged in a phosphate-buffered saline solution for 48h to rehydrate muscle tissues prior to scanning (Vickerton et al., 2013). The staining procedure was carried out at the Evolutionary Morphology of Vertebrates Lab of Ghent University, Belgium and CT-scans were performed with a custom setup [reconstructed voxel size (μm) = 30-35 (isometric); X-ray (kV) = 80; X-ray (μA) = 375; Projections = 1801; voxels = 1166] at the Center for X-ray Tomography (UGCT).

Table 1. Holding collections and field numbers of the *Blommersia* specimens whose pelvis were compared in the current study. Sex is indicated when available. Localities are indicated for Comorian specimens. In addition, average snout-vent length (SVL) and hindlimb length (HL) are given for each species in mm.

Species	Collection	Field no.	Sex	Locality	SVL	HL																																																																																																																																																																											
<i>B. blommersae</i> (Guibé, 1974)	UADBA	ZCMV8	-	-	18.4 ± 0.9	34.2 ± 1																																																																																																																																																																											
	UADBA	FG/MV633	-	-			<i>B. domerguei</i> (Guibé, 1974)	UADBA	ZCMV271	-	-	14.4 ± 0.3	23.7 ± 0.5	UADBA	ZCMV272	-	-	<i>B. grandisonae</i> (Guibé, 1974)	UADBA	MV1356	-	-	20.4 ± 0.6	35.7 ± 3.8	UADBA	ZCMV5491	-	-	<i>B. sarotra</i> (Glaw & Vences, 2002)	MNCN	DRV8867	M	-	18.6 ± 0.5	33.1 ± 1.9	MNCN	DRV8870	M	-	<i>B. alexi</i> sp. nov.	MNCN	DRV6805	F	Mont Combani	26.9 ± 2.6	54.1 ± 4.9	MNCN	DRV6807	M	Mont Sapere	MNCN	DRV6813	F	Mont Sapere	MNCN	DRV6832	M	Mont Bénara	MNCN	DRV6833	M	Mont Bénara	MNCN	DRV6835	M	Mont Choungi	MNCN	DRV6836	M	Mont Bénara	MNCN	DRV6841	M	Mont Bénara	MNCN	DRV6848	F	Mont Combani	MNCN	DRV6851	F	Mont Combani	<i>B. nataliae</i> sp. nov.	MNCN	DRV6808	F	Mont Sapere	20.1 ± 1.6	37.3 ± 2.2	MNCN	DRV6854	F	Mont Sapere	MNCN	DRV6855	F	Mont Sapere	MNCN	DRV6857	M	Mont Sapere	MNCN	DRV6859	M	Mont Sapere	MNCN	DRV6860	M	Mont Sapere	MNCN	DRV6862	M	Mont Sapere	MNCN	DRV6863	M	Mont Sapere	MNCN	DRV6864	M	Mont Sapere	MNCN	DRV6866	M	Mont Sapere	MNCN	DRV6867	M	Mont Sapere	MNCN	DRV6868	F	Mont Sapere	MNCN	DRV6869	F	Mont Sapere	<i>B. wittei</i> (Guibé, 1974)	MNCN	DRV8719	M	-	24.3 ± 1.3	41.1 ± 2.5	MNCN	DRV8755	M	-	MNCN	DRV8767	M	-	MNCN	DRV8768	M	-	MNCN	DRV8784	F	-	MNCN	DRV8816	F	-	UADBA	FGZC376	-	-	UADBA	FGZC406	-	-	UADBA	FGZC1466	-	-	UADBA
<i>B. domerguei</i> (Guibé, 1974)	UADBA	ZCMV271	-	-	14.4 ± 0.3	23.7 ± 0.5																																																																																																																																																																											
	UADBA	ZCMV272	-	-			<i>B. grandisonae</i> (Guibé, 1974)	UADBA	MV1356	-	-	20.4 ± 0.6	35.7 ± 3.8	UADBA	ZCMV5491	-	-	<i>B. sarotra</i> (Glaw & Vences, 2002)	MNCN	DRV8867	M	-	18.6 ± 0.5	33.1 ± 1.9	MNCN	DRV8870	M	-	<i>B. alexi</i> sp. nov.	MNCN	DRV6805	F	Mont Combani	26.9 ± 2.6	54.1 ± 4.9	MNCN	DRV6807	M	Mont Sapere		MNCN	DRV6813	F	Mont Sapere			MNCN	DRV6832	M	Mont Bénara	MNCN	DRV6833	M	Mont Bénara	MNCN	DRV6835	M	Mont Choungi	MNCN	DRV6836	M	Mont Bénara	MNCN	DRV6841	M	Mont Bénara	MNCN	DRV6848	F	Mont Combani	MNCN	DRV6851	F	Mont Combani	<i>B. nataliae</i> sp. nov.	MNCN	DRV6808	F	Mont Sapere	20.1 ± 1.6	37.3 ± 2.2	MNCN		DRV6854	F	Mont Sapere	MNCN			DRV6855	F	Mont Sapere	MNCN	DRV6857	M	Mont Sapere	MNCN	DRV6859	M	Mont Sapere	MNCN	DRV6860	M	Mont Sapere	MNCN	DRV6862	M	Mont Sapere	MNCN	DRV6863	M	Mont Sapere	MNCN	DRV6864	M	Mont Sapere	MNCN	DRV6866	M	Mont Sapere	MNCN	DRV6867	M	Mont Sapere	MNCN	DRV6868	F	Mont Sapere	MNCN	DRV6869	F	Mont Sapere	<i>B. wittei</i> (Guibé, 1974)	MNCN	DRV8719	M	-		24.3 ± 1.3	41.1 ± 2.5	MNCN	DRV8755			M	-	MNCN	DRV8767	M	-	MNCN	DRV8768	M	-	MNCN	DRV8784	F	-	MNCN	DRV8816	F	-	UADBA	FGZC376	-	-	UADBA	FGZC406	-	-	UADBA	FGZC1466	-	-	UADBA	FGZC3139	-
<i>B. grandisonae</i> (Guibé, 1974)	UADBA	MV1356	-	-	20.4 ± 0.6	35.7 ± 3.8																																																																																																																																																																											
	UADBA	ZCMV5491	-	-			<i>B. sarotra</i> (Glaw & Vences, 2002)	MNCN	DRV8867	M	-	18.6 ± 0.5	33.1 ± 1.9	MNCN	DRV8870	M	-	<i>B. alexi</i> sp. nov.	MNCN	DRV6805	F	Mont Combani	26.9 ± 2.6	54.1 ± 4.9	MNCN	DRV6807	M	Mont Sapere		MNCN	DRV6813	F	Mont Sapere			MNCN	DRV6832	M	Mont Bénara		MNCN	DRV6833	M	Mont Bénara			MNCN	DRV6835	M	Mont Choungi	MNCN	DRV6836	M	Mont Bénara	MNCN	DRV6841	M	Mont Bénara	MNCN	DRV6848	F	Mont Combani	MNCN	DRV6851	F	Mont Combani	<i>B. nataliae</i> sp. nov.	MNCN	DRV6808	F	Mont Sapere	20.1 ± 1.6	37.3 ± 2.2	MNCN		DRV6854	F	Mont Sapere	MNCN			DRV6855		F	Mont Sapere	MNCN	DRV6857			M	Mont Sapere	MNCN	DRV6859	M	Mont Sapere	MNCN	DRV6860	M	Mont Sapere	MNCN	DRV6862	M	Mont Sapere	MNCN	DRV6863	M	Mont Sapere	MNCN	DRV6864	M	Mont Sapere	MNCN	DRV6866	M	Mont Sapere	MNCN	DRV6867	M	Mont Sapere	MNCN	DRV6868	F	Mont Sapere	MNCN	DRV6869	F	Mont Sapere	<i>B. wittei</i> (Guibé, 1974)	MNCN	DRV8719	M	-		24.3 ± 1.3	41.1 ± 2.5	MNCN	DRV8755				M	-			MNCN	DRV8767	M	-	MNCN	DRV8768	M	-	MNCN	DRV8784	F	-	MNCN	DRV8816	F	-	UADBA	FGZC376	-	-	UADBA	FGZC406	-	-	UADBA	FGZC1466	-	-	UADBA	FGZC3139	-	-	
<i>B. sarotra</i> (Glaw & Vences, 2002)	MNCN	DRV8867	M	-	18.6 ± 0.5	33.1 ± 1.9																																																																																																																																																																											
	MNCN	DRV8870	M	-			<i>B. alexi</i> sp. nov.	MNCN	DRV6805	F	Mont Combani	26.9 ± 2.6	54.1 ± 4.9	MNCN	DRV6807	M	Mont Sapere		MNCN	DRV6813	F	Mont Sapere			MNCN	DRV6832	M	Mont Bénara		MNCN	DRV6833	M	Mont Bénara			MNCN	DRV6835	M	Mont Choungi		MNCN	DRV6836	M	Mont Bénara			MNCN	DRV6841	M	Mont Bénara	MNCN	DRV6848	F	Mont Combani	MNCN	DRV6851	F	Mont Combani	<i>B. nataliae</i> sp. nov.	MNCN	DRV6808	F	Mont Sapere	20.1 ± 1.6	37.3 ± 2.2	MNCN		DRV6854	F	Mont Sapere	MNCN			DRV6855		F	Mont Sapere	MNCN	DRV6857			M		Mont Sapere	MNCN	DRV6859	M			Mont Sapere	MNCN	DRV6860	M	Mont Sapere	MNCN	DRV6862	M	Mont Sapere	MNCN	DRV6863	M	Mont Sapere	MNCN	DRV6864	M	Mont Sapere	MNCN	DRV6866	M	Mont Sapere	MNCN	DRV6867	M	Mont Sapere	MNCN	DRV6868	F	Mont Sapere	MNCN	DRV6869	F	Mont Sapere	<i>B. wittei</i> (Guibé, 1974)	MNCN	DRV8719	M	-		24.3 ± 1.3	41.1 ± 2.5	MNCN	DRV8755				M	-				MNCN	DRV8767			M	-	MNCN	DRV8768	M	-	MNCN	DRV8784	F	-	MNCN	DRV8816	F	-	UADBA	FGZC376	-	-	UADBA	FGZC406	-	-	UADBA	FGZC1466	-	-	UADBA	FGZC3139	-	-			
<i>B. alexi</i> sp. nov.	MNCN	DRV6805	F	Mont Combani	26.9 ± 2.6	54.1 ± 4.9																																																																																																																																																																											
	MNCN	DRV6807	M	Mont Sapere																																																																																																																																																																													
	MNCN	DRV6813	F	Mont Sapere																																																																																																																																																																													
	MNCN	DRV6832	M	Mont Bénara																																																																																																																																																																													
	MNCN	DRV6833	M	Mont Bénara																																																																																																																																																																													
	MNCN	DRV6835	M	Mont Choungi																																																																																																																																																																													
	MNCN	DRV6836	M	Mont Bénara																																																																																																																																																																													
	MNCN	DRV6841	M	Mont Bénara																																																																																																																																																																													
	MNCN	DRV6848	F	Mont Combani																																																																																																																																																																													
	MNCN	DRV6851	F	Mont Combani																																																																																																																																																																													
<i>B. nataliae</i> sp. nov.	MNCN	DRV6808	F	Mont Sapere	20.1 ± 1.6	37.3 ± 2.2																																																																																																																																																																											
	MNCN	DRV6854	F	Mont Sapere																																																																																																																																																																													
	MNCN	DRV6855	F	Mont Sapere																																																																																																																																																																													
	MNCN	DRV6857	M	Mont Sapere																																																																																																																																																																													
	MNCN	DRV6859	M	Mont Sapere																																																																																																																																																																													
	MNCN	DRV6860	M	Mont Sapere																																																																																																																																																																													
	MNCN	DRV6862	M	Mont Sapere																																																																																																																																																																													
	MNCN	DRV6863	M	Mont Sapere																																																																																																																																																																													
	MNCN	DRV6864	M	Mont Sapere																																																																																																																																																																													
	MNCN	DRV6866	M	Mont Sapere																																																																																																																																																																													
	MNCN	DRV6867	M	Mont Sapere																																																																																																																																																																													
	MNCN	DRV6868	F	Mont Sapere																																																																																																																																																																													
	MNCN	DRV6869	F	Mont Sapere																																																																																																																																																																													
<i>B. wittei</i> (Guibé, 1974)	MNCN	DRV8719	M	-	24.3 ± 1.3	41.1 ± 2.5																																																																																																																																																																											
	MNCN	DRV8755	M	-																																																																																																																																																																													
	MNCN	DRV8767	M	-																																																																																																																																																																													
	MNCN	DRV8768	M	-																																																																																																																																																																													
	MNCN	DRV8784	F	-																																																																																																																																																																													
	MNCN	DRV8816	F	-																																																																																																																																																																													
	UADBA	FGZC376	-	-																																																																																																																																																																													
	UADBA	FGZC406	-	-																																																																																																																																																																													
	UADBA	FGZC1466	-	-																																																																																																																																																																													
	UADBA	FGZC3139	-	-																																																																																																																																																																													

Morphological Data Analysis

Pelvic shape was compared by means of a novel landmark-less geometric morphometric technique: Generalized Procrustes Surface Analysis (GPSA; Pomidor et al., 2016). This new method allows the exploitation of morphological output resulting from high-resolution scanning technology without the time-consuming process of identification and digitization of functionally homologous landmarks on the structure of interest. GPSA

adapts the Iterative Closest Point algorithms (Besl & McKay, 1992; Chen & Medioni, 1992) to the Generalized Procrustes Analysis paradigm (Rohlf & Slice, 1990) to perform a symmetric superimposition of model surfaces and calculate an associated distance metric, the Procrustes Surface Metric (PSM), analogous to Procrustes distance that quantifies shape difference (Pomidor et al., 2016). For accurate superimposition an individual must be chosen as the prototype in an analysis on the basis that it is the most complete, most representative, and least morphometrically atypical individual in the dataset. Analyses were performed in the Java © executable provided by Pomidor upon personal request and available at <http://morphlab.sc.fsu.edu/software/gpsa/index.html>. These were performed with and without size standardization (*i.e.* centroid size = 1) to evaluate the influence of size differences between individuals and species in intra- and inter-specific pelvic shape comparisons.

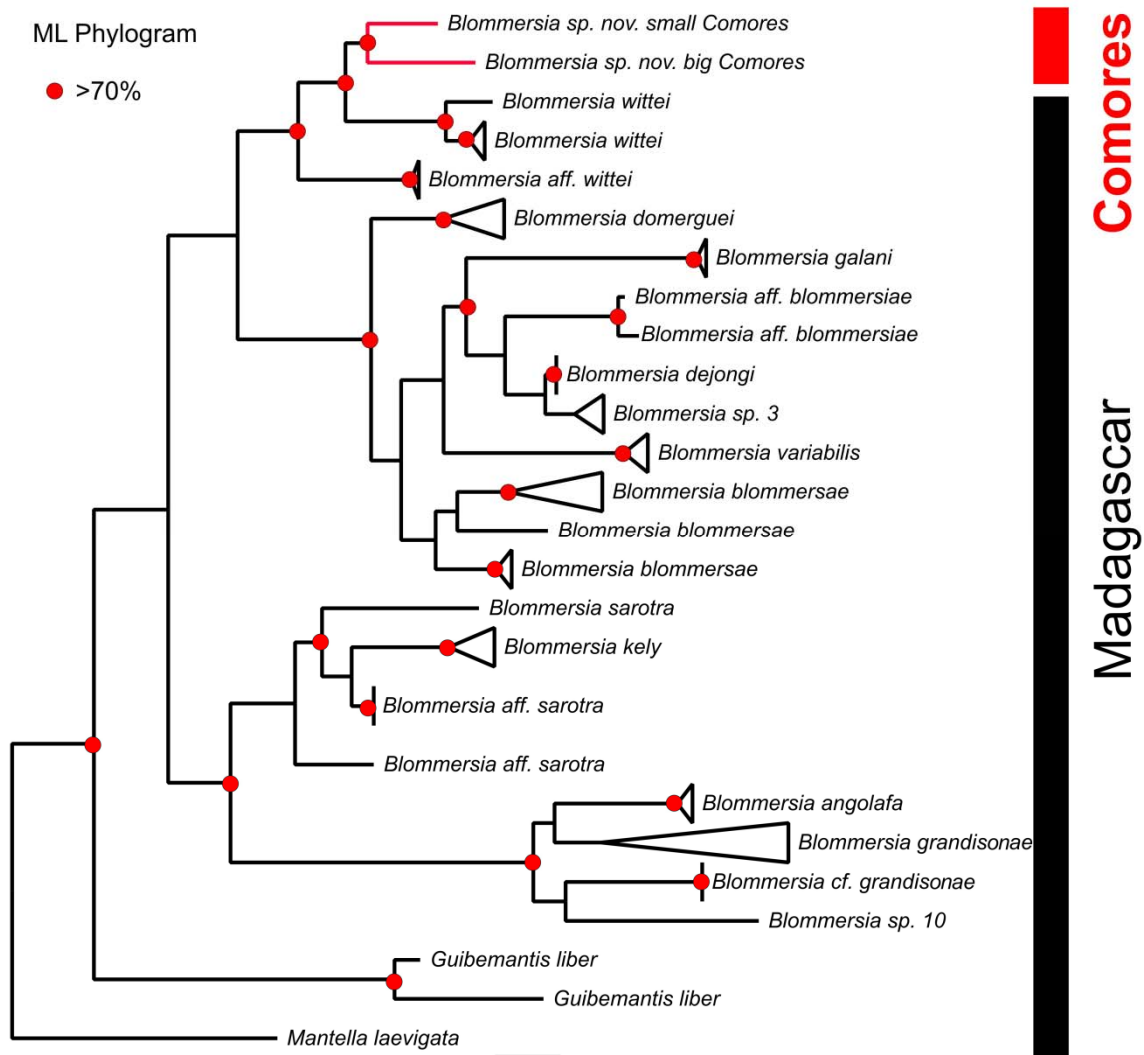


Fig. 1. Maximum Likelihood phylogenetic reconstruction of 16S rRNA relationships within *Blommersia*. Nodes with Maximum Likelihood statistical support higher than 70% are shown in red.

We assessed the intraspecific variation in pelvic morphology through GPSA on datasets of the Comorian sister species and their Malagasy sister taxon, and its interspecific variation on datasets consisting of all possible combinations of these three species. An individual of the *Blommersia wittei* sample was always used as the prototype in analyses containing the three species. In addition, to focalize pelvic shape changes on more potentially biologically-meaningful interspecific variation, we performed interspecific GPSA analyses on a dataset consisting of the mean pelvic shapes for these three species and on another dataset consisting in the mean pelvic shapes of all seven *Blommersia* species. Interspecimen PSM values were compared across analyses, and Principal Coordinate Analysis (PCoA) scores resulting from GPSA pointwise comparisons were plotted in R v3.5.1 statistical software (<https://www.R-project.org>) to visualize the distribution of specimens along PCoA shape axes. Differences between species in PSM values and PCoA loadings were evaluated statistically in IBM SPSS Statistics v23 ($\alpha = 0.05$). For each GPSA analysis, overall pelvic shape disparity and the pelvic shape variation explained by each PCoA axes are visualized independently on the sample's mean surface in 3D by means of a color-coded heatmap based on the variation in PSM value at each vertex of the model relative to the sample's consensus.

Phylogenetic Data

Mitochondrial rRNA 16S sequences were compiled from Genbank for all available *Blommersia* species. The same 16S fragment was gathered for the two Comorian species that do not appear in Genbank by the Vieites Lab from a large RNAseq dataset. Sequences were aligned under the Clustal-Wallis algorithm using Genious software, and these were filtered for the same seven species of the morphological analysis (Fig. 1). In order to estimate evolutionary divergence between species a genetic distance matrix was calculated using the Maximum Composite Likelihood model (Tamura et al., 2004). The rate variation among sites was modelled with a gamma distribution (shape parameter = 1). All positions with less than 95% coverage were eliminated, meaning that fewer than 5% alignment gaps, missing data, and ambiguous bases were allowed at any position. There were a total of 475 positions in the final dataset. Analyses were performed in MEGA6 software (Tamura et al., 2013). To determine whether or not there is correlation between observed genetic and morphological variation within the *Blommersia* genus, a Mantel test

(1000 permutations) was performed in R comparing 16S genetic and PSM distance matrices.



Fig. 2. Imprints of the pelvic musculature insertion areas on the 3D pelvic model of the DRV6834 *B. alexi* **sp. nov.** specimen. Insertion areas are not perfectly drawn to scale (see text). Numbers designate the muscles found in Table 2 [m. coccygeiliacus not drawn]. The hashed area of the m. iliacus internus indicates its position on the medial face of the iliac shaft. The * denotes the relative position of the *Blommersia* femoral gland.

RESULTS

Characterization of Blommersia Pelvic Musculature

CT-scans of stained specimens were examined to locate and identify the different muscles inserting onto the *Blommersia* pelvis. As the representative of our species, and due to its larger size that facilitates visualization, we extracted a 3D model of the pelvis of a *B. alexi* **sp. nov.** specimen (DRV6834) and mapped onto the model's surface its corresponding muscles insertions coming from the stained CT-scan of the same animal (Fig. 2). This procedure allows for a reasonable visualization of the relative positions of

Table 2. Pelvic musculature names, locomotor function, and insertion area based on Duellman & Trueb, 1994 and Prikryl et al., 2009. Muscle numbers match Figure 2.

#	Muscle Complex	Muscle	Locomotor Function	Pelvic Insertion Area
1		obliquus externus	Hypaxial flank musculature: provides support for the viscera and exerts a ventral force on the axial column	Lateral anterior ilial shaft
2		transversus	Hypaxial flank musculature: provides support for the viscera and exerts a ventral force on the axial column	Ventrolateral surface of the anterior ilial shaft
3		iliacus externus	draws the femur forward and flexes the hip joint	Mid-region of the lateral ilial shaft and crest
4	triceps femoris	glutaeus magnus	extends the knee joint and flexes the hip joint	Anterolateral region of the posterior ilial process
5		iliofibularis	abducts the femur and flexes the knee	Posteroventral region of the posterior ilial process
6		iliofemoralis	retraction and adduction of the femur; draws the femur dorsally	Posterodorsal region of the posterior ilial process
7	triceps femoris	tensor fascia latae	extends the knee joint and flexes the hip joint	Lateral surface of the ventral mid-region of the ilial shaft
8		iliacus internus	protracts and abducts the femur	Lateral and medial posterior ilium base and preacetabulum
9		coccygeollicaus	Epaxial musculature: rotates the urostyle ventrally	Medial surface of the ilial shaft and ilial crest
10		semimembranosus	adducts the femur and flexes the knee joint	Dorsoposterior ischium margin
11	obturator externus-gemellus- quadratus femoris	gemellus	pulls the femur ventrally	Anterior lateral ischium surface
12	sartoriosemitendinosus	semitendinosus (dorsal head)	abducts the femur, pulls the femur ventrally, and flexes the knee joint	Posterior lateral ischium surface
13	gracilis	gracilis major	pulls the thigh backwards, flexes the knee joint, and extends the hip joint	Posterior ischium border
14		adductor magnus (dorsal head)	adducts the hip joint	Ventral ischium margin
15		quadratus femoris	pulls the femur ventrally	Ventrolateral ischium surface
16		adductor magnus (ventral head)	adducts the hip joint	Ventral pubic margin
17	sartoriosemitendinosus	semitendinosus (ventral head)	abducts the femur, pulls the femur ventrally, and flexes the knee joint	Posteroventral pelvis lateral surface at pubis-ischium union
18	obturator externus-gemellus- quadratus femoris	obturator externus	pulls the femur ventrally	Ventral lateral pubic surface
19	sartoriosemitendinosus	sartorius	abducts the femur, pulls the femur ventrally, and flexes the knee joint	Anteroventral preacetabular ilium base and pubic margin
20	pectineus-adductor longus	adductor longus	adducts and protracts the femur	Anteroventral preacetabular ilium base and pubic lateral surface
21	pectineus-adductor longus	pectineus	adducts the femur, fixes the femur in the acetabulum	Pubic lateral surface
22		obturator internus	pulls the femur dorsally and rotates the femur	Complete outer acetabulum labrum margin, excluding its most-dorsal margin
23	triceps femoris	cruralis	extends the knee joint and flexes the hip joint	Anteroventral margin of the acetabulum

the pelvic musculature; however muscle insertion areas are not perfectly drawn to scale due to differences in the depth along the 2D plane of the volume at which muscles insert. To obtain a more precise characterization of the pelvic musculature, including muscles volumes, and its architecture, a complete segmentation of the *Blommersia* pelvic musculature is underway. For the time being we provide a video of the pelvic musculature across the frog's sagittal plane and several images of the ongoing segmentation in the Supplementary Material.

Table 3. Morphological disparity for *Blommersia* intra- and inter-specific comparisons of pelvic shape.

Species	Pelvic Morphological Disparity					
	CS = 1					
	min.	max.	range	min.	max.	range
<i>B. alexi</i>	0.006 ± 2E-6	0.059 ± 0.003	0.053	0.022 ± 2E-5	0.263 ± 0.05	0.241
<i>B. nataliae</i>	0.008 ± 6E-6	0.076 ± 0.007	0.068	0.020 ± 2E-5	0.142 ± 0.03	0.122
<i>B. wittei</i>	0.006 ± 2E-6	0.058 ± 0.007	0.052	0.016 ± 2E-5	0.340 ± 0.06	0.323
<i>B. alexi</i> - <i>B. nataliae</i>	0.009 ± 1.2E-5	0.056 ± 0.004	0.047	0.026 ± 1E-4	0.203 ± 0.05	0.177
<i>B. alexi</i> - <i>B. wittei</i>	0.009 ± 1E-5	0.116 ± 0.005	0.107	0.029 ± 1E-4	0.358 ± 0.08	0.329
<i>B. nataliae</i> - <i>B. wittei</i>	0.010 ± 1.6E-5	0.066 ± 0.015	0.056	0.022 ± 6E-5	0.253 ± 0.07	0.231
<i>B. alexi</i> - <i>B. nataliae</i> - <i>B. wittei</i>	0.010 ± 1.5E-5	0.053 ± 0.004	0.043	0.030 ± 1.6E-4	0.327 ± 0.14	0.297
<i>B. alexi</i> - <i>B. nataliae</i> - <i>B. wittei</i>	0.003 ± 3E-9	0.083 ± 0.003	0.080	0.015 ± 1E-8	0.368 ± 0.13	0.353
<i>7 Blommersia spp.</i>	0.011 ± 2.1E-5	0.060 ± 0.020	0.049	0.031 ± 2.4E-4	0.356 ± 0.15	0.325
<i>7 Blommersia spp.</i>	0.006 ± 2E-6	0.079 ± 0.007	0.073	0.023 ± 2E-5	0.339 ± 0.20	0.315

The average minimum, maximum, and range of pointwise variance are given for each comparison. Analyses in bold indicate they were performed on species' mean shape models. Values in the left column correspond to analyses standardized for size, ie. centroid size (CS) = 1.

Pelvic Morphological Disparity

Morphological disparity as reflected by variance at each vertex of the pelvis model in intraspecific pelvic shape is largest in *B. nataliae* **sp. nov.** However, when including size variation in the analyses it is *B. wittei* who presents the highest disparity followed by *B. alexi* **sp. nov.** (Table 3). PSM values of individuals to their respective consensus across intraspecific analyses were not significantly different when standardizing for size ($p =$

0.487), however there was a significant difference between *B. alexi* **sp. nov.** (0.15) and *B. wittei* (0.07) when including size variation in the analyses ($p = 0.021$).

Pelvic morphological disparity in interspecific comparisons resulted the largest between *B. alexi* **sp. nov.** and *B. wittei*, and the smallest between the Comorian sister species. When including size variation in the analyses the same pattern holds (Table 3). PSM values of individuals to their respective interspecific analysis consensus were not significantly different when standardized for size, however when including size variation in the analyses ($p < 0.05$) *B. alexi* **sp. nov.** presents the largest PSM values and *B. wittei* larger than *B. nataliae* **sp. nov.**

Differences across interspecific comparisons using either individual or species' mean models revealed that larger morphological disparity is observed when utilizing species' mean models (Table 3). As would be expected, all analyses increased in morphological disparity value when including size variation. An ANOVA on individual's centroid size values revealed significant differences between the three species ($F = 39.35$; $p < 0.001$), with *B. nataliae* **sp. nov.** presenting the smallest size (2.4) compared to *B. wittei* (2.7) and *B. alexi* **sp. nov.** (3.3). This analysis was not performed on the seven species sample due to insufficient sample size for the remaining species.

Ordination of Pelvic Shape Variation

Intraspecific

PCoA on intraspecific pelvis shape variation displayed significant differences between male and female distribution in shape space only for size-standardized *B. nataliae* **sp. nov.** (Wilk's $\lambda = 0$; $p = 0.005$). For this species, females presented significantly lower values on PCo1 ($p = 0.011$; Fig. 3).

Shape variation associated with lower PCo1 values (Fig. 3) consists in an overall decrease in size and robustness of the pelvis. This results in a relatively decreased aperture of the iliac shafts, a relative decrease in height and length of the iliac shafts, a relative decrease in the angle of inclination of the iliac crests, and a relative decrease in robustness of the entire acetabular portion of the pelvis, especially at the iliac process and posterodorsal ilium and ischium.

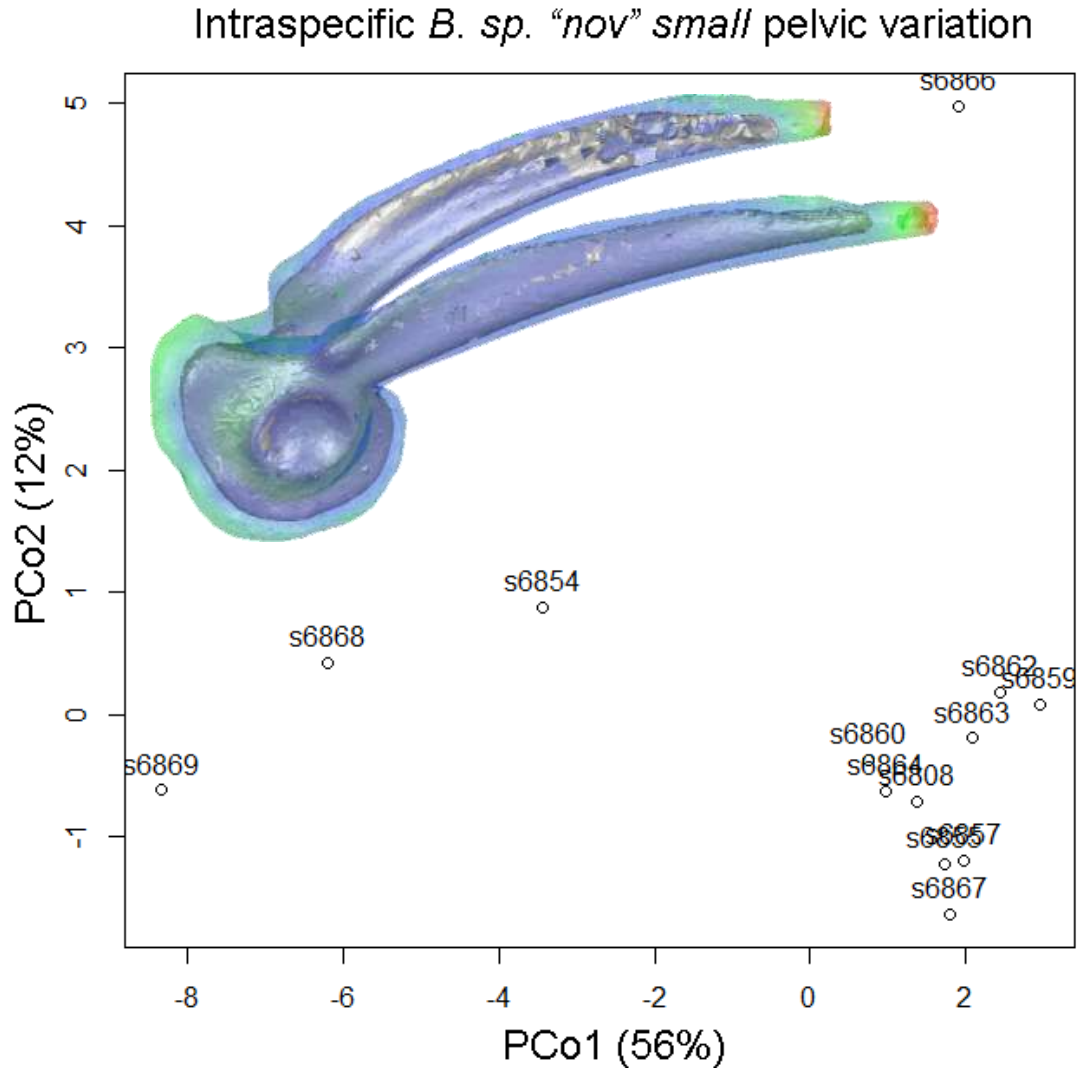


Fig. 3. Principal Coordinate PCo1 – PCo2 plot for *B. nataliae sp. nov.* intraspecific pelvic shape variation standardized for size (CS = 1). Pelvic shape variation associated to PCo1 is illustrated overlaying the pelvic models described by the most negative (grey) and the most positive PCo1 scores (transparent colored) in the lateral view.

Interspecific

PCoA on the pelvic shape variation between Comorian sister species resulted in a significant species' ordination in shape space when including size variation (Wilk's $\lambda = 0$; $p = 0.050$). This is reflected on PCo1 ($p < 0.001$) for which *B. nataliae sp. nov.* presents more negative values and *B. alexi sp. nov.* more positive values (Fig. 4).

Shape variation associated with increasing PCo1 value (Fig. 4) consists in a relatively increased width of the pelvis at the level of the iliac processes that results in a relatively increased lateral aperture of the iliac shafts, a relative increase in length of the iliac shafts, a relative increase in the angle of inclination of the iliac crests, and an extensive isometric

increase in size and robustness of the iliac processes, acetabulum, and entire acetabular portion of the pelvis.

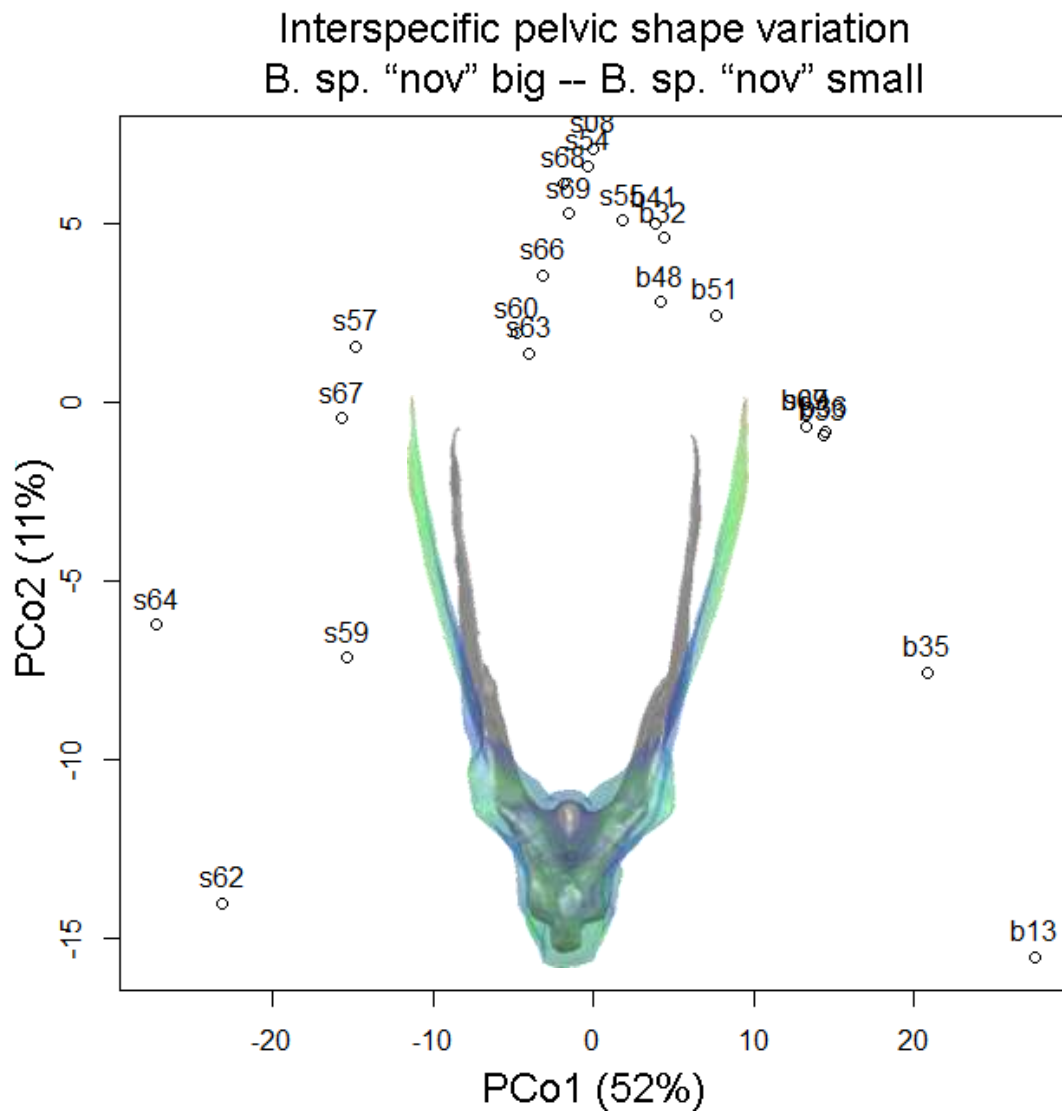


Fig. 4. Principal Coordinate PCo1 – PCo2 plot for *B. alexi* sp. nov. – *B. nataliae* sp. nov. interspecific pelvic shape variation when including size. Pelvic shape variation associated to PCo1 is illustrated overlaying the pelvic models described by the most negative (grey) and the most positive PCo1 scores (transparent colored) in the dorsal view.

PCoA on the pelvic shape variation between the Comorian sister species and their *B. wittei* sister taxon resulted in a marginally significant species' ordination in shape space when individuals were standardized for size (Pillai's Trace = 1.992, $p = 0.007$; Wilk's $\lambda = 0$, $p = 0.069$), however this outcome was better distinguished when including size variation in the analysis (Wilk's $\lambda = 0$; $p = 0.007$). To focalize biologically-relevant pelvic shape variation PCoA was repeated for the three species sample utilizing as models the species' mean pelvic shape (Fig. 5).

Shape variation associated with increasing PCo1 value (Fig. 5) consists in a relative decrease in iliac shaft length, a relative increase in height of the anterior iliac crest, a relative increase in aperture of the iliac shafts, a relative decrease in height of the posterior iliac shafts, a relative decrease in robustness of the iliac processes, the acetabulum, the ventral region of the pelvis at the pubis-ischium union, the lateral surface of the ischium and the anterior ilium base, a relative increase in length along the anterior-posterior axis of the ilium base, and a relative increase in robustness of the anterior region of the pubis, of the posterior ilium base, posterior ischium margin and at the insertion of the mm. quadratus femoris and dorsal head of the adductor magnus.

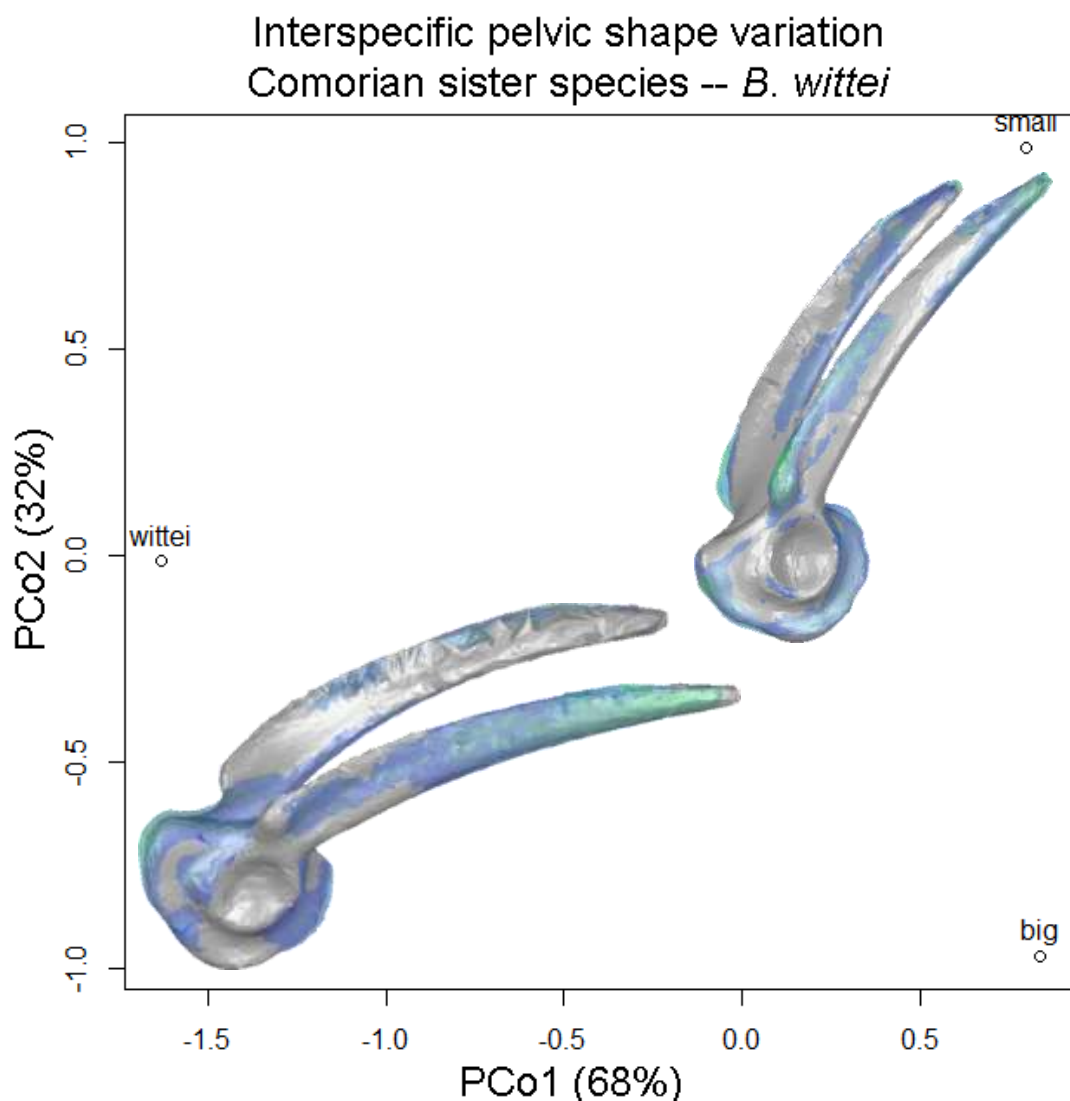


Fig. 5. Principal Coordinate PCo1 – PCo2 plot for the Comorian sister species – *B. wittei* interspecific mean pelvic shape variation standardized for size (CS = 1). Pelvic shape variation associated to PCo1 is illustrated in the bottom left corner overlaying the pelvic models described by the most negative (grey) and the most positive PCo1 scores (transparent colored) in the lateral view. Pelvic shape variation associated to PCo2 is illustrated on the right overlaying the pelvic models described by the most positive (grey) and the most negative (transparent colored) PCo1 scores in a vertical-lateral view.

Shape variation associated with decreasing PCo2 value (Fig. 5) consists in a relative increase in iliac shaft length, a relative increase in the angle of inclination of the iliac crests, a relative increase in size, height and lateral robustness of the iliac processes, and a relative increase in robustness of the anterior ilium base, anterior margin of the pubis, posterior margin of the ischium and at the insertion of the m. obturator externus.

Within-genus

PCoA on the pelvic shape variation between the seven *Blommersia* species resulted in a significant species' ordination in shape space both when standardized for size (Wilk's $\lambda = 0$, $p = 0.001$) and when including size variation (Wilk's $\lambda = 0$, $p < 0.001$). Again, PCoA was repeated for the sample utilizing as models the species' mean pelvic shape to focalize biologically-relevant pelvic shape variation (Fig. 6).

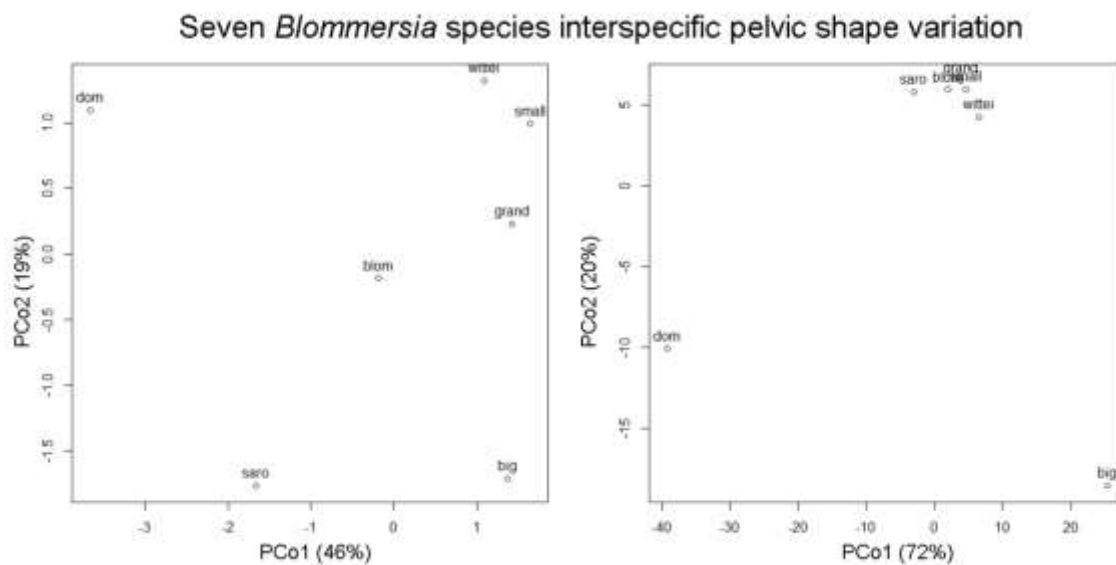


Fig. 6. Principal Coordinate PCo1 – PCo2 plot for the interspecific mean pelvic shape variation within the seven *Blommersia* species sample. Left: standardized for size (CS = 1). Right: including size variation.

Shape variation associated with increasing PCo1 values (Fig. 6 Left) consists in a relative decrease in iliac shaft length, a relative large increase in the angle of inclination of the iliac crests, a relative increase in lateral aperture of the iliac shafts starting from their posterior base, a relative increase in length along the anterior-posterior axis of the ilium base, and a relative large increase in robustness of the entire ilium base (more so anteriorly), anterior pubis, ventral pubic margin and posterior ischium margin.

Shape variation associated with decreasing PCo2 values (Fig. 6 Left) consists in a relative decrease in iliac shaft length, iliac crest height and iliac shaft aperture, a relative increase in pelvic width at the level of the iliac processes, a relative decrease in robustness of the posterior ilium base and especially of the ventral region of the pelvis at the pubis-ischium union, and a relative increase in robustness of the anterior ilium base, anterior pubic margin and ventrolateral pubic surface.

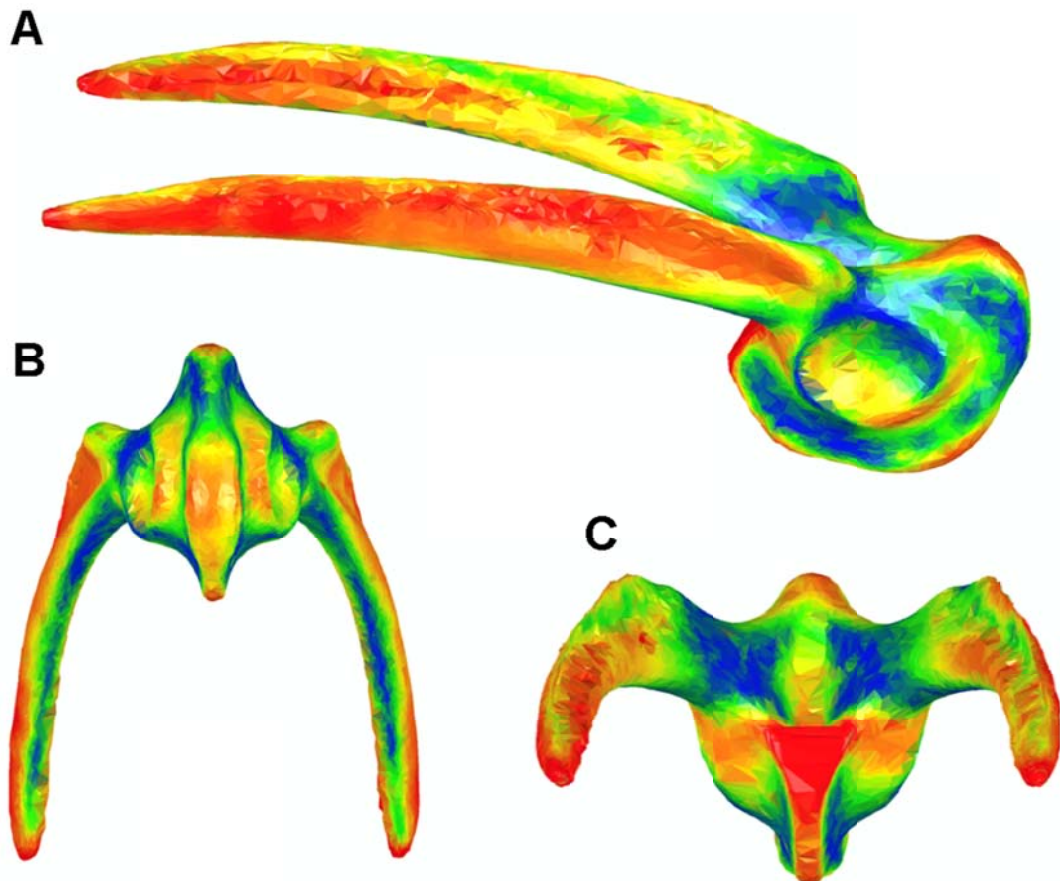


Fig. 7. Morphological disparity heatmap representation for the interspecific mean pelvic shape comparison between our seven *Blommersia* species. Variance in shape is displayed at each vertex of the 3D model obeying a color gradient from blue (lower values) to red (higher values). The range of variance values correspond to those found in the last row of the left column in Table 3.

Interspecific morphological disparity in mean pelvic shape for the seven *Blommersia* species sample (Fig. 7) illustrated high variation along the lateral surface of the iliac shafts and crests, the medial surface of the anterior iliac shafts, the anterior and posterior ilium base margins, the posteroventral acetabulum labrum, and the ventral margin of the epipubis. Low morphological disparity was observed along the ventral margin of the iliac shafts, the posterior medial base of the iliac shafts below the iliac processes, the dorsal

acetabulum labrum, the lateral surfaces of the posterior ischium, and the ventrolateral pubic surface.

Phylogenetic and Morphological Distance Mantel Test

The Mantel test between the mitochondrial rRNA 16S phylogenetic distance matrix and the morphological interspecimen PSM distance matrix (based on species' mean pelvic shapes) for the seven *Blommersia* species indicates a high positive correlation between the two datasets ($Z = 0.15775$; correlation = 0.77558; $t = 4.75825$; $\alpha=0.01$; two-tailed $p = 0.00000$). The results of 999 permutations also support this relationship (two-tailed $p = 0.001$).

DISCUSSION

Blommersia Pelvic Musculature Architecture

This is the first time that muscle insertion areas have been located and identified in a *Blommersia* species. Compared to similar previous studies in other anuran species (Duellman & Trueb, 1994; Prikryl et al., 2009) that have dissected the animals for this task, and in the process destroyed the sample for future analysis, we have been able to map the exact location of pelvic muscle insertions onto their corresponding skeletal morphology on the same individual (Fig. 2) preserving the sample for museum conservation. This has been possible thanks to the combination of CT and the application of a customized sequential two-contrast agent soft-tissue staining technique (see Materials & Methods). However, unlike these previous studies that electrically stimulated dissected muscles to determine their precise biomechanical movement, we could not evaluate the movements of the muscles in our species without destruction of the samples. Consequently, we have used their information on *Rana esculenta* as an approximation of these movements for our species due to the phylogenetic proximity of this genus to *Blommersia* (Table 2).

Comorian Pelvic Shape Evolutionary Divergence

Our analyses of intraspecific pelvic shape disparity showed an interesting pattern between the two Comorian *Blommersia* sister species and their Malagasy sister taxon. When size

variation was included for pelvic shape comparison *B. wittei* was the most variable, however when standardized for size *B. nataliae* **sp. nov.** was the most variable (Table 3). This indicates that the potential range of size variation observed in both Comorian species may have already been present in their most recent common ancestor, and that each Comorian species has diverged on the island to opposing extremities of the size range of their Malagasy sister taxon; an outcome supported by their significantly different centroid sizes. The higher intraspecific disparity observed in the smaller Comorian species when standardized for size coincides with the tendency to miniaturization in the genus and suggests that the species is still undergoing morphological changes to adjust to smaller sizes. This observation is further reinforced by the fact that we observed sexual dimorphism in *B. nataliae* **sp. nov.** pelvic shape consisting in a tendency towards an overall smaller and less robust pelvis in females (Fig. 3). What is more contrasting, however, is the opposite process of gigantism in *B. alexi* **sp. nov.** Although presenting less disparity in shape than *B. wittei*, *B. alexi* **sp. nov.** presented larger PSM values to its consensus, doubling those of its Malagasy sister taxon when including size variation. This indicates that this species is increasing almost isometrically in size without large changes in the species' general pelvic shape. Therefore, we can conjecture that there are less systemic morphological constraints on pelvic shape with increasing size, relative to reducing its size, in relation to pelvic locomotor function. This supposition, however, would have to be tested biomechanically and can be a topic for future research.

Interspecific comparisons of pelvic shape variation between the three species were consistent across size-standardized and non-standardized analyses, and reflected their size and phylogenetic relationships, respectively, the largest disparity in shape was between *B. alexi* **sp. nov.** and *B. wittei*, and the smallest between the two Comorian sister species (Table 3). However, significant patterns in pelvic shape variation between the Comorian sister species were only observed when including size variation in the analysis. Thus, we can ascertain that Comorian species present divergent size-related pelvic shape variation, but similar patterns of size-unrelated pelvic shape variation. This is reflected in the ordination of interspecific pelvic shape variation between them along PCo1 (size-related differences) and PCo2 (same pattern of size-unrelated variation) axes, respectively (Fig. 4). Pelvic shape divergence between them consisted in an isometric variation in size of the acetabular portion of the pelvis, a change in length of the iliac shafts, a change in inclination angle of the iliac crest, and in an alteration of the width of the pelvis at the

level of the iliac processes that results in a modification of the aperture between iliac shafts. Interestingly, these shape changes coincided to a large extent with those described by the PCo2 axis resulting from the ordination of the size-standardized shape variation between the three species' mean pelvic shapes (Fig. 5). Comorian sister species lie on opposite extremes of this axis of shape variation and *B. wittei* exactly in-between. Consequently, this analysis uncovers an axis of size-unrelated morphological change in pelvic shape along which the Comorian species have diverged in opposite directions from their Malagasy sister taxon. Pelvic shape variation described by this axes (PCo2, Fig. 5) differs to that described by size-related variation between Comorian species (PCo1, Fig. 4) in that the acetabular portion of the pelvis does not change isometrically, but relatively increases its robustness more towards its anterior region in *B. alexi* **sp. nov.** and more towards its posterior region in *B. nataliae* **sp. nov.** This is suggestive that development of the posterior portion of the acetabular pelvis may be more essential for conserving locomotor function during processes of miniaturization in this genus, but again, this supposition would have to be evaluated further to determine whether this is due to biomechanical and/or developmental constraints.

Both Comorian species further diverged from their sister taxon in Madagascar along an additional axis of size-unrelated pelvic shape variation (PCo1, Fig. 5). Shape changes related to the Comorian species consisted in *i)* a relative decrease in iliac shaft length accompanied by a relative increase in their lateral aperture and a variation in their height, which increases anteriorly, but decreases posteriorly, *ii)* relatively smaller iliac processes, but displaying a relatively increased length of the ilium base along its anterior-posterior axis, and *iii)* a relatively more robust lateral surface of the dorsal pubis and dorsal margin of the ischium. Apparently all these observed changes in pelvic shape may affect associated muscle architecture, and ultimately jumping locomotor performance, and will be discussed below in the context of the evolution of the anuran musculoskeletal locomotor system.

Blommersia Phylogenetic Pelvic Shape Evolution

The aforementioned axis of pelvic shape variation between Comorian sister species and their Malagasy sister taxon (PCo1, Fig. 5) coincides to a large extent with that observed between the mean pelvic shapes of the seven *Blommersia* species included in this study

(PCo1, Fig. 6 Left), albeit with slight differences on the acetabular portion of the pelvis, and may represent a major axis of pelvic shape variation in the genus. Interestingly, morphological changes along the PCo2 axis of the *Blommersia* interspecific pelvic shape analysis (PCo2, Fig. 6) also coincide to a large extent with those discriminating Comorian sister species (PCo1, Fig. 5), potentially representing an additional major axis of pelvic shape variation within the genus. We can confirm that these axes describe relevant patterns for species' pelvic shape divergence within our small subsample of the *Blommersia* genus given the high correlation (0.77; $p = 0.001$) observed between our species' morphological and genetic distance matrices. However, whether or not these patterns are phylogenetically widespread within the genus should be corroborated in the future with further analyses including the pelvic shapes of additional *Blommersia* species.

In the size-standardized PCo1-PCo2 morphospace (Fig. 6 Left) we observe several patterns of pelvic shape divergence that reflect the phylogenetic relationships between our *Blommersia* species. First of all, the oldest species pair (*B. sarotra* – *B. grandisonae*, Fig. 1) is the only one to cover the complete range of shape variation of the biplot (*i.e.* positive and negative values on both axes; first and third quadrants) potentially indicating a longer time for divergence, and the more recent *B. domerguei* – *B. blommersae* species pair essentially occupies the second quadrant (*i.e.* negative PCo1, positive PCo2 values) consequently not overlapping in morphospace with the preceding species pair. In the same manner, the *B. wittei* – *B. nataliae* **sp. nov.** species pair covers the region of the first quadrant unoccupied by previous species pairs, however *B. alexi* **sp. nov.** diverges greatly from the position of *B. wittei* and its Comorian sister species in the shared morphospace and is the only species that occupies the fourth quadrant. The great leap of *B. alexi* **sp. nov.** into an unoccupied area of the shared morphospace so far away from its phylogenetically closest relatives, and jumping over the position of *B. grandisonae*, advocates that it has potentially undergone a process of ‘morphological release’ on Mayotte by occupying part of the morphospace that is likely filled by other, larger anuran species from mainland Madagascar.

Evolution of the Blommersia Musculoskeletal Locomotor System

The morphological disparity in pelvic shape observed between the seven analyzed *Blommersia* species was largely concentrated on the lateral and medial iliac shafts and on

the anterior and posterior ilium base (red, Fig. 7). These morphological structures constitute anatomical regions that are highly derived in anurans relative to their tetrapod ancestors and that have favored the evolution of different types of locomotion (Prikryl et al., 2009). The reabsorption of the pubis and anterior expansion of the iliac shafts, simultaneously with the reduction of the tail into an urostyle, have promoted the continuous diversification of the musculature associated to these structures to adapt to diverse locomotor requirements (Gans & Parsons, 1966). This has resulted in modifications of the musculature inserting on the iliac shaft and ilium base (*i.e.* no. 1-3, 7-9; Fig. & Table 2) involved in the anterior movement of the femur and responsible for the crouching position of anurans that allows them to generate relatively large forces in short timespans (Burkholder & Lieber, 2001; Gillis, 2010; Reilly et al., 2016). Conversely, the musculature involved in thrust production (*i.e.* no. 4-6, 10, 12-13, 17, 19, 23; Fig. & Table 2) have been modified the least relative to their ancestral positions on the pelvis (Prikryl et al., 2009). Accordingly, these muscles insert on the pelvic regions of less disparity between these *Blommersia* species (blue, Fig. 7). However, in specialized terrestrial jumpers, as the majority of mantellids including the *Blommersia* genus (Reilly & Jorgensen, 2011), these muscles have become relatively larger and more diversified than in other anurans exhibiting dissimilar locomotor modes, consequently increasing absolute force production during jumping (Zug, 1978; James et al., 2007). Therefore the variation in length along the anterior-posterior axis of the ilium base we observe between our *Blommersia* species may correspond to an isometric variation in size modifying the available space below for the insertion of these muscles. In addition, while the pelvic shape disparity observed within our *Blommersia* species sample largely corresponds to the general pattern of pelvic musculature evolution from tetrapods to anurans, we observed relatively large amounts of disparity at the iliac process (yellow-green, Fig. 7). Given the stable evolutionary origin (Prikryl et al., 2009) of the musculature on this structure (no. 4-6, Fig. 7), we believe that the disparity in pelvic shape at this structure may be due more to size differentiation between *Blommersia* species than to correlation with muscular insertion.

The axes of shape variation describing significant interspecific differences in pelvic shape between the studied *Blommersia* species (see above) point to more specific differences in morphology that may be potentially implicated in their ecological diversification and correlated to a species' lifestyle, habitat use, and locomotor performance (Gomes et al.,

2009). With this in mind we hypothesize that the ecological pressures associated to the colonization of novel environments during the *Blommersia* species' divergence would have determined the development of pelvic shape through its morphofunctional association with locomotor performance. In mantellids, miniaturization parallels species diversity (Wollenberg et al., 2011). Smaller body sizes are believed to limit species' dispersal capabilities, resulting in smaller and more fragmented geographic ranges that potentially facilitate reproductive isolation and ultimately speciation. However, a smaller body size also reduces physiological tolerances and does not permit the colonization of novel areas due to limited dispersal capabilities, causing an opposite effect on the speciation process (Pabijan et al., 2012). The shape variation associated to 'miniaturization/gigantism' in our Comorian species relative to their Malagasy sister taxon were largely determined by isometric size differences in the iliac shafts' length, aperture, and width between the iliac processes (Figs. 3 & 4); the only size-unrelated variation consisting in a more developed anterior region of the acetabular region in the larger species relative to its posterior region in the smaller one (PCo2, Fig. 5). If we consider the shape variation associated to the isometric increase in size to result in a linear increase in locomotor performance (*e.g.* in jump distance; Emerson, 1978, but see James et al., 2007), this difference between the Comorian species advocates a trade-off between thigh extension and flexion during locomotion [with reference to the locomotor function of the predominant muscles inserting on these areas (no. 10 & 19, Table 2)] that may be correlated to their differential preferred habitat and lifestyle. However, to corroborate this hypothesis a reciprocal transplant experiment testing their biomechanical locomotor performance in the different environments would be necessary. Additional analogous experiments between other *Blommersia* species may as well be considered to evaluate whether the observed pelvic morphological differences correlate to contrasting locomotor performance within different habitats.

ACKNOWLEDGEMENTS

We would like to thank the members of the University of Antananarivo, Department of Animal Biology for giving us access to their museum collections, and to Christina Paradela from the internal Service of Non-destructive Techniques (MNCN-CSIC) for the hours spent CT-scanning our own specimens. This research was funded by the Spanish Ministry of Economy and Competitiveness; grant number CGL2013-40924-P.

REFERENCES

- Besl PJ, McKay ND (1992) Method for registration of 3-D shapes. In *Sensor Fusion IV: Control Paradigms and Data Structures*, pp. 586-607. International Society for Optics and Photonics.
- Burkholder TJ, Lieber RL (2001) Sarcomere length operating range of vertebrate muscles during movement. *Journal of Experimental Biology*, **204**, 1529-1536.
- Chen Y, Medioni G (1992) Object modelling by registration of multiple range images. *Image and Vision Computing*, **10**, 145-155.
- Cignoni P, Callieri M, Corsini M, Dellepiane M, Ganovelli F, Ranzuglia G (2008) Meshlab: an open-source mesh processing tool. In *Eurographics Italian Conference*, pp. 129-136.
- Descamps E, Sochacka A, De Kegel B, Van Loo D, Van Hoorebeke L, Adriaens D (2014) Soft tissue discrimination with contrast agents using micro-CT scanning. *Belgian Journal of Zoology*, **144**, 20-40.
- Duellman WE, Trueb L (1994) *Biology of Amphibians*, JHU Press.
- Duncan R, Turner C (1995) Mechanotransduction and the functional response of bone to mechanical strain. *Calcified Tissue International*, **57**, 344-358.
- Emerson SB (1978) Allometry and jumping in frogs: helping the twain to meet. *Evolution*, **32**, 551-564.
- Emerson SB (1982) Frog postcranial morphology: identification of a functional complex. *Copeia*, **1982**, 603-613.
- Emerson SB, De Jongh H (1980) Muscle activity at the ilio-sacral articulation of frogs. *Journal of Morphology*, **166**, 129-144.
- Essner RL, Suffian DJ, Bishop PJ, Reilly SM (2010) Landing in basal frogs: evidence of saltational patterns in the evolution of anuran locomotion. *Naturwissenschaften*, **97**, 935-939.
- Gans C, Parsons TS (1966) On the origin of the jumping mechanism in frogs. *Evolution*, **20**, 92-99.
- Gignac PM, Kley NJ (2014) Iodine-enhanced micro-CT imaging: methodological refinements for the study of the soft-tissue anatomy of post-embryonic vertebrates. *Journal of Experimental Zoology Part B: Molecular and Developmental Evolution*, **322**, 166-176.
- Gillis GB (2010) Frog muscles start stretched. *Journal of Experimental Biology*, **213**, vi-vi.

- Gomes F, Rezende E, Grizante M, Navas C (2009) The evolution of jumping performance in anurans: morphological correlates and ecological implications. *Journal of Evolutionary Biology*, **22**, 1088-1097.
- Handrigan GR, Wassersug RJ (2007) The anuran Bauplan: a review of the adaptive, developmental, and genetic underpinnings of frog and tadpole morphology. *Biological Reviews*, **82**, 1-25.
- Hudson CM, Brown GP, Shine R (2016) Athletic anurans: the impact of morphology, ecology and evolution on climbing ability in invasive cane toads. *Biological Journal of the Linnean Society*, **119**, 992-999.
- James RS, Navas CA, Herrel A (2007) How important are skeletal muscle mechanics in setting limits on jumping performance? *Journal of Experimental Biology*, **210**, 923-933.
- Lires AI, Soto IM, Gómez RO (2016) Walk before you jump: new insights on early frog locomotion from the oldest known salientian. *Paleobiology*, **42**, 612-623.
- Pabijan M, Wollenberg K, Vences M (2012) Small body size increases the regional differentiation of populations of tropical mantellid frogs (Anura: Mantellidae). *Journal of Evolutionary Biology*, **25**, 2310-2324.
- Pomidor BJ, Makedonska J, Slice DE (2016) A landmark-free method for three-dimensional shape analysis. *PLoS One*, **11**, e0150368.
- Přikryl T, Aerts P, Havelková P, Herrel A, Roček Z (2009) Pelvic and thigh musculature in frogs (Anura) and origin of anuran jumping locomotion. *Journal of Anatomy*, **214**, 100-139.
- Reilly SM, Jorgensen ME (2011) The evolution of jumping in frogs: morphological evidence for the basal anuran locomotor condition and the radiation of locomotor systems in crown group anurans. *Journal of Morphology*, **272**, 149-168.
- Reilly SM, Montuelle SJ, Schmidt A, Krause C, Naylor E, Jorgensen ME, Essner Jr RL (2016) Pelvic function in anuran jumping: interspecific differences in the kinematics and motor control of the iliosacral articulation during take-off and landing. *Journal of Morphology*, **277**, 1539-1558.
- Rohlf FJ, Slice D (1990) Extensions of the Procrustes method for the optimal superimposition of landmarks. *Systematic Biology*, **39**, 40-59.
- Scherz MD, Hawlitschek O, Andreone F, Rakotoarison A, Vences M, Glaw F (2017a) A review of the taxonomy and osteology of the *Rhombophryne serratopalpebrosa* species group (Anura: Microhylidae) from Madagascar, with comments on the value of volume rendering of micro-CT data to taxonomists. *Zootaxa*, **4273**, 301-340.
- Scherz MD, Razafindraibe JH, Rakotoarison A, Dixit NM, Bletz MC, Glaw FR, Vences M (2017b) Yet another small brown frog from high altitude on the Marojejy Massif, northeastern Madagascar (Anura: Mantellidae). *Zootaxa*, **4347**, 572-582.

Sigurdson T, Green DM, Bishop PJ (2012) Did Triadobatrachus jump? Morphology and evolution of the anuran forelimb in relation to locomotion in early salientians. *Fieldiana Life and Earth Sciences*, **2012**, 77-89.

Tamura K, Nei M, Kumar S (2004) Prospects for inferring very large phylogenies by using the neighbor-joining method. *Proceedings of the National Academy of Sciences*, **101**, 11030-11035.

Tamura K, Stecher G, Peterson D, Filipowski A, Kumar S (2013) MEGA6: molecular evolutionary genetics analysis version 6.0. *Molecular Biology and Evolution*, **30**, 2725-2729.

Vickerton P, Jarvis J, Jeffery N (2013) Concentration-dependent specimen shrinkage in iodine-enhanced micro CT. *Journal of Anatomy*, **223**, 185-193.

Vieites DR, Wollenberg KC, Andreone F, Köhler J, Glaw F, Vences M (2009) Vast underestimation of Madagascar's biodiversity evidenced by an integrative amphibian inventory. *Proceedings of the National Academy of Sciences*, **106**, 8267-8272.

Wainwright PC, Alfaro ME, Bolnick DI, Hulsey CD (2005) Many-to-one mapping of form to function: a general principle in organismal design? *Integrative and Comparative Biology*, **45**, 256-262.

Whittaker RJ, Fernández-Palacios JM (2007) *Island Biogeography: ecology, evolution, and conservation*, Oxford University Press.

Wollenberg KC, Vieites DR, Glaw F, Vences M (2011) Speciation in little: the role of range and body size in the diversification of Malagasy mantellid frogs. *BMC Evolutionary Biology*, **11**, 217.

Zug GR (1978) Anuran Locomotion—Structure and Function, 2: Jumping Performance of Semiaquatic, Terrestrial, and Arboreal Frogs. *Smithsonian Contributions to Zoology*, **276**.

SUPPLEMENTARY MATERIAL

Table S1. Holding collection, field number, sex, and locality of recollection of the Comorian *Blommersia* individuals that were stained to enhance muscle visualization.

Species	Collection	Field no.	Sex	Locality
<i>B. alexi</i> sp. nov.	MNCN	DRV6834	M	Mont Bénara
	MNCN	DRV6837	M	Mont Bénara
	MNCN	DRV6840	M	Mont Bénara
	MNCN	DRV6851	F	Mont Combani
<i>B. nataliae</i> sp. nov.	MNCN	DRV6809	F	Mont Sapere
	MNCN	DRV6856	M	Mont Sapere
	MNCN	DRV6864	M	Mont Sapere
	MNCN	DRV6866	M	Mont Sapere

Videos S1 & S2. Video along the 2D sagittal plane of contrast stained specimen DRV6834 *B. alexi* sp. nov. illustrating the musculature associated to the pelvis and urostyle [grey values: 12000-55500; greyscale (S1) and seismic (S2) colormaps]. The initial and final positions of the video are shown in Fig. S1. The position of the skeletal structures are visualized as a transparent renderization within the videos.

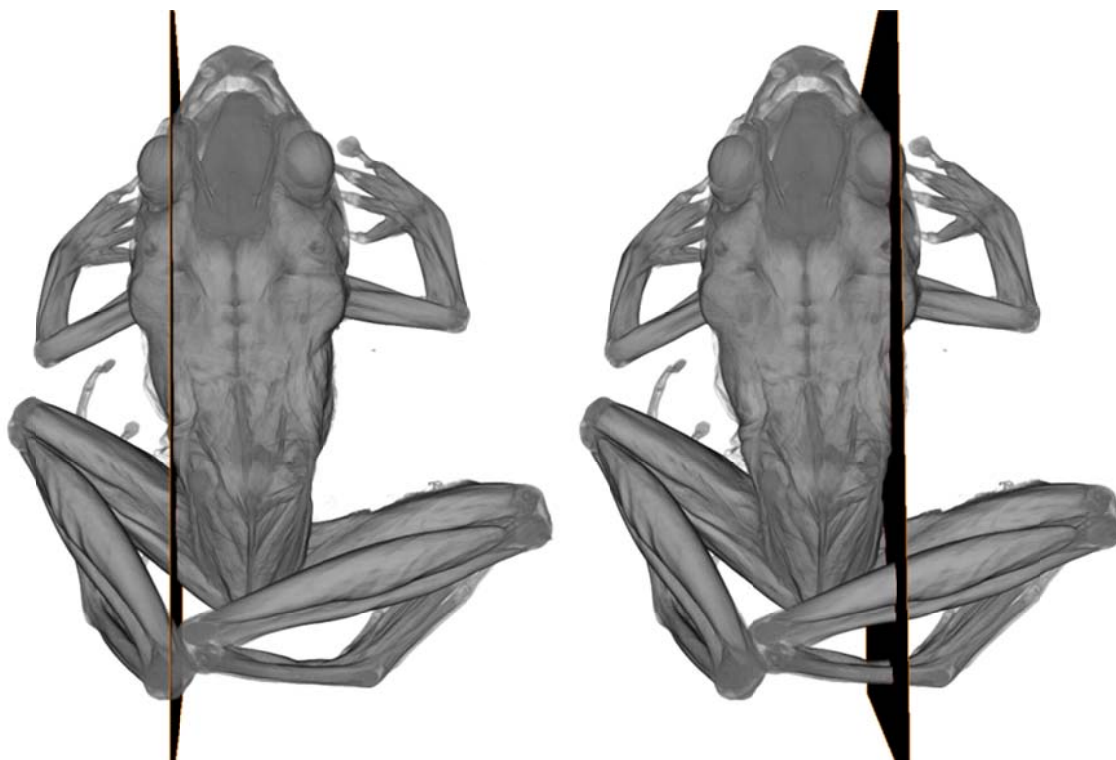


Fig. S1. Cutting planes along the sagittal axis corresponding to the visualization of Videos S1 & S2.

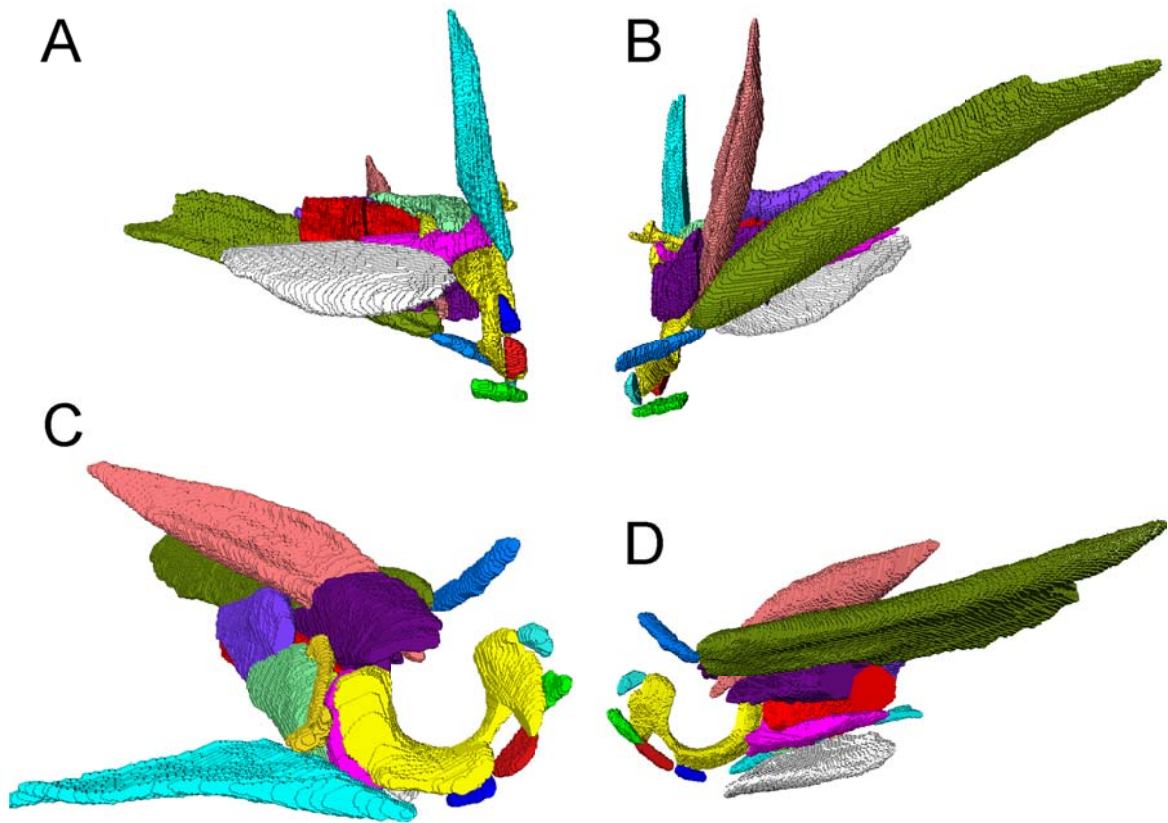
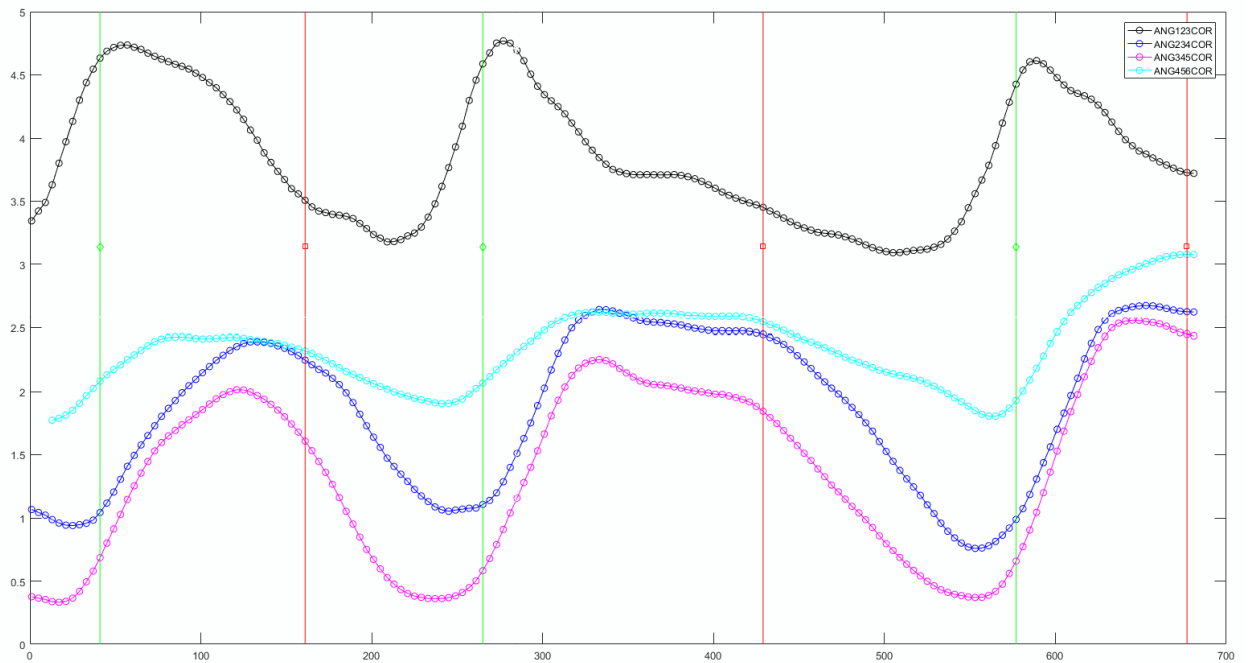
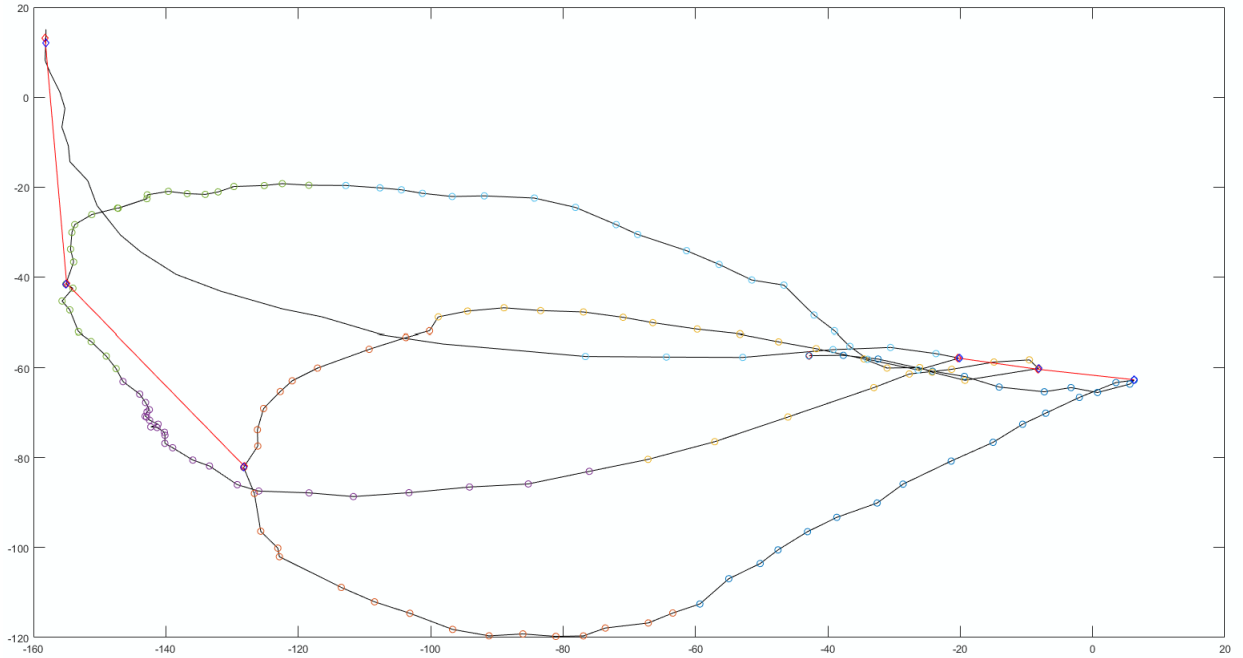


Fig. S2. Images of the ongoing segmentation of the pelvic musculature of *B. alexi* **sp. nov.** **A:** ventral view. **B:** dorsal view. **C:** medial sagittal view. **D:** lateral sagittal view. Images correspond to the right leg of specimen DRV6834.

SECTION III



Wood Frog Locomotor Biomechanics

CHAPTER 6

Kinematic performance and muscle activation patterns during post-freeze locomotion in wood frogs (*Rana sylvatica*)

Javier H. Santos-Santos^{1,2}, Brett M. Culbert³, Emily M. Standen³

¹*Department of Animal Biology, University of Barcelona, Avenida Diagonal 645, 08028, Barcelona, Spain*

²*Department of Biogeography and Global Change, Museo Nacional de Ciencias Naturales - CSIC, Calle Jose Gutierrez Abascal 2, 28006, Madrid, Spain*

³*Department of Biology, University of Ottawa, Ottawa, Canada*

ABSTRACT

Wood frogs [*Rana sylvatica* (LeConte, 1825)] exhibit one of the most extreme freeze tolerance responses found in vertebrates. While extensive work is continuing to resolve the physiological mechanisms involved, few have studied the effects of freezing on locomotor performance. The ability to mount an appropriate locomotor response is vital, as locomotion can affect both survivorship and reproductive success. To investigate how the biomechanical processes during locomotion are altered following freezing, stroke cycle timings and kinematic performance were measured prior to, and immediately following a freeze-thaw cycle. Additionally, the effects of cooling rate (0.3°C/h vs. 0.8°C/h) were also assessed. While jumping and swimming performance were both reduced post-freeze, the effects were more pronounced during swimming, with observed reductions in velocity and distance travelled. Interestingly, these changes occurred largely independent of cooling rate. Altered stroke cycle timings and highly variable muscle activation/deactivation patterns suggest an impairment in muscle function as frogs continued to recover from the effects of freezing. This was supported by the physiology of frogs post-freeze, specifically, the persistence of elevated glucose levels in muscles important during locomotion. Collectively, these findings suggest that reductions in locomotor performance observed immediately following a freeze-thaw cycle are driven by alterations in muscle function.

KEYWORDS: biomechanics, cooling rate, cryoprotectants, freeze tolerance, locomotion, *Rana sylvatica*, wood frog.

INTRODUCTION

Many animals cope with seasonally subzero ($< 0^{\circ}\text{C}$) temperatures; as such, a diverse suite of strategies to facilitate survival during these periods have evolved. Many animals seek thermal refugia, and may even enter prolonged periods of inactivity and reduced metabolism (*i.e.* hibernation) to overcome these seasonal hardships (Sømme, 1989; Heggenes et al., 1993; Terrien et al., 2011; Williams et al., 2015). However, ectotherms arguably possess the most impressive overwintering strategies of all animals. Many ectotherms, including insects, reptiles, and amphibians synthesize large quantities of cryoprotectant compounds (*e.g.* glucose and glycerol) prior to the onset of subzero temperatures (Storey & Storey, 1988). Cryoprotectants allow animals to avoid freezing by reducing the temperature at which ice crystals begin to form in tissues—allowing them to function at subzero temperatures (Storey, 1997). However, some ectotherms have taken this a step further.

Certain species can tolerate freezing (Storey & Storey, 1987; Storey & Storey 1988); relying largely on amassing high levels of cryoprotectants in tissues to discourage damage (Storey & Storey, 1992). These effects are amplified via dehydration of tissues, which further increases cryoprotectant concentrations (Lee et al., 1992; Churchill & Storey, 1993). During this period animals enter a frozen state where breathing rate, heart rate, and blood flow cease (Layne et al., 1989; Layne & First, 1991). Survival during subzero periods depends on a variety of factors, including cooling rate, freezing temperature, and the frequency of subzero episodes (Layne & Lee, 1987; Costanzo et al., 1992). Of all freeze tolerant vertebrate species, wood frogs [*Rana sylvatica* (LeConte, 1825)] have been the most thoroughly studied.

Like all freeze tolerant species, wood frogs rely on a combination of tissue dehydration and cryoprotectant synthesis to cope with freezing. In anticipation of freezing, muscle proteolysis causes an increase in urea production, while liver glycogen stores are rapidly converted to glucose immediately upon initiation of freezing—elevating levels of both cryoprotectant molecules (Costanzo et al., 2015). Similarly, as a result of an increased reliance on anaerobic metabolism during both freezing and dehydration, lactate levels rise (Churchill & Storey, 1993). However, upon thaw wood frogs reconvert the majority of the glucose mobilized as cryoprotectant back into hepatic glycogen reserves (Storey &

Storey, 1986; Costanzo et al., 2013), providing energy stores to facilitate behaviours such as mating.

Wood frogs begin to perform intense spawning behaviours immediately upon spring arousal (Wells & Bevier, 1997). However, when competing with controls that were not frozen, recently thawed male wood frogs are less successful at achieving amplexus with a female (Costanzo et al., 1997). As well, locomotor endurance remains impaired for at least 96h following thaw (Irwin et al., 2003). These combined findings suggest that despite the urge to perform and reproduce immediately upon thaw, an altered physiological condition is likely preventing them from doing so. In fact, Layne and Rice (2003) observed that jump distance and swim speed were negatively affected 6h post-freeze, only returning to pre-freeze levels after 54h. However, no studies to date have assessed how kinematics during locomotion are altered in recently thawed frogs.

We hypothesized that biomechanical performance in *R. sylvatica* post-thaw is reduced due to prolonged effects of the widespread physiological remodeling induced during freezing. To assess this, we compared the kinematics and muscle activation patterns of *R. sylvatica* before and after freezing, and measured several physiological parameters implicated in their freeze tolerance response. In addition, we assessed the effect of the rate of cooling, predicting that more abrupt decreases in temperature would cause further reductions in biomechanical performance. The effects of holding time on animal performance and condition were also assessed.

MATERIALS & METHODS

Collection and Housing

Fifty-one male wood frogs (*Rana sylvatica*) were used in this study. Animals were collected on April 1, 2016 in Bishop Mills, Ontario. Following collection, animals were transferred to holding containers at the University of Ottawa. Containers were kept in the dark at 4°C, and contained one centimeter of dechloraminated City of Ottawa tap water. Water was changed every three days. Wood frogs were not fed over the duration of the study to avoid the potentially lethal effects due to unpredictable ice nucleation occurring in the contents of the gut while freezing (Storey & Storey, 1987). All animals were checked to be sexually mature (*i.e.* inspection of nuptial pads) and in good condition (*i.e.* completely unfrozen and uninjured) prior to experimentation. All experimental protocols

were approved by the University of Ottawa animal care committee (protocol BL2548), and were in compliance with the guidelines of the Canadian Council on Animal Care (CCAC) for the use of animals in research and teaching.

Table 1. Experiment cycle timeline and procedures.

DAY	CONTROLS N=3	RAPID COOLING N=3	SLOW COOLING N=3
1	Surgery: sham (20min.)	Surgery: electrodes (30min.)	Surgery: electrodes (30min.)
	Recovery @ 4°C (24h)	Recovery @ 4°C (24h)	Recovery @ 4°C (24h)
2	Filming (30min.)	Filming (30min.)	Filming (30min.)
	Euthanized and Dissected	Cooling 4°C to -2.5°C (over 8h)	Cooling 4°C to -2.5°C (over 24h)
		Frozen @ -2.5°C (12h)	
3		Thaw @ 4°C (8h)	
		Filming (30min.)	
		Euthanized and Dissected	
4			Thaw @ 4°C (8h)
			Filming (30min.)
			Euthanized and Dissected

Columns denote cooling treatments and sample sizes. Four 4-day experiment cycles were run in total.

Experimental Procedure

All experimental procedures (*i.e.* holding, transportation, anesthesia, operation, recovery, and filming) were performed at 4°C. Experiments were conducted from April 8-24, 2016. Six non-jumped controls (twelve in total) were randomly sampled from holding on the first and last days of the experiment to assess changes in tissue metabolite concentrations over time. Each experimental cycle (four in total) included nine frogs and lasted four days (Table 1).

Treatments consisted of a slow cooling regime, where the environmental temperature was reduced from 4°C to -2.5°C over a 24h period; a rapid cooling regime, where the environmental temperature was reduced from 4°C to -2.5°C over an 8h period; and a sham treatment, where muscles were prodded without electrode insertion to control for any effects of surgery and animals were not frozen (Table 1). The order of treatment assignment was determined randomly prior to retrieving the animals for surgery. Animal temperatures were monitored throughout the cooling regime using a RDXL4SD 4-channel data logger thermometer equipped with four type T thermocouples (OMEGA), and freezing exotherms were observed during both cooling regimes.

On Day 1, frogs were randomly collected from holding and underwent surgery (see Section 2.2.1). Following surgery, animals were given 24h to recover at 4°C. On Day 2, video recordings of jumping and swimming performance were taken (see Section 2.2.2). Following filming, animals were returned to their containers and placed into their respective cooling treatment. Sham-handled animals were filmed, and immediately euthanized and dissected. On Day 3, animals in the rapid cooling treatment were placed at 4°C for 8h. Previous work has shown that sciatic nerve excitability and hind limb retraction returns within this time range (Kling et al., 1994). Following this, animals were filmed for a second time, and immediately euthanized and dissected. On Day 4, the same protocol described for Day 3 was performed on animals from the slow cooling treatment.

Surgery

Following collection from holding, animals were weighed, measured (snout-vent length (SVL)), and placed on a covered bed of ice. Bi-filament stainless steel wire electrodes (0.002 µm; California Fine Wire Co.) were surgically implanted into the gastrocnemius and semimembranosus muscles using a 26 gauge needle (Fig. 1). These muscles were selected due to their ubiquitous importance during locomotion. Electrodes were sutured together at the knee, ischium, and sacrum along the right side of the animal to prevent animal injury and damage to the wires. Over the duration of the surgery, the temperature of the animal, and its surrounding materials, were monitored using a temperature data logger with a type K thermocouple (OMEGA). After surgery, animals were placed in chilled water to recover. Animals were then individually put into containers with moist sphagnum moss and placed at 4°C. The lid of each container was modified to allow

electrode movement to prevent injury to both the animals and the wires. Animals of each regime were placed in separate incubators (Precision M815; Thermo Scientific) at 4°C.

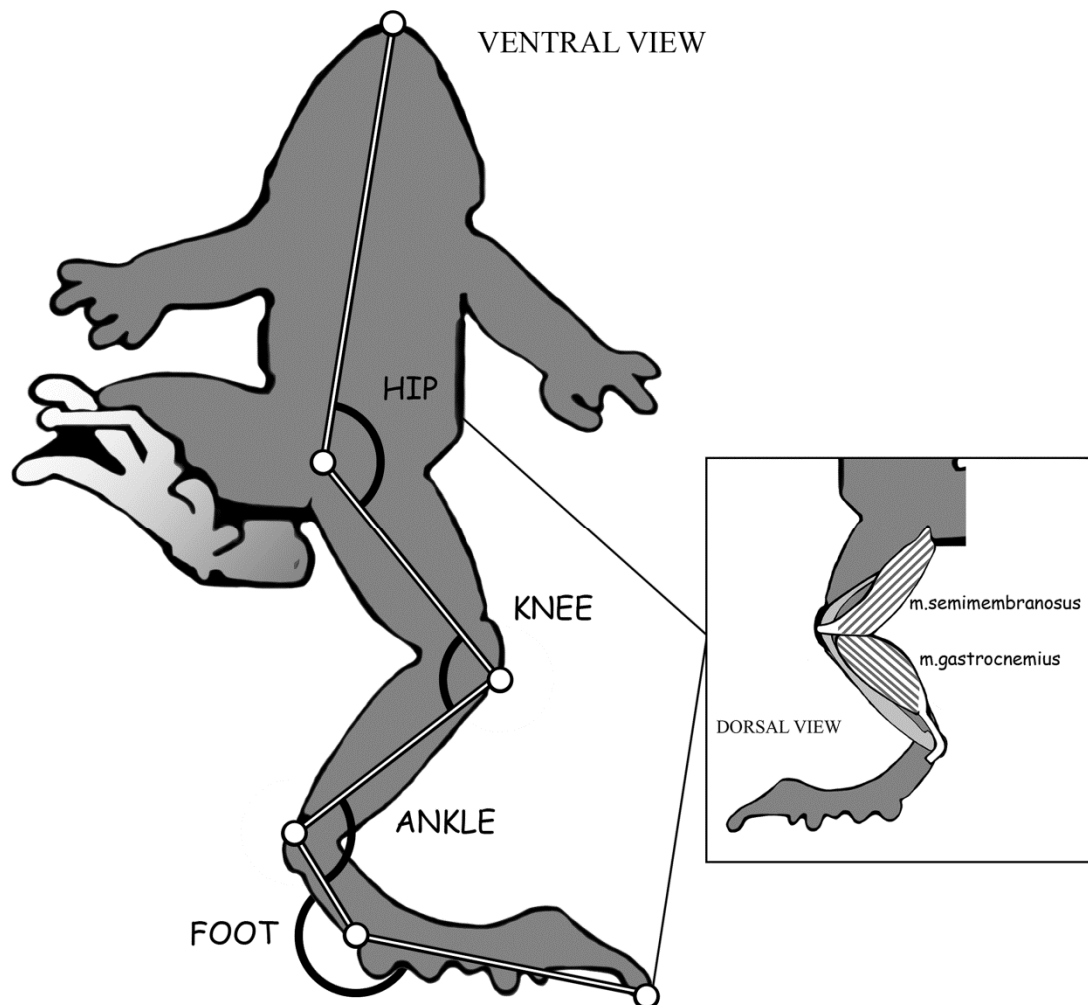


Fig. 1. Schematic representation of a wood frog (*Rana sylvatica*). Six anatomical landmarks were digitized in the ventral view to calculate animal movement. The expanded region in the dorsal view shows the position of the two muscles examined in this study. The m. semimembranosus is a hip extensor and knee flexor that originates on the ischium and inserts on the medial tibiofibula. The m. gastrocnemius originates posteriorly on the femoral condyles and inserts on the plantar aponeurosis posterior of the tibiotarsal joints acting as a foot flexor, and also flexes the leg at the knee joint. Single bipolar electromyography electrodes were implanted into each muscle to measure activation patterns during jumping and swimming.

Filming

Two high-speed video cameras (FASTCAM Mini UX100; Photron) were fixed around an 80L aquarium, containing 40L of water. The lateral camera was fixed at the same plane as the water level, while the ventral camera reflected off of a mirror positioned at a 45° angle underneath the aquarium. The tank was insulated and water chilled to 4°C. Water

temperature was monitored using a temperature data logger with a type K thermocouple throughout each trial.

Animals were placed on moist sphagnum moss on top of a brick embedded in ice, which served both to maintain water temperature and as a jumping platform that impeded the frog from swimming backwards. Ice bricks were replaced between treatments. The temperature of each animal was periodically monitored up until the point of jumping using a type K thermocouple. Each animal jumped and swam between two and four times, which was filmed at 500 frames per second.

Electromyography

The electromyography (EMG) electrodes were connected to P511 Grass amplifiers (Natus Medical Inc.). Amplifiers and camera trigger were connected to a PowerLab DAQ (ADInstruments Inc.). Synchronization of high-speed video and EMG electrode data was performed via an end trigger through the PowerLab DAQ with the LabChart (v.8.1.5) interface at a 10kHz sampling rate and a $\pm 5V$ differential signal range. A 60Hz notch filter was applied to remove potential alternating current electrical noise. Our baseline signal was 0.05V. Onset and offset were determined manually in MATLAB at approximately 0.3-0.5V.

Dissections

Immediately following final video recordings, animals were rapidly euthanized via double pithing. Mass and length (SVL) were recorded, and blood samples were collected via aortic severance into heparinized capillary tubes. Tubes were centrifuged at 10,000g for 3 minutes and hematocrit was measured. Plasma was extracted, flash frozen in liquid nitrogen, and stored at $-80^{\circ}C$ for later analysis of glucose, lactate, and urea. The liver, right gastrocnemius, and right semimembranosus were extracted, weighed, and flash frozen in liquid nitrogen. Hepatosomatic index was calculated as the percentage of the liver in relation to the mass of the entire animal. These samples were stored at $-80^{\circ}C$ for later analysis of glycogen, glucose, lactate, and urea. To calculate relative muscle water content, the right peroneus muscle was extracted, weighed, placed into an incubator at $65^{\circ}C$ for 30 minutes, and reweighed. The percent difference between these weights

represented relative water content. During dissection, proper placement of the EMG electrodes was confirmed. All dissections were performed on ice.

Tissue Preparation and Metabolite Measurements

Tissue samples were ground using a mortar and pestle on dry ice prior to analysis. Glucose/glycogen, lactate, and urea levels were determined according to the methods described by Keppler & Decker (1974), Brandt et al. (1980), and Rahmatullah & Boyd (1980), respectively. Analyses of glucose, glycogen, and lactate were performed in triplicate; however, urea was run in duplicate due to limited sample volumes. Inter- and intra-assay variations (% CV) for glucose (Inter, Intra; 6.2%, 4.4%), glycogen (1.7%, 6.1%), lactate (3.0%, 3.7%), and urea (6.1%, 9.7%) were all below 10%.

Data Processing

Single view high-speed videos were digitized in MATLAB (DLTdv5; Hedrick, 2008; Release 2016a; MathWorks). In swimming videos, six anatomical landmarks were tracked in the ventral view: (A) tip of the nose; (B) ischium; (C) femur head; (D); ankle; (E) tarsus; and (F) tip of the second (longest) phalange (Fig. 1). Animal trajectories calculated from the ischium and four angles (foot, ankle, knee, and hip) were measured to describe the motion of the leg following Peters et al. (1996; Fig. 1). The stroke cycle began with extension of the foot, and finished following the completion of foot flexion. In jumping videos, the tip of the nose was tracked in the lateral view to calculate jump height and distance. A calibration cube was used to convert pixel lengths to distance measurements in both views.

Kinematics

Peak joint extension and flexion were determined by plotting calculated angles over time. Average jump and swim velocity were calculated as the total distance covered in each trial divided by time, while instantaneous velocity was calculated at every 4th frame (*i.e.* 8ms). Distance and velocity during kick and recovery correspond to the foot extension and flexion phases, respectively, of each stroke cycle. The jump loading time was calculated as the time from the visible flexing of the stationary frog's epaxial musculature

(see beginning movement point (BM) (Peters et al., 1996)) to the first visible motion of leg extension. At this point the animal is in a characteristic position of an upward head/snout tilt; a stance that immediately leads to hind limb extension. Swimming was categorized as either synchronous, asynchronous, or both—based on the observed initiation of leg extension. Stroke cycle timings were calculated using polar coordinates so that individual stroke cycles could be compared. Peak joint angle magnitude timings, as well as EMG muscle activation timings, were transformed into stroke cycle polar coordinates in radians.

Statistical Analyses

All data are presented as means \pm SEM. Unpaired *t*-tests were used to assess whether animal physiology or kinematic locomotor performance at the end of the experiment (*i.e.* Day 16) varied from that of animals at the beginning of the experiment (*i.e.* Day 1). One-way analysis of variance was employed to detect differences in physiology and kinematic performance between cycles within treatments. Unpaired *t*-tests were used to evaluate differences between rapid and slow cooling regimes for all physiological variables, and to compare with sham-handled controls. Paired *t*-tests were employed to assess differences between pre- and post-freeze locomotor performance. For variables with more than one measure per animal, values were averaged and means were analyzed. When data did not meet the assumptions of homoscedasticity and normality, analyses were performed using transformed data. Variables that showed a von Mises distribution and equal variance were tested for directionality using Rayleigh's test. If variables are directional that means they occur at the same time in every stroke cycle. Analyses of kinematic and physiological data were performed in SigmaPlot (Version 11, Systat), while cycle timings were analyzed in MATLAB (Release 2016a; MathWorks). A significance level of 0.05 was used for all analyses.

RESULTS

Does holding duration affect physiology or locomotor performance?

When comparing the physiological characteristics of non-jumped control frogs sampled directly from holding at the beginning of the experiment (Day 1) to those sampled at the end of the experiment (Day 16), several differences were observed (Table 2A). Lactate

levels in both the gastrocnemius ($p=0.020$) and semimembranosus ($p<0.001$) increased over the duration of the experiment, along with plasma ($p=0.030$) and semimembranosus ($p<0.001$) glucose concentrations. Muscle water content ($p=0.004$) increased over this period as well. Plasma lactate ($p<0.001$), hepatic glucose ($p=0.001$), and semimembranosus glycogen ($p=0.030$) levels all decreased across time.

Locomotor performance of jumped sham-handled control frogs did not vary across time (Day 1 vs. Day 16) for any of the kinematic variables assessed (Table 2B).

Does cooling regime influence physiology?

Upon scrutiny of the data, no differences were detected for any of the kinematic or physiological variables across the four experimental cycles for any of the treatment groups. Thus, data were pooled across cycles within each treatment group for the remaining analyses.

Animals differed very little physiologically between the two cooling regimes (Table 3A); the lone difference being frogs from the rapid regime exhibited higher liver glycogen concentrations ($p=0.030$). However, when comparing pooled frogs from both cooling regimes to sham-handled control frogs, several differences were observed (Table 3B). Glucose concentrations of previously frozen frogs were elevated in the plasma ($p=0.002$), liver ($p=0.006$), gastrocnemius ($p<0.001$), and the semimembranosus ($p<0.001$). Lactate levels were reduced in the gastrocnemius ($p=0.001$) and the semimembranosus ($p<0.001$) of previously frozen frogs. Frogs from the slow cooling regime also displayed lower hepatic glycogen levels than sham-handled controls ($p<0.001$), however, rapidly cooled frogs did not differ from controls ($p=0.240$).

How does locomotor performance change following freeze?

Frogs from the slow cooling regime (Table 4A) displayed reductions in distance kicked ($p=0.040$), took longer to enter the jumping position ($p=0.020$), and had larger maximum flexion angles at the foot ($p=0.040$) post-freeze. Rapidly cooled frogs (Table 4B) exhibited reductions in mean jump velocity ($p<0.001$), kick velocity ($p=0.030$), and maximum instantaneous swimming velocity ($p=0.040$), as well as performing asynchronous swimming more frequently ($p=0.027$) following freeze. To further

investigate the effects of freezing on locomotor performance, we analyzed the before and after measures of experimental animals irrespective of treatment (Table 5). Overall, frogs displayed reductions in average jumping velocity ($p=0.007$), average swimming velocity ($p=0.013$), kick distance ($p=0.025$), kick velocity ($p=0.004$), maximum instantaneous swimming velocity ($p=0.007$), and took longer to enter a jumping position ($p=0.004$) following freeze.

Effects of freezing on cycle timing occurred for both cooling regimes (Fig. 2). Frogs from the rapid cooling regime (Table 6A) reached their maximum flexion angle at the foot later ($p=0.020$), while performing their maximum extension angles at the ankle ($p=0.049$) and hip ($p=0.030$) earlier in the stroke cycle. Frogs from the slow cooling regime, on the other hand, reached their maximum extension angles at the foot ($p<0.001$), ankle ($p=0.005$), and knee ($p=0.030$) later in the stroke cycle, as well as their maximum flexion angle at the ankle ($p=0.003$) earlier (Table 6B).

Following the slow cooling regime, muscle activation timings of the both the gastrocnemius and the semimembranosus were highly variable and did not occur at a particular time during the stroke cycle (non-directional; Raleigh's test ($p>0.05$); Table 6A). Similarly, the muscle activation of the semimembranosus in rapidly cooled frogs was also non-directional. The gastrocnemius of rapidly cooled frogs did occur at the same point in each stroke cycle (directional; Raleigh's test ($p<0.05$)). Rapidly cooled frogs did not display changes in either the start ($p=0.500$) or end ($p=0.520$) of activation in the gastrocnemius as a consequence of freezing (Fig. 2C).

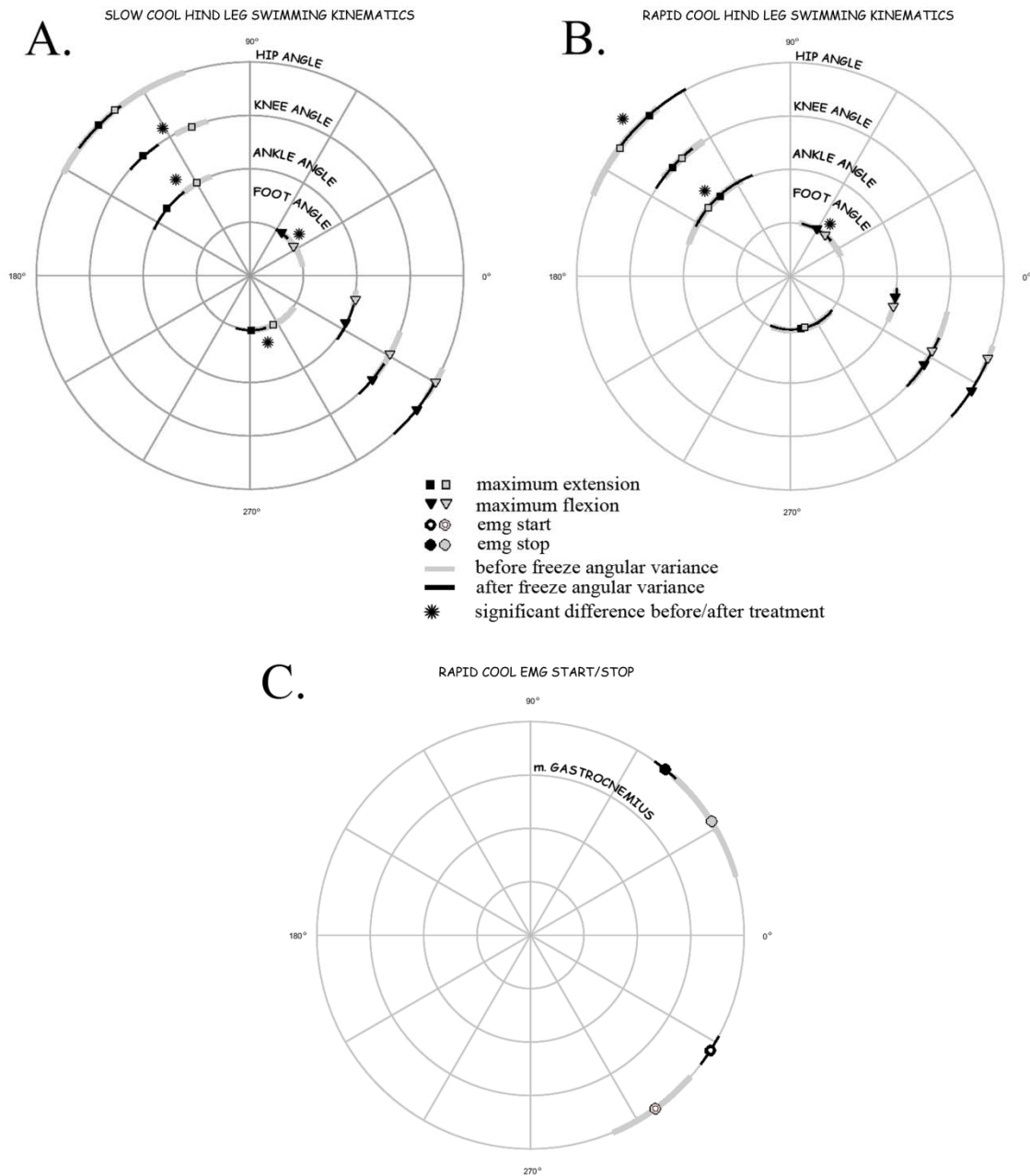


Fig. 2. Timing of kinematic variables for the right leg of wood frogs (*Rana sylvatica*) during swimming before (thick grey) and after (thin black) freeze. One complete stroke cycle is represented by 360 degrees; 0 degrees represents the start of extension and 180 degrees the start of flexion. **A)** Timing of leg extension and flexion before and after the slow cooling treatment. **B)** Timing of leg extension and flexion before and after the rapid cooling treatment. **C)** EMG muscle activation/deactivation timing differences before and after the rapid cooling treatment. Significant differences before and after treatment are denoted with an asterisk.

Table 2A. Differences in physiological measures of non-jumped control wood frogs (*Rana sylvatica*) over the duration of the experiment. Frogs were sampled directly from their holding tanks on Days 1 and 16. Data are presented as means \pm the standard error of the mean (SEM) and significant results are shown in **bold**.

Tissue	N		Day 1		Day 16		<i>t</i>	<i>p</i>
	Day 1	Day 16	Mean \pm SEM	Mean \pm SEM	Mean \pm SEM	Mean \pm SEM		
Glucose ($\mu\text{mol mL}^{-1}$ or g^{-1})	Plasma	6	5	3.70 \pm 0.75	13.42 \pm 4.09	2.57	0.030	
	Liver	6	6	13.18 \pm 1.21	5.65 \pm 1.22	4.38	0.001	
	Semimembranosus	6	6	2.06 \pm 0.20	9.38 \pm 0.34	18.59	<0.001	
Glycogen ($\mu\text{mol mL}^{-1}$ or g^{-1})	Gastrocnemius	6	6	1.92 \pm 0.29	1.24 \pm 0.15	2.06	0.700	
	Liver	6	6	30.85 \pm 2.12	23.50 \pm 5.99	1.16	0.270	
	Semimembranosus	6	6	2.76 \pm 0.50	1.39 \pm 0.19	2.59	0.030	
Lactate ($\mu\text{mol mL}^{-1}$ or g^{-1})	Gastrocnemius	6	6	3.01 \pm 0.60	1.78 \pm 0.30	1.83	0.100	
	Plasma	6	5	6.45 \pm 0.82	1.57 \pm 0.34	5.13	<0.001	
	Liver	6	6	2.74 \pm 0.25	2.37 \pm 0.33	0.91	0.390	
Urea ($\mu\text{mol mL}^{-1}$ or g^{-1})	Semimembranosus	6	6	10.5 \pm 0.85	26.08 \pm 0.84	13.02	<0.001	
	Gastrocnemius	6	6	5.91 \pm 0.66	8.96 \pm 0.80	2.94	0.020	
	Plasma	6	6	6.94 \pm 0.64	6.09 \pm 0.67	0.92	0.380	
Hepatosomatic Index (%)	Liver	6	6	3.31 \pm 0.21	3.32 \pm 0.50	0.01	0.990	
	Semimembranosus	6	6	3.61 \pm 0.30	3.02 \pm 0.14	1.79	0.100	
	Gastrocnemius	6	6	2.97 \pm 0.12	3.04 \pm 0.12	0.45	0.660	
Muscle H ₂ O Content (%)		6	6	3.62 \pm 0.34	2.97 \pm 0.23	1.59	0.140	
		6	6	37.48 \pm 1.49	47.80 \pm 2.35	3.71	0.004	
Hematocrit (%)		6	6	30.50 \pm 3.14	19.15 \pm 4.62	2.03	0.070	
		6	6					

Table 2B. Differences in kinematic measures of sham-handled control wood frogs (*Rana sylvatica*) over the duration of the experiment. Data are presented as means \pm the standard error of the mean (SEM). No significant differences were detected. Angles are reported in radians.

Variable	N		Day 1		Day 16		t	p
	Day 1	Day 16	Mean \pm SEM	Mean \pm SEM	Mean \pm SEM	Mean \pm SEM		
Jumping	3	6	123.03 \pm 12.15	199.22 \pm 37.93	1.36	0.220		
	3	5	26.65 \pm 5.40	31.04 \pm 4.67	0.60	0.570		
	3	6	0.06 \pm 0.06	16.53 \pm 7.21	1.56	0.160		
	3	6	14.67 \pm 3.53	9.33 \pm 0.67	2.13	0.070		
Swimming	3	5	26.65 \pm 5.40	31.04 \pm 4.67	0.60	0.570		
	3	5	54.91 \pm 11.33	78.71 \pm 15.07	1.10	0.320		
	3	5	38.66 \pm 7.42	46.35 \pm 6.54	0.75	0.480		
	3	5	29.57 \pm 5.38	57.09 \pm 8.30	2.34	0.060		
	3	5	18.34 \pm 2.49	23.02 \pm 2.31	1.31	0.240		
	3	5	46.89 \pm 7.72	65.04 \pm 10.23	1.23	0.270		
Maximum Extension Angles	3	5	3.17 \pm 0.01	3.09 \pm 0.05	1.33	0.230		
	3	5	3.07 \pm 0.06	3.06 \pm 0.05	0.11	0.920		
	3	5	2.60 \pm 0.06	2.56 \pm 0.06	0.39	0.710		
	3	5	2.56 \pm 0.07	2.77 \pm 0.06	2.12	0.080		
Maximum Flexion Angles	3	5	4.17 \pm 0.15	4.20 \pm 0.07	0.22	0.840		
	3	5	0.92 \pm 0.04	0.83 \pm 0.08	0.82	0.440		
	3	5	0.24 \pm 0.07	0.19 \pm 0.05	0.61	0.560		
	3	5	1.63 \pm 0.01	1.48 \pm 0.07	1.50	0.190		

Table 3A. Physiological differences between wood frogs (*Rana sylvatica*) from the slow and rapid cooling regimes. Data are presented as means \pm the standard error of the mean (SEM). Significant results are shown in **bold**.

	Tissue	N		Slow Cooling		Rapid Cooling		t	p
		Slow Cooling	Rapid Cooling	Mean \pm SEM	Mean \pm SEM	Mean \pm SEM	Mean \pm SEM		
Glucose ($\mu\text{mol mL}^{-1}$ or g^{-1})	Plasma	11	12	25.77 \pm 2.95	25.55 \pm 5.11	0.90	0.380		
	Liver	12	12	25.27 \pm 2.69	25.11 \pm 3.40	0.04	0.970		
	Semimembranosus	12	12	9.29 \pm 0.74	10.27 \pm 1.30	0.03	0.890		
Glycogen ($\mu\text{mol mL}^{-1}$ or g^{-1})	Gastrocnemius	12	12	10.78 \pm 0.75	11.49 \pm 1.61	0.34	0.740		
	Liver	12	10	8.33 \pm 2.43	18.50 \pm 3.71	2.367	0.030		
	Semimembranosus	12	12	3.05 \pm 0.40	2.52 \pm 0.32	1.22	0.240		
Lactate ($\mu\text{mol mL}^{-1}$ or g^{-1})	Gastrocnemius	12	12	3.15 \pm 0.42	2.11 \pm 0.35	1.93	0.070		
	Plasma	11	12	10.13 \pm 0.86	9.34 \pm 0.72	0.79	0.490		
	Liver	12	12	3.48 \pm 0.31	4.18 \pm 0.23	1.81	0.080		
Urea ($\mu\text{mol mL}^{-1}$ or g^{-1})	Semimembranosus	12	12	8.09 \pm 1.15	9.19 \pm 0.75	0.80	0.430		
	Gastrocnemius	12	12	2.99 \pm 0.18	2.68 \pm 0.18	1.26	0.220		
	Plasma	11	12	6.69 \pm 0.49	6.90 \pm 0.91	0.15	0.880		
Hepatosomatic Index (%)	Liver	12	12	3.57 \pm 0.24	3.41 \pm 0.38	0.68	0.510		
	Semimembranosus	12	12	3.65 \pm 0.25	3.21 \pm 0.19	1.43	0.170		
	Gastrocnemius	12	12	2.99 \pm 0.18	2.68 \pm 0.18	1.19	0.250		
Muscle H ₂ O Content (%)		12	12	2.80 \pm 0.18	2.90 \pm 0.19	0.36	0.720		
		11	12	38.08 \pm 2.20	40.49 \pm 3.04	0.59	0.570		
Hematocrit (%)		11	12	24.57 \pm 2.23	25.29 \pm 1.17	0.29	0.770		

Table 3B. Physiological differences between combined treatment and sham-handled control wood frogs (*Rana sylvatica*). Liver glycogen was compared separately for each cooling regime as a difference was detected between cooling regimes (see Table 3A). Data are presented as means \pm the standard error of the mean (SEM). Significant results are shown in **bold**.

Tissue	N		Treatments		Controls		t	p
	Treatments	Controls	Mean \pm SEM	SEM	Mean \pm SEM	SEM		
Glucose ($\mu\text{mol mL}^{-1}$ or g^{-1})	Plasma	23	15	25.65 \pm 2.95		10.44 \pm 3.61	3.26	0.002
	Liver	24	15	25.19 \pm 2.12		16.04 \pm 2.04	2.92	0.006
	Semimembranosus	24	15	9.78 \pm 0.74		5.21 \pm 0.81	4.04	<0.001
	Gastrocnemius	24	14	11.13 \pm 0.87		3.31 \pm 0.38	6.63	<0.001
Glycogen ($\mu\text{mol mL}^{-1}$ or g^{-1})	Liver	Slow-12	15	8.33 \pm 2.43		23.81 \pm 2.61	4.25	<0.001
		Rapid-10		18.50 \pm 3.71			1.21	0.240
Semimembranosus		24	15	2.79 \pm 0.25		2.30 \pm 0.26	1.27	0.210
	Gastrocnemius	24	15	2.63 \pm 0.29		2.16 \pm 0.29	1.10	0.280
Lactate ($\mu\text{mol mL}^{-1}$ or g^{-1})	Plasma	23	15	9.72 \pm 0.55		7.96 \pm 0.96	1.71	0.090
	Liver	24	15	3.83 \pm 0.20		4.54 \pm 0.35	1.92	0.060
Semimembranosus		24	15	8.64 \pm 0.68		19.83 \pm 1.56	7.48	<0.001
	Gastrocnemius	24	15	8.96 \pm 0.91		14.32 \pm 1.23	3.57	0.001
Urea ($\mu\text{mol mL}^{-1}$ or g^{-1})	Plasma	23	14	6.80 \pm 0.52		6.62 \pm 0.44	0.24	0.810
	Liver	24	15	3.49 \pm 0.22		3.25 \pm 0.21	0.73	0.470
	Semimembranosus	24	15	3.43 \pm 0.16		3.25 \pm 0.14	0.80	0.430
	Gastrocnemius	24	15	2.84 \pm 0.13		2.87 \pm 0.17	0.14	0.890
Hepatosomatic Index (%)		24	15	2.85 \pm 0.13		2.69 \pm 0.15	0.81	0.420
Muscle H ₂ O Content (%)		23	13	39.34 \pm 1.88		42.53 \pm 2.94	0.96	0.350
Hematocrit (%)		23	15	24.95 \pm 1.20		25.34 \pm 1.87	0.19	0.850

Table 4A. Effects of the slow cooling regime on wood frog (*Rana sylvatica*) kinematics. Data are presented as means \pm the standard error of the mean (SEM). Significant results are shown in **bold**. Angles are reported in radians.

Variable	N	Before		After		<i>t</i>	<i>p</i>
		Mean \pm SEM	SEM	Mean \pm SEM	SEM		
Jumping	12	161.41 \pm 25.67		170.15 \pm 28.31		0.23	0.820
	12	56.04 \pm 7.59		49.54 \pm 8.30		0.53	0.610
	12	4.28 \pm 3.77		8.75 \pm 5.81		0.63	0.540
	12	23.33 \pm 5.25		59.83 \pm 11.15		2.80	0.020
Swimming	8	29.08 \pm 3.76		17.45 \pm 3.15		2.18	0.060
	8	74.45 \pm 10.18		42.17 \pm 4.70		2.54	0.040
	8	44.49 \pm 6.81		25.92 \pm 5.00		2.14	0.070
	8	48.61 \pm 6.95		46.61 \pm 6.67		0.01	0.990
	8	20.98 \pm 2.46		13.81 \pm 2.55		1.75	0.120
	8	56.74 \pm 7.74		34.10 \pm 6.31		2.03	0.080
Maximum Extension Angles	8	3.05 \pm 0.04		3.08 \pm 0.03		0.47	0.650
	8	2.88 \pm 0.04		2.91 \pm 0.05		0.55	0.600
	8	2.37 \pm 0.06		2.32 \pm 0.06		1.04	0.330
Maximum Flexion Angles	8	2.63 \pm 0.06		2.55 \pm 0.09		0.75	0.480
	8	4.42 \pm 0.10		4.65 \pm 0.09		2.47	0.040
	8	0.94 \pm 0.08		0.83 \pm 0.09		0.08	0.940
Hip	8	0.21 \pm 0.03		0.24 \pm 0.07		0.41	0.690
	8	1.56 \pm 0.08		1.38 \pm 0.12		1.45	0.190

Table 4B. Effects of the rapid cooling regime on wood frog (*Rana sylvatica*) kinematics. Data are presented as means \pm the standard error of the mean (SEM). Significant results are shown in **bold**. Angles are reported in radians.

Variable	<i>N</i>	Before		After		<i>t</i>	<i>P</i>
		Mean \pm SEM	SEM	Mean \pm SEM	SEM		
Jumping							
Distance (mm)	12	237.62 \pm 31.93		183.94 \pm 28.15		1.56	0.150
Avg Velocity (cm sec ⁻¹)	12	86.52 \pm 9.49		42.82 \pm 7.61		4.57	<0.001
Max Height (mm)	12	8.72 \pm 3.65		10.81 \pm 4.94		0.36	0.730
Jump Loading Time (msec)	9	20.67 \pm 4.67		34.67 \pm 6.27		1.84	0.100
Swimming							
Avg Velocity (cm sec ⁻¹)	10	26.33 \pm 3.48		18.26 \pm 2.53		1.63	0.140
Kick Distance (mm)	10	60.36 \pm 7.49		46.62 \pm 7.05		1.01	0.340
Kick Velocity (cm sec ⁻¹)	10	41.29 \pm 5.63		24.45 \pm 4.13		2.49	0.030
Distance Recovery (mm)	10	46.07 \pm 7.30		60.53 \pm 9.48		0.89	0.400
Velocity Recovery (cm sec ⁻¹)	10	18.58 \pm 2.45		17.78 \pm 2.33		0.22	0.830
Max Instantaneous Velocity (cm sec ⁻¹)	10	53.32 \pm 6.95		34.02 \pm 5.36		2.28	0.040
Maximum Extension Angles							
Foot	10	3.12 \pm 0.03		3.18 \pm 0.05		0.97	0.360
Ankle	10	3.03 \pm 0.03		2.91 \pm 0.05		2.02	0.070
Knee	10	2.55 \pm 0.04		2.37 \pm 0.06		2.04	0.070
Hip	10	2.74 \pm 0.06		2.66 \pm 0.04		1.88	0.090
Maximum Flexion Angles							
Foot	10	4.39 \pm 0.18		4.69 \pm 0.15		1.14	0.280
Ankle	10	0.96 \pm 0.10		1.14 \pm 0.08		0.89	0.400
Knee	10	0.32 \pm 0.07		0.36 \pm 0.07		0.22	0.830
Hip	10	1.49 \pm 0.06		1.63 \pm 0.07		1.02	0.340

Table 5. Effects of freezing on wood frog (*Rana sylvatica*) kinematics. Data are pooled across the rapid and slow cooling regimes to assess the general effects of freezing on kinematics. Data are presented as means \pm the standard error of the mean (SEM). Significant results are shown in **bold**.

Variable	N	Before		After		<i>t</i>	<i>p</i>
		Mean \pm SEM	Mean \pm SEM	Mean \pm SEM	Mean \pm SEM		
Jumping	Distance (mm)	24	199.51 \pm 21.55	177.05 \pm 19.58	0.86	0.400	
	Avg Velocity (cm sec ⁻¹)	24	71.28 \pm 6.74	46.18 \pm 5.55	2.95	0.007	
	Max Height (mm)	24	6.50 \pm 2.61	9.78 \pm 3.73	0.73	0.470	
Jump Loading Time (msec)	21	22.19 \pm 3.54	47.25 \pm 6.78	3.31	0.004		
Swimming	Avg Velocity (cm sec ⁻¹)	18	27.64 \pm 2.51	17.90 \pm 1.94	2.76	0.013	
	Kick Distance (mm)	18	67.07 \pm 6.28	44.62 \pm 4.34	2.46	0.025	
	Kick Velocity (cm sec ⁻¹)	18	42.81 \pm 4.28	25.11 \pm 3.11	3.30	0.004	
	Distance Recovery (mm)	18	47.28 \pm 4.94	54.26 \pm 6.08	0.71	0.490	
	Velocity Recovery (cm sec ⁻¹)	18	19.72 \pm 1.71	16.00 \pm 1.74	1.37	0.190	
Max Instantaneous Velocity (cm sec ⁻¹)	18	54.95 \pm 5.06	34.06 \pm 3.99	3.10	0.007		

Table 6A. Effects of the slow cooling regime on wood frog (*Rana sylvatica*) stroke cycle and muscle activation timings. Data are presented as means \pm angular variance in radians. Significant results are shown in **bold**. Data that were non-directional were excluded from the analysis.

Variable	<i>N</i>	Before Mean \pm Ang Var	After Mean \pm Ang Var	<i>F</i>	<i>p</i>
Maximum Angular Timings	9	Extension	-1.12 \pm 0.48	23.67	<0.001
		Flexion	0.59 \pm 0.37	12.38	0.003
Ankle	9	Extension	2.09 \pm 0.14	10.04	0.005
		Flexion	-0.21 \pm 0.06	2.19	0.160
Knee	9	Extension	1.94 \pm 0.09	5.49	0.030
		Flexion	-0.50 \pm 0.15	1.76	0.200
Hip	9	Extension	2.25 \pm 0.37	1.19	0.290
		Flexion	-0.52 \pm 0.07	0.90	0.360
EMG Timings	4	Gastrocnemius	-0.89 \pm 0.14	NA	NA
		End	0.12 \pm 0.09	NA	NA
Semimembranosus	6	Start	Non-Directional	NA	NA
		End	Non-Directional	NA	NA

Table 6B. Effects of the rapid cooling regime on wood frog (*Rana sylvatica*) stroke cycle and muscle activation timings. Data are presented as means \pm angular variance in radians. Significant results are shown in **bold**. Data that were non-directional were excluded from the analysis.

Variable	N	Before		After		F	p
		Mean \pm Ang Var	Mean \pm Ang Var	Mean \pm Ang Var	Mean \pm Ang Var		
Maximum Angular Timings	Foot	Extension	11	-1.30 \pm 0.55	-1.31 \pm 0.61	0.02	0.890
		Flexion	11	0.86 \pm 0.46	1.04 \pm 0.28	6.65	0.020
Ankle		Extension	11	2.44 \pm 0.38	2.29 \pm 0.35	4.40	0.049
		Flexion	11	-0.28 \pm 0.14	-0.19 \pm 0.07	0.39	0.540
	Knee	Extension	11	2.31 \pm 0.16	2.39 \pm 0.16	0.62	0.440
		Flexion	11	-0.48 \pm 0.24	-0.58 \pm 0.17	1.01	0.330
	Hip	Extension	11	2.50 \pm 0.25	2.29 \pm 0.20	5.55	0.030
		Flexion	11	-0.39 \pm 0.06	-0.56 \pm 0.15	1.24	0.280
EMG Timings	Gastrocnemius	Start	3	-0.95 \pm 0.22	-0.57 \pm 0.07	0.52	0.500
		End	3	0.56 \pm 0.27	0.89 \pm 0.06	0.46	0.520
	Semimembranosus	Start	3	-0.94 \pm 0.10	Non-Directional	NA	NA
		End	3	0.22 \pm 0.10	Non-Directional	NA	NA

DISCUSSION

Physiology

Wood frogs undergo drastic physiological remodeling to tolerate freezing. As such, it is not surprising that frogs which underwent freezing had different physiological responses than non-frozen sham-handled controls. Elevated levels of glucose along with low levels of hepatic glycogen in previously frozen animals suggest that the resorption of this cryoprotectant molecule occurs over a longer duration than the 8 hour recovery period provided. Indeed, prior studies have shown that the effects of freezing on glucose metabolism persist even following 5 days of recovery from freezing at 4°C (Costanzo et al., 2013). As well, consistent with previous findings, this universal rise in glucose occurred independently of muscle glycogen stores (Storey, 1984), instead relying solely on hepatic glycogen levels (Table 3B). The functional outcome of this being that glycogen stores remain high in muscle tissues where they are required for high intensity locomotor and reproductive behaviours. Interestingly, there were almost no physiological differences between frogs that were cooled at different rates (Table 3A), suggesting that the physiological effect of cooling rate is minor when compared to the broad responses induced by freezing in general.

Lactate is known to accumulate while frozen (Storey & Storey, 1984), owing to an increased reliance on anaerobic metabolism. Lactate levels negatively correlate with muscle performance in frogs (Fitts & Holloszy, 1976), therefore, it would be feasible to expect that elevated lactate would be associated with reductions in post-freeze locomotor performance (Layne & Rice, 2003; current study). However, in contrast, we observed lower levels of muscle lactate in previously frozen animals compared to sham-handled controls (Table 3B), and previous studies suggest that either lactate does not accumulate in the leg muscles (Costanzo et al., 1997), or that it is rapidly cleared upon thaw (<24hr; Irwin et al., 2003). In support of the latter, Sinclair et al. (2013) observed that whole animal metabolic rate increases during thaw, probably due in part to lactate clearance. This is supported by elevated post-freeze activity levels of lactate dehydrogenase (Cowan & Storey, 2001), which converts lactate to pyruvate. Overall, these data suggest that lactate is not the cause of the reduction in locomotor performance observed post-thaw.

Muscle atrophy induced while frozen may also cause reduced locomotor performance, however, immobility while frozen does not seem to cause muscle atrophy in wood frogs

(Irwin et al., 2003; Layne & Rice, 2003). More likely, reductions in creatine phosphate (PCr) levels that occur as a result of freezing may be influencing performance (Storey & Storey, 1984). PCr stores are relied upon by frogs while frozen to maintain constant levels of adenosine triphosphate, and thus become depleted (Storey & Storey, 1984; Layne & Kennedy, 2002). However, PCr is also used by anurans as a fuel source during periods of high intensity muscle activation, such as burst locomotion (Miller & Sabol, 1989). Therefore, it is likely that decreased PCr levels are, at least partly, responsible for the observed reductions in post-freeze locomotor performance. We also observed elevated levels of glucose in both the gastrocnemius and the semimembranosus muscles (Table 3B)—a persisting artifact of the prior freeze response. It is possible that excess of this cryoprotectant molecule may have further inhibitory effects on muscle function and thus locomotor performance in anurans, and future work should investigate this.

Layne & Rice (2003) found that lower freezing temperatures required longer recovery periods before pre-freeze levels of locomotor performance returned. While we did not vary freezing temperatures in the present study, we did vary the rate of temperature decline. Costanzo et al. (1992) reported significant differences in organ dehydration and glucose content due to cooling rate, with both being impaired in frogs cooled at a rate of $-1.6^{\circ}\text{C}/\text{h}$ compared to $-0.2^{\circ}\text{C}/\text{h}$. The rapid cooling rate used in the present study was $\sim 50\%$ less than that used in Costanzo et al. (1992), however, previous work has shown that cooling rates $\leq -1.0^{\circ}\text{C}/\text{h}$ are associated with high rates of mortality (Costanzo et al., 1991). While no mortalities as a result of freezing were observed in the current study, we also did not detect any differences in glucose levels indicative of impaired glucose mobilization, despite hepatic glycogen levels being higher in rapidly cooled frogs. It is therefore likely that cooling rates necessary to impair glucose mobilization in this species are lethal.

In contrast to earlier studies (Layne, 1992; Costanzo et al., 1997) that required a 24h thaw at 3°C for wood frogs to respond by jumping, frogs from both of our cooling regimes recovered jumping and swimming ability within 8h thawing at 4°C . That our frogs recovered coordinated motor function sooner than those of earlier studies (southern Ohio spring emergers) could be due to intraspecific differences originating from their postglacial colonization biogeography, however, divergence between wood frog populations' may already predate the last glacial maximum. Lee-Yaw et al. (2008) defined

two distinct mitochondrial lineages (*i.e.* Eastern and Western) expanding from two different glacial refugia. Our frogs' lineage (Western lineage), which has colonized from Alaska to the Great Lakes region, may have inherited superior freeze-tolerance mechanisms than those from southern Ohio (Eastern lineage) due to the lower temperatures encountered at higher latitudes. This is supported by the fact that genetics appear to have a strong effect on the thermal physiology of wood frogs (Manis & Claussen, 1986), and that morphological variation reflects the genetic differences between lineages (Martof & Humphries, 1959; Lee-Yaw et al., 2008).

Biomechanics

While frogs in the current study underwent significant physiological changes as a result of holding over the 16 day period of experiments (Table 2A), their kinematic performance measures were unaffected (Table 2B). The lack of quantifiable change in biomechanical performance hints at the resilience of the frog musculoskeletal system to function effectively at a broad range of physiological parameters.

Frogs that underwent freezing, however, displayed reduced kinematic performance. Previous work shows that freezing dramatically decreases *in vitro* muscle function in wood frogs up to 24h following thaw (Layne, 1992), and reduces locomotor performance even following 11 days of recovery (Layne & Rice, 2003). These findings have important ecological implications, as wood frogs experience highly variable conditions over the winter, potentially undergoing dozens of repeated freeze-thaw cycles (Sinclair et al., 2013). This not only increases their odds of being preyed upon, but given that wood frogs spawn immediately after thawing (Wells & Bevier, 1997), a reduction in locomotor performance may lead to a reduction in reproductive success.

The decrease in locomotor performance suggests a decrease in muscle output and, thus, a less explosive locomotor event. This hypothesis is partially supported by changes observed in kinematic and muscle activation patterns of treatment animals. For example, in slowly cooled animals, leg extension starts earlier and ends later in the stroke cycle, occupying a larger portion of the stroke cycle via a slower motion pattern (Fig. 2A). Rapidly cooled animals did not exhibit this extended power phase, but rather they delayed their knee extension, while accelerating extension of their hip and ankle (Fig. 2B)—a

seemingly variable pattern suggestive of decreased function and control. Of more direct interest is the change in the rotation of the foot during swimming. Richards (2008) showed that foot rotation of a swimming frog is an important mechanism affecting thrust production. The position of the foot during the recovery stroke is also essential for reducing drag during flexion. If this timing is altered, the foot is not streamlined and can increase drag, explaining the decreases in swimming velocity and distance travelled.

During this study, we also measured muscle activation timing in the gastrocnemius and the semimembranosus muscles. Both muscles flex the knee, while the semimembranosus also extends the hip and the gastrocnemius flexes the foot. Therefore, both muscles are important in successful thrust production during jumping and swimming. Wood frogs recover hind limb muscle contractility within 1-2h post-thaw, however, coordinated motor function and body posturing remains impaired for 14-24h (Layne & Lee, 1995; Costanzo et al., 1997). During this time, processes such as muscle fiber recruitment may be suboptimal, affecting locomotor performance. In the current study, we observed highly variable EMG timings for both the gastrocnemius and the semimembranosus muscles of the leg following freezing (Tables 6A and 6B). Also notable, frogs from the rapid cooling treatment exhibited an increase in asynchronous kicking behavior when swimming post-freeze. This behavioral modification has performance consequences and may be a result of post-freeze neuromotor control impairment (Kling et al., 1994); frogs that activate all joints synchronously during swimming produce higher thrust forces (Nauwelaerts & Aerts, 2003; Johanssen & Lauder, 2004).

Jumping performance does not appear to be as affected as swimming performance post-freeze (Table 5). This difference in response may be the result of the mechanical differences between forces produced on land vs. in water. Muscle forces produced during jumping are transferred into more effective ground reaction forces compared with the more lateral production of forces during swimming (Nauwelaerts & Aerts, 2003). In addition, elastic energy storage may differ between terrestrial and aquatic locomotion such that loading of elastic elements during jumping is more effective than during swimming (Aerts & Nauwelaerts, 2009). If ground reaction forces and elastic storage are more important during jumping, impaired muscle function may not be as detrimental to jump performance as it is to swim performance, which relies more directly on muscle contraction and contraction rate.

Over the course of the experiment we observed rehydration of the leg muscles and reductions in circulating lactate levels in our frogs (Table 2A), changes consistent with recovering from freezing. Given that we collected these animals in April, immediately following spring emergence, these changes suggest that the frogs in the current study may still have been recovering from the effects of winter freezing. Both reduced muscle pH (Renaud & Stevens, 1984) and muscle dehydration (Preest & Pough, 1989) negatively affect contractile function in the muscles of anurans, suggesting that our frogs may have already exhibited muscle impairment prior to experimental freezing. While kinematic performance did not vary over the duration of the experiment (Table 2B), future studies should investigate whether the degree of biomechanical resilience varies seasonally (*i.e.* spring vs. fall).

ACKNOWLEDGEMENTS

This work was supported by a NSERC Discovery Grant and a Canadian Foundation for Innovation Grant to EMS, and an ERASMUS MUNDUS – NOVA DOMUS CHEMEDPHO Action 2 Grant to JHS-S. We also acknowledge the University of Barcelona and the University of Ottawa for their collaboration in the ERASMUS MUNDUS framework financed by the European Commission. Many thanks are extended to Vance Trudeau, Michal Galus, Maria Vu, and Brad Weiler for assistance with frog collection and care, Nicolas Corradi for allowing us to use his incubators, Kathleen Gilmour for letting us use her plate reader and reagents, Riley Jones for performing the urea analysis, and the many undergraduate students who assisted with conducting experiments, performing surgeries, processing tissues, and digitizing videos.

REFERENCES

- Aerts P, Nauwelaerts S (2009) Environmentally induced mechanical feedback in locomotion: frog performance as a model. *Journal of Theoretical Biology*, **261**, 372–378.
- Brandt RB, Siegel SA, Waters MG, Bloch MH (1980) Spectrophotometric assay for D-(-)-lactate in plasma. *Analytical Biochemistry*, **102**, 39–46.
- Churchill TA, Storey KB (1993) Dehydration tolerance in wood frogs: a new perspective on development of amphibian freeze tolerance. *American Journal of Physiology-Regulatory, Integrative and Comparative Physiology*, **265**, R1324–R1332.

Costanzo JP, do Amaral MFC, Rosendale AJ, Lee RE (2013) Hibernation physiology, freezing adaptation and extreme freeze tolerance in a northern population of the wood frog. *Journal of Experimental Biology*, **216**, 3461–3473.

Costanzo JP, Irwin JT, Lee RE (1997) Freezing impairment of male reproductive behaviors of the freeze-tolerant wood frog, *Rana sylvatica*. *Physiological Zoology*, **70**, 158–166.

Costanzo JP, Lee RE, Wright MF (1992) Cooling rate influences cryoprotectant distribution and organ dehydration in freezing wood frogs. *Journal of Experimental Biology*, **261**, 373–378.

Costanzo JP, Lee JR, Wright MF (1991) Effect of cooling rate on the survival of frozen wood frogs, *Rana sylvatica*. *Journal of Comparative Physiology B*, **161**, 225–229.

Costanzo JP, Reynolds AM, Clara M, Do Amaral F, Rosendale AJ, Lee RE (2015) Cryoprotectants and extreme freeze tolerance in a subarctic population of the wood frog. *PLoS One*, **10**, 3461–3473.

Cowan KJ, Storey KB (2001) Freeze-thaw effects on metabolic enzymes in wood frog organs. *Cryobiology*, **43**, 32–45.

Fitts R, Holloszy J (1976) Lactate and contractile force in frog muscle during development of fatigue and recovery. *American Journal of Physiology*, **231**, 430–433.

Hedrick TL (2008) Software techniques for two- and three-dimensional kinematic measurements of biological and biomimetic systems. *Bioinspiration & Biomimetics*, **3**, 034001.

Heggenes J, Krog OMW, Lindås OR, Dokk JG, Lindas OR, Dokk JG (1993) Homeostatic behavioural responses in a changing environment: brown trout (*Salmo trutta*) become nocturnal during winter. *Journal of Animal Ecology*, **62**, 295–308.

Irwin JT, Costanzo JP, Lee RE (2003) Postfreeze reduction of locomotor endurance in the freeze tolerant wood frog, *Rana sylvatica*. *Physiological and Biochemical Zoology*, **76**, 331–338.

Johansson LC, Lauder GV (2004) Hydrodynamics of surface swimming in leopard frogs (*Rana pipiens*). *Journal of Experimental Biology*, **207**, 3945–3958.

Kepler D, Decker K (1974) Methods for determination of metabolites. I. Carbohydrate metabolites: glycogen determination with amyloglucosidase. In *Methods of Enzymatic Analysis* (ed Bergmeyer HU), pp. 1127–1131. Academic Press, New York.

Kling KB, Costanzo JP, Lee RE (1994) Post-freeze recovery of peripheral nerve function in the freeze-tolerant wood frog, *Rana sylvatica*. *Journal of Comparative Physiology B*, **164**, 316–320.

Layne JR (1992) Postfreeze survival and muscle function in the leopard frog (*Rana pipiens*) and the wood frog (*Rana sylvatica*). *Journal of Thermal Biology*, **17**, 121–124.

Layne JR, First MC (1991) Resumption of physiological functions in the wood frog (*Rana sylvatica*) after freezing. *American Journal of Physiology-Regulatory, Integrative and Comparative Physiology*, **261**, R134–R137.

Layne JR, Kennedy SD (2002) Cellular energetics of frozen wood frogs (*Rana sylvatica*) revealed via NMR spectroscopy. *Journal of Thermal Biology*, **27**, 167–173.

Layne JR, Lee RE (1987) Freeze tolerance and the dynamics of ice formation in wood frogs (*Rana sylvatica*) from Southern Ohio. *Canadian Journal of Zoology*, **65**, 2062–2065.

Layne JR, Lee RE (1995) Adaptations of frogs to survive freezing. *Climate Research*, **5**, 53-59.

Layne JR, Lee RE, Heil TL (1989) Freezing-induced changes in the heart rate of wood frogs (*Rana sylvatica*). *American Journal of Physiology-Regulatory, Integrative and Comparative Physiology*, **257**, R1046–R1049.

Layne JR, Rice ME (2003) Postfreeze locomotion performance in wood frogs (*Rana sylvatica*) and spring peepers (*Pseudacris crucifer*). *Canadian Journal of Zoology*, **81**, 2061-2065.

Lee RE, Costanzo JP, Davidson EC, Layne JR (1992) Dynamics of body water during freezing and thawing in a freeze-tolerant frog (*Rana sylvatica*). *Journal of Thermal Biology*, **17**, 263–266.

Lee-Yaw JA, Irwin JT, Green DM (2008) Postglacial range expansion from northern refugia by the wood frog, *Rana sylvatica*. *Molecular Ecology*, **17**, 867-884.

Manis, M.L., and Claussen, D.L. 1986. Environmental and genetic influences on the thermal physiology of *Rana sylvatica*. *Journal of Thermal Biology*, **11**, 31–36.

Martof BS, Humphries RL (1959) Geographic variation in the wood frog, *Rana sylvatica*. *American Midland Naturalist*, **61**, 350–389.

Miller K, Sabol JL (1989) The role of phosphocreatine breakdown in the metabolic support of locomotion by clawed frogs, *Xenopus laevis*. *Comparative Biochemistry and Physiology Part B: Biochemistry and Molecular Biology*, **93**, 251–254.

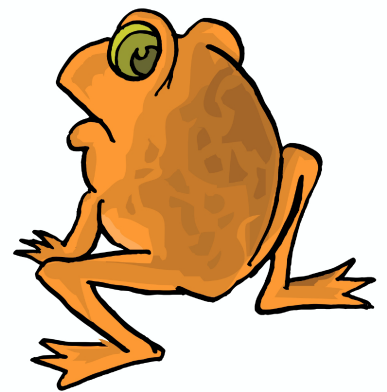
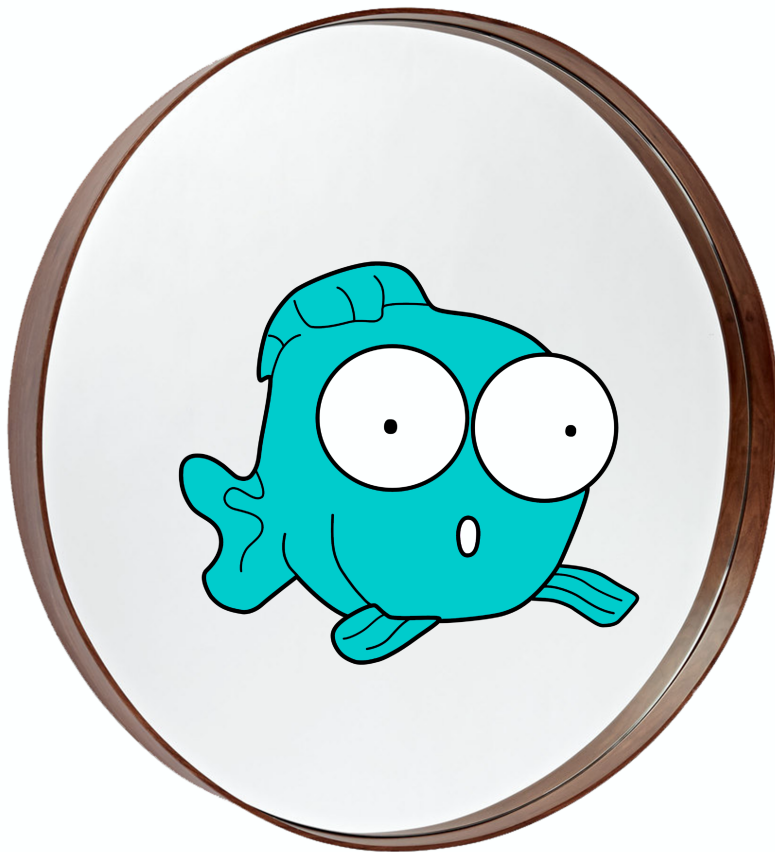
Nauwelaerts S, Aerts P (2003) Propulsive impulse as a covarying performance measure in the comparison of the kinematics of swimming and jumping in frogs. *Journal of Experimental Biology*, **206**, 4341–4351.

Peters SE, Kamel LT, Bashor DP (1996) Hopping and swimming in the leopard frog, *Rana pipiens*. I. Step cycles and kinematics. *Journal of Morphology*, **230**, 1–16.

Preest MR, Pough FH (1989) Interaction of temperature and hydration on locomotion of toads. *Functional Ecology*, **3**, 693–699.

- Rahmatullah M., Boyde TR (1980) Improvements in the determination of urea using diacetyl monoxime; methods with and without deproteinisation. *Clinica Chimica Acta*, **107**, 3–9.
- Renaud JM, Stevens ED (1984) The extent of short-term and long-term compensation to temperature shown by frog and toad sartorius muscle. *Journal of Experimental Biology*, **75**, 57–75.
- Richards CT (2008) The kinematic determinants of anuran swimming performance: an inverse and forward dynamics approach. *Journal of Experimental Biology*, **211**, 3181–3194.
- Sinclair BJ, Stinziano JR, Williams CM, Macmillan HA, Marshall KE, Storey KB (2013) Real-time measurement of metabolic rate during freezing and thawing of the wood frog, *Rana sylvatica*: implications for overwinter energy use. *Journal of Experimental Biology*, **216**, 292–302.
- Sømme L (1989) Adaptations of terrestrial arthropods to the alpine environment. *Biological Reviews of the Cambridge Philosophical Society*, **64**, 367–407.
- Storey K (1984) Freeze tolerance in the frog, *Rana sylvatica*. *Experientia*, **40**, 1261–1262.
- Storey KB (1997) Organic solutes in freezing tolerance. *Comparative Biochemistry and Physiology Part A: Molecular & Integrative Physiology*, **117**, 319–326.
- Storey KB, Storey JM (1984) Biochemical adaptation for freezing tolerance in the wood frog, *Rana sylvatica*. *Journal of Comparative Physiology B*, **155**, 29–36.
- Storey KB, Storey JM (1986) Freeze tolerant frogs: cryoprotectants and tissue metabolism during freeze-thaw cycles. *Canadian Journal of Zoology*, **64**, 49–56.
- Storey KB, Storey JM (1987) Persistence of freeze tolerance in terrestrially hibernating frogs after spring emergence. *Copeia*, **1987**, 720–726.
- Storey KB, Storey JM (1988) Freeze tolerance in animals. *Physiological Reviews*, **68**, 27–84.
- Storey KB, Storey JM (1992) Natural freeze tolerance in ectothermic vertebrates. *Annual Review of Physiology*, **54**, 619–637.
- Terrien J, Perret M, Aujard F (2011) Behavioral thermoregulation in mammals: a review. *Frontiers in Bioscience*, **16**, 1428–1444.
- Wells KD, Bevier CR (1997) Contrasting patterns of energy substrate use in two species of frogs that breed in cold weather. *Herpetologica*, **53**, 70–80.
- Williams CM, Henry HAL, Sinclair BJ (2015) Cold truths: How winter drives responses of terrestrial organisms to climate change. *Biological Reviews of the Cambridge Philosophical Society*, **90**, 214–235.

INTEGRATIVE DISCUSSION



ADVANCES IN MORPHOMETRIC METHODS

In Section I landmark-based Geometric Morphometrics (GMM) was applied with the intention of finding morphological differences in body shape between phenotypically very similar sister species, namely the as of yet phylogenetically unresolved [at the species level] *Haplochromis* cichlids due to their recent divergence (Wagner et al., 2012; Takahashi & Sota, 2016; but see Keller et al., 2013). The analyses validated GMM as a very powerful method for morphological discrimination, identifying the slightest of variations in anatomical structures despite the apparent similarity between individuals upon visual inspection (Van Oijen et al, 1981). However, the adequate functioning of this method cannot be taken for granted and involves standardization in the acquisition of image data and comprehensive error testing to assure that the calculated shape corresponds to biological, rather than methodological variation. This involves an exhaustive labor of landmark placement on images (*i.e.* digitization), which has to be performed on all individuals of the sample by the same person to avoid inter-observer differences in structure recognition. In 2D analyses, additional care has to be taken to standardize image capture, and orientation error in the placement of the sample prior to image capture must be considered. In the analyses of an ontogenetic series of individuals, image parallax can also become an issue due to the curved surface of the body of the animal, which in fish increases with their increasing size, thus potentially inducing non-standardized shape variation in the analysis (Fruciano, 2016). To correct for this potential source of error, however, there exists an unbending procedure that corrects landmarks' coordinates based on a subset located along one of the animal's body axes. For my analyses of cichlid ontogenetic series, I performed the unbending procedure along their anteroposterior axis, successfully removing this source of variation and improving their shape comparisons (Santos-Santos et al., 2015).

Luckily, throughout the years, comprehensive software packages have been developed (*e.g.* Morpho, IMP, Morphologika, tps Series, Past, MorphoJ, *geomorph* R-package) that have allowed for a progressive improvement in the visualization of shape deformation corresponding to GMM output. In this manner, in my cichlid manuscripts (Chapters 1 & 2) I have illustrated the shape variation as superimposed wireframes that aid an untrained observer significantly in the interpretation of the patterns of shape variation. In addition, there have been improvements in the statistical analysis of shape data, resulting in the

advancement of shape analyses to take into account the effect of additional factors on shape variation and better estimate significance levels based on non-parametric permutation, which adjusts more realistically to the structure of shape data (Collyer & Adams, 2018). In my comparison of cichlid species with their hybrid (Chapter 2), I adopted a couple of these methods: Allometry analyses were carried out taking into account factor-specific allometric relationships with the `procD.allometry()` and `[advanced.]procD.lm()` functions in the *geomorph* R-package; Phenotypic Trajectory Analysis (Adams & Collyer, 2009; Collyer & Adams, 2013) that tests for [dynamic] differences in the way groups' change shape across the different states of their [for example] developmental/ontogenetic gradient was carried out with the `trajectory.analysis()` function, as well, in *geomorph*; and Between-group Principal Component Analysis that has been demonstrated to not overestimate group differences and to be a better statistical procedure than the previously widely used Canonical Variate Analysis to calculate the axes of shape variation that best discriminate groups (Mitteroecker & Bookstein, 2011) was carried out in the most recent version of MorphoJ, where it is now available under a relatively user-friendly interface.

All in all, landmark-based GMM constitutes a non-destructive method that allows to extract patterns of shape based on the coordinated variation of a configuration of anatomical landmarks. Furthermore, the multivariate nature of shape allows to test for covariation between different anatomical regions, defined as subsamples of landmarks within the entire configuration, potentially identifying integrative (Mitteroecker & Bookstein, 2007) and modular (Klingenberg, 2009) patterns of shape development (Santos-Santos, unpublished data). When these landmarks are located at anatomical structures that are previously known to be implicated in an organism's functional design, ecomorphological approximations can be inferred from the observed patterns of shape variation. However, additional studies relating the range of observed shape variation to the organism's functional performance must be carried out to demonstrate whether or not it constitutes an adaptive advantage for the organism, and accordingly could increase its fitness in nature (Arnold, 1983).

Section II further reflects the search for ecomorphological variation, albeit this time in internal anatomical structure and with 3D volumetric images due to the advent, and affordability, of modern X-ray computed tomography (CT) techniques. The application of

these techniques have become widespread thanks to the preservation of the sample following scanning [as opposed to microtome sectioning], however they are mostly utilized for paleontological or skeletal samples. The accurate scanning of samples that must remain submerged in alcohol pose an additional difficulty due to the density and movement of the liquid during X-ray image capture. This aspect, although not reflected in the manuscripts, lead to long hours of exploring calibrations and sample preparations in order to come up with a standardized protocol to scan the frogs used in this study. Even so, the scan times to obtain the volumetric anatomy of an individual (4-8h) can be considered relatively worthwhile. In this manner, in Chapter 4 I explore the internal anatomy for the first time of a *Blommersia* species. In contrast to 2D photographs or 3D surfaces, volumetric data provides an additional dimension of morphological variation: density value. Thanks to the density histogram that is produced from the reconstruction of X-ray images, I was able to characterize this species' osteological morphology to the precision of micrometers, measuring distances directly on the rendered volumes and describing intraspecific variation in structures presenting different levels of ossification.

On the other hand, to compare shapes one must segment (*i.e.* assign density values to coordinates) the sub-region of the volume that corresponds to the structure of interest, and extract it as a 3D mesh or surface. This was done for the pelvis of *Blommersia* frogs in Chapter 5. However, real biological structures are far from flawless and must be standardized as well before between-individual comparisons. This obliges to post-process the 3D models, correcting for any computational errors in their geometry that could have arisen in their segmentation/generation and removing individual-specific variations that could obfuscate group-specific trends in shape variation. These processes used to require extremely expensive software licenses (*e.g.* Amira/Avizo™, Geomagic®), however nowadays, due to the extended use of these methods in economically-deficient fields, such as biology, more and more new open source resources are becoming available that nearly match in performance their licensed counterparts, albeit with a little bit more user interaction (*e.g.* 3D Slicer, Meshlab). Nonetheless, the economical obtainment of high-resolution 3D morphology brings about another matter in shape comparison. In contrast to traditional GMM approaches that rely on a limited number of user-defined landmarks to describe shape, 3D models consist in tens to hundreds of thousands of points that describe a structure's morphology. Performing traditional GMM analysis on these datasets would result in unrealistic statistically-sound sample sizes and computation

times, not to mention the biological non-homology between the models' pointclouds. The solution to these problems comes from the hand of the recently developed Generalized Procrustes Surface Analysis (Pomidor et al., 2016), which adapts the Iterative Closest Point algorithms (Besl & McKay, 1992; Chen & Medioni, 1992) to the Generalized Procrustes Analysis paradigm (Rohlf & Slice, 1990) of traditional GMM. I explored this method for the analysis of the *Blommersia* pelvis due to the absence of obvious anatomical landmarks on the bone's smooth surface that could serve to perform traditional landmark-based GMM. After several attempts I was able to create a workflow from 3D model generation and post-processing to their analysis, and the results obtained were biologically coherent with visualization of shape variation easily interpretable in the manner of a color-coded heatmap upon the sample's 3D model template. Although this method of GMM analysis requires a relatively more elaborate process of data acquisition and post-processing than traditional GMM, these procedures are more repeatable, eliminating inter-observer differences in landmark placement, and involve much less interaction of the researcher who would have to manually digitize all specimens, albeit the longer computational times.

In Chapter 5 as well, I make use of the combination of a traditional histological technique with that of CT-scanning to shed light on another aspect of the organism's internal morphology: soft tissues. Contrast agents for histological sectioning have been around since the early 20th century, but it has only been until the last decade that these techniques have been started to be used in conjunction with X-ray tomography (Metscher, 2009; Pauwels et al., 2013). Staining chemicals modify the density of targeted tissues, expanding the range of effective density values in resulting CT data, consequently enhancing the contrast between different tissue types and allowing for an easier visual discrimination and segmentation of different anatomical structures. However, the histochemical bonding of certain staining chemicals to tissue may be irreversible and imbue the sample with an unnatural hue. In my analysis of *Blommersia* locomotor morphology I was interested in mapping the associated musculature in search for relationships between variation in its architecture and skeletal shape variation, which could potentially exert an influence on the functioning of the musculoskeletal system. To discriminate the different muscle bundles and the position of their insertions, tendons, and ligaments I developed a staining protocol involving two contrast agents: iodine and phosphomolibdic acid. The first has been reported as the best contrast agent for muscle

tissue in vertebrates, resulting in images that allow discrimination up to individual muscle fibers (current study; Jeffery et al., 2011; Gignac & Kley, 2014). In addition, although imbuing the sample with a reddish hue, iodine staining is completely reversible and can be washed out simply with running tap water. The second is a slightly more aggressive staining chemical, which can decalcify osteological structures if used [inappropriately] in excessive concentrations and/or staining times. Although irreversible, it imbues the sample with a light translucent greenish hue that does not belie the sample's anatomy. The use of this contrast agent enhances discrimination of connective tissues, such as cartilage (Metscher, 2009; Descamps et al., 2014). By employing these two chemicals sequentially, the effective range of density values compared to non-stained scans increased two-fold and different tissue types were delimited to less overlapping ranges of values (data not shown). The application of this technique is remarkable not only in the capture of soft tissue morphology, but also in the potential of the resulting data for biomechanical studies. In my drive to link morphology to functional performance, a plausible next step would be the creation of musculoskeletal models for biomechanical simulation (*e.g.* Kargo et al., 2002; Johansson & Lauder, 2004; O'Higgins et al., 2011). The combination of a skeletal CT-scan previous to a stained CT-scan of the same individual would provide the most precise biomechanical model possible; and if performed for several individuals with body sizes at the extremes of a species' size range would also allow for an exhaustive validation of the allometric scaling between morphological variation and performance (Dick & Clemente, 2016; Heinen et al., 2016). These could be future lines of work with the *Blommersia* species once muscle segmentation has been completed.

Despite the possibility of simulating locomotor performance without physically invading the anatomy of the organism, validation of a simulation's outcome cannot be evaluated without certain performance measurements *in vivo*. Following this line of thought, in Chapter 6 I applied several biomechanical techniques to evaluate jumping and swimming locomotor performance in a common North American frog. Contrary to the rest of techniques used in the current tome, animals tested biomechanically are normally sacrificed [in my case for physiological data], thus the unfeasibility of performing these studies with rare, non-model organisms. Ideally, my biomechanical studies performed *in vivo* should have been with the same *Blommersia* species, and individuals, for which I described their morphology. In that way the data obtained from high-speed video

kinematics (*e.g.* joint extension/flexion timings/angles) and electromyography recordings (*i.e.* muscle activation/deactivation timings); and optimistically also from sonomicrometry (*i.e.* timed changes in muscle length) and particle image velocimetry (*i.e.* resulting fluid wake dynamics), can all be incorporated into the biomechanical model to further increase the precision of performance simulations for hyper-realistic interpretations.

ECOMORPHOLOGICAL DISCRIMINATION OF SISTER SPECIES

Phylogenetically proximal sister species pose an added challenge to discriminate morphologically due to their relatively recent divergence, which in contrast to more distantly related lineages have not disposed of as much time for the accumulation of directed phenotypic divergence. However, the retention of ancestral polymorphism (Moran & Kornfield, 1993; Meier et al., 2018) and phenotypic plasticity potential (Wimberger, 1994; Wagner & Altenberg, 1996) can make their morphology diverge faster than expected in response to the environmental factors of contrasting habitats or ecological niches. This is especially true when sister species occur in syntopy. If their ancestor colonized a novel environment void of competitors, for example an island, the divergence of the ancestral population towards differing ecological niches may result in a process of ecological release (Bolnick et al., 2010; Yoder et al., 2010), which [analogously] may be accompanied in parallel by a process of morphological release. In this thesis I studied two groups of syntopic vertebrate sister species with different divergence times: the recent modern haplochromines of Lake Victoria, and the relatively more ancient mantellid frogs from Madagascar and Comoros.

In Chapter 1 I described the divergence in trophic morphology of two syntopic *Haplochromis* sister species from Lake Victoria with contrasting feeding habits (*i.e.* ecological niches) in nature. The morphological specializations for biting and suction feeding in cichlids had been described before (Barel, 1977; 1983); however I tracked the morphological change of trophic specialization through ontogeny for the first time. In addition, the application of Geometric Morphometric techniques allowed to ‘quantify’ the amount of shape change that is associated to these specializations not only in biometric lengths, but also in the qualitative description of shape based on the coordinated displacement of the configuration of anatomical landmarks. In this manner covariation in

shape development between different subsets of landmarks was also observed, discovering a link between shape variation associated with trophic morphology and that related to locomotor specialization (Santos-Santos et al., 2015). This observation contrasted with earlier studies that ordered vertebrate evolutionary radiations in three stages (*i.e.* habitat, trophic morphology and communication, respectively; Streebman & Danley, 2003) and has been observed to hold true in other cichlid flocks, such as those of Lake Malawi (Hulsey et al., 2017). Furthermore, I observed this coordinated development of trophic and associated locomotor morphology to show different relationships depending on ontogenetic stage and described how shape changes could have developed in response to meet the differing functional demands in species' known ontogenetic shifts in habitat and diet (Katunzi, 1983; Witte, 1981; Galis & De Jong, 1988; Goldschmidt et al., 1990).

In general, ontogenetic shape variation in my Lake Victoria cichlid species showed that fry already displayed differences uncorrelated with size associated to their ecomorphological specializations and that these are magnified through ontogeny due to species-specific allometries (Santos-Santos et al., 2015). Growth along the antero-posterior body axis explained large part of the shape variation during size category I in accordance with the selective advantage of increased growth in juvenile fish (Galis & De Jong, 1988), while size category II shape variation was less correlated with size and corresponded more to changes along the dorso-ventral body axis. In size category III allometry again showed to be an important factor in shape differentiation, especially of the body's streamline, however species diverged at this stage presenting different allometric trajectories (Chapter 2). Furthermore, the observed locomotor morphological specialization was in accordance with that reported for other freshwater fish along the benthic-limnetic axis of differentiation (Hollingsworth et al., 2013; Hulsey et al., 2013; Kusche et al., 2014).

The Lake Victoria cichlid fauna was affected *circa* 18000-15000 years ago by an incomplete desiccation of the lake, which resulted in a genetic bottleneck of its extant fauna (Seehausen, 2002; Elmer et al., 2009). The persistence of [most likely benthic] species in shallow refugia and the posterior migration of [most likely riverine] cichlids from neighboring Lake Kivu, probably recolonized the lake and occupied the novel niches that appeared as lake levels rose again. In this situation hybridization between

species can be expected, and in accordance introgression of mitochondrial genes from Lake Kivu into Lake Victoria cichlids has been observed (Loh et al., 2012). The adaptive potential of the Lake Victoria haplochromine fauna however is attributed to the sharing of ancestral [nuclear] genetic polymorphism with the most recent common ancestor of the other African lacustrine radiations (Elmer et al., 2009). My analysis of the Lake Victoria cichlid hybrid displayed an intermediate mosaic of parental morphological features, albeit occupying its unique area of the morphospace along the second major axes of shape variation (~20%). This reinforces the documented idea that hybridization has promoted phenotypic variation in cichlid fish adaptive radiations (Salzburger et al., 2002; Seehausen, 2004; Selz et al., 2014; Meier et al., 2017), especially in view of heterochrony (Meyer, 1987) and phenotypic plasticity potential (Ghalambor et al., 2007; Magalhaes et al., 2009; Genner & Turner, 2012; Husemann et al., 2017) in combination with the many-to-one mapping of form to function (Martinez & Sparks, 2017) that together can result in a fast response of the phenotype to adapt to the ecological opportunity offered by fluctuating environmental conditions such as those during Lake Victoria's Pleistocene desiccation/restoration. The area of morphospace occupied by the hybrid was especially large during size category I in my analysis, indicating that during this ontogenetic stage individuals can modify their shape to a greater extent than later in ontogeny when constructional constraints may begin to limit certain directions of phenotypic change (Barel et al., 1989). This appears to hold true in my Lake Victoria species in view of reciprocal transplant experiments that were performed in relation to their dietary niches (unpublished data). Fish fry developed the corresponding morphological specializations to feed on either biting or suction diet items irrespective of their species' natural adult morphotype, emphasizing the phenotypic plastic potential of these cichlids at this ontogenetic stage, their low genetic differentiation, and the retention of ancestral polymorphisms. In any case, the closer morphological proximity of the hybrid to the benthic morphotype in my analysis leads to the hypothesis that the benthic species may be genetically more conservative and that the pelagic species constitutes a more derived condition. This interpretation would match the paleogeographic history of Lake Victoria as mentioned beforehand and the direction of genetic introgression of Lake Kivu pelagic/riverine haplotypes into relic Lake Victoria benthic haplotypes.

In contrast to Lake Victoria modern haplochromines [thousands of years of divergence], which constitute the fastest adaptive radiation known in vertebrates (Seehausen, 2006),

Malagasy mantellid frogs have diverged within a larger timespan [millions of years] (Wollenberg et al., 2011). This increased amount of time has probably aided in the evolution of stronger reproductive isolation mechanisms between mantellid species. Nonetheless, hybridization is further prevented in this group of frogs due to their unique reproductive behavior that involves the recognition of species-specific chemicals produced in male femoral glands (Glaw & Vences, 2006; Vences et al., 2007); a key innovative trait that has also probably promoted evolutionary divergence in the subfamily Mantellinae. The absence of apparent hybridization in these frogs elicits functionally-relevant phenotypic divergence between species to be interpreted more as a result of directional selection than of ecological opportunism in a fluctuating, heterogeneous environment. Likewise, although both vertebrate adaptive radiations have occurred in the tropics, the terrestrial lifestyle of adult mantellid frogs leads to different behaviors: dispersal in anurans is common and associated to movements to and from breeding habitats (Russell et al., 2005), while African cichlid fish present low dispersal and highly philopatric behavior (Witte, 1981). In addition, ecological pressures on locomotor morphology are different in aquatic versus terrestrial environments. Whereas African cichlid fish mainly diversify in locomotor morphology along the benthic-limnetic axis of the lakes' water column, terrestrial locomotion presents many more dimensions of potential phenotypic divergence (*e.g.* burrowers, climbers, gliders, jumpers). On the other hand, the opposite holds true in trophic morphology, for which cichlids display a much larger array of morphological specializations to disparate dietary niches (*e.g.* algae scrapers, detritivores, piscivores, ram suction feeders, scale eaters, zooplanktivores). Allometric shape development also entails different evolutionary trends between fish and anurans. Beforehand it was mentioned how increased growth rate in juvenile fish is correlated with increased survival rate, whereas many groups of anurans, including *Blommersia* species, present trends of miniaturization (Glaw & Vences, 2007; Klages et al., 2013).

The aspect of size evolution appears to play a major role in *Blommersia* divergence. In this genus, miniaturization parallels species diversity (Wollenberg et al., 2011). Smaller body sizes are believed to limit species' dispersal capabilities, resulting in smaller and more fragmented geographic ranges that potentially facilitate reproductive isolation and ultimately speciation. However, a smaller body size also reduces physiological tolerances and does not permit the colonization of novel areas due to limited dispersal capabilities, causing an opposite effect on the speciation process (Pabijan et al., 2012). It appears that

the evolution of these anurans in a tropical area where trophic resources are in general widely available, rather than being predominantly conditioned by trophic ecology as in aquatic cichlids, present stronger ecological pressures on locomotor morphology linked to the species' lifestyle, habitat use, and dispersal capabilities. In this context, when speciation occurs in sympatry, certain phenotypic trends relating size and dispersal processes can be expected in tropical anurans. If species have the opportunity to disperse, they will tend to increase hindlimb length to increase mobility and undergo morphological differentiation in response to the novel habitats they colonize. If species are already large and present low dispersal capabilities, the evolution of poisonous chemicals can deter predation. On the other hand, if species do not have the opportunity to disperse, they will tend to become smaller and depend on crypsis for predator avoidance (Van Bocxlaer et al., 2010). In the case of *Blommersia* miniaturization, the functional morphology of a species is assumed to be adequate for a given (micro)habitat and morphology evolves to decrease in size without largely affecting fitness. The reproductive isolation associated to lower range sizes and dispersal behaviors later generates an increased accumulation of genetic divergence giving way to the formation of cryptic species in a non-adaptive radiation. However, why is it that species in this genus tend to decrease in size? When considering their biogeographic setting on mainland Madagascar, which is one of the global hotspots of biodiversity and especially of anurans (Glaw & Vences, 2007), the competition with other anuran species for space is most likely large. This situation for this relatively small anuran genus (<25mm; now <30mm due to the description of *B. alexi* **sp. nov.**) has probably limited their options of dispersal relative to larger anuran species in Madagascar and consequently has promoted their ecological strategy of miniaturization.

In Chapters 3-5 I explored the morphological evolution of the *Blommersia* locomotor musculoskeletal system in the search of potential anatomical regions implicated in species divergence. For this purpose I counted on a naturally occurring evolutionary experiment on the island of Mayotte, Comoros. The syntopic radiation on the island of a *B. wittei* ancestor from Madagascar, which arrived in an event of transoceanic dispersal 6-8 Mya (Vences et al., 2003), into two new *Blommersia* species provided an unique opportunity to study the morphological evolution of this genus in the absence of gene flow and competition evolutionary processes. Interestingly, the two species have diverged in reproductive ecology and morphology, but most importantly they have also diverged in

size in opposite directions. One of the species (*B. alexi* **sp. nov.**) has become 20% larger than any known *Blommersia* on Madagascar (25 to 30 mm SVL), while its sister species (*B. nataliae* **sp. nov.**) has followed the trend of miniaturization of the genus. Processes of gigantism/nanism on islands are common in vertebrates, leading to the conception of what is known as the Island Rule (Van Valen, 1973; Lomolino, 2005) that states that there is a graded trend from gigantism in small species to dwarfism in larger species. It appears that the constrained area and the absence of competitors and predators on islands favor the evolution of body size towards its optimal condition based on a particular *bauplan* and ecological strategy, whereas in species-rich mainland communities interspecific interactions facilitate the evolutionary divergence of this trait (Whittaker et al., 2007). From what is observed in Madagascar, the optimal *Blommersia* body size appears to be small and restricted to small ranges. In accordance, *B. nataliae* **sp. nov.** has occupied a restricted empty niche in waterlogged cut bamboo shoots, however its sister species presents a shift towards a different *bauplan* that better represents the ecological strategy of the larger *Mantydactylus* (Mantellinae) present on mainland Madagascar. Intraspecific competition in the founding Comorian population in conjunction with the ecological release from competitors and predators on the island may have driven this opposing trend in size diversification (Lomolino, 2005). In this manner the gigantism of *B. alexi* **sp. nov.** can be interpreted as a process of morphological release within the genus in parallel with the ecological release this species has undergone on Mayotte, effectively occupying part of the functional ecological and morphological spaces that are filled by other frog taxa on mainland Madagascar. My results in Chapter 5 on the patterns of pelvic shape variation within the *Blommersia* genus appear to support this hypothesis for this morphological trait given the position of *B. alexi* **sp. nov.** in the shared morphospace and the high correlation between the observed morphological and phylogenetic distances.

In addition, in Chapter 4 I presented the first complete osteological description of a *Blommersia* species, identifying several clade-specific osteological traits probably implicated in their reproductive behavior and locomotor performance. The most exceptional skeletal characteristic was that of the clavicular process. Since there is no report of this structure in any other anuran clade, it can be presumed that it serves a function specific to the *Blommersia* genus, and most likely is linked to the mantellines' unique reproductive behavior. However, in the absence of the detailed muscular architecture of this genus, an extensive work which is currently underway (see Chapter

5), the exact biomechanical function of this structure, and of others that were observed, cannot be described in detail. Other approaches to approximate observed morphological variation with locomotor performance potentially implicated in species ecomorphological divergence include whole organism biomechanical studies (Lailvaux & Husak, 2014). In Chapter 6 I explore these techniques, albeit with another non-*Blommersia* neobatrachian species. The anuran *bauplan* is highly derived and allows optimal locomotion in both aquatic and terrestrial mediums (Handrigan & Wassersug, 2007). This is due not only to an extensive osteological reorganization relative to their tetrapod ancestor (Zug, 1972; Sigurdson et al., 2012), but also to the modification of the muscular architecture associated with locomotor function (Prikryl et al., 2009; Fabrezi et al., 2014). In my whole organism biomechanical experiments I focused on two of the hindlimb muscles that are implicated in thrust production during both jumping and swimming locomotor modes in anurans: the m. gastrocnemius and the m. semimembranosus. The wood frog (*Rana sylvatica*) is an extraordinary species in that it is able to freeze during winter at sub-zero temperatures (Storey, 1984) and initiate reproductive behaviors almost immediately upon thaw in spring (Layne & Rice, 2003). What I observed in this species is a remarkable resilience of muscular physiology and kinematic performance despite the extreme stress imposed by the seasonal phenomenon it experiences each year in its natural habitat. In like manner, similar studies with *Blommersia* species in the future could shed light on how differential locomotor performance between species is related to the observed underlying patterns of shape variation in locomotor morphology that is potentially linked to their diverging lifestyles, habitats, and life histories.

REFERENCES

- Adams DC, Collyer ML (2009) A general framework for the analysis of phenotypic trajectories in evolutionary studies. *Evolution: International Journal of Organic Evolution*, **63**, 1143-1154.
- Arnold SJ (1983) Morphology, performance and fitness. *American Zoologist*, **23**, 347-361.
- Barel C (1983) Towards a constructional morphology of cichlid fishes (Teleostei, Perciformes). *Netherlands Journal of Zoology*, **33**, 357-424.
- Barel C, Anker GC, Witte F, Hoogerhoud R, Goldschmidt T (1989) Constructional constraint and its ecomorphological implications. *Acta Morphologica Neerlando-Scandinavica*, **27**, 83-109.

Barel C, Van Oijen M, Witte F, Witte-Maas EL (1977) An introduction to the taxonomy and morphology of the haplochromine Cichlidae from Lake Victoria. *Netherlands Journal of Zoology*, **27**, 333-380.

Besl PJ, McKay ND (1992) Method for registration of 3-D shapes. In *Sensor Fusion IV: Control Paradigms and Data Structures*, pp. 586-607. International Society for Optics and Photonics.

Bolnick DI, Ingram T, Stutz WE, Snowberg LK, Lau OL, Paull JS (2010) Ecological release from interspecific competition leads to decoupled changes in population and individual niche width. *Proceedings of the Royal Society of London B: Biological Sciences*, **277**, 1789-1797.

Chen Y, Medioni G (1992) Object modelling by registration of multiple range images. *Image and Vision Computing*, **10**, 145-155.

Collyer ML, Adams DC (2013) Phenotypic trajectory analysis: comparison of shape change patterns in evolution and ecology. *Hystrix*, **24**, 75.

Collyer ML, Adams DC (2018) RRPP: An R package for fitting linear models to high-dimensional data using residual randomization. *Methods in Ecology and Evolution*, **9**, 1772-1779.

Descamps E, Sochacka A, De Kegel B, Van Loo D, Van Hoorebeke L, Adriaens D (2014) Soft tissue discrimination with contrast agents using micro-CT scanning. *Belgian Journal of Zoology*, **144**, 20-40.

Dick TJ, Clemente CJ (2016) How to build your dragon: scaling of muscle architecture from the world's smallest to the world's largest monitor lizard. *Frontiers in Zoology*, **13**, 8.

Elmer KR, Reggio C, Wirth T, Verheyen E, Salzburger W, Meyer A (2009) Pleistocene desiccation in East Africa bottlenecked but did not extirpate the adaptive radiation of Lake Victoria haplochromine cichlid fishes. *Proceedings of the National Academy of Sciences*, **106**, 13404-13409.

Fabrezi M, Manzano AS, Abdala V, Lobo F (2014) Anuran locomotion: ontogeny and morphological variation of a distinctive set of muscles. *Evolutionary Biology*, **41**, 308-326.

Fruciano C (2016) Measurement error in geometric morphometrics. *Development Genes and Evolution*, **226**, 139-158.

Galis F, De Jong P (1988) Optimal foraging and ontogeny; food selection by *Haplochromis piceatus*. *Oecologia*, **75**, 175-184.

Genner MJ, Turner GF (2012) Ancient hybridization and phenotypic novelty within Lake Malawi's cichlid fish radiation. *Molecular Biology and Evolution*, **29**, 195-206.

Ghalambor CK, McKay JK, Carroll SP, Reznick DN (2007) Adaptive versus non-adaptive phenotypic plasticity and the potential for contemporary adaptation in new environments. *Functional Ecology*, **21**, 394-407.

Gignac PM, Kley NJ (2014) Iodine-enhanced micro-CT imaging: methodological refinements for the study of the soft-tissue anatomy of post-embryonic vertebrates. *Journal of Experimental Zoology Part B: Molecular and Developmental Evolution*, **322**, 166-176.

Glaw F, Vences M (2006) Phylogeny and genus-level classification of mantellid frogs (Amphibia, Anura). *Organisms Diversity & Evolution*, **6**, 236-253.

Glaw F, Vences M (2007) *A Field Guide to the Amphibians and Reptiles of Madagascar*, Vences & Glaw.

Goldschmidt T, Witte F, De Visser J (1990) Ecological segregation in zooplanktivorous haplochromine species (Pisces: Cichlidae) from Lake Victoria. *Oikos*, **58**, 343-355.

Handrigan GR, Wassersug RJ (2007) The anuran Bauplan: a review of the adaptive, developmental, and genetic underpinnings of frog and tadpole morphology. *Biological Reviews*, **82**, 1-25.

Heinen F, Lund ME, Rasmussen J, de Zee M (2016) Muscle–tendon unit scaling methods of Hill-type musculoskeletal models: An overview. *Proceedings of the Institution of Mechanical Engineers, Part H: Journal of Engineering in Medicine*, **230**, 976-984.

Hollingsworth PR, Simons AM, Fordyce JA, Hulsey CD (2013) Explosive diversification following a benthic to pelagic shift in freshwater fishes. *BMC Evolutionary Biology*, **13**, 272.

Hulsey C, Roberts R, Loh YH, Rupp M, Streelman J (2013) Lake Malawi cichlid evolution along a benthic/limnetic axis. *Ecology and Evolution*, **3**, 2262-2272.

Hulsey CD, Zheng J, Faircloth BC, Meyer A, Alfaro ME (2017) Phylogenomic analysis of Lake Malawi cichlid fishes: further evidence that the three-stage model of diversification does not fit. *Molecular Phylogenetics and Evolution*, **114**, 40-48.

Husemann M, Tobler M, McCauley C, Ding B, Danley PD (2017) Body shape differences in a pair of closely related Malawi cichlids and their hybrids: Effects of genetic variation, phenotypic plasticity, and transgressive segregation. *Ecology and Evolution*, **7**, 4336-4346.

Jeffery NS, Stephenson RS, Gallagher JA, Jarvis JC, Cox PG (2011) Micro-computed tomography with iodine staining resolves the arrangement of muscle fibers. *Journal of Biomechanics*, **44**, 189-192.

Johansson LC, Lauder GV (2004) Hydrodynamics of surface swimming in leopard frogs (*Rana pipiens*). *Journal of Experimental Biology*, **207**, 3945-3958.

- Kargo WJ, Nelson F, Rome LC (2002) Jumping in frogs: assessing the design of the skeletal system by anatomically realistic modeling and forward dynamic simulation. *Journal of Experimental Biology*, **205**, 1683-1702.
- Katunzi EF (1983) Seasonal variation in the food of a molluscivorous cichlid *Haplochromis sauvagei* Pfeffer 1896. *Netherlands Journal of Zoology*, **33**, 337-341.
- Keller I, Wagner C, Greuter L, Mwaiko S, Selz O, Sivasundar A, Wittwer S, Seehausen O (2013) Population genomic signatures of divergent adaptation, gene flow and hybrid speciation in the rapid radiation of Lake Victoria cichlid fishes. *Molecular Ecology*, **22**, 2848-2863.
- Klages J, Glaw F, Köhler J, Müller J, Hipsley CA, Vences M (2013) Molecular, morphological and osteological differentiation of a new species of microhylid frog of the genus *Stumpffia* from northwestern Madagascar. *Zootaxa*, **3717**, 280-300.
- Klingenberg CP (2009) Morphometric integration and modularity in configurations of landmarks: tools for evaluating *a priori* hypotheses. *Evolution and Development*, **11**, 405-421.
- Kusche H, Recknagel H, Elmer KR, Meyer A (2014) Crater lake cichlids individually specialize along the benthic–limnetic axis. *Ecology and Evolution*, **4**, 1127-1139.
- Lailvaux SP, Husak JF (2014) The life history of whole-organism performance. *The Quarterly Review of Biology*, **89**, 285-318.
- Layne JR, Rice ME (2003) Postfreeze locomotion performance in wood frogs (*Rana sylvatica*) and spring peepers (*Pseudacris crucifer*). *Canadian Journal of Zoology*, **81**, 2061-2065.
- Loh Y-HE, Bezault E, Muenzel FM, Roberts RB, Swofford R, Barluenga M, Kidd CE, Howe AE, Di Palma F, Lindblad-Toh K (2012) Origins of shared genetic variation in African cichlids. *Molecular Biology and Evolution*, **30**, 906-917.
- Lomolino MV (2005) Body size evolution in insular vertebrates: generality of the island rule. *Journal of Biogeography*, **32**, 1683-1699.
- Magalhaes I, Mwaiko S, Schneider M, Seehausen O (2009) Divergent selection and phenotypic plasticity during incipient speciation in Lake Victoria cichlid fish. *Journal of Evolutionary Biology*, **22**, 260-274.
- Martinez CM, Sparks JS (2017) Malagasy cichlids differentially limit impacts of body shape evolution on oral jaw functional morphology. *Evolution*, **71**, 2219-2229.
- Meier JJ, Marques DA, Mwaiko S, Wagner CE, Excoffier L, Seehausen O (2017) Ancient hybridization fuels rapid cichlid fish adaptive radiations. *Nature Communications*, **8**, 14363.

- Meier JI, Marques DA, Wagner CE, Excoffier L, Seehausen O (2018) Genomics of parallel ecological speciation in Lake Victoria cichlids. *Molecular Biology and Evolution*, **35**, 1489-1506.
- Metscher BD (2009) MicroCT for comparative morphology: simple staining methods allow high-contrast 3D imaging of diverse non-mineralized animal tissues. *BMC Physiology*, **9**, 11.
- Meyer A (1987) Phenotypic plasticity and heterochrony in *Cichlasoma managuense* (Pisces, Cichlidae) and their implications for speciation in cichlid fishes. *Evolution*, **41**, 1357-1369.
- Mitteroecker P, Bookstein F (2007) The conceptual and statistical relationship between modularity and morphological integration. *Systematic Biology*, **56**, 818-836.
- Mitteroecker P, Bookstein F (2011) Linear discrimination, ordination, and the visualization of selection gradients in modern morphometrics. *Evolutionary Biology*, **38**, 100-114.
- Moran P, Kornfield I (1993) Retention of an ancestral polymorphism in the Mbuna species flock (Teleostei: Cichlidae) of Lake Malawi. *Molecular Biology and Evolution*, **10**, 1015-1029.
- O'Higgins P, Cobb SN, Fitton LC, Gröning F, Phillips R, Liu J, Fagan MJ (2011) Combining geometric morphometrics and functional simulation: an emerging toolkit for virtual functional analyses. *Journal of Anatomy*, **218**, 3-15.
- Pabijan M, Wollenberg K, Vences M (2012) Small body size increases the regional differentiation of populations of tropical mantellid frogs (Anura: Mantellidae). *Journal of Evolutionary Biology*, **25**, 2310-2324.
- Pauwels E, Van Loo D, Cornillie P, Brabant L, Van Hoorebeke L (2013) An exploratory study of contrast agents for soft tissue visualization by means of high resolution X-ray computed tomography imaging. *Journal of Microscopy*, **250**, 21-31.
- Pomidor BJ, Makedonska J, Slice DE (2016) A landmark-free method for three-dimensional shape analysis. *PLoS One*, **11**, e0150368.
- Přikryl T, Aerts P, Havelková P, Herrel A, Roček Z (2009) Pelvic and thigh musculature in frogs (Anura) and origin of anuran jumping locomotion. *Journal of Anatomy*, **214**, 100-139.
- Rohlf FJ, Slice D (1990) Extensions of the Procrustes method for the optimal superimposition of landmarks. *Systematic Biology*, **39**, 40-59.
- Russell AP, Bauer AM, Johnson MK (2005) Migration in amphibians and reptiles: An overview of patterns and orientation mechanisms in relation to life history strategies. In *Migration of Organisms: Climate Geography Ecology* (ed Elewa AMT), pp. 151-203. Berlin, Heidelberg: Springer Berlin Heidelberg.

- Salzburger W, Baric S, Sturmbauer C (2002) Speciation via introgressive hybridization in East African cichlids? *Molecular Ecology*, **11**, 619-625.
- Santos-Santos JH, Audenaert L, Verheyen E, Adriaens D (2015) Divergent ontogenies of trophic morphology in two closely related haplochromine cichlids. *Journal of Morphology*, **276**, 860-871.
- Seehausen O (2002) Patterns in fish radiation are compatible with Pleistocene desiccation of Lake Victoria and 14 600 year history for its cichlid species flock. *Proceedings of the Royal Society of London B: Biological Sciences*, **269**, 491-497.
- Seehausen O (2004) Hybridization and adaptive radiation. *Trends in Ecology & Evolution*, **19**, 198-207.
- Seehausen O (2006) African cichlid fish: a model system in adaptive radiation research. *Proceedings of the Royal Society of London B: Biological Sciences*, **273**, 1987-1998.
- Selz O, Lucek K, Young KA, Seehausen O (2014) Relaxed trait covariance in interspecific cichlid hybrids predicts morphological diversity in adaptive radiations. *Journal of Evolutionary Biology*, **27**, 11-24.
- Sigurdsen T, Green DM, Bishop PJ (2012) Did Triadobatrachus jump? Morphology and evolution of the anuran forelimb in relation to locomotion in early salientians. *Fieldiana Life and Earth Sciences*, 77-89.
- Storey K (1984) Freeze tolerance in the frog, *Rana sylvatica*. *Experientia*, **40**, 1261-1262.
- Streelman JT, Danley PD (2003) The stages of vertebrate evolutionary radiation. *Trends in Ecology & Evolution*, **18**, 126-131.
- Takahashi T, Sota T (2016) A robust phylogeny among major lineages of the East African cichlids. *Molecular Phylogenetics and Evolution*, **100**, 234-242.
- Van Bocxlaer I, Loader SP, Roelants K, Biju SD, Menegon M, Bossuyt F (2010) Gradual adaptation toward a range-expansion phenotype initiated the global radiation of toads. *Science*, **327**, 679-682.
- Van Oijen M, Witte F, Witte-Maas E (1981) An introduction to ecological and taxonomic investigations on the haplochromine cichlids from the Mwanza Gulf of Lake Victoria. *Netherlands Journal of Zoology*, **31**, 149-174.
- Van Valen L (1973) Body size and numbers of plants and animals. *Evolution*, **27**, 27-35.
- Vences M, Vieites DR, Glaw F, Brinkmann H, Kosuch J, Veith M, Meyer A (2003) Multiple overseas dispersal in amphibians. *Proceedings of the Royal Society of London B: Biological Sciences*, **270**, 2435-2442.
- Vences M, Wahl-Boos G, Hoegg S, Glaw F, Spinelli Oliveira E, Meyer A, Perry S (2007) Molecular systematics of mantelline frogs from Madagascar and the evolution of their femoral glands. *Biological Journal of the Linnean Society*, **92**, 529-539.

Wagner CE, Harmon LJ, Seehausen O (2012) Ecological opportunity and sexual selection together predict adaptive radiation. *Nature*, **487**, 366-370.

Wagner GP, Altenberg L (1996) Perspective: complex adaptations and the evolution of evolvability. *Evolution*, **50**, 967-976.

Whittaker RJ, Fernández-Palacios JM (2007) *Island Biogeography: ecology, evolution, and conservation*, Oxford University Press.

Wimberger PH (1994) Trophic polymorphisms, plasticity, and speciation in vertebrates. In *Theory and Application of Fish Feeding Ecology* (eds Stouder D, Fresh K, Feller R). Columbia, SC: University of South Carolina Press.

Witte F (1981) Initial results of the ecological survey of the haplochromine cichlid fishes from the Mwanza Gulf of Lake Victoria (Tanzania): breeding patterns, trophic and species distribution, with recommendations for commercial trawl-fishery. *Netherlands Journal of Zoology*, **31**, 175-202.

Wollenberg KC, Vieites DR, Glaw F, Vences M (2011) Speciation in little: the role of range and body size in the diversification of Malagasy mantellid frogs. *BMC Evolutionary Biology*, **11**, 217.

Yoder J, Clancey E, Des Roches S, Eastman JM, Gentry L, Godsoe W, Hagey TJ, Jochimsen D, Oswald BP, Robertson J, Sarver BA (2010) Ecological opportunity and the origin of adaptive radiations. *Journal of Evolutionary Biology*, **23**, 1581-1596.

Zug GR (1972) Anuran locomotion: structure and function. I. Preliminary observations on relation between jumping and osteometrics of appendicular and postaxial skeleton. *Copeia*, **4**, 613-624.

CONCLUSIONS

1. Landmark-based Geometric Morphometric techniques allow the discrimination of subtle morphological differences in shape between phenotypically-similar sister species and do not imply the destruction of the samples.
2. *Haplochromis fischeri* and *H. piceatus* display ontogenetic shape variation proper of their trophic and locomotor ecological specializations. Development of divergent morphological specializations display a relevant allometric component as well as a species-specific allometric component of shape variation. In addition, trophic and locomotor morphological specializations display an integrated development through ontogeny.
3. The *Haplochromis* hybrid displayed an intermediate morphology relative to its parentals along their major axis of shape variation, albeit occupying a discrete region of the shared morphospace along its secondary axis. Its mosaic of parental and unique features coincides with other studies in cichlid fish that support hybridization as an evolutionary mechanism that has promoted phenotypic divergence in African adaptive radiations.
4. The *Haplochromis* hybrid's ontogenetic phenotypic trajectory was significantly closer to that of the biter morphotype (*H. fischeri*), advocating the belief that this morphotype is more genetically conserved in this Lake Victoria species pair and that the sucker morphotype (*H. piceatus*) comprises a more derived condition.
5. *Blommersia alexi* **sp. nov.** and *B. nataliae* **sp. nov.** are syntopic sister species on the island of Mayotte, Comoros that have diverged genetically and in body size, morphology, and reproductive ecology from a transoceanic colonization event of a Malagasy ancestor.
6. The advent of advancements in X-ray computed tomography technology allows the convenient obtainment of data on the internal anatomy of vertebrates without the necessity of damaging the samples. This technology combined with histological chemical staining techniques can further improve the contrast between different tissue types and their visual discrimination, such as of muscle.

7. The *Blommersia* genus presents a relatively hyperossified skeleton and several osteological peculiarities likely involved in their locomotor function and unique reproductive behavior. The presence of the clavicular process is specific to the genus and probably plays a role in vertical adhesion during the reproductive act.
8. Generalized Surface Procrustes Analysis is an extension of traditional landmark-based Geometric Morphometric methods that allows for a holistic comparison of featureless anatomical structures, such as the *Blommersia* pelvis. In addition, this method allows for the utilization of high-resolution anatomical data obtained from the segmentation of computed tomography volumes and exported as 3D pointcloud surfaces.
9. Within-genus patterns of *Blommersia* pelvic shape variation are highly correlated with the phylogenetic distances between species.
10. Pelvic shape divergence between the Comorian *Blommersia* sister species is largely isometric and occurs in opposite directions from their Malagasy sister taxon, with *Blommersia alexi* **sp. nov.** presenting a trend of increasing size and *B. nataliae* **sp. nov.** one of decreasing size.
11. The wood frog's musculoskeletal system displays an incredible resilience at a broad range of physiological parameters as reflected by their relatively unaltered biomechanical performance before freezing versus after thawing.
12. Morphological evolution in tropical cichlid radiations appears to be influenced to a larger degree by trophic ecological pressures, whereas in tropical mantellids it is body size variation and locomotor performance that condition species' divergence.

